ORGANO FUNCTIONALIZED Zr-TMS CATALYSTS: SYNTHESIS, CHARACTERIZATION AND THEIR APPLICATIONS IN ENVIRONMENTALLY BENIGN ORGANIC TRANSFORMATIONS

A THESIS
SUBMITTED TO THE
UNIVERSITY OF PUNE

FOR THE DEGREE OF
DOCTOR OF PHILOSOPHY
IN
CHEMISTRY

BY
M. CHIDAMBARAM

UNDER THE GUIDANCE OF
Dr. A.P. SINGH

CATALYSIS DIVISION
NATIONAL CHEMICAL LABORATORY
PUNE 411 008
INDIA

DECEMBER 2005

DECLARATION BY RESEARCH GUIDE

Certified that the work incorporated in the thesis entitled: **"Organo functionalized Zr-TMS catalysts: synthesis, characterization and their applications in environmentally benign organic transformations",** submitted by **Mr. M. Chidambaram,** for the Degree of ***Doctor of Philosophy*****,** was carried out by the candidate under my supervision at Catalysis Division, National Chemical Laboratory, Pune 411 008, India. Material that has been obtained from other sources is duly acknowledged in the thesis.

Signature of the Research Supervisor
(Dr. Anand Pal Singh) **Date:**

DECLARATION BY THE CANDIDATE

I declare that the thesis entitled **"Organo functionalized Zr-TMS catalysts: synthesis, characterization and their applications in environmentally benign organic transformations"**, submitted by me for the Degree of ***Doctor of Philosophy*** in the record of work carried out by me during the period from December 2000 to till date under the guidance of Dr. A.P. Singh at Catalysis Division, National Chemical Laboratory, Pune and has not formed the basis for the award of any degree, diploma, associateship, fellowship, titles in this or any other University or other institution of Higher learning.

I further declare that the material obtained from other sources has been duly acknowledged in the thesis.

Signature of the candidate

(M. Chidambaram) **Date:**

Dedicated to my beloved...

Parents,

Brother, Sister-in-law &

Teachers

ACKNOWLEDGEMENTS

I find it very difficult to write something in short to acknowledge my research guide, **Dr Anand Pal Singh**. His constant inspiration, invaluable guidance and constructive criticism helped me a lot to focus my views in proper perspective. I take this opportunity to express my intense reverence towards him for guiding me in the right direction throughout the course of this work. My deepest personal regards are due for him forever.

I am highly indebted to Dr. A. V. Ramaswamy and Dr. S. Sivasanker, former Heads of Catalysis Division, and Dr. Rajiv Kumar, Head of Catalysis Division, not only formally for allowing me to use all the available facilities in the division but also personally for many stimulating discussions and valuable guidance throughout the course of this investigation.

I owe my sincere gratitude to Dr. S.B. Halligudi for FT-IR analysis, Dr. C.S. Gopinath for XPS analysis and discussion, Dr. P.R. Rajamohanan of NMR Division for solid and liquid state NMR analysis and discussions, Dr. Pradeep Kumar Tripati of OCS Division for catalysis related discussions, Dr. B.G. Anderson of Schuit Institute of Catalysis, Eindhoven University of Technology, The Netherlands and Prof. S. Vasudevan of Department of Inorganic and Physical Chemistry of Indian Institute of Science, Bangalore for FT-Raman analysis and discussions, Dr. P.N. Joshi for AAS analysis, Dr. Sainkar of CMC and Dr. A.A. Bhalekhar for SEM analysis, Dr. N.E. Jacob and Mr. R.K. Jha for N_2-sorption analysis, Ms. V. Samuel for XRD, Dr. (Mrs.) S.S. Deshpande for GC-MS analysis, Micro analysis laboratory staffs for elemental analysis, Mrs. R. Pasricha for TEM analysis and Mr. Marimuthu of CMET for Thermal analysis.

My heartfelt thanks are due Dr. (Mrs.) V. Ramaswamy, Dr. D. Srinivas, Dr. C. V. V. Satyanarayana, Dr. P. Manikandan, Dr. T. Raja, Dr. K. Selvaraj and

all other scientific and non-scientific staff of the division for their valuable help and cooperation during my tenure as a research scholar. I further, take this moment to thank my guide's better-half Mrs. Rita Rani Singh (Aunty), for her greatness and care towards me and treating me as one of her sons. I also thank other divisional scientists Dr. K.V. Srinivas, Dr. A. Sudalai for constructive discussions. I take this opportunity to show my deepest gratitude towards my flute Guru Sri. V.G. Kulkarni of CEPD Division for his generous nature.

I take this golden opportunity to convey my earnest gratitude to my friend Dr. C. Venkatesan, without his invariable help and regular scientific discussions; it would have not been possible for me to submit this thesis. Dear Venki I salute for your all helps and cares. I am also very much thankful to my senior colleagues Dr. Sahida, Dr. Sushama, Dr. Amit Dubey, Dr. Mukherjee, Dr. Laha, Dr. Patra and Dr. Mandal and my colleagues Dr. Amit Dubey, Vandana, Muthukumar, Sachin, Surendran, Shylesh, Shainaz, Shrikant, Selvakumar, Sanskriti, Neelu, Jino, Sana and Tamil selvi for their helpful hand, sympathetic ears and making the lab feel like a family. Special thanks to Dr. Anirban, Satyajyoti, Mahesh, Raina, Amit, Sonu and Pranjal. I thank Dr. Kala, Dr. Sarada, Dr. Bennur, Dr. Shiju, Biju, Pai, Vasudev, Sanbag, Prasant, Sachin, Satyanarayana, Surekha and all other research scholars in Catalysis Division for their constant support throughout my stay in NCL. I thank the staffs of Accounts, Administration, Engineering and Stores & Purchase sections for their help in a way or the other.

I would like to express my appreciation to my friends, Dr. Venkatathri, Dr. Murugan, Dr. Thiagarajan, Balki, Devaraj (Captain), Peter, Pradeep, Ramesh, Selvakannan, Selvanathan, M. Sankar, S. Sankar, Senthil, KT, Thirumoorthy, Vijayaraj, Lakshmi, Kamal, Vijayanand, Khaja, Sasi,

Kamalraj for the wonderful time I had with them. It will remain in my memories of life that I had wonderful time, fun and enjoyment at SA-49, SA-9 and 201 Venkatesh Apartments during my research time. It gives me great pleasure to thank my old friends I.S Sundaram, Ramakrishnan, Dr. Sivakumar, Dr. Sathiyendiran, Kalimuthu, Selva, Ragavendran, Ramalakshmi, kumeresh, Vasanth, from whom I have received unfailing support and encouragement during many years of studies that they have shown to me in their own special way. I also take this golden opportunity to convey my earnest respect to my schoolteachers Mr. Senathipathy, Mr. Samual, and Mr. Balakrishnan, my graduation tutors Dr. Eswaran, Dr. Thamarai selvan, Mr. Elangovan of Department of Chemistry, Thiagarajar College, Madurai, for their extraordinary way of teaching that build up my research career in science. I further, thank Mr. Damodharan, Mr. Ramakrishnan, Mr. Raju and their family for having given food throughout this course of study.

The thesis could not have been completed without the endless love and blessings from my family. Amma and Appa, I should not belittle you by thanking; you taught me how to dream, gave me the skills to chase after those dreams, and encouraged me to reach for the unreachable star. Due adoration to my brothers Mr. Sekaran, Mr. Ganesh, Mr. Ragu, my sisters Mrs. Dhanam, Mrs. Bavani, Ms. Vijayaboopathy and my sister-in-laws, Mrs. Vasantha, Mrs. Subbulakshmi, Mrs. Selvarani and my brother-in-laws Mr. Kamaraj and Mr. Karthikeyan and my Sister Viji's would-be husband Mr. Jagadhesan their steadfast faith in my capability has always spurred me to go ahead, especially in difficult times. I appreciate the supports and fun given by my nephews Mahesh, Praveen, Guru, Manoj, Pirithivi, Dharan kutty, Kishor and Vijay.

Finally, my thanks are due to Council of Scientific and Industrial Research, Government of India, for awarding the Senior Research Fellowship, and to Dr. P. Ratnasamy (former Director), Dr. S. Sivaram, Director, and Dr. B. D. Kulkarni, Deputy Director, National Chemical Laboratory, to carry out my research work and extending all possible infrastructural facilities, and to submit this work in the form of a thesis for the award of Ph.D. degree.

M. Chidambaram

CONTENTS

LIST OF FIGURES

LIST OF TABLES

LIST OF SCHEMES

LIST OF ABBREVIATIONS

AAS	Atomic Absorption Spectroscopy	KCP	Kinetically Controlled Product
AES	Atomic Emission Spectroscopy	LCT	Liquid Crystal Template
APTS	3-Aminopropyltrimethoxy silane	MCM	Mobil's Crystalline Material
CP MAS	Cross Polarization Magic Angle Spinning	MPTS	3-Mercaptopropyltrimethoxy Silane
BET	Brunauer-Emmett-Teller	NMR	Nuclear Magnetic Resonance
BJH	Barrett-Joyner-Halenda	ODA	Octadecylamine
BTSE	1,2-Bis(triethoxysilyl)ethane	PMO	Periodic Mesoporous Organosilica
DD MAS	Dipolar-Decoupled Magic Angle Spinning	OSA	Organosilanolsulfonic Acid
CMC	Critical Micelle Concentration	SAED	Selected Area Electron Diffraction
BSA	Benzylsulfonic Acid	TFA	Trifluromethanesulfonic Acid
TMAOH	Tetramethyl Ammonium Hydroxide	GHSV	Gram Hourly Space Velocity
BE	Binding Energy	SAMS	Self-Assembled Monolayers
CTMABr	Cetyltrimethylammonium Bromide	SBA	Santa Barbara Amorphous
DCM	Dichloromethane	DDA	Dodecylamine
SDPEN	(*S*,*S*)-DPEN or (*S*,*S*)-1,2-Diphenylethylenediamine	SEM	Scanning Electron Microscopy

DNA	Deoxyribonucleic acid	SLC	Silicatropic Liquid Crystals
DPEN	1,2-Diphenylethylenediamine	TCP	Thermodynamically Controlled Product
DTA	Differential Thermal Analysis	TEOS	Tetraethyl orthosilicate
ee	enantiomeric Excess	TGA	Thermogravimetric Analysis
EN	Ethylenediamine	THF	Tetrahydrofuran
FSM	Folded Sheet Materials	TOF	Turnover Frequency
FTIR	Fourier Transform Infrared	TON	Turnover Number
GC	Gas Chromatography	TPD	Temperature Programmed Desorption
GCMS	Gas Chromatography – Mass Spectroscopy	TPEN	*N*-[3-(trimethoxysilyl)propyl]-ethylenediamine
TG-DTA	Thermogravimetric-Differential Thermal analysis	UOFMN	Unified Organically Functionalized Mesoporous Network
HMM	Hybrid Mesoporous Material	UV-Vis	Ultraviolet-Visible
HMS	Hexagonal Mesoporous Silica	XPS	X-Ray Photoelectron Spectroscopy
HRTEM	High Resolution Transmission Electron Microscopy	XRD	X-Ray Diffraction
ICP-AES	Inductively Coupled Plasma – Atomic Emission Spectrometry	XRF	X-Ray Fluorescence
SEM	Scanning Electron Microscopy	TPD	Temperature Programmed Desorption
Zr-TMS	Zirconia-Transition metal oxide Mesoporous molecular Sieves	ETMS	Ethoxytrimethylsilane

ABSTRACT OF THE THESIS

The present work aims at the design and development of transition metal oxide based mesoporous molecular sieves (TMS) using zirconia as transition metal oxide support (Zr-TMS) synthesized by adopting suitable templating route to get high surface area with narrow pore size distributions. Further, the surface modification of Zr-TMS was done using various organic and organosilane groups, such as benzylsulfonic acid (BSA), trifluromethanesulfonic acid (TFA) and organosilanolsulfonic acid (OSA) by post synthetic route to develop new class of highly acidic mesoporous catalysts for catalytic activity in acylation, acetalization, condensation and esterification reactions.

The present work is comprised of **six chapters**.

Chapter 1: Introduction and Literature survey

This chapter presents an over view of various physical and chemical aspects of mesoporous molecular sieve materials, precisely transition metal oxide based mesoporous materials, more particularly zirconia. The different characteristic properties of these materials include shape selectivity, formation mechanisms, acidity etc., have been discussed. Detailed literature surveys over synthesis aspects, characterization techniques, and different catalytic applications have been given. The scopes and objectives of the present work have been outlined at the end of this chapter.

Chapter 2: Synthesis methodologies and characterization techniques

This chapter describes the general synthesis procedures of mesoporous zirconia (Zr-TMS) material, functionalization of benzylsulfonic acid over Zr-TMS (Zr-TMS-BSA) material, triflic acid over Zr-TMS (Zr-TMS-TFA) material, and organosilanolsulfonic acid over Zr-TMS (Zr-TMS-OSA) material and some amorphous functionalized materials such as A-Zr-BSA, A-Zr-TFA and A-Zr-OSA also.

Further, the complete general physicochemical characterization techniques such as powder X-ray diffraction (XRD), atomic absorption spectroscopy (AAS), nitrogen sorption technique, FT-IR spectroscopy, FT-Raman spectroscopy, X-ray photoelectron spectroscopy (XPS), elemental analysis, temperature programmed desorption (TPD) of ammonia, solid state ^{29}Si and ^{13}C CP/DD MAS NMR (cross polarization/dipolar decoupled nuclear magnetic resonance) spectroscopy, scanning electron microscopy (SEM), transmission electron microscopy (TEM), and thermo gravimetric analysis (TG-DTA) are discussed and their principles have also been discussed. The general catalytic reactions such as acylation, condensation, acetalization and esterification reaction and the basic principles of product analytical tools, such as gas chromatography (GC) gas chromatography/mass spectrometry (GC/MS) and liquid state nuclear magnetic resonance (NMR) have also been studied.

Chapter 3: Benzylsulfonic acid functionalized mesoporous zirconia (Zr-TMS-BSA) catalysts

This chapter deals with the synthesis of Zr-TMS high surface area, functionalization with benzyl sulphonic acid by post synthetic route using etherification and subsequently followed by sulphonation reactions to achieve covalently bonded Zr-TMS-BSA (-Zr-O-CH_2-Φ-SO_3H) catalysts. Different amounts of sulphonic acid were loaded over Zr-TMS-BS and the maximum amount of sulphonic acid loading was optimized to 9.1 wt % (input 10 wt %) without destroying the mesoporous structure of the material. The powder XRD patterns at low angle confirm the mesoporous nature of the materials. The N_2 adsorption-desorption studies ascribed the high surface area and considerable pore size distribution, which is in general agreement with previous values reported for mesoporous ZrO_2. The FT-IR study revealed the successful anchoring of benzyl group and the subsequent functionalization of –SO_3H group. The NH_3 TPD measurements showed that the

catalysts are acidic in nature with proper acid strength. The synthesized catalysts were used in the benzoylation of diphenyl ether with benzoyl chloride to 4-phenoxybenzophenone and condensation of 2-methylfuran with acetone to 2,2-bis(5-methylfuryl)propane and found to be more active and selective due to increase in the number of acid sites and their mesoporosity, respectively. Zr-TMS, A-Zr-BSA-10 and SO_4^{2-}/ZrO_2 were found to be poorly active and selective because of the lower acidic and non- mesoporous nature, respectively.

Catalysts optimization study was done in condensation of anisole to 4,4'-DMDPM reactions on Zr-TMS-BSA-X, (where X=5, 10, 15), Zr-TMS, sulfated zirconia and *p*-TSA catalysts. Zr-TMS-BSA-15 catalyst catalyzes the condensation of anisole efficiently with *para*-formaldehyde and is superior to other Zr-TMS-BSA catalysts due to its higher acidity. *P*-TSA, the conventional homogeneous catalyst and sulfated zirconia showed high activity than Zr-TMS and Zr-TMS-BSA catalysts. Whereas Zr-TMS-BSA catalysts found to be more selective than any other catalysts studied. Total acidity obtained at 30℃ of Zr-TMS and Zr-TMS-BSA with different wt% loading of benzylsulfonic acid show direct co-relationship between acidity and catalytic activity. The influence of the duration of the run, catalyst concentration, reaction temperature and anisole / *p*-HCHO molar ratio on the catalyst performance is examined in order to optimize the conversion of anisole and selectivity to 4,4'-DMDPM. The conversion of anisole using Zr-TMS-BSA-10 increased significantly with an increase in reaction time, catalyst concentration, and reaction temperature and decreased for anisole to *p*-HCHO molar ratio. Zr-TMS-BSA-10 was recycled and a decrease in anisole conversion is observed after two cycles, which is related leaching of BSA.

Chapter 4: Triflic acid functionalized mesoporous zirconia (Zr-TMS-TFA) catalysts

This chapter describes the synthesis of Zr-TMS catalysts based on the sol-gel method. The template was extracted from the synthesized materials with by using

ethanol and HCl. The extracted Zr-TMS was successfully functionalized with triflic acid by post synthesis treatment to obtain covalently-bonded Zr-TMS-TFA catalysts. Different loadings (5, 10, 15, 20, 25 and 30 wt %) of triflic acid over Zr-TMS were prepared by varying the molar ratios of $Zr(OC_4H_9)_4$, CTMABr, TMAOH, H_2O and CF_3SO_3H. Triflic acid functionalized amorphous (A-Zr-TFA) catalysts were also synthesized for comparison study. The catalysts were characterized by various physico-chemical techniques such as powder XRD, N_2 adsorption-desorption, FTIR, FT-Raman, elemental analysis, ^{13}C DD/MAS NMR, TPD of NH_3, SEM, TEM, and thermal analysis. The powder XRD patterns at low angle confirm the mesoporous nature of the materials. BET surface area and pore size distribution results were in general agreement with previous values reported for mesoporous ZrO_2. The NH_3 TPD measurements showed that the catalysts were highly acidic. ^{13}C DD/MAS NMR revealed that the $–CF_3$ group remained intact in the material. FT-Raman analysis demonstrated that the triflic acid was bonded in an identical fashion on both amorphous $Zr(OH)_4$ and Zr-TMS for all loadings. Triflate ligands bound via 3 equivalent oxygen atoms to zirconium atoms forming tripod structures. TEM studies showed that the material contained disordered channels, unlike MCM-41 mesoporous molecular sieves. Acetalization of EAA to fructone and benzoylation of BP to 4-PBP reactions were performed on Zr-TMS-TFA, A-Zr-TFA, triflic acid and SO_4^{2-}/ZrO_2. Zr-TMS-TFA catalysts were found to be the most active and selective in both reactions due to increase in the number of acid sites and their mesoporosity, respectively. The stability and recycle effect of the catalysts were checked in the acetalization reaction by using Zr-TMS-TFA-30. No major loss of activity was observed after two recycles, but a decrease of the sulfur content and catalyst crystallinity was observed.

The catalysts optimization study was done in benzoylation of toluene to 4,4'-dimethylbenzophenone reactions over Zr-TMS-TFA-5, Zr-TMS-TFA-15, Zr-TMS-

TFA-30, Zr-TMS and TFA catalysts. Zr-TMS-TFA-30 catalyst catalyzes the benzoylation of toluene efficiently with *para*-toluoyl chloride and is superior to other Zr-TMS-TFA catalysts due to its higher acidity. The influence of the duration of the run, catalyst concentration, reaction temperature and toluene / *p*-T-Cl molar ratio on the catalyst performance is examined in order to optimize the conversion of *p*-T-Cl and selectivity to 4,4'-DMBP. The formation of acylated products of toluene is explained by an electrophilic attack of acyl cation ($R\text{-}CO^+$; where R = $CH_3\text{-}C_6H_5\text{-}$) on the toluene ring, whose formation is facilitated by acid sites on Zr-TMS-TFA catalysts.

Chapter 5: Organosilanolsulfonic acid functionalized mesoporous zirconia (Zr-TMS-OSA) catalysts

This chapter explains a simple and efficient procedure has been developed for the syntheses of Zr-TMS and functionalization of OSA by post synthesis route over Zr-TMS to achieve Zr-TMS-OSA catalysts. Four different loadings (5, 10, 20 and 30 wt %) of OSA over Zr-TMS were prepared by varying the molar ratios. OSA functionalized non-porous catalyst (A-Zr-OSA-20) was also synthesized for comparison study. The powder XRD patterns at low angle confirm the mesoporous nature of the materials. The high BET surface area and uniform pore size distribution explains that the material is in mesoporous range. AAS experimental results reveal that more than 99 % of sodium (Na^+) was replaced by H^+ to form organosilanolsulfonic acid Zr-TMS catalysts. The NH_3 TPD measurements proved that the catalysts were comparatively highly acidic in nature. Solid-state ^{13}C CP/MAS NMR demonstrated that the OSA group remained intact in the material and there is no disulphide formation under the present synthesis condition. FT-Raman analysis illustrate that organosilanolsulfonic acid was bonded in an identical fashion on Zr-TMS at all loadings measured and found correct. The XPS measurements show peak broadening and shift in the binding energies of zirconium 3d, Silicon 2p, carbon

1s, sulfur 2p (both sulfide and sulfate sulfur) and lines in the case of Zr-TMS-OSA catalysts. Further, it explains that the OSA is anchored on the surface of zirconia linearly and sulfonic acid group is easily accessible for catalysis. TEM studies showed that the material contained uniform square like and disordered hexagonal channels, unlike MCM-41 mesoporous molecular sieves. Thermal analytical results demonstrate that the material is highly pure and it cannot be treated above 300°C. After having demonstrated the syntheses of stable, mesoporous, OSA functionalized Zr-TMS catalysts; their catalytic performance was assessed for the liquid phase esterification of glycerol with lauric acid and condensation of aniline with p-formaldehyde, which are industrially equally important reactions. Zr-TMS-OSA catalysts were found to be the most active and selective in both the reactions due to their mesoporosity and to an increase in number of acid sites with the "right" acid strength. The stability and recycle effect of the catalysts were checked in the esterification reaction using Zr-TMS-OSA-20 and found no major deactivation.

Chapter 6: Summary and Conclusions

This last chapter elaborately presents the summary and conclusions of the present thesis work. The arrival at the earlier set scopes and objectives of thesis have been achieved and discussed, like,

Zr-TMS material has been synthesized and functionalized with benzylsulfonic acid, triflic acid and organosilanolsulfonic acid. The synthesized catalysts have been characterized by various instrumental techniques to confirm the existence of mesoporous nature and to confirm the presence of organic functional groups. Then catalytic applications have been performed in various reactions to prove the promising catalytic nature of the catalysts.

CHAPTER-1

INTRODUCTION AND LITERATURE SURVEY

1.1. HISTORY

The term “catalysis” was coined by Berzelius in 1853 and used to cover a number of physiological and chemical reactions, discovered at that time, all with the common feature that they proceeded in the presence of a further substance which did not itself alter during the course of the reaction. Among these reactions were the oxidation of ethyl alcohol yielding acetic acid and the combustion of hydrogen, both of which take place in the presence of platinum at room temperature, the decomposition of ammonia and hydrogen peroxide in the presence of different metals, the conversion of starch in to sugar in the presence of acids or ferments and the cleavage of amygdaline in the presence of emulsion.

Berzelius defined a catalyst as a substance, which by its mere presence evokes chemical actions, which would not take place in its absence. In brief “the presence of a catalyst awaking the affinities which are asleep. The idea of “marriage broker” about the phenomenon of catalysis put forwarded by Chinese scientists. After sixty years W. Ostwald, introduced a new definition of catalysis based on the knowledge of chemical equilibrium that all chemical reactions precede via a number of more or less stable intermediates. According to Ostwald the phenomenon catalysis can be understood as an acceleration of a thermodynamically feasible reaction through the presence of a substance, the catalyst, which it self is either essentially altered or consumed by this chemical action. Further, from thermodynamics it is obvious that a catalyst, which increases the rate of the forward reaction, must also increase the rate of the reverse process.

In addition to this thermodynamic definition of catalysis, several other approaches have been put forward during the last hundred years, including the concept of “intermediate chemical compounds” by Sebatier. This concept returns in a modified version in the activated complex theory. The “active site theory” suggested by Taylor in 1925 postulates that distinct sites on a catalytic surface can interact with

the reactants; he also expressed that “the amount of surface which is catalytically active is determined by the reaction itself”. The geometric theory attributed the active sites to geometric formation of what were assumed to be perfect crystal planes whereas earlier formulation of the electronic theory regarded surface energetic as more important than surface atoms, as distinct geometric entities.

Catalysts are conveniently divided into two groups, homogeneous and heterogeneous catalysts. It is interesting to note that first industrial catalytic process, soap making and alcoholic fermentation, used homogeneous catalysts or enzymes with out knowing anything of catalysis. The first “modern” process also used a homogeneous catalyst; nitric oxide, to oxidize SO_2 to SO_3 in the earlier sulphuric acid manufacture. However, the homogeneous catalysts have several disadvantages if applied in industrial processes such as wasting large amounts of catalysts, corrosion of reactors, water pollution by acidic wastewater and difficulties of catalyst recovery. The use of heterogeneous catalysts helped scientists for overcoming the practical difficulties when using homogeneous catalysts. To combine the advantages of homogeneous and heterogeneous catalytic reaction systems, homogeneous catalyst heterogenized by anchoring through coordinating groups like phosphines to polymers like cross-linked polystyrene or even to traditional oxide supports.

Further, catalysis is a process in which the chemical reactions are facilitated by mere presence of catalysts and plays a vital role in nature and society since almost every reaction requires a catalytic material [1]. Catalysts are substances that facilitate a chemical reaction by lowering the energy barrier of the reaction pathway and thus increasing the reaction rate [2]. Three groups of materials can be recognized as catalysts on the basis of nature of the substances: homogeneous catalysts, bio-catalysts (e.g. enzyme), and heterogeneous catalysts. The description of a catalyst as homogeneous or heterogeneous, generally taken to refer to its phase relative to that of substrate, is equally applicable to the structural anisotropy of the

active site. Homogeneous catalysts, mainly soluble transition metal complexes do offer a potentially well-defined metal environment, which translates into greater selectivity in the transformations effected at the metal center [3]. Rapid developments in homogeneous catalysts can accrue because soluble catalyst systems are much more amenable to study than bulk metals: the ability to monitor molecular changes in organo-metallic complexes enables a level of mechanistic understanding which remains without parallel in the long established field of heterogeneous catalysis [4]. Bio-catalytic methods based on enzyme catalysis, originally limited to the production of natural microbial metabolites, have expanded greatly in the last decade, to encompass synthesis not only of natural and unnatural products of opposite configuration, but of chiral synthons for use in building up novel chemical entities [5]. Porous solids (zeolites, charcoal, etc.), layered silicate sheets (clays), layered metal oxides (sulfated zirconia, tungstated zirconia, etc.), and bulk metal oxides (spinels, MgO, etc.), heteropoly acids are some of the well-known heterogeneous catalysts [6-10].

1.2. SOLID ACIDS

Solid acids have been the subjects of the most extensive and detailed studies of all heterogeneous catalysts**.** A solid acid may be a solid on which the color of a basic indicator changes or a solid on which a base is chemically adsorbed. They are used in such important processes as catalytic cracking (X and Y zeolites), paraffin isomerization (chlorinated Pt-Al_2O_3) [11], refining (silica-alumina, noble metal support) [1], alcohol from olefin formation (SiO_2-H_3PO_4) [12], alkylation (SiO_2-H_3PO_4) and many others. The first solid acid catalysts commercially used on a large scale were acid-leached natural aluminosilicates such as clays. They were the first cracking catalysts in the Houndry's processes [13]. All these catalysts are characterized by the presence of protons or coordinatively unsaturated metal cation

on their surfaces. The number of these sites determines the total surface acidity while their structure is responsible for the acid strength.

The acidity and acid strength of a solid acid depend upon the following factors.

1. The kind of cation in the crystal lattice of the oxide.
2. The kind of two or more cation in the crystal lattice of the oxide.
3. The preparation method of the catalyst. (Co-precipitation, melting, calcination)
4. The means of activation.

The modification of the acid properties on the surface can be accomplished by depositing atoms or groups of atoms of high acidic character on the surface of the oxides. Usually atoms having strong acceptor properties are used for increasing the acidic nature of solid oxides. They increase the acceptor ability, and in consequence of that, the acidic strength of the surface by pulling away electrons from the active centers. Depositing on the surface, such atoms as Cl, F, or their compounds achieve this, e.g. CCl_4, while deposition of atoms having donor properties increase the basic strength of the metal oxide. The general principle has several variations. As an e.g. one can deposit on surface, a group of atoms or whole molecules containing in their structures. Atoms, which are strong acceptors, can be in the form of protonic acids; H_3PO_4, HCl, FPO_3H, etc. such Lewis acids as for e.g.$AlCl_3$, SbF_5, P_2O_5 or finally both of them together.

They are either highly crystalline or amorphous in nature. According to the inherent size of the pores or voids the substances possess, the materials are further divided into three types: Microporous (pore size ca. 0.3-2 nm), mesoporous (pore size ca. 2 –20 nm) and macroporous (pore size >20 nm). Microporous materials include zeolites, clays, and sulfated metal oxides and mesoporous materials (M41S family, SBA family) are both academically and industrially interested and as the pores are small enough to sieve the molecules of certain molecular diameter these

materials are called as molecular sieves. Table 1.2 typically lists some zeolites and molecular sieves with variable pore sizes, mostly in the microporous range prior to the discovery of MCM-41.

Table 1.1. General classification and applications of heterogeneous catalysts.

Class of catalysts	Examples	Applications
Metals (supported-mono, bi-, multi-metallic), alloys, etc.,	Pt, Pd, Rh, Ni, Fe, Co, Cu, Ag, etc., on SiO_2, Al_2O_3, activated carbon, and others.	Hydrogenation-dehydrogenation, aromatization, oxidation.
Metal oxides (amorphous and crystalline) and mixed metal oxides (acidic or basic or redox)	MgO, CuO, SiO_2-Al_2O_3, zeolites, mesoporous metal oxides, AlPOs, SAPOs, oxides of Bi-Mo, Fe-Mo, perovskites, spinels, fluorites	Alkylation, cracking, isomerization, disproportionation, selective oxidation, dehydration-hydration, ammoxidation, amination.
Metal sulfides (supported)	Co-Mo, Ni-Mo, Ni-W on Al_2O_3, SiO_2 or other supports.	Hydrodesulfurisation, hydrotreating, hydrogenation
Metal salts	$Zr_3(PO_4)_4$, ZnS, $LaPO_4$, sulfates, carbonates.	Etherification, amination
Ion-exchange resins	Nafion-H, amberlyst resins	Etherification, dehydration-hydration, esterification
Heteropolyacids (supported)	$H_3PW_{12}O_{40}$, $H_3PMo_{12}O_{40}$, $H4SiW_{12}O_{40}$	Acid catalyzed reactions, oxidation condensation
Clays and pillared clays, hydrotalcites.	Kaolinite, K-10 Montmorillonite, Al-pillared montmorillonite	Acid-catalyzed reactions, cracking, alkylation, nitration
Immobilized enzymes	Aspartase, nitrilase, amylase	Hydration, amination
Metal complexes (supported or encapsulated)	Metal porphyrins, salens and pthalocyanins)	Selective oxidation

Table 1.2. Pore size definition of zeolites and molecular sieves

Pore size (Å)	definition	Typical material	Ring size	Pore diameter (Å)
>500	macroporous			
20-500	mesoporous	MCM-41, Zr-TMS		15-100
<20	microporous			
	ultra-large pore	Cloverite	20	6.0 x 13.2
		JDF-20	20	6.2 x 14.5
		VPI-5	18	12.1
		$AlPO_4$-8	14	7.9 x 8.7
	Large pore	Faujasites	12	7.4
		Beta	12	
		Mordenite	12	6.7 x7.0
		$AlPO_4$-5	12	7.3
		ZSM-12	12	5.5 x 5.9
	Medium pore	ZSM-48	10	5.3 x 5.6
		ZSM-5	10	5.3x 5.6; 5.1 x 5.5
	Small pore	CaA	8	4.2
		SAPO-34	8	4.3

It is estimated that molecular sieves are responsible for the production of more than 85% of all bulk chemicals as well as intermediates and fine chemicals, and for the destruction of pollutants, such as NO_x and chlorinated hydrocarbons. Fine chemicals are used as intermediates in the manufacturing of various chemical substances such as pharmaceuticals, flavors, essences, agro-chemicals and detergents etc. Among the solid acid-base catalyst that are employed in various industrial processes for the production of fine chemicals, zeolite catalysts represent 45% in different processes such as for alkylation, acylation, amination, cracking, etherification, esterification, condensation reactions etc.

1.3. ACID PROPERTIES OF SOLID ACIDS

Acids can be classified into two categories, Brönsted and Lewis acids. According to Brönsted and Lewis definitions, a solid acid shows a tendency to donate a proton or to accept an electron pair. In zeolites the hydroxyl groups with in the channels produce the active Brönsted sites. These are usually prepared by ammonium ion exchange method. Acids do not destroy the structure of zeolites. The hydroxyl may

be regarded as protons bonded to negatively charged framework oxygens associated with AlO_4^- tetrahedra. At higher temperature (greater than 200°C) these can be mobile [14], and at even higher temperature (greater than 550°C) they may lose to form Lewis sites (Figure 1.1).

Brönsted sites,

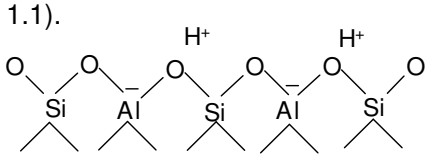

(A)

$+H_2O$ $-H_2O$

Lewis sites

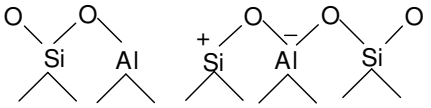

(B)

Figure 1.1. Formation mechanism of Brönsted and Lewis acid sites.

The cationic species present in the catalyst framework can act as Lewis acid site, because of their electron acceptor properties. These sites function frequently as sorption sites [15]. Studies in zeolites showed that there is a distribution of acid site strength i.e. some sites have strength greater than 90 percent sulphuric acid [16]. Such acids are called super acids. There has been rapid development of solid super acids, which include,

1.3.1. Lewis acid

'True Lewis site'

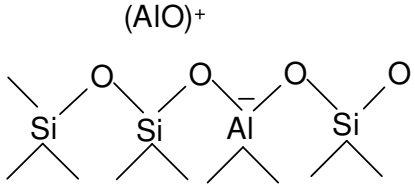

(C)

Figure 1.2. True Lewis acid in sites solid acid catalysts

Lewis acid sites (electron pair acceptor sites) are related to the formation of positively charged oxide clusters or ions within the porous structures of the zeolites. These species are typically alumina or silica/alumina, formed by extraction of aluminum from the lattice, or metal ions exchanged for the protons of acid sites. The

former type of Lewis acidity, i.e. aluminum oxide clusters containing alumina in octahedral and tetrahedral coordination will usually be a stronger Lewis acid than exchangeable metal cations, "true" Lewis acids (Figure 1.2) [17].

Lewis acid sites are acting also as hydride (or anion) receptors in a variety of reactions.

1. Supported acids e.g. liquid acids such as SbF_5 on high surface-area solids.
2. Synergism of metal halides and metal salt e.g. $AlCl_3$-$CuCl_2$; $AlCl_3$-$CuSO_4$.etc.
3. Sulfate-promoted metal oxides. e.g. ZrO_2-SO_4^{2-}, TiO_2-SO_4^{2-}.etc.
4. Metal-promoted super acids, and
5. Polymeric super acids. eg. Nafion H

1.3.2. Brönsted acid

Pure siliceous zeolites are electrically neutral. By replacing silicon (tetrahedrally coordinated with oxygen atoms) having a formal charge of 4^+ in the zeolite lattice with aluminum (formal charge 3^+) a negatively charged tetrahedron is created. The negative charge is balanced by a cation either NH_4^+, alkali cations like Na^+, K^+ or H^+ ions. The protons are formally assigned as bonded to the bridging oxygen of a Si-O-Al bond to form hydroxyl groups that act as strong Brönsted acids at the solid/gas interface. The overwhelming evidence is that hydroxyls within the zeolite channels provide the active Brönsted sites [18]. These are usually prepared via ammonium ion exchange:

$$NaZ + NH_4^+(aq) \rightleftharpoons NH_4Z + Na^+(aq)$$

$$NH_4Z \rightleftharpoons NH_3(g) + HZ$$

They are also prepared via hydrolytic process involving water coordinated to polyvalent cations: $M(H_2O)^{n+} \rightleftharpoons MOH^{(n-1)+} + H^+$

This generates protonic sites within the zeolite. In silica rich zeolites, where acids do not destroy the structure, the hydrogen forms (HZ) can be prepared by direct exchange of Na^+ by H^+ using mineral acids. Brönsted acid sites will have acid strength, which depends on their environment, i.e. depending on chemical composition and the structure of the zeolite [19]. The local environment of the acid site in a molecular sieve is determined by the structure, i.e. the coordination of the TO_4 tetrahedra in the framework (topology). This leads to different amounts of topologically different T sites, i.e. sites in tetrahedral position. In this way, LTL zeolites would have two, MOR four and MFI twelve different T sites [20], while FAU structures have no inequivalent T sites. These different tetrahedral positions differ in T-O-T bond angles and T-O bond lengths [21, 22].

1.3.3. Super acids

The super acid may be obtained by,

1. Lewis acid action on metal oxide,
2. Synthesis of Lewis acids on metal oxide surface.
3. Lewis acid action on salts,
4. Lewis acid action on ion exchange resins,
5. Lewis acid action on graphite.

The presence of sulfur in oxide species plays a good role in the generation of super acid sites. e.g. solid super acids such as sulfated zirconia, sulfated titania etc. have been reported to exhibit extremely high catalytic activities for acylation [23 ,24] and alkylation [25] of aromatics, isomerization of paraffins [26, 27] etc, Beckmann rearrangement of oximes [28] etc. In these catalysts, the S=O group have a high double bond nature. The strength of super acid depends on the extent of losing the double bond character by an electron shift from an adsorbed basic molecule to the sulfur complex [29]. The larger the shift, the higher the acid strength. The generation of super acidity is independent of sulfur source such as $(NH_4)_2SO_4$, SO_3, SO_2, or H_2S,

provided that the oxidation state of sulfur is brought to its highest one [30, 31]. The surface sulfur complex in the highly active catalysts or highly acidic catalysts has a strong tendency of reducing the bond order of S=O from a highly covalent double-bond character to a lesser double-bond character when a basic molecule is adsorbed on its central metal cation. The strong ability of the sulfur complex with structure to accommodate electrons from a basic molecule is a driving force to generate highly acidic properties (Figure 1.3).

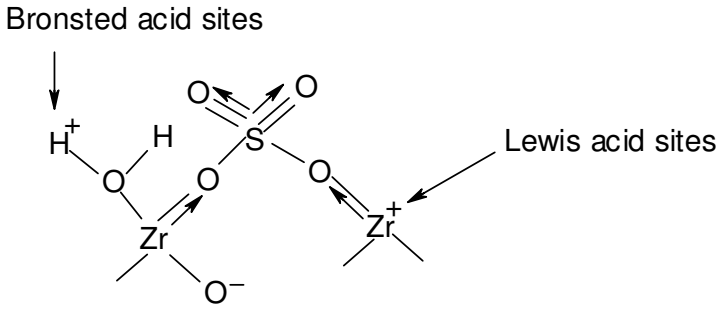

Figure 1.3. Lewis and Brönsted Acid sites in solid super acids

1.4. NEED FOR MESOPOROUS MATERIALS

Even though, zeolites, having pore dimensions of 5 to 7 Å, served the purpose of most of the industrial reactions by providing high surface area, the pore dimensions are not sufficient enough to accommodate broad spectrum of larger molecules. The performance of zeolite systems is limited by diffusion constraints associated with smaller pores. To a certain extent it is possible overcome this problem with aluminophosphates (ALPOs) [32-36], microporous crystalline materials with pore dimensions up to 13 Å. However, these materials suffer from limited thermal stability as well as negligible catalytic activity due to framework neutrality. Moreover, the need for present day heterogeneous catalysts in processing hydrocarbons with high molecular weight made researchers to think for better systems. These limitations led to the discovery of mesoporous materials.

With the first successful report on the mesoporous materials (M41S) by Mobil researchers [37], with well-defined pore sizes of 20-500Å, the pore-size

constraint (15Å) of microporous zeolites was broken. The high surface area (>1000m^2/g) and precise tuning of the pores are among the desirable properties of these materials. Mainly these materials used in a new synthetic approach where, instead of a single molecule as templating agent as in the case of zeolites, self-assembly of molecules aggregates or supramolecular assemblies are employed as templating agent. M41S series of mesoporous materials consists of uni-dimensional hexagonal MCM-41 [38], three-dimensional cubic MCM-48 [39] and lamellar MCM-52 [40]. In this series MCM-41 is the most investigated, which has a honeycomb structure as a result of hexagonal packing of uni-dimensional cylindrical pores. The pore dimensions of this is in a range of 20-100 Å. MCM-48 having cubic structure is thought to be based on the gyroid form of an infinite periodic minimal surface model, which means that two molecules on each side of a surface will not meet.

The purpose and advantages of synthesizing mesoporous materials is as follows.

1. To overcome the diffusional constraints with zeolites.
2. Very high surface are (>1000m^2/g) and pore size distribution (20-100 Å).
3. Good host material for guest species (i.e. heterogenization of homogeneous species or metal complexes on the walls).
4. Easier to monitor the changes made with active species via surface are measurement and pore size distribution experiment.

1.5. MECHANISM OF FORMATION OF MESOPOROUS MATERIAL

An ever growing interest in expanding the pore sizes of zeotype materials from micropore region to mesopores region in response to the increasing demands in both industrial and fundamental studies, the mechanism of formation should be understand clearly. Examples are treating heavy feeds, separating and selective synthesizing large molecules and intra zeolite fabricating technology [41, 42]. Zeolitic materials, typically have a surface area of ca. >700 m^2 g^{-1}, which are not truly crystalline like microporous zeolites but because of rapid growth of the research on

these materials make them to be classified as mesopore zeolites, with the majority of this surface inside the pores and accessible only through apertures of well-defined dimensions [43]. In 1992, researchers at Mobil Corporation discovered the M41S family of silicate/aluminosilicates mesoporous molecular sieves with exceptionally large uniform pore structures, which has resulted in a worldwide resurgence in this area [37, 38]. Three different mesophases in this family have been identified, i.e. lamellar [40], hexagonal [38], and cubic phases [39], in which the hexagonal mesophase, MCM-41, possesses highly regular arrays of uniform-sized channels whose diameters are in the range of 15-100 Å depending on the templates used, the addition of auxiliary organic compounds (co-template) and the reaction parameters. The pores of this novel material are nearly as regular, yet considerably larger than those present in crystalline materials such as zeolites, thus offering new opportunities for applications in catalysis [44] and advanced composite materials [45]. Accordingly, MCM-41 has been investigated extensively because the other members in this family are either thermally unstable or difficult to obtain.

The M41S family of mesoporous materials is synthesized using a silica source and different organic structure directing agents, *e.g.*, cationic surfactants containing long alkyl chain quaternary ammonium compounds containing 10–20 carbons, often followed with addition of co-surfactants. The dependence of surfactant/silica molar ratio in a ternary synthesis system containing tetraethylorthosilicate (TEOS, silica source), water and cetyltrimethylammonium ($C_{16}TMA^+$) cations (surfactant) at 100°C on appearance of different phases of M41S family is summarized in Table 1.2.

A number of models have been proposed to rationalize the mechanism of formation of mesoporous materials by various synthesis routes. All these models are based on the role of surfactants in solution to direct the formation of silicate mesostructure. In solution, the surfactants have a hydrophilic head group and a long chain hydrophobic tail group within the same molecule, which will aggregate and self-

organize in such a way so as to minimize the contact between the incompatible ends. Different types of interaction between the surfactant and the inorganic precursor under different synthesis conditions leads to different postulates for the mechanism of formation of mesoporous materials, which will be discussed briefly in this section.

1.5.1. Liquid Crystal Templating (LCT) Mechanism

The researchers of Mobil Corporation proposed a 'liquid crystal templating (LCT) mechanism' to explain the formation of M41S type mesoporous materials [37, 38]. The mesostructure formation depends on the hydrocarbon chain length of the surfactant tail group and the effect of variation of the surfactant concentration and the additional organic swelling agents. The lowest concentration at which surfactant molecules aggregate to form spherical isotropic micelles is called critical micelle concentration (CMC_1). Further increase in the surfactant concentration initiates aggregation of spherical into cylindrical or rod-like micelles (CMC_2). There are three main liquid crystalline phases with hexagonal, cubic and lamellar structures. The hexagonal phase is the result of hexagonal packing of cylindrical micelles, the lamellar phase corresponds to the formation of surfactant bilayers and the cubic phase may be regarded as a bicontinuous structure.

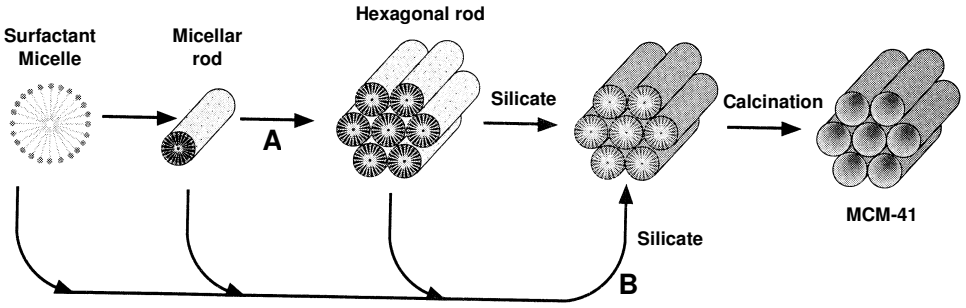

Scheme 1.1. Liquid crystal templating (LCT) mechanism proposed for the formation of MCM-41; (A) liquid crystal phase initiated and (B) silicate anion initiated. [Source: Ref.38].

The Mobil researchers proposed two synthesis mechanisms [37, 38]. In the first route, the $C_nH_{2n+1}(CH_3)_3N^+$ surfactant species organize into lyotropic liquid crystal phase, which can serve as template for the formation of hexagonal MCM-41 structure. Firstly the surfactant micelles aggregate into a hexagonal array of rods, followed by interaction of silicate or aluminate anions present in the reaction mixture with the surfactant cationic head groups. Thereafter condensation of the silicate species occurs, leading to the formation of an inorganic polymeric species. After combusting off the surfactant template by calcination, hexagonally arranged inorganic hollow cylinders are produced (Scheme 1.1). However, the drawbacks of this synthesis pathway was pointed out by Cheng et al.[46], according to whom the hexagonal liquid-crystal phase does not form below 40% of surfactant concentration. It is known that MCM-41 may be formed at low surfactant concentrations (1 wt %) with respect to water content, and *in situ* ^{15}N NMR spectra indicated that the hexagonal liquid-crystalline phase was not present anytime during formation of MCM-41 [47].

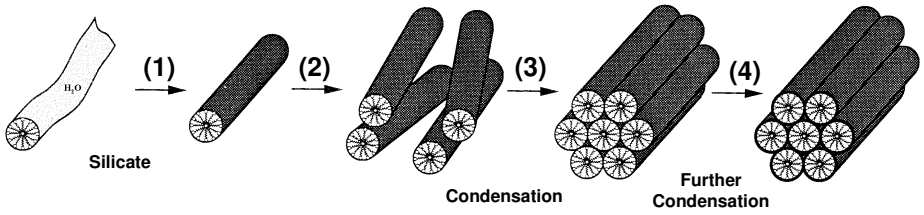

Scheme 1.2. Silicate rod assembly proposed for the formation of MCM-41; (1) and (2) random ordering of rod-like micelles and interaction with silicate species, (3) spontaneous packing of the rods, and (4) remaining condensation of silicate species on further heating. [Source: Ref.47].

In the second route, the hexagonal ordering is initiated by the presence of silicate species in the reaction mixture [37, 38]. Chen et al. explained that randomly distributed surfactant micelles with rod-like morphology form initially, and their interaction with silicate oligomers generate randomly oriented surfactant micelles surrounded by two or three silica monolayers [47]. The presence of rod-like micelles

in solution was supported by isotropic *in situ* ^{14}N NMR [47]. Further condensation between silicate species on adjacent rods occurs on heating, initiating the long-range hexagonal ordering (Scheme 1.2).

1.5.2. Charge Density Matching

The 'charge density matching' model proposed by Stucky *et al*. suggested that condensation occurs between initially formed silicate species by the electrostatic interaction between the anionic silicates and the cationic surfactant head groups [48, 49]. This eventually reduces the charge density and therefore, curvature was introduced into the layers to maintain the charge density balance with the surfactant head groups, which leads the transformation of lamellar mesostructure into the hexagonal one (Scheme 1.3.A). Although silica-initiated synthesis mechanism has been widely accepted, the presence of an intermediate lamellar species has been disputed.

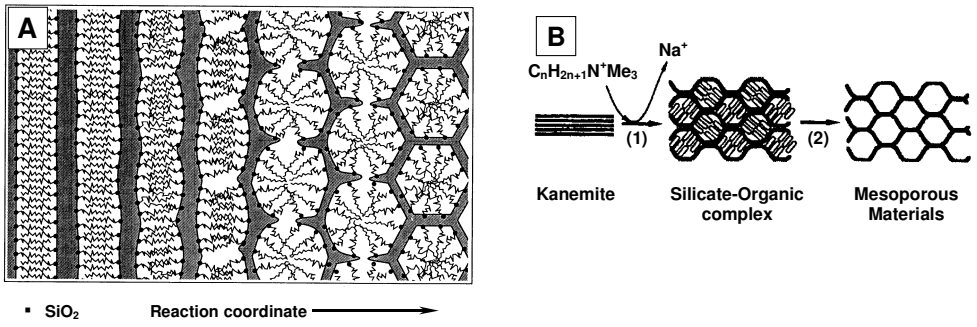

Scheme 1.3. Transformation of surfactant-silicate systems from lamellar to hexagonal mesophases; (A) hexagonal mesophase obtained by charge density matching, and (B) folding of kanemite silicate sheets around intercalated surfactant molecules. [Source: Refs. 48, 49 and 50].

1.5.3. Folded Sheet Mechanism

The 'folded-sheet mechanism' postulated by Inagaki et al. indicated the presence of intercalated silicate phases in the synthesis medium of the reaction products (Scheme 1.3.B) [50]. The flexible silicate layers of kanemite fold around the

surfactant cations, and cross-linking of the interlayer occurs by condensation of silanol groups on adjacent silicate sheets. On increase of pH, the amount of occluded $C_nH_{2n+1}(CH_3)_3N^+$ cations in kanemite increase resulting in expansion of the kanemite interlayers to form another class of regular hexagonal structure called FSM-16.

1.5.4. Silicatropic Liquid Crystals

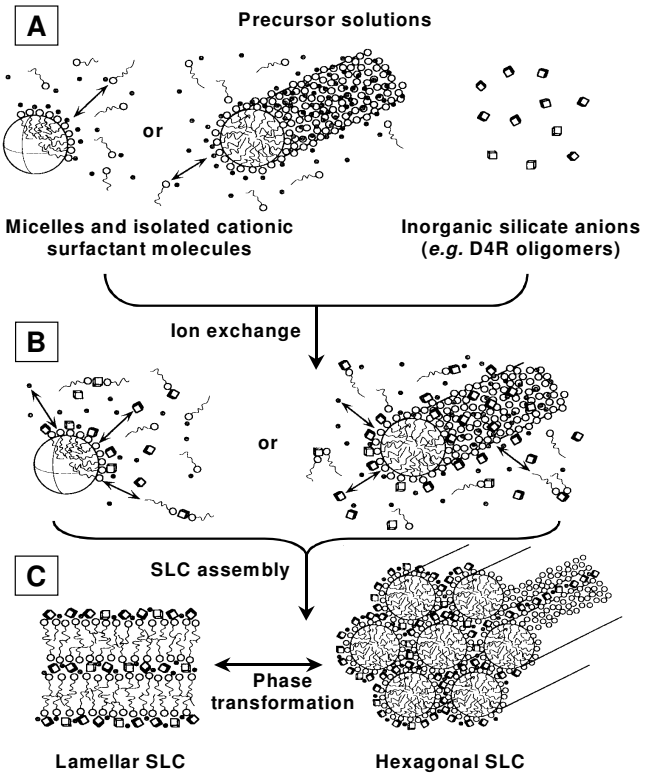

Scheme 1.4. Cooperative organization for the formation of silicatropic liquid crystal phase / silicate-surfactant mesophases; (A) organic and inorganic precursor solutions, (B) preliminary interaction of the two precursor solutions after mixing, and (C) multidentate interaction of the oligomeric silicate units with the surfactant molecules. [Source: Ref.51, 52].

Firouzi et al. have developed a model based on cooperative organization of inorganic and organic molecular species into 3D structured arrays [51, 52]. According to this model, the physicochemical properties of a particular system were not determined by the organic arrays having long-range preorganized order, but by the

dynamic interplay among ion-pair inorganic and organic species, so that different phases can readily be obtained through small variation of controllable synthesis parameters. The exchange of silicate anions with the surfactant halide counter ions formed the 'silicatropic liquid crystal' (SLC) phase (Scheme 1.4), which exhibited very similar behavior to that of typical lyotropic systems and finally condensed irreversibly in to MCM-41.

1.5.5. Generalized Liquid Crystal Templating Mechanism

1.5.5.1. Ionic Route (Electrostatic Interaction)

Huo et al. proposed a generalized mechanism for the formation of mesostructures, which was based on specific types of electrostatic interaction between an inorganic precursor (I) and a surfactant head group (S) [53, 54]. In this concept, four different approaches were proposed to synthesize transition metal oxide mesostructures [53]. The first route involves the charge density matching between surfactant cations and inorganic anions (will be referred to as S^+I^- hereafter). The second route deals with the charge-reversed situation, *i.e.*, anionic surfactant and cationic inorganic species (S^-I^+). Both the third and fourth routes are counterion-mediated pathways. The third one demonstrates the assembly of cationic species *via* halide ions ($S^-X^+I^-$), while the fourth one depicts the assembly of anionic species *via* alkali metal ions ($S^+X^-I^+$). These syntheses strategies are acceptable for the formation of a wide variety of lamellar, hexagonal or cubic mesophases. However, a general problem negotiated very often is the poor stability of the inorganic framework, which frequently collapses after removal of the surfactant.

1.5.5.2. Neutral Templating Route (Hydrogen Bonding Interaction)

Tanev and Pinnavaia proposed another route to synthesize hexagonal mesoporous silicas (HMS) having thicker pore walls, high thermal stability and smaller crystallite size but, having higher amounts of interparticle mesoporosity and lower degree of long-range ordering of pores than MCM-41 materials [55-57]. This

route is essentially based on hydrogen bonding between neutral primary amines (S^0) and neutral inorganic precursors (I^0), wherein hydrolysis of tetraethyl orthosilicate (TEOS) in an aqueous solution of dodecylamine yields neutral inorganic precursor. Using the same approach, porous lamellar silicas with vesicular particle morphology have been synthesized with the aid of double headed alkylamines linked by a hydrophobic alkyl chain (α,ω-dialkylamine) [57].

1.5.5.3. Ligand-Assisted Templating Route (Covalent Interaction)

Antonelli and Ying have proposed a ligand-assisted templating mechanism for the synthesis of hexagonally packed mesoporous metal oxide completely stable to surfactant removal.[i] In a typical synthesis, the surfactant was dissolved in the metal alkoxide precursor before addition of water to allow nitrogen–metal covalent bond formation between the surfactant head group and the metal alkoxide precursor. The existence of this covalent interaction was confirmed by ^{15}N NMR spectroscopic studies. In this approach, the structure of the mesophases could be controlled by adjustment of the metal/surfactant ratio, which led to a new class of mesoporous transition metal oxides analogous to M41S family.

1.6. CONTROL OF CRYSTAL SIZES, PORE SIZES AND MORPHOLOGY

The past decade saw extensive research to control the crystal size, pore dimensions and pore sizes of ordered mesoporous materials, particularly for MCM-41 with unidirectional channels. The control of crystal size is of immense importance when these materials are to be used in catalytic processes. The length of the pores must be decreased as much as possible to overcome diffusion limitations, which is normally done by decreasing crystallite size. Wu et al. have synthesized thermally stable hexagonal mesoporous materials of smaller crystal sizes (~100 nm) by microwave heating of precursor gels at 150 ºC for not more than 1 h [58]. The fast and homogeneous condensation reactions occurring during microwave synthesis leads to smaller crystal sizes and high thermal stability.

The characteristic feature of the M41S type molecular sieves is the flexibility to synthesize these materials with different pore diameters ranging from 2–10 nm. This can be achieved by the following ways: (i) variation of the chain length of the hydrophobic alkyl group (8 to 22 carbon atoms) in the surfactant molecules [37], (ii) addition of organic swelling agents such as 1,3,5-trimethylbenzene [37], or alkanes of different chain length [59], which will increase the micellar size by solvation of the added hydrophobic molecules in the hydrophobic region of the micelles, and (iii) by adjusting the composition of the gel and the crystallization variables [60]. Sun and Ying have demonstrated the tailoring of pore sizes between 0.5 and 2 nm employing short-chain alkylamines as supramolecular templates, *via* the "ligand-assisted templating" route [61, 62].

The morphology of the mesoporous materials obtained by Beck et al. consisted of aggregates and loose agglomerates of small particles [37, 38]. However, well-defined morphologies like fibers, thin films, spheres, monoliths *etc*. of these mesoporous materials are required for a wide range of applications such as membranes for large molecule catalysis, separation, optical sensors, slow drug release systems, templates for the assembly of nanostructures, masks for high-resolution lithography, low dielectric constant films for microelectronics and other interface-controlled processes. Huo et al. [53] and Yang et al. [63] have synthesized mesoporous silica with highly curved morphologies (toroidal, disk-like, spiral and spheroidal shapes) in acidic medium *via* the $S^+X^-I^+$ route. Mesoporous fibers (length 50–1000 μm) have been prepared in oil-in-water emulsions [64] and in aqueous phase [65] under acidic conditions ($S^+X^-I^+$). Highly oriented mesoporous free-standing films (diameter ≤10 cm, thickness ~10–500 mm) have been synthesized at the air-water [66] and oil-water [64] interfaces, on both mica [67] and the graphite [68] surfaces and by using dip- or spin-coating [69] methods. The syntheses of hollow (diameter 1–100 μm) [64] as well as hard (diameter 0.1–2 mm) [70] mesoporous silica spheres were achieved

through emulsion biphasic chemistry, whereas monolithic periodic mesoporous silica (diameter 150–500 nm, interparticle pores on the order of particle size) was prepared by different systems using ionic [71] and neutral surfactants [72]. Another morphology with vesicle like hierarchical structures, consisting of one or more undulated silica sheets (thickness 3 nm, mesopore diameter 2.7–4.0 nm) running both parallel and orthogonal to the silica sheets, was prepared by Kim et al. using neutral gemini surfactants [73].

1.7. REMOVAL OF TEMPLATE

Removal of template plays a crucial role in the preparation of mesoporous materials. Depending on the preparative method, template can be removed either by calcination [74] in air or by solvent extraction [75]. Calcination is the better method than removal by extraction techniques. This is due to the strong interaction between template and inorganic species in the case of direct pathways or mediated pathways where electrostatic interactions play a key role for the formation of meso-structure. The calcination has to be done in the flow of inert gases at the initial stages followed by the flow of air. This is due to maintain the crystallinity of the material. But extraction prefers when we need rich amount of hydroxyl groups in the catalysts [76].

1.8. SURFACE MODIFICATION OF MESOPOROUS MATERIALS

The application of pure mesoporous silicates or aluminosilicates as catalysts is rather limited because of the limitations in the nature of their active sites, leading to limited scope of the reactions they could accomplish. To utilize these mesoporous materials for several specific applications including catalysis and also sorption, ion exchange, sensing *etc.*, the introduction of reactive organic functional groups by modifying the inner surfaces of these materials, to form inorganic–organic hybrid materials, is essential [77]. The inorganic components of these inorganic–organic hybrid materials can provide mechanical, thermal or structural stability, while the organic components can introduce flexibility into the framework and can more readily

be modified for specific applications [78]. The presence of large amount of silanol groups on the surfaces of M41S materials could be exploited for anchoring of desired organic functional groups by condensation with necessary alkoxysilane precursors [79]. These parent organic functional groups, with or without further modification; can facilitate anchoring of different types of catalytically reactive metal particles or organometallic complexes inside the mesoporous network [80]. Different methods for organic modification of mesoporous surfaces will be briefly highlighted in this section.

1.8.1. Grafting Methods

Grafting refers to post synthesis modification of the inner surface of mesoporous silica, where the organic functional groups are introduced as the terminal groups of an organic monolayer [81]. The large concentration of surface silanol [$(–SiO)_3Si–OH$)] groups present in mesoporous silica can be utilized as convenient moieties for anchoring of organic functional groups [82]. The surface modification with organic functional groups is generally carried out by silylation, as depicted in Scheme 1.5.

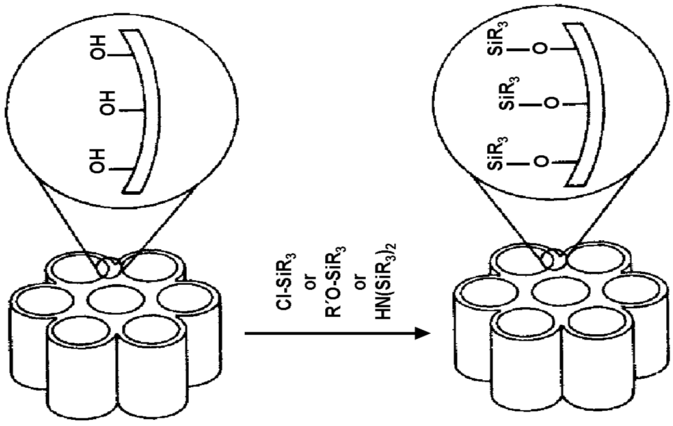

Scheme 1.5. Functionalization of inner walls of mesoporous silicates by grafting. [Source: Ref.77].

The surfactant molecules from the mesopores are usually removed either by calcination or by extraction with appropriate solvents. At typical calcinations temperatures (~500 °C) several surface silanol groups are lost after condensation of

unreacted silanol groups. However, it is necessary to maintain a large concentration of surface silanol groups after calcination, if a high coverage of organic functional groups on the surfaces is desired. This can be achieved by treatment of calcined mesoporous silica with boiling water [83] or steam [84], or by acid hydrolysis [85]. Solvent-extraction processes reduce the possibility of loss of surface silanol groups, although thermal treatments after extraction can increase the surface reactivity towards silylation.

1.8.1.1. Grafting with Passive Surface Groups

Organic functional groups with lower reactivity such as alkyl or phenyl groups could be grafted to alter the accessible pore volume of mesoporous silica, thereby enhancing the hydrophobicity of the surface and protecting towards hydrolysis. The pore diameters of ordered mesoporous materials could be adjusted by varying the alkyl chain length of the silylating agent or the quantity of the silylating agent [86]. The most commonly used surface modifying agents containing lower reactive functional groups are trimethylchlorosilane (Me_3SiCl) [87], and hexamethyldisilazane [$(Me_3Si)_2NH$] [88].

1.8.1.2. Grafting with Reactive Surface Groups

Grafting of the mesopore surfaces with reactive functional groups like olefin, cyanide, thiol, amine, halide, epoxide *etc*. permits further functionalization of the surface. Further functionalization includes hydroboration [89] and bromination [88] of olefins (vinyl groups), hydrolysis of cyanides to carboxylic acids [90], oxidation of thiols to sulfonic acids [91, 92], alkylation and nucleophilic substitution of amines [93], and nucleophilic substitution of halides [94]. After the desired modification of the reactive functional groups, a rational design for anchoring of catalytically active transition metal complexes onto mesoporous network could be made [95].

1.8.1.3. Site-Selective Grafting

For grafting of organic functional groups, the external surface of the mesoporous materials is kinetically more accessible than the internal surface and is functionalized predominantly [96]. To minimize the grafting on the external surface, it is necessary to passivate the silanol groups on the external surface before functionalizing those on the internal surface. Shephard et al. have carried out the passivation of external surface with dichlorodiphenylsilane (Ph_2SiCl_2) first, and functionalization of internal surface with 3-aminopropyltrimethoxysilane [$(MeO)_3Si(CH_2)_3NH_2$] thereafter [97]. The existence of the amine functional groups almost entirely on the internal surface was confirmed by high-resolution transmission electron microscopy (HRTEM).

In a different approach, grafting of the external surface by Me_3SiCl was carried out on the as-prepared mesoporous material without the surfactant being removed from the mesopores [98]. Grafting occurred mainly on the external surface due to steric constraint of the surfactant. After solvent extraction of the surfactant the internal surface was functionalized with the desired organic group. An alternate pathway by Antochshuk and Jaroniec describes simultaneous grafting of Me_3SiCl and extraction of surfactant template, by refluxing as-synthesized MCM-41 material with neat Me_3SiCl [99]. Since the calcination step is not required in these two processes, larger number of surface silanol groups is likely to be present inside the mesopores.

1.8.2. Co-condensation Reactions

In the grafting methods, incorporation of organic groups is done by attachment of the organosiloxane precursor with surface Si atoms through Si–O–Si–C covalent bond formation (Scheme 1.5). Then Si–O can be cleaved at some reaction conditions as experienced by Price et al. [81]. Therefore, in some cases it would be desirable to have direct formation of a C–Si (surface) covalent bond. Thus,

the "one-pot" co-condensation method, where condensation occurs between a tetraalkoxysilane and one or more trialkoxyorganosilanes through sol-gel chemistry, seems to have distinct advantages over the grafting methods (Scheme 1.6) [100]. Several research groups have employed this method to prepare inorganic–organic hybrid mesoporous materials under a wide range of synthesis conditions [89, 101-104]. Usually the solvent extraction technique is used to remove the surfactant from the resultant materials. The co-condensation reactions proceed through different pathways, which will be discussed briefly in this section.

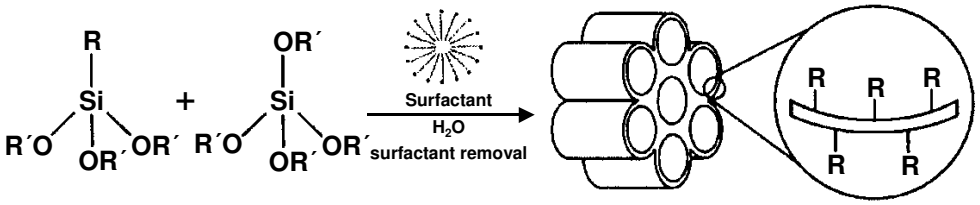

Scheme 1.6. Synthesis of organo-functionalized mesoporous silicates by co-condensation. [Source: Ref.78].

1.8.2.1. S^+I^- Pathway

This pathway refers to condensation between anionic silica precursors (I^-), obtained under basic conditions, initiated by cationic surfactant (S^+) micelles. The surfactants are normally extracted with acid-alcohol mixtures [47, 88]. It has been observed that the d_{100} spacing and the pore size of the channels are significantly reduced as the concentration of the trialkoxyorganosilanes increases, even when the same surfactant is used [96, 102]. Simultaneously, an increase in wall thickness has been observed, probably because of protrusion of organic groups into the channels. The decrease in cell dimensions may be attributed to the interaction between nonpolar organic groups and the surfactant tails, which drag the organic precursor further into the micelles. Functionalization with two or more organic groups is also possible in this pathway [105, 106]. However, the functional groups are randomly

distributed in the resultant material, and their location cannot be controlled as precisely as done by the grafting processes mentioned earlier.

1.8.2.2. $S^+X^-I^+$ Pathway

In this pathway interaction of cationic silicate precursors (I^+), obtained under acidic conditions, occurs with the S^+X^- pair, where S^+ represents cationic surfactant species and X^- denotes anions generated from the acid [104, 107, 108]. Unlike the S^+I^- pathway, a simple extraction technique using pure solvent can be used to remove the surfactant.

1.8.2.3. S^0I^0 Pathway

This mechanism deals with a weak interaction between a neutral silica precursor (I^0) and neutral surfactant micelles (S^0) [103, 109, 110]. In this case also, surfactant removal can be achieved by extraction with pure solvent. The pore volume and surface area do not vary systematically with increasing concentration of the organosilane, but smaller pore sizes have been obtained with increasing the same [110].

1.8.2.4. N^0I^0 Pathway

In this pathway, non-ionic surfactants (N^0) like alkylpoly ethyleneoxide are used as the template, and the syntheses are carried out at neutral P^H [111, 112]. Worm-like channel structures have been obtained in this method. The cell dimensions usually get reduced with higher loading of organic functional groups [111].

1.8.2.5. Inorganic–Organic Hybrids with Organic Moiety in the Framework

The co-condensation method has recently been employed to create organic–inorganic hybrid materials lacking long-range ordering and containing the organic moiety as component of the solid network [113-116]. The templates used in the syntheses of these materials consist of two trialkoxysilyl groups connected by an aliphatic chain (Scheme 1.7). Inagaki et al. have first reported the synthesis of "periodic mesoporous organosilica" (PMO) with organic functional groups uniformly

incorporated in the mesoporous walls, using 1,2-bis(trimethoxysilyl)ethane (BTME) as the framework precursor and octadecyltrimethylammonium chloride as the surfactant [113, 114]. By varying the synthesis conditions, three highly ordered mesoporous structures have been obtained: (a) a 2D hexagonal mesophase (hexagonal rod-like morphology), denoted as HMM-1; (b) a 3D hexagonal mesophase (spherical morphology), denoted as HMM-2; and (c) a cubic mesophase (decaoctahedral morphology), denoted as HMM-3.

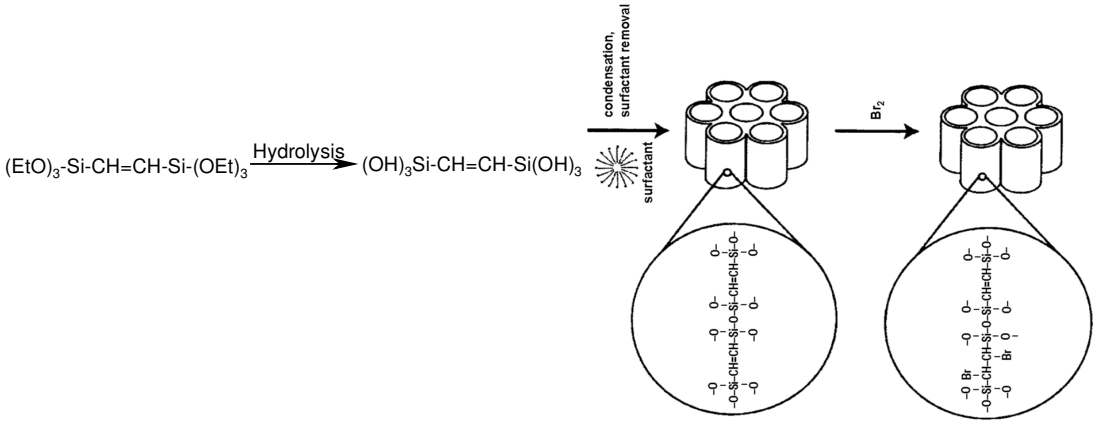

Scheme 1.7. Synthesis of mesoporous materials with reactive organic functional groups on the solid framework. [Source: Ref.77].

Asefa et al. [115] and Melde et al. [116] have studied the co-condensation of either 1,2-bis(triethoxysilyl)ethane (BTSE) or 1,2-bis(triethoxysilyl)ethylene BTSEY with silica precursors to synthesize hexagonal hybrid framework materials under basic reaction conditions. Melde et al. have designated their materials as "unified organically functionalized mesoporous networks" (UOFMN), having worm-like channel systems and lacking long-range ordering [116]. Both of the materials synthesized by Asefa et al. and Melde et al. have higher hydrothermal stability than M41S materials synthesized under identical conditions.

1.9. ORGANO-FUNCTIONALIZED MESOPOROUS MATERIALS

The mesoporous MCM-41 materials add a new dimension due to their large and variable pore diameters. Grafting of functional organosilanes by using surface hydroxyl groups as anchor points has been widely used in the field of catalysis. Important applications of these modified and functionalized systems are heterogeneous catalysis and photocatalysis involving bulky grafted catalysts and/or the conversion of large substrates. Other potential applications include ion exchange and separations, removal of heavy metals, chromatography, stabilization of quantum wires, stabilization of dyes, and polymer composites [91, 117]. The introduction of functional organic groups is usually performed through attachment of silane-coupling agents to mesoporous walls of previously synthesized and calcined materials. The functional group is either directly incorporated in the silane-coupling agent or it is grafted onto it in a second or further reaction step. Co-condensation of reactive species during the mesopores synthesis is a method to incorporate functionality into the walls of the channel system [78, 118]. Macquarrie et al. and Brunel et al. have detailed the covalent attachment of basic function such as amino group on the MCM-41 surface which can be either used as base catalysts or used as an anchor point for asymmetric ligands assembly [93, 94, 119]. Surface modification techniques are enjoying a renewed interest, and it is clear that the pore walls of mesoporous materials are easily modified with either purely inorganic or with hybrid, semi-organic functional groups and can be successfully used as catalysts for green chemistry [120, 121].

1.10. ZIRCONIA IN CATALYSIS

Over the last ten years, the zirconia used as catalyst or catalytic support has attracted much attention due to its high thermal stability, remarkable mechanical strength, easy availability, high melting point, low thermal conductivity, high corrosion resistance, amphoteric behavior and unique properties of the surface [9, 122-125].

Zirconia exhibits several crystalline modifications: monoclinic, that is thermally stable at the temperature below 1172 °C, tetragonal, stable at the temperature range 1172-2347 °C, cubic, stable above 2347 °C and rhombic, stable at a high pressure. However, tetragonal and cubic Zirconia can be prepared at low temperatures (in the range of 550-750 °C) in the form of highly dispersed metastable phase. Zirconia can be prepared by precipitation as well as sol-gel [126] method. The source may be zirconyl chloride, zirconium n-butoxide, zirconium propoxide, zirconium nitrate etc. The hydrolysis of these materials results the formation of zirconium hydroxide and the calcination leads to the zirconium oxide. The traditional precipitation technique may give rise to microcrystalline zirconia; but the sol-gel method produces nanocrystalline zirconia, which is very attractive for novel applications. The crystalline structures, concentrations, transformation between each other and catalytic properties of zirconia are generally depends upon its synthesis method and thermal treatment.

Doping of other elements will also affect the catalytic properties of zirconia. High surface area zirconia is widely used as a catalytic support or oxygen censor electrolytes in automobile exhaust emission control system. Doping of Zirconium with small amounts of rare earth elements may tailor its properties for better catalytic performance. The incorporation of redox Cu^{2+} active species into the structure of cubic [127] zirconia (Cu-ZrO_2) combined with oxygen mobility due to oxygen vacancies leads to the formation of catalyst, which are superior to either CuO or ZrO_2 or CuO supported on ZrO_2. Tungsten oxide [128] species form strong acid sites on zirconia supports (WO_x-ZrO_2) and inhibit ZrO_2 crystallite sintering and tetragonal to monoclinic structural transformation. The catalyst is active for isomerization reactions such as o-xylene isomerization [129].

Zirconia and its mixed oxides can be used as an acid-base bifunctional catalyst [126]. In this case where an acid site act as an active site in one step of a

reaction and a basic site acts as an active site in another step and is called acid-base concerted bifunctional [130] catalysis. This is due to its pronounced catalytic behavior in spite of its almost neutral surface property. The co-operation of weakly acid sites and weakly basic sites of which acid-base pair sites are suitably oriented on zirconia surface is surprisingly powerful for particular reactions and causes highly selective reactions and long catalytic life. Sulfated-zirconia and modified sulfated-zirconia form an important class of catalysts, as is evidenced from the voluminous research that has appeared in the last decade [131].

1.11. MESOPOROUS ZIRCONIA

The discovery of silica-based mesoporous materials raised an enormous interest in catalysis because of the possibility to extent the concept of shape selectivity to large molecules [37, 38]. Soon after the discovery of the MCM materials, various researchers put forward an idea of non-silica-based mesoporous oxides. Titanium[132,133], zirconium [134-147], niobium [148], tantalum [149], aluminum [150], hafnium [151], tin [152], and manganese [153] have been synthesized using ionic or neutral templates as structure directing agents, although most of them were comprised of mainly non-porous framework walls, which would limit their thermal and hydrothermal stability and greatly compromise their usefulness in catalytic application. Stucky et al. then synthesized mesoporous metal oxides with a semi crystalline framework by block copolymer templating materials [154].

Hudson and Knowels [134, Scheme 1.8], first achieved the synthesis of zirconium-based mesoporous materials by cationic surfactant adopting the scaffolding mechanism, where the preparation of mesoporous zirconium (IV) oxide samples was obtained by surfactant exchanged hydrous zirconium (IV) oxide. The proposed scaffolding mechanism by the authors is given in scheme 1.8. Ciesla et al. [135, 136] studied the formation of porous zirconium oxo phosphate by a surfactant-assisted synthesis, where they used two different syntheses leading to zirconia

compounds with high surface areas and regular pore systems, in which either zirconium sulfate or zirconium propoxide is used as zirconia source with cationic surfactant to obtain sulfate containing material. Blin et al. [137] synthesized the mesoporous zirconia using cationic surfactant with zirconyl chloride as zirconia source and studied the kinetics of synthesis mechanism.

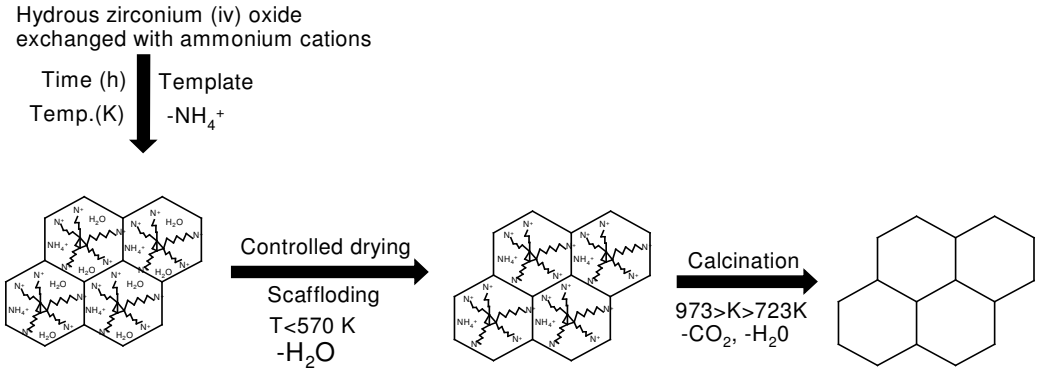

Scheme 1.8. Synthesis of mesoporous zirconia using zirconium (IV) oxide with cationic surfactant via scaffolding mechanism [Source. Ref.134].

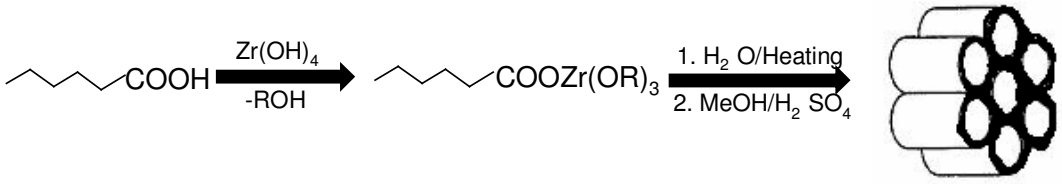

Scheme 1.9. Synthetic strategy for mesoporous zirconia. In the first step the metal alkoxide is combined with the carboxylic acid prior to addition of water. After addition of water and aging from ambient to 150 ℃ over several days the mesostructure is obtained. [Source: Ref.139].

Ulagappan et al. [138] reported the preparation of lamellar and hexagonal forms of mesoporous zirconia by the neutral amine route. They further reported that they found the lamellar form of mesoporous zirconia turned in to hexagonal form upon removal of template. Antonelli [139] reported the synthesis and mechanistic studies of sulfated mesoporous zirconia with chelating carboxylate surfactants where he used long chain acid as surfactant (Scheme 1.9). Reddy and Sayari [140] studied

the formation of nanoporous zirconium oxide using cationic template at acidic pH via supramolecular templating approach. Zhao et al. [141] reported metal doped mesoporous zirconia using anionic surfactants with various Al/Zr ratios. Pacheco et al. [142] studied the formation of mesoporous zirconia from anionic and neutral surfactants.

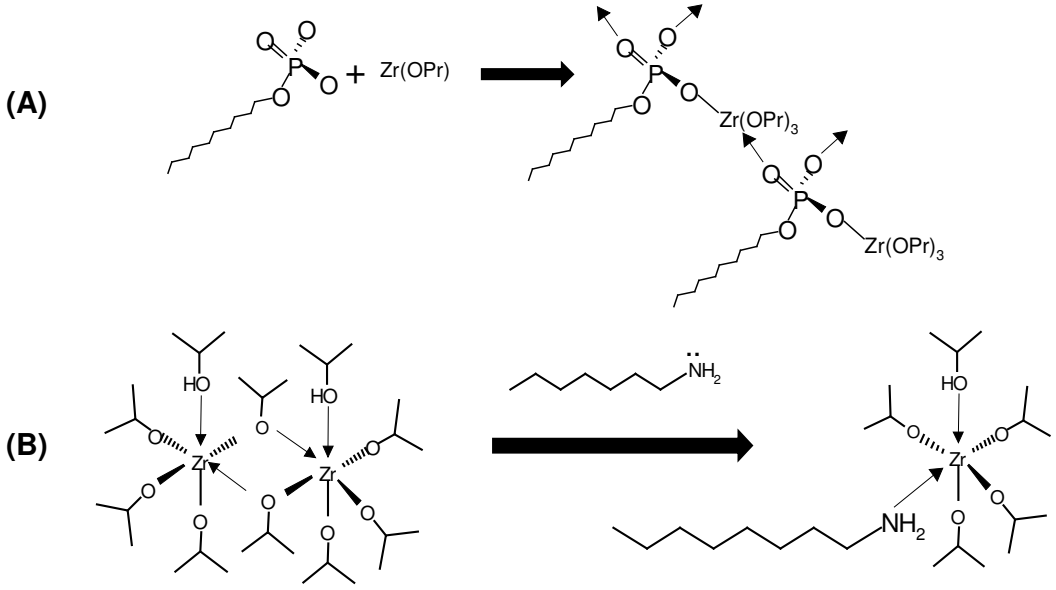

Scheme 1.10. Representative schematic drawings of (A) the anionic amphiphile-zirconium n-propoxide interaction, and (B) the nonionic amphiphile-zirconium isopropoxide interaction. [Source: Ref. 143].

Wong and Ying [143] reported the extensive study of mesostructured zirconium oxide via amphiphilic templating mechanism with a variety of headgroups (anionic and nonionic) and tail group chain lengths (1-18 carbons). They claimed the mesoporous material based on zirconia as Zr-TMS (zirconium oxide with a mesostructured framework) and in this thesis the same name is used. They further proposed two types of interaction between the surfactants and zirconium source (Scheme 1.10). Huang et al. [144] demonstrated synthesis of mesoporous sulfated zirconium dioxide with partially tetragonal wall structure and successfully tested in n-

butane isomerization and alkylation of 1-naphthol reactions. Chen et al. [145] studied the metal oxide containing ordered porous zirconium oxide. McIntosh and Kydd [146] studied the tailoring of pore size of mesoporous sulfated zirconia via liquid crystal templating mechanism using neutral template. Synthesis of mesoporous sulfated zirconium dioxide by surfactant-assisted mechanism by Larsen et al. [147], are attracting increased interest in the use of zirconia as a catalyst support. Great effort has been made to prepare mesoporous zirconium hydroxide with high surface area via a surfactant templating route. Further, Zirconia based mixed oxides are of great importance due to their multiple applications, including catalysis and solid-oxide fuel cells [155]. Many heterogeneous catalysts are less active for fast reactions than the corresponding homogeneous catalysts because the reaction rates are limited by the transport of reactant to the active sites on the particle surface. The rate of a reaction that is limited only by mass transfer is directly proportional to the particle surface area [156]. The best approach to get highly active heterogeneous catalysts is to use porous supports such as mesoporous silica or mesoporous metal oxides. Porous zirconia is attracting increasing interest on account of its use as a catalyst support or membrane partially because it is chemically more stable. Usually it has been prepared through a template-assisted mechanism. After the formation of pore structure, the template will be removed by extraction or calcination at 550 °C. If the temperature is going above 600 °C zirconia starts to transform from the metastable (tetragonal) phase to the stable monoclinic phase. This phase transformation is accompanied by a dramatic change in pore structure of zirconia. At temperatures lower than phase transformation temperature, the pore structure of zirconia also changes, but to a lesser extent, as a result of sintering and grain growth. Metal oxides like yttria, ceria, magnesia or lanthana can stabilize the tetragonal phase through doping. It is further known that the catalytic efficiency of metal oxides can be

improved by doping the metal oxide with a metal [157] and functionalizing the acidic organo-species over support materials [158].

Transition metal oxides are widely used as industrial catalysts and as catalysts supports. Unfortunately they usually have poorly defined pore structures. The synthesis of mesoporous silica partially substituted by titanium and zirconium has been attempted to circumvent the difficulty of preparing stable mesoporous titania and zirconia. Zirconium oxide is of particular interest because it contains both acidic and basic surface sites. Further, we have chosen zirconium as the metal species because it has only one stable oxidation state and exhibit pronounced polyoxo ion chemistry in aqueous solutions [159]. These are critical for some reactions that need bifunctional catalysts. The search for zirconium oxide as supports for various catalysts has received keen interest in the past decade. In the recent years SO_4^{2-}/ZrO_2 has attracted attention as it catalyzes various industrially important reactions such as: isomerization; condensation; Friedel-Crafts acylation reactions; etc [131]. However, its non-uniform pore size, low porosity, and small surface area limit its potential application for catalyzing reactions of bulky molecules. Despite these limitations zirconia has a high melting point, low thermal conductivity, high corrosion resistance, and amphoteric behavior, all of which can be useful properties for a support material. Parvulescu et al. studied extensively the synthesis of mesoporous zirconium oxide using cationic surfactant and claimed that the synthesis occurred via a scaffolding mechanism [160]. The possibility of obtaining such material with a mesoporous texture has made this oxide even more interesting.

1.12. PHYSICO-CHEMICAL CHARACTERIZATION

Characterization of the catalysts and catalysis process by means of analytical techniques is far most important to know about the properties of the catalysts. By proper characterization studies, it is possible to propose models of the systems and according to the needs one can design the properties of the system associated with

structural or functional modules. Table 1.3 shows characterization techniques frequently utilized to determine the structure and composition of catalysts.

Table 1.3. Physico-chemical characterization techniques, basis and information.

Analysis method	Physical basis	Information
Infra red spectroscopy (FT-IR)	Vibrational excitation of surface atoms by adsorption of infrared radiation	Structure and bonding of adsorbates
X-ray diffraction (XRD)	Monochromatic beam of X-rays of wavelength λ, incident on a sample made of small crystallites, will be diffracted by sets of planes of high atomic concentrations.	Crystallinity of the samples, unit cell parameter, particle size, composition, etc.,
X-ray photoelectron spectroscopy (XPS)	Energy distribution of electrons that are emitted from the catalyst due to photoelectric effect	Composition at the surface, valency and binding energy of an atom.
Electron microscope (TEM, SEM)	Interaction of electron with matter	Morphology, particle size and compositions.
Thermogravimetry analysis (TGA/DTA)	Change in weight of a system under examination as the temperature is increased at a predetermined and preferably at a linear rate/Measuring of thermal effects associated with physical and chemical changes by a differential method	Determination of compositions of complex mixture, purity and thermal stability associated with physical/ chemical changes with respect to temperature.
Adsorption/desorption of gases at low temperature	Adsorptions of gaseous molecules or liquids at lower temperature and high pressure and desorption of the same at decreased pressure.	Surface area pore size distribution and pore volume of solid materials.
Atomic absorption spectroscopy (AAS)	Measurement of intensities of the emission forms the basis of quantitative determinations	Presence/absence of metals/metalloids.
FT-Raman	Frequency of the light scattered by molecules as they undergo rotations and vibrations.	Determining the organic/inorganic functional molecules/groups/atom

Temperature programmed adsorption/desorption (TPD)	Adsorption of base over the acid sites and desorption of the same at elevated temperatures.	Nature of acid sites and acid strength.
Chemical characterization of functional groups (NMR)	Change in the direction of nuclear spin quantum number in the presence of strong magnetic field.	Structural determination by means of coupling, decoupling, co-ordination position of an atom/element

1.13. REACTIONS OF INTEREST

1.13.1. Acylation Reaction

Friedel-Crafts acylation reactions are widely used in the manufacture of arylketones, which are of interest in the synthesis of a large number of fine chemicals such as drugs, fragrances, dyes, and pesticides [161]. This process has been carried out in industry by working under batch conditions using acyl halides as acylating agent and homogeneous Lewis acids such as anhydrous metal halides ($FeCl_3$, $FeBr_3$, $SbCl_5$, $TiCl_4$, $ZrCl_4$) as catalyst [162]. Conventionally, in the Friedel-Crafts ketone synthesis, homogeneous Lewis acid catalysts such as $AlCl_3$, BF_3 and HF have been used. However Lewis acids must be used in higher than stoichiometric amounts and the catalyst must be destroyed at the end of the reaction with a significant production of undesirable wastes [163]. In order to overcome all these difficulties of Lewis acid catalysts, several other acid catalysts such as iron sulfate [164], iron oxide [165], heteropoly acids [166], trifluromethanesulfonic acids [167] have been used as alternate catalysts. Various metal salts supported on zeolites and clays have also been reported for Friedel-Crafts reactions [168]. Besides, the use of solid acids, zeolites enable one to use beneficially their shape selective properties (molecular sieving mechanism) to obtain the desired products.

1.13.2. Esterification Reaction

Monoglycerides (MG), which are produced by esterification of glycerol with fatty acid, are very important chemicals from industrial point of view. Monoglycerides posses a hydrophilic head and a hydrophobic tail due to which they act as detergent. Due to this property they are widely used as emulsifier in food, pharmaceutical and cosmetic industries. They can be used in low calorie margarines as they increase skin permeability and they have been considered to use in low calorie margarines. There are two major industrial routes to monoglycerides [169, 170]. First they are manufactured by glycerolysis i.e. a base catalyzed transesterification of triglycerides with glycerol at elevated temperature approximately (528K). Second monoglycerides may be produced by a direct single esterification of glycerol with fatty acid.

Direct esterification of glycerol with fatty acid requires high temperature so that the mutual solubility of immiscible reactant phase's increase but it causes loss of selectivity. In order to lower the temperature of process an acid catalyst is required eg. H_2SO_4, phosphoric acid or organic sulfonic acids. The use of zeolite USY gives high monoglycerides selectivity but their activity is low because of the limited acidity [171, 172]. At this point mesoporous materials gain importance, which are more easily accessible for large reactant molecules like fatty acids and their esters. The best mesoporous sulfonic catalyst offers a unique combination of high selectivity and activity, which is not obtained with homogeneous or traditional heterogeneous catalyst [173].

1.13.3. Acetalization Reaction

The acetalization reaction is required to protect carbonyl groups in presence of other functional groups when processing multifunctional organic molecules [175]. Besides the interest in acetals as protecting groups, many of them have found direct application as fragrances, in cosmetics, as food and beverage additives, in pharmaceuticals, in detergents, and in lacquer industries [175].

Acetalization of ketones needs stronger acidic conditions provided by strong acid catalyst. But due to the drawbacks of homogeneous catalysts we can not use H_2SO_4, HCl or p-toluene sulfonic acids. Thus solid acid catalysts are required for the reaction. Zeolites and mesoporous materials are successfully used in the preparation of fructone, a flavoring material with apple scent. It is produced by the acetalization of ethylacetoacetate (EAA) with ethylene glycol (EG). Zeolite-β, ZSM 5 and USY are used successfully in this process [176].

1.13.4. Condensation Reaction

A condensation reaction (also known as a dehydration reaction) is a chemical reaction in which two molecules or moieties react with each other with the concurrent loss of water or ammonia [177]. It may be considered as the opposite of a hydrolysis reaction, i.e., the cleavage of a chemical entity into two parts by the action of water. A condensation reaction proceeds in two steps: 1 Nucleophilic addition, 2. Elimination.

This type of reaction is used as a basis for making of many important polymers for example: in the rubber industry as a curative for neoprene [178], polyurethane [179] and various epoxies [180]. It is also the basis for the laboratory formation of silicates and polyphosphates. The reactions that form acid anhydrides from their constituent acids are typically condensation reactions.

1.14. LITERATURE SURVEY

1.14.1. Mesoporous zirconia:

1. Preparation and characterisation of mesoporous, high surface area zirconium (iv) oxides. J.A. Knowles, M.J. Hudson, *J. Chem. Soc., Chem. Commun. (1995) 2083.*
2. Formation of a porous zirconium oxo phosphate with a high surface area by a surfactant-assisted synthesis. U. Ciesla, S. Schacht, G.D. Stucky, K.K. Unger, F. Schuth. *Angew. Chem. Int. Ed. Engl.* 35 (1996) 541.

3. Preparation of lamellar and hexagonal forms of mesoporous silica and zirconia by the neutral amine route: lamellar–hexagonal transformation in the solid state. N. Ulagappan, V.N. Raju, C.N.R. Rao, *Chem. Commun. (1996) 2243.*
4. Highly ordered porous zirconia from surfactant-controlled syntheses: Zirconium oxide-sulfate and zirconium oxo phosphate. U. Ciesla, M. Froba, G.D. Stucky, F. Schuth. *Chem. Matet. 11 (1999) 227.*
5. Synthesis and mechanistic studies of sulfated meso- and microporous zirconias with chelating carboxylate surfactants. D.M. Antonelli. *Adv. Mater. 11 (1999) 487.*

1.14.2. Organo functionalization over mesoporous material:

1. An ordered mesoporous organosilica hybrid material with a crystal-like wall structure. S. Inagaki, S. Guan, T. Ohsuna, O. Terasaki, *Nature 416 (2002) 304.*
2. Synthesis of large-pore phenylene-bridged mesoporous organosilica using triblock copolymer surfactant. Y. Goto, S. Inagaki. *Chem. Commun. (2002) 2410.*
3. Ordered benzene-silica hybrids with molecular-scale periodicity in the walls and different pore sizes. N. Bion, P. Ferreira, A. Valente, I.S. Goncalves, J. Rocha. *J. Mater. Chem. 13 (2003) 1910.*
4. Novel mesoporous materials with a uniform distribution of organic groups and inorganic oxide in their frameworks. S. Inagaki, S. Guan, Y. Fukushima, T. Ohsuna and O. Terasaki, *J. Am. Chem. Soc., 121 (1999) 9611.*
5. Periodic mesoporous organosilicas with organic groups inside the channel walls. T. Asefa, M. J. Mac Lachlan, N. Coombs, G. A. Ozin, *Nature, 402 (1999)867.*

6. Periodic mesoporous organosilicas, PMOs: Fusion of organic and inorganic chemistry 'inside' the channel walls of hexagonal mesoporous silica. C.Y. Ishii, T. Asefa, N. Coombs, M.J. Mac Lachlan, G.A. Ozin. *Chem. Commun. (1999) 2539.*
7. A versatile ruthenium catalyst for the tetrahydropyranylation of alcohols and phenols. S. Ma, L.M. Venanzi, *Tetrahedron Lett. 34 (1993) 5269.*
8. Solid superacid, silica-supported polytrifluoromethanesulfosiloxane catalyzed Friedel–Crafts benzylation of benzene and substituted benzenes. D.Q. Zhou, J.H. Yang, G.M. Dong, M.Y. Huang, Y.Y. Jiang. *J. Mol. Catal. A: Chem.* 159 (2000) 85.
9. Silica-embedded *tert*-butyldimethylsilyltrifluoromethanesulfonate catalysts as new solid acid catalysts. A.N. Parvulescu, B.C. Gagea, M. Alifanti, V. Parvulescu, V.I. Parvulescu, S. Nae, A. Razus, G. Poncelet, P. Grange;. *J. Catal.* 202 (2001) 319.
10. Novel heterogeneous zinc triflate catalysts for the rearrangement of α–pinene oxide. K. Wilson, A. Renson, J.H. Clark. *Catal. Lett.* 61 (1999) 51.
11. Trifluoromethanesulfonic acid and derivatives. R.D. Howells, J.D. Mc. Cown. *Chem. Rev.* 77 (1977) 69.
12. Noncoagulating surfaces. R.H. Krahnke. *U.S. Patent, US3508959 (1970).*
13. Solfonato-organosilanol compounds and aqueous solutions. B.R. Beck, F.T. Sher, G.V.D. Tiers. *U.S. Patent, US4235638 (1980).*

1.15. OBJECTIVES AND SCOPES OF THE THESIS

The surface modification of M41S type mesoporous materials by reactive organic functional groups allows the preparation of multifunctional molecular sieves with desired catalytic properties [77]. The mesoporosity and very high surface area of

these surface-functionalized mesoporous materials can be exploited for the immobilization of different catalytically reactive species [80].

The present work aims at the design and development of mesoporous solid catalysts for selective acylation, acetalization, condensation, and esterification reactions. In the first phase, zirconium based mesoporous molecular sieves (Zr-TMS) will be synthesized by adopting suitable templating route to get high surface area with narrow pore size distributions. Further, the surface modification of Zr-TMS shall be done using various organic and organosilane compounds, such as benzylsulfonic acid (BSA), trifluromethanesulfonic acid (TFA) and organosilanolsulfonic acid (OSA) by post synthetic route to develop new class of highly acidic mesoporous catalysts. In the second phase, the characterization of all synthesized catalysts will be done by various physico-chemical techniques. In the third phase, the catalytic activity will be studied in acylation, acetalization, condensation and esterification reactions. Most of the reactions in organic synthesis and numerous industrial processes are still running with hazardous, homogeneous catalysts, which are non-recommendable. The development of new catalytic process using solid catalysts is becoming increasingly interest. With the ever growing environmental and economic concerns, the present study comprises the following: Design and development of benzylsulfonic acid containing mesoporous zirconia (Zr-TMS-BSA) catalysts for acylation of aromatics with an acylating agent and solvent free condensation of heterocyclic and aromatic molecule using a condensation agent, triflic acid containing mesoporous zirconia (Zr-TMS-TFA) catalysts for selective acylation of deactivated and hindered bulky aromatic molecule, acetalization of ethylacetoacetate, and organosilanolsulfonic acid containing mesoporous zirconia (Zr-TMS-OSA) catalysts for esterification of alcohol and solvent free condensation reaction of aromatics.

The following objectives have been set for the present study:

i. Synthesis of Zr-TMS by using various zirconium precursors and structure directing agents and successful removal of template without mesoporous structure collapse with enriched hydroxyl groups for functionalization will be discussed.

ii. The successful functionalization of BSA over Zr-TMS (Zr-TMS-BSA) and their characterization to confirm the functionalized sulphonic acid group in the benzyl ring.

iii. Another successful functionalization of TFA over Zr-TMS to get Zr-TMS-TFA will be done by post synthesis method and their complete characterization to confirm the successful anchoring of organic moiety over inorganic support will be explained.

iv. Yet another functionalization of OSA over Zr-TMS (Zr-TMS-OSA) and their characterization to confirm the functionalized organosilanolsulphonic acid group.

v. Further, functionalization of BSA over amorphous zirconia (A-Zr-BSA), TFA over amorphous zirconia (A-Zr-TFA) and OSA over amorphous zirconia (A-Zr-OSA) will be discussed for comparison with the functionalized mesoporous materials.

vi. Characterization of all the developed catalysts by powder XRD, atomic absorption spectroscopy, Nitrogen sorption, FT-IR, FT-Raman, ^{29}Si, ^{13}C CP/DD MAS NMR, TPD of ammonia, scanning electron microscopy, transmission electron microscopy, X-ray photoelectron spectroscopy, thermal analysis will be demonstrated to understand the physicochemical aspects of the functionalized organic moieties over zirconia support.

vii. The catalytic applications of functionalized catalysts will be discussed in shape selective acylation of diphenyl ether with benzoyl chloride,

condensation of 2-methylfuran with acetone using benzylsulfonic acid functionalized catalysts; shape selective benzoylation of biphenyl with benzoyl chloride, acetalization of ethylacetoacetate with ethylene glycol using triflic acid functionalized catalysts; and esterification of glycerol with lauric acid, condensation of aniline with para-formaldehyde using organosilanolsulfonic acid functionalized catalysts will be discussed.

viii. Further, the catalysts optimization study will be discussed in benzoylation of toluene with p-toluoyl chloride and condensation of anisole with p-formaldehyde reactions.

ix. Finally the stability and utility of the all catalysts shall be achieved by screening all catalysts in various recycling studies.

1.16. OUTLINE OF THE THESIS

The present work has been sequentially placed under six chapters for a thesis entitled “Organo functionalized Zr-TMS catalysts: Synthesis, characterization and their applications in environmentally benign organic transformations” as follows:

Chapter 1: Introduction and literature survey

This chapter presents an over view of various physical and chemical aspects of mesoporous molecular sieve materials, precisely transition metal oxide based mesoporous materials, more particularly zirconia. The different characteristic properties of these materials include shape selectivity, formation mechanisms, acidity etc., have been discussed. Detailed literature surveys over synthesis aspects, characterization techniques, and different catalytic applications have been given. The scopes and objectives of the present work are also outlined at the end of this chapter.

Chapter 2: Synthesis methodologies and characterization techniques

This chapter briefly gives an account about the general synthesis procedures of mesoporous zirconia (Zr-TMS) material, functionalization of benzylsulfonic acid over Zr-TMS (Zr-TMS-BSA) material, triflic acid over Zr-TMS (Zr-TMS-TFA) material, and organosilanolsulfonic acid over Zr-TMS (Zr-TMS-OSA) material and some amorphous functionalized materials such as A-Zr-BSA, A-Zr-TFA and A-Zr-OSA are also described. Further, the complete general physicochemical characterization techniques such as powder X-ray diffraction (XRD), atomic absorption spectroscopy (AAS), nitrogen sorption technique, FT-IR spectroscopy, FT-Raman spectroscopy, X-ray photoelectron spectroscopy (XPS), elemental analysis, temperature programmed desorption (TPD) of ammonia, solid state ^{29}Si and ^{13}C CP/DD MAS NMR (cross polarization/dipolar decoupled magic angle spinning nuclear magnetic resonance) spectroscopy, scanning electron microscopy (SEM), transmission electron microscopy (TEM), and thermo gravimetric analysis (TG-DTA) and their general principles have also been discussed. The chemical reactions such as acylation, condensation, acetalization, esterification reaction and the basic principles of product analytical tools, such as gas chromatography (GC) gas chromatography/mass spectrometry (GC/MS) and liquid state nuclear magnetic resonance (NMR) have also been discussed.

Chapter 3: Benzylsulfonic acid functionalized mesoporous zirconia (Zr-TMS-BSA) catalysts

This chapter deals the synthesis of benzylsulfonic acid functionalized mesoporous zirconia via covalent route by post synthetic procedure. The functionalization of benzyl alcohol and further with chlorosulfonic acid over Zr-TMS-BS (Zr-TMS-BSA) and an amorphous functionalized catalyst (10 wt % BSA loaded Zr-TMS, A-Zr-BSA-10) are discussed. The catalysts characterization by XRD, surface area measurements, FT-IR spectroscopy, elemental analysis; TPD of

ammonia, SEM and TEM are also discussed. Further, the catalytic application in liquid phase benzoylation of diphenyl ether with benzoyl chloride, and liquid phase condensation of 2-methylfuran with acetone have been discussed. Furthermore, the liquid phase condensation of anisole with *p*-formaldehyde is briefly explained as catalysts optimization study. Catalysts recycles studies are also described in 2-methylfuran and anisole condensation reactions.

Chapter 4: Triflic acid functionalized mesoporous zirconia (Zr-TMS-TFA) catalysts

This chapter describes the synthesis of triflic acid functionalized mesoporous zirconia (Zr-TMS-TFA) and amorphous triflic acid functionalized zirconia (A-Zr-TFA) via covalent bond formation mechanism. Further, the characterization of mesoporous materials synthesized during this investigation by XRD, nitrogen sorption technique, FT-IR spectroscopy, FT-Raman spectroscopy, elemental analysis, TPD of ammonia, solid state ^{13}C CP and DD/MAS NMR spectroscopy, SEM, TEM, and thermo gravimetric analysis are also explained. Then the catalytic application of the catalysts has been discussed in liquid phase benzoylation of biphenyl with benzoyl chloride and in liquid phase acetalization of ethylacetoacetate with ethylene glycol reactions. Furthermore, the catalytic reaction parameters, such as, activity of various catalysts, duration of run, influence of catalyst/acylation agent, reaction temperature, influence of molar ratios of reactants have also been demonstrated in the liquid phase benzoylation of toluene with *p*-toluoyl chloride as catalysts optimization study. Catalysts recycles studies are also discussed in ethylacetoacetate acetalization and toluene benzoylation reactions.

Chapter 5: Organosilanolsulfonic acid functionalized mesoporous zirconia (Zr-TMS-OSA) catalysts

This chapter gives an account of synthesis of organosilanolsulfonic acid functionalized mesoporous zirconia (Zr-TMS-OSA) and an amorphous OSA

functionalized (A-Zr-OSA-20) zirconia catalyst via bottom up route by post synthetic procedure. The characterization of catalysts by powder XRD, atomic absorption spectroscopy, nitrogen sorption technique, FT-IR spectroscopy, FT-Raman spectroscopy, elemental analysis, TPD of ammonia, solid state ^{29}Si and ^{13}C CP/MAS NMR spectroscopy, scanning electron microscopy, transmission electron microscopy, and thermo gravimetric analysis have been briefly discussed. Further, the catalytic applications of the catalysts have been explained in the liquid phase esterification of glycerol with lauric acid and liquid phase condensation of aniline with para-HCHO. Catalyst recycle study is also described in glycerol esterification reaction.

Chapter 6: Summary and conclusions

The summary and conclusions of the present work are drawn in this chapter. The arrival at the earlier set scope and objectives of thesis have also been discussed.

1.17. REFERENCES

1. G. Ertl, H. Knozinger, J. Weitkamp, *Handbook of Heterogeneous Catalysis,* Willey-VCH, Weinheim **1997**.
2. J.M. Thomas, *Principles and Practice of Heterogeneous Catalysis,* VCH, Weinheim, **1997**.
3. G. Parshall, S.D. Ittel, *Homogeneous Catalysis: The Applications and Chemistry of Soluble Transition-Metal Complexes*, 2nd Ed. John Wiley & Sons, New York, **1992.**
4. B.C. Gates, *Catalytic Chemistry,* John Wiley & Sons, New York, **1992**, 310.
5. E. Santaniello, P. Ferraboschi, P. Grisenti, A. Manzocchi, *Chem. Rev.,* 92, **1992**, 1071.
6. P.B.Venuto, P. S. Landis, *Adv. Catal.,* 18, **1968**, 259.
7. P.B. Venuto, *Micropor. Mater.,* 2, **1994,** 297.

8. K. Tanabe, W.F. Hoelderich, *Appl. Catal. A: Gen.*, 181, **1999,** 399.
9. A. Corma, *Chem. Rev.,* 95, **1995,** 559; 97, **1997** 2373.
10. N. Mizuno, M. Misono, *Chem. Rev.,* 98, **1998**, 199.
11. A. Corma, A. Martinez, *Catal. Rev. Sci. Eng.,* 35, **1993**, 483.
12. K. Gaare, D. Akporiaye*, J. Mol. Catal.,* 49, **1989**, 109.
13. E. Houdry, A. Joseph, *Bull. Assoc. Fr. Tech. Pet.,* 117, **1956**, 177.
14. M.M. Mestdagh, E.E.W. Stone, J.J. Fripiat, *J. Chem. Soc., Farad. Trans., I.* 72, **1976**, 154.
15. A. Baranski, S. Ceckiewicz, *J. Chem. Soc., Farad. Trans., I.* 74, **1978**, 146.
16. R. Beamont, D. Barthomeuf, *J. Catal.,* 26, **1972**, 218.
17. H.G. Karge, *Stud. Surf. Sci. Catal.,* 65, **1991**, 133.
18. R.S. Hansford, *Ind. Eng. Chem.,* 39, **1947,** 849.
19. D. Barthomeuf, *Mat. Chem. Phys.,* 17, **1987**, 49.
20. W.M. Meir, D.H. Olson, C. Baerlocher, *Atlas of Zeolite Structure types,* 4th Ed. Elsevier, London. **1996**.
21. A. Redondo, P.J. Hay, *J. Phys. Chem.,* 97, **1993**, 11754.
22. R.A. van Santen, G.J. Kramer, W.P.J.H. Jacobs, *Theory of Brönsted acidity in zeolites.* In: R.W. Joyner, R.A. van Santen (Ed) *Elementary reaction steps in heterogeneous catalysis,* Kluwer Academic Publishers, **1993**, 113.
23. K. Tanabe, T. Yamaguchi, K. Akiyama, A. Mitoh, K. Awabuchi, K. Isogai, *Proc. 8th Inter. Cong. Catal.,* 6 **1984**, 601, Verlag Chemie, Berlin.
24. K. Arata, M. Hino, *Bull. Chem. Soc. Jpn.,* 53, **1980**, 446.
25. K. Tanabe, T.Yamaguchi, *Successful design of catalysts,* Ed. T. Inui, Elsevier Science Publishers, Amsterdam, Vol. 44, **1989**.
26. M. Hino, S. Kobayshi, K. Arata, *J. Am. Chem. Soc.,* 101, **1979**, 6439.
27. M. Hino, K. Arata, *J. Chem. Soc., Chem. Commun.,* **1979**, 1148.
28. K. Iida S. Nojima, *Jpn. Patent,* 62169769, **1987**.

29. T. Jin, T. Yamaguchi, K. Tanabe, *J. Phys. Chem.,* 90, **1986**, 4794.

30. T. Yamaguchi, T. Jin, K. Tanabe, *J. Phys. Chem.,* 90, **1986**, 3148.

31. Y. Nagase, T. Jin, H. Hattori, T. Yamaguchi, K. Tanabe, *Bull. Chem. Soc. Jpn.,* 58, **1985**, 916.

32. T. Kimura, *Micropor. Mesopor. Mater.,* 77, **2005**, 97.

33. U. Schuchardt, D. Cardoso, R. Sercheli, R. Pereira, R.S. da Cruz, M.C. Guerreiro, D. Mandelli, E.V. Spinace, E.L. Pires, *Appl. Catal. A: Gen.,* 211, **2001**, 1.

34. A.K. Sinha, S. Sainkar, S. Sivasanker, *Micropor. Mesopor. Mater.,* 31, **1999**, 321.

35. A.K. Sinha, S. Sivasanker, *Catal. Today,* 49, **1999**, 293.

36. N. Venkatathri, S.G. Hedge, V. Ramaswamy, S. Sivasanker, *Micropor. Mesopor. Mater.,* 23, **1998**, 277.

37. C.T. Kresge, M.E. Leonowicz, W.J. Roth, J.C. Vartulli, J.S. Beck, *Nature,* 359 **1992**, 710.

38. J.S. Beck, J.C. Vartulli, W.J. Roth, M.E. Leonowicz, C.T. Kresge, K.D. Schmitt, C.T.W. Chu, D.H. Olson, E.W. Sheppard, S.B. McCullen, J.B. Higgins, J.L. Schlenker, *J. Am. Chem. Soc.,* 114, **1992**, 10834.

39. J.C. Vartulli, K.D. Schmitt, C.T. Kresge, W.J. Roth, M.E. Leonowicz, S.B. McCullen, S.D. Hellring, J.S. Beck, J.L. Schlenker, D.H. Olson, E.W. Sheppard, *Chem. Mater.,* 6, **1994**, 2317.

40. M. Dubois, Th. Gulik-krzywicki, B. Cabane, *Langmuir,* 9, **1993**, 673.

41. G.A. Ozin, C. Gil, *Chem. Rev.,* 89, **1989**, 1749.

42. M.E. Davis, R.F. Loba, *Chem. Mater.,* 4, **1992**, 756.

43. X.S. Zhao, G. Q. Lu, G. J. Millar, *Ind. Eng. Chem. Res.,* 35, **1996**, 2075.

44. A. Corma, A. Martinez, *Adv. Mater.*, 7, **1995**, 137.

45. C. Huber, K. Moller, T. Bein, *J. Chem. Soc., Chem. Commun.*, **1994**, 2619.

46. C. F. Cheng, H. He, W. Zhou, J. Klinowski, *Chem. Phys. Lett.,* 244, **1995**, 117.

47. C-Y. Chen, S.L. Burkett, H-X. Li, M.E. Davis, *Micropor. Mater.*, 2, **1993**, 27.

48. A. Monnier, F. Schuth, Q. Huo, D. Kumar, D.I. Margolese, R.S. Maxwell, G.D. Stucky, M. Krishnamurthy, P. Petroff, A. Firouzi, M. Janicke, B.F. Chmelka, *Science*, 261, **1993**, 1299.

49. G.D. Stucky, A. Monnier, F. Schuth, Q. Huo, D.I. Margolese, D. Kumar, R.S. Maxwell, M. Krishnamurthy, P. Petroff, A. Firouzi, M. Janicke, B.F. Chmelka, *Mol. Cryst. Liq. Cryst.*, 240, **1994**, 187.

50. S. Inagaki, Y. Fukushima, K. Kuroda, *J. Chem. Soc., Chem. Commun.*, **1993**, 680.

51. A. Firouzi, D. Kumar, L. M. Bull, T. Besier, P. Sieger, Q. Huo, S. A. Walker, J. A. Zasadzinski, C. Glinka, J. Nicol, D. I. Margolese, G. D. Stucky, B. F. Chmelka, *Science*, 267, **1995**, 1138.

52. A. Firouzi, F. Atef, A. G. Oertli, G. D. Stucky, B. F. Chmelka, *J. Am. Chem. Soc.,* 119, **1997**, 3596.

53. Q. Huo, D.I. Margolese, U. Ciesla, P. Feng, P. Sieger, R. Leon, P. Petroff, F. Schuth, G.D. Stucky, *Nature*, 368, **1994**, 317.

54. Q. Huo, D.I. Margolese, U. Ciesla, D.G. Demuth, P. Feng, T.E. Gier, P. Sieger, A. Firouzi, B.F. Chmelka, G.D. Stucky, *Chem. Mater.*, 6, **1994**, 1176.

55. P. T. Tanev, T. J. Pinnavaia. *Science,* 267, **1995**, 865.

56. P.T. Tanev, T.J. Pinnavaia, *Chem. Mater.*, 8, **1996**, 2068.

57. P.T. Tanev, T.J. Pinnavaia, *Science,* 271, **1996**, 1267.

58. C.G. Wu, T. Bein, *J. Chem. Soc., Chem. Commun.*, **1995**, 925.

59. N. Ulagappan, C.N.R. Rao, *Chem. Commun.*, **1996**, 2759.

60. D. Khushalani, A. Kuperman, G. A. Ozin, K. Tanaka, J. Garces, M. M. Olken, A. Kuperman, *Adv. Mater.*, 7, **1996**, 842.

61. D. M. Antonelli, J. Y. Ying, *Angew. Chem. Int. Ed.*, 35, **1996**, 426.

62. T. Sun, J. Y. Ying, *Nature,* 389, **1997**, 704.

63. H. Yang, N. Coombs, G. A. Ozin, *Nature,* 386, **1997,** 692.

64. S. Schacht, Q. Huo, I. G. V. Martin, G. D. Stucky, F. Schuth, *Science*, 273, **1996**, 768.

65. Q. Huo, D. Zao, J. Feng, K. Weston, S.K. Burratto, G.D. Stucky, S. Schacht, F. Schuth, *Adv. Mater.*, 9, **1997**, 974.

66. H. Yang, N. Coombs, I. Sokolov, G. A. Ozin, *Nature*, 381, **1996**, 589.

67. H. Yang, A. Kuperman, N. Coombs, S. M. Afara, G. A. Ozin, *Nature*, 379, **1996**, 703.

68. I. A. Aksay, M. Trau, S. Manne, I. Honma, N. Yao, L. Zhou, P. Fenter, P. M. Eisenberger, S. M. Gruner, *Science*, 273, **1996**, 892.

69. M. Ogawa, *Chem. Commun.,* **1996**, 1149.

70. Q. Huo, J. Feng, F. Schuth, G.D. Stucky, *Chem. Mater.*, 9, **1997** 14.

71. G.S. Attard, J.C. Glyde, C.G. Goltner, *Nature*, 378, **1995**, 366.

72. M. T. Anderson, J. E. Martin, J. G. Odinek, P. P. Newcomer, J. P. Wilcoxon, *Micropor. Mater.*, 10, **1997**, 13.

73. S. S. Kim, W. Zhang, T. J. Pinnavaia, *Science*, 282, **1998**, 1302.

74. F. Kleitz, W. Schmidt, F. Schüth, *Micropor. Mesopor. Mater.*, 65, **2003**,1 and references therein.

75. A. Doyle, B. K. Hodnett, *Micropor. Mesopor. Mater.*, 58, **2003**, 251 and references therein.

76. W.J. Hunks, G.A. Ozin, *Adv. Fun. Mater.*, 15, **2005**, 259.

77. A. Stein, B.J. Melde, R.C. Schroden, *Adv. Mater.*, 12, **2000**, 1403.

78. A.P. Wight, M.E. Davis, *Chem. Rev.*, 102, **2002**, 3589.

79. X. Feng, G. E. Fryxell, L. -Q. Wang, A. Y. Kim, J. Liu, K. M. Kemner, *Science*, 276, **1997**, 923.

80. D. E. De Vos, M. Dams, B. F. Sels, P. A. Jacobs, *Chem. Rev.*, 102, **2002**, 3615.

81. P.M. Price, J.H. Clarck, D.J. Macquarrie, *J. Chem. Soc., Dalton Trans.* **2000**, 101.

82. K. Moller, T. Bein, *Stud. Surf. Sci. Catal.***,** 117, **1998**, 53.

83. J. Liu, X. Feng, G. E. Fryxell, L. -Q. Wang, A. Y. Kim, M. Gong, *Adv. Mater.*, 10, **1998**, 161.

84. K. K. Unger, *Porous Silica – Its Properties and Use as Support in Column Liquid Chromatography,* Vol. 16, Elsevier, Amsterdam, **1979**.

85. L. Mercier, T. J. Pinnavaia, *Environ. Sci. Tech.*, 32, **1998**, 2749.

86. T. Kimura, S. Saeki, Y. Sugahara, K. Kuroda, *Langmuir*, 15, **1999**, 2794.

87. J. S. Beck, D. C. Calabro, S. B. McCullen, B. P. Pelrine, K. D. Schmitt, J. C. Vartuli, *Method for Functionalizing Synthetic Mesoporous Crystalline Material,* Mobil Oil Corporation, USA, **1992**.

88. R. Anwander, I. Nagl, M. Widenmeyer, G. Engelhardt, O. Groeger, C. Palm, T. Roser, *J. Phys. Chem. B*, 104, **2000**, 3532.

89. M. H. Lim, C. F. Blanford, A. Stein, *J. Am. Chem. Soc.*, 119, **1997**, 4090.

90. M. H. Lim, C. F. Blanford, A. Stein, *Chem. Mater.*, 10, **1998**, 467.

91. W. M. van Rhijn, D. E. De Vos, B. F. Sels, W. D. Bosaert, P. A. Jacobs, *Chem. Commun.,* **1998**, 317.

92. D. Margolese, J.A. Melero, S.C. Christiansen, B.F. Chmelka, G.D. Stucky, *Chem. Mater.,* 12, **2000**, 2448.

93. J. H. Clark, D. J. Macquarrie, *Chem. Commun.*, **1998**, 853.

94. D. Brunel, *Micropor. Mesopor. Mater.*, 27, **1999**, 329.

95. P. Sutra, D. Brunel, *Chem. Commun.*, **1996**, 2485.

96. M. H. Lim, A. Stein, *Chem. Mater.*, 11, **1999**, 3285.

97. D. S. Shephard, W. Zhou, T. Maschmeyer, J. M. Matters, C. L. Roper, S. Parsons, B. F. G. Johnson, M. J. Duer, *Angew. Chem. Int. Ed.*, 37, **1998**, 2719.

98. F. De Juan, E. Ruiz-Hitzky, *Adv. Mater.,* 12, **2000**, 430.

99. V. Antochshuk, M. Jaroniec, *Chem. Commun.,* **1999**, 2373.

100. C. Sanchez, F. Ribot, *New. J. Chem.* 18, **1994**, 1007.

101. S. L. Burkett, S. D. Sims, S. Mann, *Chem. Commun.,* **1996**, 1367.

102. S. D. Sims, S. L. Burkett, S. Mann, *Mater. Res. Soc. Symp. Proc.* 8, **1996**,

103. D. J. Macquarrie, *Chem. Commun.,* **1996**, 1961.

104. Q. Huo, D. I. Margolese, G. D. Stucky, *Chem. Mater.,* 8, **1996**, 1147.

105. P. Mukherjee, S. Laha, D. Mandal, R. Kumar, *Stud. Surf. Sci. Catal.,*129, **2000**, 283.

106. S. R. Hall, C. E. Fowler, B. Lebeau, S. Mann, *Chem. Commun.,* **1999**, 201.

107. F. Babonneau, L. Leite, S. Fontlupt, *J. Mater. Chem.,* 9, **1999**, 175.

108. V. Goletto, V. Dagry, F. Babonneau, *Mater. Res. Soc. Symp. Proc.,* 576, **1999**, 229.

109. L. Mercier, T. J. Pinnavaia, *Chem. Mater.,* 12, **2000**, 188.

110. M. Koya, H. Nakajima, *Stud. Surf. Sci. Catal.,* 117, **1998**, 243.

111. R. Richer, L. Mercier, *Chem. Commun.,* **1998**, 1775.

112. J. Brown, R. Richer, L. Mercier, *Micropor. Mesopor. Mater.,* 37, **2000**, 41.

113. S. Inagaki, S. Guan, Y. Fukushima, T. Ohsuma, O. Terasaki, *J. Am. Chem. Soc.,* 121, **1999**, 9611.

114. S. Guan, S. Inagaki, T. Ohsuma, O. Terasaki, *J. Am. Chem. Soc.*, 122, **2000**, 5660.

115. T. Asefa, M. J. McLachlan, N. Coombs, G. A. Ozin, *Nature,* 402, **1999**, 867.

116. B. J. Melde, B. T. Holland, C. F. Blanford, A. Stein, *Chem. Mater.,* 11, **1999**,

3302.

117. K. Moller, T. Bein, *Chem. Mater.,* 10, **1998**, 2950.

118. C.E. Fowler, S.L. Burkett, S. Mann, *J. Chem. Soc., Chem. Commun.,* **1997**, 1769.

119. D.J. Macquarrie, D.B. Jackson, *J. Chem. Soc., Chem. Commun.,* **1997**, 1781.

120. X.S. Zhao, G.Q. Lu, A.K. Whittakar, G.J. Millar, *J. Phys. Chem. B*, 101, **1997**, 6525.

121. K. A. Koyano, T. Tatsumi, Y. Tanaka, S. Nakata, *J. Phys. Chem. B*, 101, **1997**, 9436.

122. K. Tanabe, T. Yamaguchi, *Stud. Surf. Sci. Catal*., 44, **1989**, 99.

123. K. Tanabe M. M. Ono, H. Hattori, *Stud. Surf. Sci. Catal*., 51, **1989**, 219.

124. B.H. Davis, R. A. Keogh, R. Srinivasan, *Catal. Today*, 20, **1994**, 219.

125. X. Song, A. Sayari, *Catl. Rev.-Sci. Eng.,* 38, **1996**, 329.

126. K. Tanabe, T. Yamaguchi, *Catal.Today*, 20, **1994**, 185.

127. M.K. Dongre, V. Ramaswamy, C. S. Gopinath, A.V. Ramaswamy, S. Scheurell, M. Brueckner, E. Kemnitz., *J. Catal*., 199, **2001**, 209.

128. G.D. Yadav, J. J. Nair, *Micropor. Mesopor. Mater*., 33, **1999**,1.

129. R. D. Wilson, D.G. Barton, C.D. Baertsch, E. Iglesia, *J. Catal*.,194, **2000**,175.

130. R.P. Bell, *Portion in Chemistry,* Cornell Univ. Press, Ithaca, **1959**.

131. G. D. Yadav, J. J. Nair, *Mircopor. Mesopor. Mater*., 33, **1999**, 1.

132. D.M. Antonelli, J.Y. Ying, *Angew. Chem., Int. Ed. Engl.,* 34, **1995**, 2014.

133. H. Yoshitake, T. Sugihara, T. Tatsumi, *Chem. Mater.,* 14, **2002**, 1023.

134. J.A. Knowles, M.J. Hudson, *J.Chem. Soc., Chem. Commun.* **1995**, 2083. *J. Mater. Chem*., 6, **1996**, 89.

135. U. Ciesla, S. Schacht, G.D. Stucky, K.K. Unger, F. Schuth, *Angew. Chem. Int. Ed. Engl.,* 35, **1996**, 541.

136. U. Ciesla, M. Froba, G.D. Stucky, K.K. Unger, F. Schuth, *Chem. Matet.,* 11, **1999**, 11, 227.

137. J.L. Blin, R. Flamant, B.L. Su, *Inter. J. Inorg. Mater.*, 3, **2001**, 959.

138. N. Ulagappan, V.N. Raju, C.N.R. Rao, *Chem. Commun.,* **1996**, 2243.

139. D.M. Antonelli, *Adv. Mater.*, 11, **1999**, 487.

140. J. S. Reddy, A. Sayari, *Catal. Lett.*, 38, **1996**, 219.

141. E. Zhao, S.E. Hardcastle, G. Pacheco, A. Garcia, A.L. Blumenfeld, J.J. Fripiat, *Micropor. Mesopor. Mater.,* 31, **1999**, 9.

142. G. Pacheco, E. Zhao, A. Garcia, A. Sklyarov, J. Fripiat, *Chem. Commun.*, **1997**, 491.

143. M.S. Wong, J.Y. Ying, *Chem. Mater.*, 10, **1998**, 2067.

144. Y.Y. Huang, T.J. McCarthy, W.M.H. Sachtlet, *Appl. Catal. A: Gen.*, 148, **1996**, 135.

145. H-R. Chen, J-L. Shi, W-H. Zhang, M-L. Ruan, D-S. Yan, *Micropor. Mesopor. Mater.,* 47, **2001**, 173.

146. D.J. Mcntosh, R.A. Kydd, *Micropor. Mesopor. Mater.*, 37, **2000**, 281.

147. G. Larsen, E. Lotero, M. Nabity, L.M. Petkovic, D.S. Shobe, *J. Catal.* 164, **1996**, 246.

148. B. Lee, D.L. Lu, J.N. Kondo, K. Domen, *J. Am. Chem. Soc.,* 124, **2002**, 11256.

149. D.M. Antonelli, J.Y. Ying, *Chem. Mater.,* 8, **1996**, 874.

150. S.A. Bagshaw, T.J. Pinnavaia, *Angew. Chem. Int. Ed. Engl.,* 35, **1996**, 1102.

151. P. Liu, J. Liu, A. Sayari, *Chem. Commun.,* **1997**, 577.

152. K.G. Servin, T.M. AbdeFattah, T.J. Pinnavaia, *Chem. Commun.,* **1998**, 1471.

153. Z. Tian, W. Tong, J. Wang, N. Duan, V.V. Krishnan, S.L. Suib, *Science,* 276, **1997**, 926.

154. P. Yang, D. Zhao, D.I. Margolese, B.F. Chmelka, G.D. stucky, *Nature*, 396, **1998**, 152.

155. T. Takahashi, N.Q. Minh, *Science and Technology of Ceramic Fuel Cells*; Elsevier: New York, **1995**.

156. C.N. Satterfield, *Mass Transfer in Heterogeneous Catalysis,* MIT Press, Cambridge, MA, **1970**.

157. J.B. Miller, E.I. Ko, *Catal. Today,* 35, **1997**, 269.

158. M. Chidambaram, D. Curulla-Ferre, A.P. Singh, B.G. Anderson, *J. Catal*. 220, **2003**, 442.

159. C.J. Brinker, G.W. Xcherer, *Sol-gel Science,* academic Press, New York, **1990**.

160. V.I. Parvulescu, H. Bonnemann, V. Parvulescu, B. Endruschar, A.Ch.W. Rufinska, B. Tesche, G. Poncelet, *Appl. Catal. A: Gen.,* 214, **2001**, 273.

161. H.W. Kouwenhoven, H. van Bekkum, *Handbook of Heterogeneous Catalysis,* (G. Ertl, H. Knozinger, J. Weitkamp, Eds), Vol. 5, P.2358. VCH, Weinheim, **1997**.

162. G.A. Olah, *Friedel-Crafts and Related Reactions*, Vols. I- IV. Wiley-Interscience, New York, **1963-64**.

163. A. Kaward, S. Mitamurd, S. Kobayashi, *J. Chem. Soc., Chem. Commun*., **1993**, 1157.

164. M. Hino, K. Arata, *Chem. Lett.,* **1978**, 325.

165. K. Arata, M. Hino, *Chem. Lett.,* **1980**, 1479.

166. K. Nomiya, Y. Sugaya, S. Sasa, M. Miwa, *Bull. Chem. Soc. Jpn*., 53, **1980**, 2089.

167. F. Effenberger, G. Epple, *Angew. Chem. Int. Ed. Eng*., 11, **1972**, 300.

168. D.B. Baudry, A. Dormond, F.D. Montagne, *J. Mol. Catal. A: Chem.*, 149, **1999**, 215.

169. A.Corma, S. Iborra, S. Miquel, J. Primao, *J. catal.,* 173, **1998**, 315.

170. N.O.V. Sonntag, *J. Am. Oil. Chem. Soc.,* 59A, **1982**, 795.

171. J. Aracil, M. Martinez, N. Sanchez, A. Corma, *Zeolites,* 12, **1992**, 233.

172. N. Sanchez, M. Martinez, J. Aracil, *Ind. Eng. Chem. Res.* 36, **1997**, 1524; 36 **1997**, 1529.

173. W.D. Bossaert, D.E. De Vos, W.M. Van Rhijin, J.Bullen, P.J. Grobet, P.A. Jacobs, *J. Catal.*, 182, **1999**, 156.

174. T.W. Green, P.G.M. Wats, *Protective groups in organic synthesis,* 2nd Ed. Vol.4, P.212, Willey, New York. **1991**.

175. K. Bauer, D. Garbe, H. Surburg, *Common fragrances and flavours materials,* 2nd Ed. VCH, New York, **1990**.

176. M.J Climent, A. Corma, A. Velty, M. Susarte. *J. Catal.*, 196, **2000**, 345.

177. *IUPAC compendium of Chemical Terminology*, 2nd Edition, **1997**.

178. J.W. Lloyd, P. DeCoufle, R.M. Moore, *J. Occup. Med.,* 17, **1975**, 263.

179. K. Schmeidl, E. Manfred, *German Patent,* DE 2729918, **1979**.

180. J. I. Kroschwitz, *Kirk-Othmer Encyclopedia of chemical Technology*, Vol. 21, **1997**, P. 470.

CHAPTER-2

SYNTHESIS METHODOLOGIES AND CHARACTERIZATION TECHNIQUES

2.1. INTRODUCTION

The syntheses of mesoporous zirconia materials *via* liquid crystal templates have opened up new possibilities for preparing heterogeneous catalysts containing uniform pores in the mesoporous regime [1-3]. This new family of material is termed as Zr-TMS (Zirconia based Tech Molecular Sieves or Zirconia based Transition metal oxide Mesoporous molecular Sieves) [4]. Organo-functionalization of the internal surfaces of mesoporous material can be achieved either by covalent grafting of various organic species onto the channel walls or by incorporating functionalities directly during the synthesis [5, 6]. The grafting process has been widely applied to anchor desired organic functional groups *via* condensation with surface silanol groups of the mesoporous silicate. However, it is somewhat difficult to control the concentration and distribution of organic moieties in the mesoporous surface mainly due to non-uniform presence of silanol groups in different mesoporous samples [7]. Another phenomenon to be taken into consideration is the greater accessibility of the silanol groups of the external surface towards functionalization [7]. This grafting on the external surface can be minimized by passivating the external silanol groups before functionalization of those on the internal surface [8].

In the preceding chapter, the synthesis procedure of mesoporous zirconia and surface modification of mesoporous materials by different routes have been reviewed. This chapter will present the experimental data regarding (i) the synthesis of mesoporous zirconia (Zr-TMS), (ii) surface modification of these materials by different organic functional groups, *viz*., benzyl alcohol, trifluromethanesulfonic acid, thiol (–SH) with sultone, through grafting and co-condensation routes, and (iii) comparison of the products obtained from both methods with respect to different physicochemical characteristics. In this context, an efficient room temperature grafting process will also be discussed.

2.2. MATERIALS

2.2.1. Primary Chemicals

1. Zirconium (IV) butoxide [$Zr(C_4H_9O)_4$, 80 wt% solution in 1-butanol, Aldrich, USA]
2. Tetramethyl ammonium hydroxide [$(CH_3)_4$-N-OH, TMAOH, 25 wt % aqueous solution, Loba Chemie, India]
3. N-cetyl-N,N,N trimethyl ammonium bromide [$C_{16}H_{33}$-N-$(CH_3)_3$Br, CTMABr, 25 wt% aqueous solution, Loba Chemie, India]
4. Acetyl acetone [$CH_3COCH_2COCH_3$, acac, 98%, Merck, India]
5. Benzyl alcohol [$C_6H_5CH_2OH$, 99%, Lancaster, UK]
6. Ethoxytrimethylsilane [C_2H_5O-Si-$(CH_3)_3$, ETMS, 98%, Sigma-Aldrich, USA]
7. Chlorosulphonic acid [Cl-SO_3H, CSA, 98%, Spectrochem, India]
8. Trifluoromethanesulphonic acid [CF_3SO_3H, TFA, 98+%, Lancaster, UK]
9. 3-(mercaptopropyl) trimethoxysilane [$(CH_3O)_3$-Si-$(CH_2)_3SH$, 3-MPTS, 95%, Alrdich, USA]
10. 1, 4-butanesultone [$(CH_2)_4$-SO_3, 1, 4-BS, 99%, Lancaster, UK]
11. Sodium hydroxide [NaOH, 97%, Merck, India]

2.2.2. Solvents

1. Cyclohexane [C_6H_{12}, 99%, Thomas Baker, India]
2. Benzene [C_6H_6, 99.7%, S.d. Fine, India]
3. Acetone [CH_3COCH_3, 99.5%, S.d. Fine, India]
4. Dry toluene [C_6H_5-CH_3, 99.5%, Thomas Baker, India]
5. Dichloromethane [CH_2Cl_2, 99.5%, Merck, India]
6. Chloroform [$CHCl_3$, Merck, India]
7. Diethyl ether [C_2H_5-O-C_2H_5, 98%, Sisco, India]

8. Methanol [CH_3OH, 99.8%, Merck, India]

9. Hydrochloric acid [HCl, 35%, Merck, India]

2.2.3. Chemicals used for catalytic reactions

1. Diphenyl ether [C_6H_5-O-C_6H_5, S.d. fine-Chem. Ltd, India]

2. Benzoyl chloride [C_6H_5COCl, 99 %, Loba Chemie, India]

3. 2-methylfuran [C_5H_6O, 99 %, Aldrich, USA]

4. Acetone [CH_3COCH_3, 99.5%, S.d. Fine-Chem. Ltd, India]

5. Nitrobenzene [$C_6H_5NO_2$, 98 %, Sisco Research Laboratory, India]

6. Ethylacetoacetate [$CH_3COCH_2COOC_2H_5$, 98 %, Merck, India]

7. Ethylene glycol [$HOCH_2$-CH_2OH, 99 %, S.d. fine-Chem. Ltd, India]

8. Biphenyl [C_6H_5-C_6H_5, 99.5 %, Aldrich, USA]

9. Toluene [C_6H_5-CH_3, 99.5 %, Merck, India]

10. *p*-toluoyl chloride [C_7H_7COCl, 98 %, Aldrich, USA]

11. Glycerol [$HOCH_2$-$CHOH$-CH_2OH, 99+ %, Aldrich, USA]

12. Lauric acid [$C_{11}H_{23}COOH$, 99.5+ %, Aldrich, USA]

13. Aniline [C_6H_5-NH_2, 99.5 %, S.d. fine-Chem. Ltd, India]

14. *p*-formaldehyde [$(CH_2O)n$, 95 %, Thomas Baker, India]

15. Anisole [$C_6H_5OCH_3$, 99 %, Thomas Baker, India]

2.3. SYNTHESIS

2.3.1. Synthesis of Zr-TMS material

The synthesis of Zr-TMS was carried out using the following gel composition and procedure:

0.1 $Zr(OC_4H_9)_4$:0.05 acac: 0.025 CTMABr:0.02 TMAOH:8.5 H_2O

In a typical synthesis of Zr-TMS, zirconium (IV) butoxide and acetyl acetone was mixed well by stirring at room temperature. Then the mixture was slowly added to an aqueous solution of CTMABr and TMAOH, which are well dissolved in required amount

of water. After further stirring the resulting synthesis gel was refluxed at 90 °C for about 50 h. The solid product was recovered, washed with deionised water and acetone, and dried. The surfactant was removed from the synthesized material by solvent extraction under reflux condition. The solid product was recovered by filtration, washed with deionised water and acetone, and dried. The procedure adopted here is the modified procedure of already reported by Hudson and Knowles [1].

2.3.2. Synthesis of Zr-TMS-BSA catalysts

Functionalization of benzyl alcohol over Zr-TMS was carried out by etherification reaction using cyclohexane as solvent at 80 °C for 10 h. To protect the unloaded hydroxyl groups, after modification with benzyl alcohol, desired amount of material was degassed at 80 °C for 2 h and dry toluene was added. Then an excess of ethoxytrimethylsilane was added and the suspension was refluxed at 70 °C under nitrogen atmosphere for 12 h. Further, sulphonation of the resulting material was done with the appropriate amount of chlorosulphonic acid using chloroform as solvent at 70 °C for 3 h. Thus the material obtained was washed with chloroform and soxhlet extraction was done with a mixture of 1:1 diethyl ether and dichloromethane and dried at 50 °C for 6 h.

2.3.3. Synthesis of A-Zr-BSA catalyst

Synthesis of BSA functionalized non-porous zirconia catalyst was carried out via the following procedure. A mixture of zirconium (IV) butoxide (0.09 mol) and 1-butanol was taken in a two-necked 250 ml round bottom flask equipped with a magnetic stirrer and a septum. The flask was held at 100 °C and stirred for 10 min. Then required amount of water was added drop-wise into this mixture under stirring to hydrolyze the zirconium (IV) butoxide to $Zr(OH)_4$. Further, after 30 min of stirring, benzyl alcohol (0.01 mol), was added and stirred for 1 h, then methoxy trimethyl silane (MTMS) was added and stirred for another 1 h. Further, chlorosulphonic acid (0.01 mol) was slowly added by

syringe and stirring was continued for 2 h. The mixture was cooled, filtered, washed with deionised water, acetone and then dried at 100 °C for 6 h. Soxhlet extraction was carried out for 24 h. Then the sample was dried at 100 °C for 10 h. The synthesized material was white in colour. Functionalized non-porous material is designated as A-Zr-BSA-10.

2.3.4. Synthesis of Zr-TMS-TFA catalysts

Triflic acid was added drop wise into the mixture of toluene and Zr-TMS at 90 °C under nitrogen atmosphere and further refluxed for 2 h. The mixture was cooled, filtered, washed with deionised water and acetone and then dried at 100 °C for 6 h. Soxhlet extraction of the material was carried out at 75 °C for 24 h using a mixture of dichloromethane and diethyl ether. The syntheses of different loadings of triflic acid over amorphous $Zr(OH)_4$ (5 to 25 wt %) were carried out by varying the molar ratios of zirconium (IV) butoxide, water, and CF_3SO_3H. The sample was then dried at 200 °C for 10 h.

2.3.5. Synthesis of A-Zr-TFA catalysts

Synthesis of functionalized amorphous ≡ Zr-O-SO_2-CF_3 (A-Zr-TFA) catalysts was carried using mixture of zirconium (IV) butoxide and 1-butanol. The flask was held at 90 °C and stirred for 10 min. Then desired amount of water was added drop-wise into this mixture under stirring to hydrolyze the zirconium (IV) butoxide to $Zr(OH)_4$. Further, after 30 min of stirring, triflic acid was slowly added by syringe into the above mixture and stirring was continued for 2 h. The mixture was cooled, filtered, washed with deionised water and acetone and then dried at 100 °C for 6 h. Soxhlet extraction was carried out for 24 h. Then the sample was dried at 200 °C for 10 h. The synthesized materials were white in colour.

2.3.6. Synthesis of Zr-TMS-OSA catalysts

Zr-TMS was taken in a two necked round bottom flask; dry toluene was added and stirred for 10 min. at 100 °C. Then 3-MPTS was slowly added into the above mixture

by syringe and continued the stirring for another 2 h. Simultaneously sodium hydroxide was dissolved in methanol, at room temperature 1,4-butane sultone was added drop by drop and continued the stirring for another 30 min. This whole solution was added by syringe in to the Zr-TMS, 3-MPTS mixture, and the reflux was continued for another 4 h. Then the mixture was cooled, filtered, washed with water, acetone and then dried at 100°C for 10 h. Soxhlet extraction was carried out. The sample was then dried at 100°C for 10 h. The different loadings of OSA over Zr-TMS were also done.

2.3.7. Synthesis of A-Zr-OSA catalysts

Synthesis of OSA functionalized non-porous zirconia catalyst was carried out via the following procedure. A mixture of zirconium (IV) butoxide and 1-butanol was taken in a two-necked 250 ml round bottom flask and stirred at 100 °C for 10 min. Then water was added drop-wise into this mixture under stirring. Further, after 30 min of stirring, 3-MPTS, and mixture of CH_3OH, NaOH and 1, 4-BS was slowly added by syringe and stirring was continued for 2 h. The mixture was cooled, filtered, washed with deionised water, acetone and then dried at 100 °C for 6 h. Soxhlet extraction was carried out for 24h. Then the sample was dried at 100 °C for 10 h. The synthesized material was white in colour.

2.3.8. Synthesis of Zr-TMS-SO_3H catalyst

Well-dried Zr-TMS was taken in a two-necked round bottom flask connected with water condenser through one neck, which was equipped with nitrogen atmosphere. Dry toluene was added through another neck fitted with septum and stirred for 10 min at 100 °C. Then 3-MPTS (20 wt %) was introduced into the mixture by syringe and continued the stirring for another 2 h under nitrogen atmosphere. Then the mixture was cooled to room temperature, filtered, washed with acetone and then dried at 100 °C for 10 h. The obtained Zr-TMS-SH-20 was oxidized with three fold excess of H_2O_2 at room temperature under nitrogen atmosphere for 10 h, filtered and washed with water,

acetone and then dried at 100 °C for 10 h. The obtained catalyst is designated as Zr-TMS-SO_3H-20.

2.4. PHYSICOCHEMICAL CHARACTERIZATION

The inorganic–organic hybrid mesostructured materials can be characterized by various techniques, which provide important information about different physicochemical features. The most extensively used techniques can be categorized into the following.

1. Spectroscopic techniques:

(a) Powder X-ray diffraction (XRD), (b) Fourier transform infrared (FTIR) spectroscopy, (c) FT-Raman spectroscopy, (d) Solid state nuclear magnetic resonance (NMR) spectroscopy, (e) X-ray photoelectron spectroscopy (XPS), (f) Atomic absorption and emission spectrometry (AAS and AES).

2. Microscopic techniques:

(a) Scanning electron microscopy (SEM), (b) Transmission electron microscopy (TEM).

3. Volumetric techniques:

(a) Porosity measurements by nitrogen (N_2) adsorption (BET method), (b) Acidity measurements by pyridine or ammonia (NH_3) adsorption.

4. Gravimetric techniques:

(a) Thermo gravimetric analyses (TGA), (b) Differential thermal analysis (DTA).

2.4.1. X-Ray diffraction

It is well recognized that X-ray diffraction, based on wide-angle elastic scattering of X-rays, has been the single most important tool to determine the structure of the materials characterized by long-range ordering. The X-ray diffraction patterns are obtained by measurement of the angles at which an X-ray beam is diffracted by the sample. Bragg's equation relates the distance between two *hkl* planes (d) and the angle of diffraction (2θ) as: $n\lambda = 2d\sin\theta$, where λ = wavelength of X-rays, n = an integer known as the order of reflection (h, k and l represent Miller indices of the respective planes) [9].

From the diffraction patterns, the uniqueness of mesoporous structure [10], phase purity [11], degree of crystallinity [11] and unit cell parameters [10] of the semi crystalline hybrid materials can be determined.

The identification of phase is based on the comparison of the set of reflections of the sample with that of pure reference phases distributed by International Center for Diffraction Data (ICDD). Unit cell parameter (a_0) of a cubic lattice can be determined by the following equation: $a_0 = d_{hkl}\sqrt{(h^2 + k^2 + l^2)}$, where d = distance between two consecutive parallel lattice planes having Miller indices h, k and l [9].

X-ray diffraction broadening analysis has been widely used to characterize supported metal crystallites in the nanoscale. The average size of the nanoparticles can be estimated using the Debye-Scherrer equation: $D = k\lambda / \beta\cos\theta$, where D = thickness of the nanocrystal, k is a constant, λ = wavelength of X-rays, β = width at half maxima of (111) reflection at Bragg's angle 2θ [12]. In this study, all the synthesized catalysts were characterized by a Rigaku Miniflex instrument using Cu K_α radiation (30 kV, 15 mA), λ=1.5404 Å between 1.5 to 60° (2θ) with a scan rate of 4°/min.

2.4.2. Chemical composition by CHN-S analysis

Analysis of the organic content, carbon and sulfur present in the catalysts was estimated using a Carlo-Erba CHN-S analyzer (EA1108 Elemental Analyzer).

2.4.3. Fourier transform infrared spectroscopy

Fourier transform infrared (FT-IR) spectroscopy deals with the vibration of chemical bonds in a molecule at various frequencies depending on the elements and types of bonds. After absorbing electromagnetic radiation the frequency of vibration of a bond increases leading to transition between ground state and several excited states. The energy corresponding to these transitions corresponds to the infrared region (4000–400 cm^{-1}) of the electromagnetic spectrum. The term Fourier transform (FT) refers to a recent development in the manner in which the data are collected and converted from an

interference pattern to an infrared absorption spectrum that is like a molecular "fingerprint" [13].

In the case of porous zirconia, the FTIR spectra in the 650–750 cm^{-1} region provides information about the structural details including isomorphous substitution in framework, whereas the bands in the 3000–4000 cm^{-1} region allows to determine different Brönsted and Lewis acid sites [14]. In this study, all the synthesized catalysts FT-IR spectra were obtained in a range of 400 to 4000 cm^{-1} on a Shimadzu FTIR 8201 PC using a Diffuse Reflectance scanning disc technique.

2.4.4. FT-Raman spectroscopy

In contrast to infrared spectroscopy, where we have been concerned with the absorption of infrared light, Raman spectroscopy depends on the frequency of the light scattered by molecules as they undergo rotations and vibrations. When monochromatic light of frequency υ_0 is directed at a cell containing a dust-free transparent substance, most of the light passes through unaffected. Some of the light, however (~0.1%) is scattered by the sample molecules in all directions. The scattered radiation contains photons which have the same frequency υ_0 as the incident light (elastic scattering), but in addition the emergent radiation contains other frequencies (due to inelastic scattering) such as $(\upsilon_0-\upsilon_1)$ and $(\upsilon_0+\upsilon_1)$. The lines of lower frequency than the incident light $(\upsilon_0-\upsilon_1)$ are known as stokes lines, while the high-frequency lines $(\upsilon_0+\upsilon_1)$ are termed as anti-stokes lines. Normally, an intense monochromatic source of light in the visible region is employed as the incident or exciting radiation. Raman scattered light is due to rotations and vibrations of the compounds under investigation. Since the wavenumber position of the exciting line is approximately 20000 cm^{-1}, the Raman scattered light will have frequencies which are displaced from 20000 cm^{-1} by amounts which lie somewhere in the range ±10-4000cm^{-1}. The exact wavenumber displacements, $\Delta\upsilon$, will depend upon

the rotational and vibrational energies of the particular compound causing the Raman scattering. The same displacement will occur on the either side of the exciting line.

Raman spectra may be obtained from solids, liquids, gases and solutions. All Raman spectrometers consist basically of four units, such as a source, sample optics, a monochromator, and a detector/electronics/recorder system [15, 16]. In the present work a Bruker RFS/100S FT-Raman spectrometer. An Nd-YAG laser (1064 cm^{-1}; 50 mW) was used as an excitation source.

2.4.5. Cross-polarization magic angle spinning NMR spectroscopy

Nuclear magnetic resonance (NMR) spectroscopy is one of the most powerful tools to investigate structure and dynamics of a molecular system in liquid phase. Atomic nuclei consisting of odd number of protons and/or neutrons possessing a nuclear spin $I \neq 0$ and consequently a magnetic moment $\mu = \gamma \hbar I$ (γ = gyromagnetic ratio), when placed in a magnetic field of strength B_0, Zeeman interaction results in quantized orientations of the nuclear magnetic moments [17]. The nucleus can adopt $2I + 1$ Eigen states with energies $E(m) = -m\gamma\hbar B_0$, where m = (I, I–1,…., –I). Transitions between neighboring energy states ($\Delta m = \pm 1$) can be induced by electromagnetic radiation (energy $E = h\nu$) of frequency $\nu_0 = \gamma B_0/2\pi$.

The chemical shift interaction arises from secondary local magnetic fields induced by the interaction of the electrons surrounding the nucleus. The induced local field opposes B_0 and hence shields the nucleus under observation. The shielding is spatially anisotropic due to the nonspherical electron distribution around the nucleus [18].

With the advent of sophisticated solid-state NMR techniques, it has become possible to obtain NMR spectra of solids with spectral resolution comparable to that of liquids [19]. Modern high-resolution solid-state NMR spectroscopy allows elucidating the chemical and structural environment of several atoms (*e.g.* ^{13}C, ^{27}Al, ^{29}Si, ^{31}P, ^{51}V *etc.*) in

a solid matrix like that of porous materials [20]. The most popular technique to get high-resolution NMR spectra with narrow line width is the magic angle spinning (MAS), where the solid sample is fast rotated about an axis inclined at a "magic" angle $\theta = 54°44'$ to the direction of B_0 [21].

Cross-polarization (CP) technique does not affect the line width of the spectra, but is applied to improve the sensitivity, *i.e.*, the signal to noise ratio (SNR) of the spectra of nuclei with low natural abundance (*e.g.* ^{13}C, ^{29}Si, ^{31}P *etc.*), and to monitor the spatial proximity of nuclei [21]. CP involves indirect excitation of the less abundant nucleus through magnetization transfer from an abundant spin system (*e.g.* ^{1}H).

Bruker DRX-500 and DSX-300 NMR spectrometers were used. The resonance frequencies of ^{29}Si and ^{13}C were 59.6 and 75.5 MHz, respectively. The chemical shifts were determined using tetraethyl orthosilicate (δ=82.4 ppm from TMS) and adamantane (δ =28.7 ppm from TMS) as the reference compounds for ^{29}Si and ^{13}C, respectively.

2.4.6. X-Ray photoelectron spectroscopy

XPS is based on the photoelectric effect. Routinely used X-ray sources are Mg Kα (*hv*=1253.6 eV) and Al Kα (*hv*=1486.3 eV). In XPS one measures the intensity of photoelectrons N(E) as a function of their kinetic energy E_k. Because a set of binding energies is characteristic for an element, XPS can be used to analyze the composition of samples. Binding energies are not only element specific but contain chemical information as well. The energy levels of core electrons depend on the chemical state of the atom. Photoelectron peaks are labeled according to the quantum numbers of the level from which the electron originates. An electron coming from an orbital with main quantum number *n*, orbital quantum number *l* (0,1,2,3,.. indicated as *s,p,d,f,*..) and spin quantum number *s* (+1/2 or –1/2) is indicated as nl_{l+s}. Almost all photoelectrons used in the laboratory XPS have kinetic energy in the range of 0.2 to 1.5 keV, and probe the outer layer of the catalyst.

X-ray photoelectron spectra (XPS) were obtained using a VG Microtech Multilab-ESCA-3000 spectrometer equipped with a twin anode of Al and Mg. All the measurements are made on as received powder samples using Mg Kα X-ray at room temperature. Base pressure in the analysis chamber was 4 x 10^{-10} Torr. Multichannel detection system with nine channels is employed to collect the data. The overall energy resolution of the instrument is better than 0.7 eV, determined from the full width at half maximum of $4f_{7/2}$ core level of gold surface. The errors in all BE (binding energy) values were with in ±0.1 eV.

2.4.7. Atomic absorption and emission spectrometry

The principle of atomic absorption is based on energy absorbed during transitions between electronic energy levels of an atom. When some sort of energy is provided to an atom in ground state by a source such as a flame (temperature ranging from 2100–2800 °C), outer-shell electrons are promoted to a higher energy excited state. The radiation absorbed as a result of this transition between electronic levels can be used for quantitative analysis of metals and metalloids present in solid matrices, which have to be dissolved by appropriate solvents before analysis. The basis of quantitative analysis depends on measurement of radiation intensity and the assumption that radiation absorbed is proportional to atomic concentration. Analogy of relative intensity values for reference standards is used to determine elemental concentrations [22].

Atomic emission spectrometry (AES) is similar to atomic absorption spectrometry (AAS). In both the cases the sample must be atomized in order to obtain usable absorption spectra. However, in contrast to AAS, in AES the sample is heated at a very high temperature (8000–10000 °C), where the atoms in the sample are excited to higher energy levels. When the excited atoms are relaxed and fall back to the ground energy level, radiations are emitted. Measurement of the intensities of the emission forms the

basis of quantitative determination [23]. Here, the synthesized catalysts were studied by Varian Spectra AA220.

2.4.8. Scanning electron microscopy

Scanning electron microscopy (SEM) is an important tool for morphological characterization of mesoporous molecular sieve materials. A scanning electron microscope can generate an electron beam scanning back and forth over a solid sample. The interaction between the beam and the sample produces different types of signals providing detailed information about the surface structure and morphology of the sample. When an electron from the beam encounters a nucleus in the sample, the resultant coulombic attraction leads to a deflection in the electron's path, known as Rutherford elastic scattering. A fraction of these electrons will be completely backscattered, reemerging from the incident surface of the sample. Since the scattering angle depends on the atomic number of the nucleus, the primary electrons arriving at a given detector position can be used to produce images containing topological and compositional information [24].

The high-energy incident electrons can also interact with the loosely bound conduction band electrons in the sample. However, the amount of energy given to these secondary electrons as a result of the interactions is small, and so they have a very limited range in the sample. Hence, only those secondary electrons that are produced within a very short distance from the surface are able to escape from the sample. As a result, high-resolution topographical images can be obtained in this detection mode [25]. Here, all the synthesized catalysts were studied by JEOL-JSM-5200 scanning microscopy.

2.4.9. Transmission electron microscopy

Transmission electron microscopy (TEM) is typically used for high resolution imaging of thin films of a solid sample for microstructural and compositional analysis.

The technique involves: (i) irradiation of a very thin sample by a high-energy electron beam, which is diffracted by the lattices of a crystalline or semi crystalline material and propagated along different directions, (ii) imaging and angular distribution analysis of the forward-scattered electrons (unlike SEM where backscattered electrons are detected), and (iii) energy analysis of the emitted X-rays [26]. The topographic information obtained by TEM in the vicinity of atomic resolution can be utilized for structural characterization and identification of various phases of mesoporous materials, *viz*., hexagonal, cubic or lamellar [27]. TEM also provides real space image on the atomic distribution in the bulk and surface of a nanocrystal [28]. A JEOL JEM-1200EX instrument with 120 kV of acceleration voltage was used to probe the materials.

2.4.10. Porosity measurements by N_2 adsorption

Despite of some theoretical limitations, the Brunauer-Emmett-Teller (BET) method continues to be the most widely used method for the evaluation of surface area, pore volumes and pore size distributions of porous solids from N_2 physisorption isotherm data. The BET equation can be represented as follows: $\frac{p}{v(p_0 - p)} = \frac{1}{v_m c} + \frac{c-1}{v_m c}\frac{p}{p_0}$,

where v = volume of N_2 adsorbed by the sample under pressure p, p_0 = saturated vapor pressure at the same temperature, v_m = volume of N_2 adsorbed when the surface is covered with a unimolecular layer, and c = constant for a given adsorbate [29].

The equation suggests that the plot of $\frac{p}{v(p_0 - p)}$ versus $\frac{p}{p_0}$ should be linear, and from the intercept $\frac{1}{v_m c}$ and slope $\frac{c-1}{v_m c}$, the values of v_m and c can be determined as follows: v_m = (slope + intercept)$^{-1}$.

Thus the specific surface area (*S*) of a sample can be determined as follows: $S = \frac{N_0 v_m A}{22414m}$, where N_0 = Avogadro number, m = amount of solid adsorbent, A = cross-section of the gas molecules (16.2 Å^2 for N_2), and S is expressed in cm^2 g^{-1} unit.

Several computational procedures are available for the derivation of pore size distribution of mesoporous samples from physisorption isotherms. Most popular among them is the Barrett-Joyner-Halenda (BJH) model, which is based on speculative emptying of the pores by a stepwise reduction of p/p_0, and allowance being made for the contraction of the multilayer in those pores already emptied by the condensate [30]. The mesopores size distribution is usually expressed as a plot of $\Delta V_p/\Delta r_p$ versus r_p, where V_p = mesopore volume, and r_p = pore radius. It is assumed that the mesopores volume is completely filled at high p/p_0. N_2 adsorption-desorption was conducted by NOVA 1200 (Quantachrome) at –196°C. For this particular measurement, before analysis the samples were oven-dried at 100 °C and evacuated at 180 °C for 3 h under vacuum and then the adsorption-desorption was conducted by passing nitrogen into the sample, which was kept under liquid nitrogen.

2.4.11. Thermal analyses

The thermoanalytical techniques, *viz*., thermogravimetric analysis (TGA) and differential thermal analysis (DTA) have been widely used to establish the thermal stability of ordered mesoporous silica. Both TGA and DTA provide important information about the following: (i) temperature programmed desorption (TPD) and removal of physisorbed water below 150 °C, (ii) oxidative decomposition of the occluded organic materials, accompanied by one or several exotherms within 150 °C and 600 °C, and (iii) dehydroxylation occurring from condensation of adjacent silanol groups to form siloxane bonds at or above 600 °C [31]. Further, DTA can also detect any phase transitions if occur. Thermal analysis of all the samples were carried out by Mettler Toledo 851^e using

an alumina pan under a nitrogen (80ml min^{-1}) atmosphere from ambient to 1000 °C with the increasing rate of 20 K min^{-1}.

2.4.12. Acidity measurement

The acidity and the acid strength distribution of the solid materials were measured by the temperature programmed desorption (TPD) of ammonia [32-34]. The sample 20-30 mesh size (~ 1.0 g) was activated in a flow of N_2 at 200 °C for 6 h and cooled to room temperature. NH_3 gas (25 ml min^{-1}) was then passed continuously for a period of 30 min, and then the physically adsorbed NH_3 was desorbed by passing N_2 for 15 h (15 ml min^{-1}). Acid-strength distribution was obtained by raising the temperature with a ramping rate of 10 °C /min, from 30 to 300 °C in a number of steps in a flow of N_2 (10 ml min^{-1}). The NH_3 evolved was trapped in HCl solution and titrated with a standard NaOH solution. The higher the temperature required for desorption the stronger is the acidity of that portion of acid sites. It gives quantitative (total number of acid sites either Brönsted or Lewis) information about acid sites.

2.5. CATALYSIS

The commercialization of quite a few homogeneous catalytic systems consisting of transition metal complexes is difficult due to some inherent shortcomings, *viz*., (i) complicated work-up of the reaction mixture, (ii) preparation of the pure products not contaminated with catalysts or constituents thereof, (ii) isolation of the valuable catalyst or its constituents, which can be achieved only with high technical complexity and expenditure [35]. The most feasible way to circumvent this problem is to "*heterogenize*" the homogeneous catalyst, by means of immobilization, anchoring, or encapsulation in an inorganic (zeolites or mesoporous materials) [36] or organic (polymeric) [37] solid support.

The concept of heterogenization provides the prospective for extending the benefits of heterogeneous catalysis to homogeneous systems. These benefits include

easier separation of catalyst and reaction products leading to shorter work up times, improved process efficiency, the potential for re-activation and reuse of the supported catalyst comprising of expensive ligands. However, the prime requirement of the heterogenization approach is to maintain the stability of the heterogenized complex, such that it does not decompose or leach out from the solid matrix to the liquid phase during the course of reaction, and at the same time retains high activity, selectivity and original configuration.

Anhydrous AR grade chemicals were used without further purification. The liquid phase reaction was carried out in a 50 ml two necked flask attached to a condenser and a septum. The temperature of the reaction vessel was maintained using an oil bath. The reaction mixture was magnetically stirred and heated to the required temperature at atmospheric pressure. The product samples were withdrawn at regular intervals of time and analyzed periodically on a gas-chromatograph (HP 6890) equipped with a flame ionization detector and a capillary column (5 μm thick cross-linked methyl silicone gum, 0.2 mm x 50 m long). The products were also identified by injecting authentic samples and GCMS (Shimadzu 2000 A) and ^{1}H and ^{13}C-NMR (Bruker AC200) analysis.

Finally, the percentage conversion of reactant is defined as the total percentage of reactant transformed. The rate of reactant conversion (TOF) was calculated as the moles of reactant converted per second per mol of active site. The selectivity to a product is expressed as the amount of a particular product divided by the amount of total products and multiplied by 100.

Eight different reactions were done using different catalysts.

1. Liquid phase benzoylation of diphenyl ether with benzoyl chloride to 4-phenoxybenzo-phenone using Zr-TMS-BSA catalysts at 160°C in an oil bath at atmospheric pressure.
2. Liquid phase condensation of 2-methylfuran with acetone to 2,2-bis(5-methylfuryl)-

propane using Zr-TMS-BSA catalysts at 70℃ in an autoclave circulating cold water

3. Liquid phase condensation of anisole with p-formaldehyde to 4,4'-dimethoxydiphenlymethane using Zr-TMS-BSA catalysts at 100℃ in an oil bath at atmospheric pressure.
4. Liquid phase acetalization of ethylacetoacetate with ethylene glycol to fructone using Zr-TMS-TFA catalysts at 100 ℃ in an oil bath.
5. Liquid phase benzoylation of biphenyl with benzoyl chloride to 4-phenylbenzophenone using Zr-TMS-TFA catalysts at 170℃ in an oil bath at atmospheric pressure.
6. Liquid phase benzoylation of toluene with p-toluoyl chloride to 4,4'-dimethylbenzophenone using Zr-TMS-TFA catalysts at 130 ℃ in an oil bath using nitrogen atmosphere.
7. Liquid phase condensation of aniline with acetone to 4,4'-diaminodiphenylmethane using Zr-TMS-OSA catalysts at 150 ℃ in an oil bath using nitrogen atmosphere.
8. Liquid phase esterification of glycerol with lauric acid to monoglycerides using Zr-TMS-OSA catalysts at 100 ℃ in an oil bath.

2.6. ANALYSIS OF PRODUCTS

2.6.1. Gas Chromatography

Gas chromatography – specifically gas-liquid chromatography involves a sample being vaporized and injected onto the head of the chromatographic column. The sample is transported through the column by the flow of inert, gaseous mobile phase. The column itself contains a liquid stationary phase, which is adsorbed onto the surface of an inert solid. The carrier gas must be chemically inert. Commonly used gases are Nitrogen, Helium, Argon and Carbon dioxide. For optimum column efficiency, the sample should not be too large and should be introduced onto the column as a plug of vapor. Micro-syringe is used to inject sample through a rubber septum into a flash vaporizer port at the head of the column.

Two types of column are present, Packed and Capillary columns. For precise work, column temperature must be controlled within tenths of a degree. Many detectors are used in Gas chromatography.

Different detectors give different selectivity. Flame ionization detector (FID), Thermal conductivity detector, Electron Capture detector, Flame photometric detector, Photo ionization detector, Nitrogen–Phosphorous detector, Hall electrolytic conductivity. Flame ionization detector is a useful general detector for the analysis of organic compounds, has high sensitivity, large linear response range, low noise, robust, easy to use but destroys the sample.

2.6.2. Gas chromatography/Mass spectrometry (GC/MS)

GC/MS is a GC detector that is very expensive but very powerful version of the mass spectrometer. When coupled to a GC the detection system itself is often referred to as the mass selective detector or more simply the mass detector. This powerful analytical technique belongs to the class of hyphenated analytical instrumentation (since each part had a different beginning and can exist independently) and is called gas chromatography/mass spectrometry (GC/MS).

The power of this technique lies in the production of mass spectra from each of the analytes detected instead of merely an electronic signal that varies with the amount of analyte. These data can be used to determine the identity as well as the quantity of unknown chromatographic components with a conviction simple unavailable by other techniques. Major components of the GC/MS are Ionization source, Mass separator Quadrapole, Ion trap and Ion detector.

2.6.3. Liquid State NMR

NMR (Nuclear Magnetic Resonance) spectra arise from the spinning of nucleus. It is widely used as one of an armory of instrumental techniques available for structure analysis.

Modern NMR spectroscopy is frequently divided into several categories;

1. High-resolution mode on homogenous solutions.
2. High power mode on highly relaxing nuclei, which exhibit very broad lines, or polymers etc.
3. The study of solids using magic angle spinning techniques.
4. NMR 3D imaging to resolutions of ~ 1 mm.

The types of information accessible *via* high resolution NMR include;

1. Functional group analysis (chemical shifts)
2. Bonding connectivity and orientation (J coupling),
3. Through space connectivity (Over Hauser effect)
4. Molecular conformations, DNA, peptide and enzyme sequence and structure.
5. Chemical dynamics (Line shapes, relaxation phenomena).

The number of peaks in the low-resolution spectrum depends on the number of different environments that the hydrogen atoms have in the molecule. There are four aspects of an NMR spectrum that will allow us to determine the identity of the molecule.

1. The number of NMR signals
2. The position of each signal relative to a reference signal
3. The relative area under each signal
4. The spin coupling or spin-spin splitting pattern of each signal

2.7. CONCLUSION

In this chapter, synthesis of mesoporous zirconia (Zr-TMS) material and functionalization of benzylsulfonic acid (BSA), trifluromethanesulfonic acid (TFA) and organosilanolsulfonic acid (OSA) over Zr-TMS material have been discussed. Further, various physicochemical characterization techniques and their principles have been

elaborately demonstrated to conclude that the synthesized catalysts are in good textural and active nature. Catalysis and analysis of products are also discussed.

2.8. REFERENCES

1. M.J. Hudson, J.A. Knowles, *J. Mater. Chem.*, 6, **1996**, 89.
2. U. Ciesla, S. Schacht, G.D. Stucky, K.K. Unger, F. Schuth, *Angew. Chem. Int. Ed. Engl.,* 35, **1996**, 541.
3. D.M. Antonelli, *Adv. Mater.* 11, **1999**, 487.
4. M.S. Wong, J.Y. Ying, *Chem. Mater.,* 10, **1998**, 2067.
5. A. Stein, B. J. Melde, R. C. Schroden, *Adv. Mater.,* 12, **2000**, 1403.
6. A. P. Wight, M. E. Davis, *Chem. Rev.,* 102, **2002**, 3589.
7. M. H. Lim, A. Stein, *Chem. Mater.,* 11, **1999**, 3285.
8. D. S. Shephard, W. Zhou, T. Maschmeyer, J. M. Matters, C. L. Roper, S. Parsons, B. F. G. Johnson, M. J. Duer, *Angew. Chem. Int. Ed.,* 37, **1998**, 2719.
9. W. H. Bragg, W. L. Bragg, *The Crystalline State*, *Vol. 1*, McMillan, New York, **1949**.
10. S. Biz, M. Occelli, *Catal. Rev. Sci. Eng.,* 40, **1998**, 329.
11. G. Bergeret, *Handbook of Heterogeneous Catalysis*, *Vol. 2*, Eds: G. Ertl, H. Knozinger, J. Weitkamp, Wiley-VCH, Weinheim, **1997**, P. 464.
12. R. C. Rau, *Advances in X-Ray Analysis*, *Vol. 5*, Ed: W. M. Mueller, Sir Isaac Pitman and Sons, Ltd., London, **1962**, P. 104.
13. P. R. Griffiths, J. A. De Haseth, *Fourier Transform Infrared Spectrometry*, John Wiley and Sons, Inc., New York, **1986**.
14. C. C. Freyhardt, M. Tsapatsis, R. F. Lobo, K. J. Balkus, M. E. Davis, *Nature,* 381, **1996**, 295.
15. D.A. Long, *Raman Spectroscopy,* McGraw-Hill International Book Company, **1977**.

16. B.P. Straughan, S. Walker, *Spectroscopy,* Chapman and Hall, London, Vol.2, **1976**.

17. F. A. Rushworth, D. P. Tunstall, *Nuclear Magnetic Resonance*, Gordon and Breach Science, Publishers Ltd., London, **1973**.

18. W. W. Paudler, *Nuclear Magnetic Resonance: General Concepts and Applications*, John Wiley and Sons Inc., New York, **1987**.

19. M. Mehring, *High Resolution NMR Spectroscopy in Solids*, Springer-Verlag, Berlin, **1976.**

20. G. Engelhardt, D. Michel, *High-Resolution Solid-State NMR of Silicates and Zeolites*, John Wiley and Sons Ltd., Chichester, **1987**.

21. G. Engelhardt, in: *Handbook of Heterogeneous Catalysis*, *Vol. 2*, Eds: G. Ertl, H. Knozinger, J. Weitkamp, Wiley-VCH, Weinheim, **1997**, P. 525.

22. J. W. Robinson, *Atomic Absorption Spectroscopy*, Marcel Dekker, New York, **1975**.

23. G. L. Moore, *Introduction to Inductively Coupled Plasma Atomic Emission Spectrometry*, Elsevier, Amsterdam, **1988**.

24. G. Lawes, *Scanning Electron Microscopy And X-Ray Microanalysis*, John Wiley and Sons Ltd., Chichester, **1987**.

25. D. E. Newbury, D. C. Joy, P. Echlin, C. E. Fiori, J. I. Goldstein, *Advanced Scanning Electron Microscopy and X-Ray Microanalysis*, Plenum Press, New York, **1986**.

26. J. R. Fryer, *Chemical Applications of Transmission Electron Microscopy*, Academic Press, San Diego, **1979**.

27. V. Alfredsson, M. Keung, A. Monnier, G. D. Stucky, K. K. Unger, F. Schuth, *J. Chem. Soc., Chem. Commun.,* **1994**, 921.

28. Z. L. Wang, in: *Characterization of Nanophase Materials*, Ed: Z. L. Wang, Wiley-VCH, Weinheim, **2000**, Chapter 3, P. 37.

29. S. Brunauer, P. H. Emmett, E. Teller, *J. Am. Chem. Soc.,* 60, **1938**, 309.

30. E. P. Barrett, L. G. Joyner, P. P. Halenda, *J. Am. Chem. Soc..,* 73, **1951**, 373.

31. C. -Y. Chen, H. -X. Li, M. E. Davis, *Micropor. Mater.,* 2, **1993**, 17.

32. M. Chamumi, D. Brunel, F. Fajula, P. Geneste, P. Moreau, J. Solof, *Zeolites,* 14, **1994**, 283.

33. A.P. Singh, D. Bhattacharya, *Catal. Lett.*, 32, **1995**, 327.

34. A.P. Singh, D. Bhattacharya, S. Sharma, *Appl. Catal. A: Gen.,* 150, **1997**, 53.

35. J. Manassen, *Catalysis, Progress in Research*, Eds: F. Basolo, R. E. Burwell Jr., Plenum Press, New York, **1973**, P. 177.

36. D. E. De Vos, M. Dams, B. F. Sels, P. A. Jacobs, *Chem. Rev.,* 102, **2002**, 3615.

37. P. Ermert, *Solid-Supported Combinatorial and Parallel Synthesis of Small-Molecular-Weight Compound Libraries*, Eds: D. Obrecht, J. M. Villalgordo, Elsevier, Oxford, **1998**, P. 44.

CHAPTER-3

BENZYLSULFONIC ACID FUNCTIONALIZED Zr-TMS CATALYSTS (Zr-TMS-BSA)

3.1. INTRODUCTION

The Mobil researchers opened a new area in the synthesis of mesoporous materials through the discovery of M41S family of silicate mesoporous molecular sieves, particularly, MCM-41 by liquid-crystal templating mechanism [1]. Because of thermal stability, high surface area (around 1000 m^2 g^{-1}) and narrow pore-size distribution, these materials have invited a great deal of attention for the synthesis of wide range of bulky organic molecules. However, the MCM-41 type materials showed weak acid sites [2]. Synthesis of transition metal oxide based mesoporous materials such as titanium [3, 4], zirconium [5-7], niobium [8], tantalum [9], aluminum [10], hafnium [11], tin [12], and manganese [13] have been synthesized using ionic or neutral templates as structure directing agents, although most of them were comprised of mainly non-porous framework walls, which would limit their thermal and hydrothermal stability and greatly compromise their usefulness in catalytic application. Among these materials, zirconia [14] and alumina [10], only maintain the mesoporous structure upon the removal of template from the material by calcination or solvent extraction methods. Transition metal oxides are widely used as industrial catalysts and as catalysts supports. Unfortunately, they usually have poorly defined pore structures. Further, among the mesoporous materials, zirconia is of particular interest due to the high thermal stability and ease of synthesis [15, 16]. In the recent years SO_4^{2-}/ZrO_2 has attracted attention as it catalyzes various industrially important reactions such as: isomerization; condensation; Friedel-Crafts acylation reactions; etc [17]. However, its non-uniform pore size, low porosity, and small surface area limit its potential application for catalyzing reactions of bulky molecules. Because of the various oxidation states of zirconia, in addition to the high surface area, moderate acidity and the attractive porous nature have advantages over aluminosilicate materials for use in electromagnetic, photoelectronics and as a good support in catalysis [18].

The bifunctional nature of mesoporous zirconia has an unusual interest in the field of acidic catalysis. However, many attempts have been made to increase the acidity of these materials by using dopants or functional groups. Doping phosphates [19] or sulfates [20-22] result not only in an increase in the acidity but also a relative increase in thermal stability. These attempts result the preparation of mesoporous sulfated zirconia having partially tetragonal wall structure and narrow distribution of pore sizes by controlled hydrolysis of zirconium propoxide [23]. Moreover, the addition of the sulfate ion stabilizes the mesoporous morphology and delays crystallization. MCM-41 analogous materials have been synthesized together with zirconium oxide-sulfate and zirconium oxo phosphate [6] and a special post synthetic treatment has been developed in the later case. There has been considerable interest in the development of heterogeneous solid acid catalysts to avoid the use of traditional homogeneous acid catalytic systems (H_2SO_4, HF, $AlCl_3$, BF_3, etc.) which present serious drawbacks including hazards in handling, corrosiveness, production of toxic waste, and difficulties in separation. In this context, as an alternative, the covalent attachment of alkylsulfonic acid groups to the surface of molecular sieves has been proposed by several authors and successfully tested in several acid catalyzed reactions, including esterification [24-28] and condensations [28-31]. Sulphonic acid functionalized MCM-41 [29], SBA-2 [26] and SBA-15 [26, 32] were prepared through a thiol oxidation route. As a result, one-pot sol-gel route has been employed to achieve high levels of (3-mercaptopropyl) trimethoxysilane (3-MPTS) incorporation into mesoporous silica with >90 % efficiency and characterized by XPS and Raman spectroscopy [31].

In resent years, further, ordered mesoporous organosilica hybrid material is extended to the surfactant-mediated synthesis of benzene-silica hybrid material, phenylene-biphenylene materials, and benzene-silica hybrids with molecular-scale periodicity, large-pore phenylene-bridged mesoporous organosilica using triblock

copolymer surfactant [33-36]. Among the functionalized MCM-41 type materials, phenyl sulphonic acid functionalized MCM-41 exhibits better performance than the alkyl sulphonic acid functionalized MCM-41 in the esterification reactions. Using both catalysts, the esterification of glycerol with lauric acid and oleic acid were studied by Sastre and co-workers [24, 29]. Sohn et al. [37] reported a modified silica catalyst with derivatives of benzene-sulfonate groups and studied the catalytic activity in dehydration reactions. In order to establish novel environmentally benign materials, in the present chapter, I report the functionalization of benzyl group loaded mesoporous zirconium hydroxide with various amounts of chlorosulphonic acid without damaging the mesostructure of Zr-TMS. The functionalized materials were characterized by various physico-chemical techniques. The performance of the catalysts was tested in the benzoylation of diphenyl ether and condensation of 2-methylfuran and the results were compared with the SO_4^{2-}/ZrO_2. Further, liquid phase condensation of anisole with p-formaldehyde is also discussed as a catalysts optimization study.

3.2. EXPERIMENTAL

3.2.1. Materials

The syntheses of Zr-TMS-BSA catalysts were carried out using zirconium (IV) butoxide (80 wt % solution in 1-butanol, Aldrich, USA), a 25 wt % aqueous solution of tetramethyl ammonium hydroxide (TMAOH, Loba Chemie, India), a 25 wt % aqueous solution of N-cetyl-N, N, N trimethyl ammonium bromide (CTMABr, Loba Chemie, India), acetyl acetone (acac, 98%, Merck, India), benzyl alcohol (99%, Lancaster, UK) ethoxytrimethylsilane (ETMS, 98%, Sigma-Aldrich, USA) and chlorosulphonic acid (CSA, 98%, Spectrochem, India).

3.2.2. Synthesis of Zr-TMS material

The Zr-TMS was synthesized by adopting the following molar composition,

0.1 $Zr(OC_4H_9)_4$:1.4 BuOH:0.025 CTMABr:0.02 TMAOH:4 H_2O:0.05 Acac:0.5 EtOH

Mesoporous zirconium hydroxide (Zr-TMS) was synthesized by sol-gel route using zirconium (IV) butoxide as the zirconia source and N-Cetyl-N, N, N trimethyl ammonium bromide (CTMABr) as surfactant at a pH of 11.5, which was maintained by tetramethyl ammonium hydroxide (TMAOH) solution. Acetyl acetone (Acac) and ethanol controlled the rate of hydrolysis of zirconium butoxide in water. In a mixture of water (4 mol) and TMAOH (0.03 mol), CTMABr (0.025 mol) was dissolved and stirred for 1 h. Then a mixture of zirconium butoxide (0.1mol), acetyl acetone (0.05mol) and ethanol (0.5mol) were added to the template solution slowly and allowed to stir for 3 h. Further, the mixture was refluxed under stirring for 48 h at 90 °C. The resulting solid was filtered, washed with acetone and dried for 10 h at 100 °C (Step 1 of Scheme 3.1).

3.2.3. Surfactant removal

The solvent extraction method was employed to remove the template from the pores of the mesostructure without destroying the structure of the molecular sieves using ethanol and HCl mixture. The efficiency of the process was confirmed by elemental analysis and powder x-ray diffraction studies. 1 g as-synthesized Zr-TMS was taken and refluxed with a mixture of 100 g of distilled ethanol and 1 g of conc. HCl (36 wt.%) for 6 h, 8 h and 10 h at 80 °C. Fresh samples were used for each extraction. The extracted samples were washed several times with pure distilled ethanol and acetone. The resulting solid was dried at 100 °C for 10 h.

3.2.4. Synthesis of Zr-TMS-BSA catalysts

In the first step, the functionalization of benzyl alcohol (0.1 mol) over Zr-TMS (1g) was carried out by etherification reaction using cyclohexane (0.35 mol) as solvent at 80 °C for 10 h (Step 2 of Scheme 3.1). The sample was filtered and washed with cyclohexane, benzene and finally with acetone and dried for 6 h at 50 °C. To protect the unloaded hydroxyl groups, after modification with benzyl alcohol, desired amount of Zr-TMS-B was degassed at 80 °C for 2 h and dry toluene was

added. Then an excess of ethoxytrimethylsilane was added and the suspension was refluxed at 70 °C under nitrogen atmosphere for 12 h (Step 3 of Scheme 3.1).

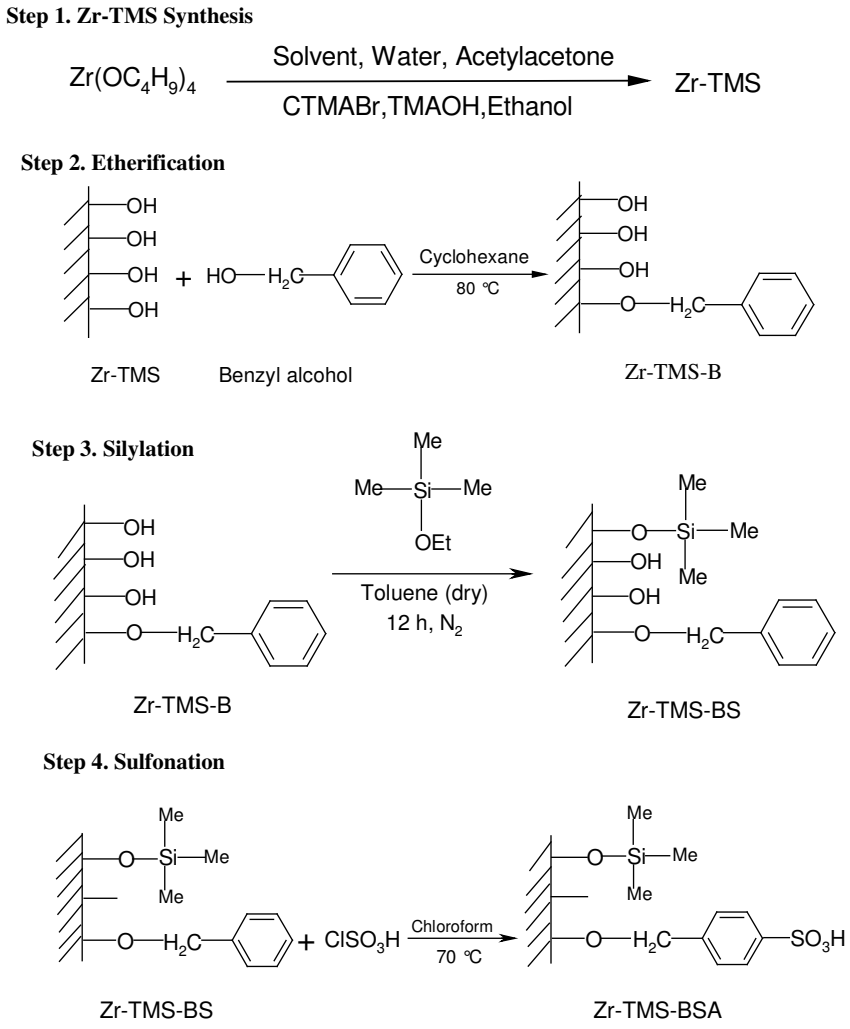

Scheme 3.1. Synthesis of benzylsulfonic acid functionalized Zr-TMS catalysts: 1. Synthesis of Zr-TMS; 2. Etherification of Zr-TMS (Zr-TMS-B); 3. Silylation of Zr-TMS-B (Zr-TMS-BS); 4. Sulfonation of Zr-TMS-BS (Zr-TMS-BSA)

The solid was filtered and soxhlet extraction was done with dichloromethane for 12 h and dried at 50 °C for 5 h. Further, sulphonation of the resulting material, Zr-TMS-BS was done with the appropriate amount of chlorosulphonic acid (Spectrochem, India) using chloroform (0.12 mol) as solvent at 70 °C for 3 h (Step 4

of Scheme 3.1). The chlorosulphonic acid was added slowly sulphonation by a syringe to the mixture of Zr-TMS-BS and chloroform. Thus the material obtained was washed with chloroform and soxhlet extraction was done with a mixture of 1:1 diethyl ether and dichloromethane and dried at 50 °C for 6 h. Benzyl alcohol, ethoxytrimethylsilane and sulphonic acid functionalized Zr-TMS are designated as, Zr-TMS-B, Zr-TMS-BS and Zr-TMS-BSA, respectively.

SO_4^{2-}/ZrO_2 was obtained from MEL Chemicals, Manchester UK and activated at 500 °C for 10 h under static air prior to reaction.

3.2.5. Synthesis of A-Zr-BSA-10 catalyst

Synthesis of BSA functionalized non-porous zirconia catalyst was carried out via the following procedure. A mixture of zirconium (IV) butoxide (0.09 mol) and 1-butanol was taken in a two-necked 250 ml round bottom flask equipped with a magnetic stirrer and a septum. The flask was held at 100 °C and stirred for 10 min. Then required amount of water was added drop-wise into this mixture under stirring to hydrolyze the zirconium (IV) butoxide to $Zr(OH)_4$. Further, after 30 min of stirring, benzyl alcohol (0.01 mol), was added and stirred for 1 h, then methoxy trimethyl silane (MTMS) was added and stirred for another 1 h. Further, chlorosulphonic acid (0.01 mol) was slowly added by syringe and stirring was continued for 2 h. The mixture was cooled, filtered, washed with deionised water, acetone and then dried at 100 °C for 6 h. Soxhlet extraction was carried out for 24 h. Then the sample was dried at 100 °C for 10 h. The synthesized material was white in colour. Functionalized non-porous material is designated as A-Zr-BSA-10.

3.2.6. Catalyst characterization

The synthesized materials were mainly characterized by powder X-ray diffraction (XRD) for phase purity and crystallinity, N_2 adsorption-desorption techniques for specific surface area, total pore volume and average pore diameter, Fourier transform infrared (FTIR) spectroscopy for functional group confirmation,

elemental analysis for C and S to measure the triflic acid loading in the material, temperature programmed desorption (TPD) of NH_3 measurement for total acidity, scanning electron microscopy (SEM) for the particle size and morphology, transmission electron microscopy (TEM) to view the crystalline structure and thermo gravimetric-differential thermal analysis (TG-DTA and DTG) to study the decomposition and thermal stability of the catalysts.

The powder X-ray diffraction patterns of synthesized Zr-TMS, and Zr-TMS-BSA were recorded on a Rigaku Miniflex instrument using Cu K_α radiation (30 kV, 15 mA), λ=1.5404 Å between 1.5 to 60° (2θ) with a scan rate of 4°/min. The BET surface area, total pore volume, and average pore diameter were measured by N_2 adsorption-desorption method by NOVA 1200 (Quantachrome) at –196°C. For this particular measurement, the samples were activated at 100°C for 2 h under vacuum and then the adsorption-desorption was conducted by passing nitrogen onto the sample, which was kept under liquid nitrogen.

The FT-IR spectra were obtained in a range of 400 to 4000 cm^{-1} on a Shimadzu FTIR 8201 PC using a Diffuse Reflectance scanning disc technique. Elemental analysis for C and S were done by EA1108 Elemental Analyzer (Carlo Erba Instruments).

Temperature programmed desorption (TPD) was carried out to determine the total acidity and strength of acid sites on the catalysts using ammonia as an adsorbate [38]. In a typical run, 1.0 g of activated sample was placed in a silica tubular reactor and heated at 200 °C under nitrogen flow of 50-ml min^{-1} for 6 h. The reactor was then cooled at 30 °C and adsorption conducted at that temperature by exposing the sample to ammonia (10 ml min^{-1}) for 30 min. Physically adsorbed ammonia was removed by purging the sample with a nitrogen stream flowing at 50 ml/min for 15 h at 30 °C. The acid strength distribution was obtained by raising the catalyst temperature (10 K min^{-1}) from 30 to 300 °C in a number of steps with the

flow of nitrogen (50 ml min^{-1}). The NH_3 evolved was trapped in the HCl solution and titrated with a standard NaOH solution.

The SEM micrographs of Zr-TMS and Zr-TMS-BSA-10 materials were taken by JEOL-JSM-5200 scanning microscopy. TEM was performed on a JEOL JEM-1200EX instrument with 100 kV of acceleration voltage to probe the mesoporosity of the materials. The TG-DTA and DTG analysis of the Zr-TMS and Zr-TMS-BSA-10 catalysts were carried out with Mettler Toledo 851^e equipment using an alumina pan under a nitrogen (80ml min^{-1}) atmosphere from ambient to 1000°C with the increasing rate of 20°C min^{-1}.

3.2.7. Liquid phase benzoylation of diphenyl ether

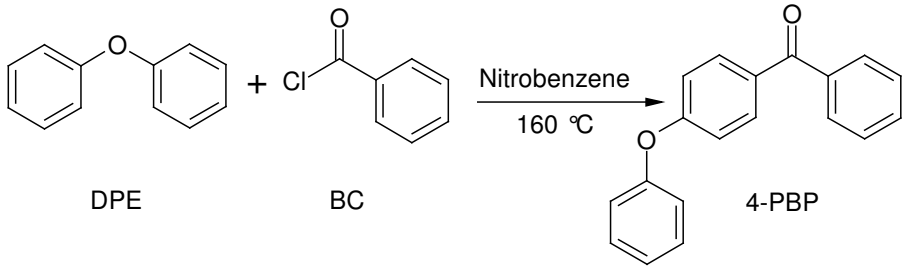

Scheme 3.2. Liquid phase benzoylation of diphenyl ether with benzoyl chloride to 4-phenoxybenzophenone (4-PBP).

Benzoylation of diphenyl ether (DPE) with benzoyl chloride (BC) has been used to study the catalytic performance of the catalysts in a batch reactor using nitrobenzene (NB) as solvent at 160 °C (Scheme 3.2). 1:1 molar ratio (0.01 mol each) of diphenyl ether (S.d. fine-Chem. Ltd, India) and benzoyl chloride (S.d. fine-Chem. Ltd, India) were taken along with nitrobenzene (S.d. fine-Chem. Ltd, India) in a 50 ml two-necked round bottom flask attached to a condenser and a septum. A required amount of activated catalyst (0.5g) was added to the reaction mixture. An oil bath was used to maintain the reaction temperature at 160 °C. The reaction was carried out for 30 min. and the product mixture was analyzed by a gas

chromatograph (HP 6890) equipped with a flame ionization detector (FID) and a capillary column (HP, 5 μm thick cross-linked methyl silicone gum, 0.2mm×50 m). The product was identified by injecting authentic samples in gas-chromatograph and by GC-MS (Shimadzu 2000 A) analysis. The geometry optimization of diphenyl ether has been done by performing a restricted Hartree-Fock (RHF) calculation using a STO-3G basis set. The calculations are done in Gamess US ab-initio quantum chemistry package.

3.2.8. Liquid phase condensation of 2-methylfuran

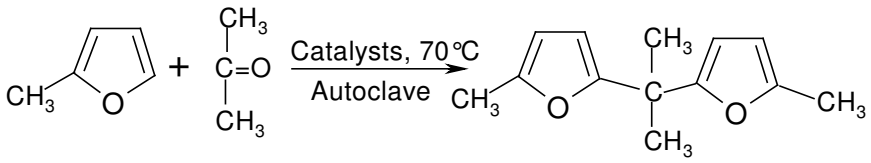

Scheme 3.3. Liquid phase condensation of 2-methylfuran with acetone to 2,2-bis(5-methylfuryl)propane.

In another study, condensation of 2-methylfuran (2-MF) with acetone (AC) has been used to study the catalytic performance of the catalysts in a pressure reactor at 70 °C (Scheme 3.3). 2:1 molar ratio (0.02 mol each) of 2-MF (Aldrich, USA) and acetone (S.d. fine-Chem. Ltd, India) were taken in a 100 ml pressure reactor and the reaction was carried out at ambient pressure circulating cold water. A required amount of activated catalyst (0.1 g) was added to the reaction mixture. The reaction was carried out for 3 h and the product mixture was analyzed by a gas chromatograph (HP 6890) equipped with a flame ionization detector (FID) and a capillary column (HP, 5 μm thick cross-linked methyl silicone gum, 0.2mm×50 m). The product was identified by injecting authentic samples in gas-chromatograph and by GC-MS (Shimadzu 2000 A) analysis. Further, the products were confirmed by ^{1}H and ^{13}C NMR analysis.

3.2.9. Catalysts recycle study

Recycling of the catalyst was done during the condensation of 2-methylfuran reaction by using Zr-TMS-BSA-10. After workup of the reaction, the catalyst was separated by filtration, washed with acetone and dried at 100 ºC for 10 h in the presence of air. Thus, the recovered catalyst after each cycle was characterized for its crystallinity by XRD and its chemical composition by elemental analysis.

3.2.10. Liquid phase condensation of anisole (Catalysts optimization study)

High purity anisole and A.R. grade *p*-HCHO were used without further purification. The catalyst was activated at 100ºC for at least 4 h before use in the experiments, so as to maintain the dry conditions. The liquid phase catalytic condensation was performed in a 50 ml round bottom flask fitted with a condenser, N_2 gas supply tube and a septum. The temperature of the reaction vessel was maintained using an oil bath. In a typical run, a mixture of anisole (0.02 mol), *p*-HCHO (0.01 mol) and activated catalyst (0.1 gm), was magnetically stirred and heated to attain the reaction temperature (100ºC) in the presence of N_2 gas. The product samples were withdrawn at regular intervals of time and analyzed periodically on a gas-chromatograph (Agilent 6890N) equipped with a flame ionization detector and a capillary column (5 μm thick cross-linked methyl silicone gum, 0.2mm x 50 m long). The product samples were also identified by GCMS (Shimadzu 2000 A) analysis. The main product, 4,4'-dimethoxydiphenylmethane was separated by column chromatography and confirmed by ^1H and ^{13}C NMR analysis.

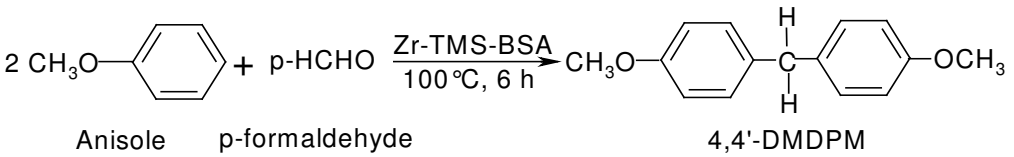

Scheme 3.4. Liquid phase condensation of anisole with *p*-formaldehyde to 4,4'-dimethoxydiphenlymethane (4,4'-DMDPM).

Conversion of anisole is defined as the weight percentage of anisole consumed. The turnover rates for anisole conversion (TOF, $h^{-1}mol^{-1}S$) were calculated as the mol of anisole converted per hour over per mol of sulfur. The selectivity to a product is expressed as the amount of a particular product divided by the amount of total products and multiplied by 100.

The main product of our interest, 4,4'-dimethoxydiphenylmethane has been identified by GC, GC-MS, ^{1}H and ^{13}C liquid state nuclear magnetic resonance techniques. GC gave three disguisable product peaks with one prominent peak. The GC-MS gave the molecular weight of dimethoxydiphenlymethane. Further, the main product (4,4'-DMDPM) has been separated by column chromatography and analyzed by ^{1}H and ^{13}C NMR. ^{13}C NMR ($CDCl_3$, adamantane) δ 40.08 ($-CH_2$), 55.18 ($-OCH_3$), 133.68 (1), 157.89 (4), 113.82 (2, 6), 129.68 (3, 5). ^{1}H NMR ($CDCl_3$, TMS) δ 3.78 (S, 6H), 3.87 (S, 2H), 6.83 (D, J=8Hz, 2H), 7.10 (D, J=8Hz, 2H).

3.3. RESULTS AND DISCUSSION

3.3.1. Synthesis of catalysts

In order to immobilize the catalytically active species on a heterogeneous solid surface, an organic linker group is needed. Organic functionalization of the internal surfaces of any mesoporous materials can be achieved, either by covalently grafting of various organic species onto the surface or by incorporating of functionalities directly during the synthesis. Zr-TMS material has been synthesized by the procedure given in experimental part and obtained dry material before functionalization. For functionalization of BSA over Zr-TMS, two different methods were adopted and based on our preliminary instrumental techniques; the procedure given in experimental part was found suitable for the preparation of proposed Zr-TMS-BSA catalysts.

Five samples of BSA functionalized Zr-TMS (denoted as Zr-TMS-BSA-5, -10, -15, -20, and -25 wt %) were prepared and their compositions are listed in Table 3.1

and the generalized synthesis scheme of Zr-TMS-BSA is given in Scheme 3.1. Zr-TMS material (Step 1 of Scheme 3.1.) was treated with was treated with benzyl alcohol to get Zr-TMS-BZ material having the Equation 2 of Scheme 3.1. Further, Zr-TMS-B was treated with ethoxytrimethylsilane to get Zr-TMS-BS having the Step 3 of Scheme 3.1 and sulfonation was chlorosulfonic acid to get benzylsulfonic acid functionalized Zr-TMS catalyst having the Step 4 of Scheme 3.1. Five different loading of BSA, such as 5, 10, 20, and 25 wt % over Zr-TMS was done and designated as Zr-TMS-BSA-5, Zr-TMS-BSA-10, Zr-TMS-BSA-20, and Zr-TMS-BSA-25, respectively; where as the effective loading is tabulated in Table 3.1, based on the sulfur concentration by elemental analysis of sulfur.

The amorphous zirconia functionalized with BSA was also synthesized with 10 wt% loading of BSA and designated as A-Zr-BSA-10 catalyst.

Table 3.1. Physico-chemical properties of Zr-TMS, Zr-TMS-BS, Zr-TMS-BSA and sulfated zirconia catalysts.

Catalyst	Elemental Analysis (Output) [a] (Wt %)		Loading of sulphonic acid (Wt %)		BET surface area (m^2g^{-1})[b]	NH_3 desorbed (mmol/g)				NH_3 Chemisorbed at 30 °C (mmol/g)[c]
	C	S	input	output		30-70°C	70-110°C	110-150°C	150-200°C	
Zr-TMS[d]	--	--	--	--	370	0.06	0.15	0.19	0.10	0.50
Zr-TMS-BS	--	--	--	--	308	--	--	--	--	--
Zr-TMS-BSA-5[e]	2.9	2.0	5	4.7	229	0.11	0.26	0.31	0.04	0.72
Zr-TMS-BSA-10[f]	1.6	2.5	10	9.1	198	0.23	0.38	0.41	0.17	1.19
Zr-TMS-BSA-15	1.1	2.8	15	10.3	179	0.22	0.39	0.43	0.18	1.22
Zr-TMS-BSA-20	0.9	3.2	20	11.6	158	0.25	0.40	0.46	0.20	1.31
Zr-TMS-BSA-25	0.7	3.3	25	12.0	98	0.25	0.41	0.48	0.20	1.34
A-Zr-BSA-10[h]	1.7	2.6	10	9.3	49	0.24	0.38	0.42	0.19	1.23
SO_4^{2-}/ZrO_2[i]	--	2.6	10	7.9	101	--	--	--	--	1.45[h]

[a]Measured by EA 1108 CHN/S Elemental analyzer to measure the acid loading.
[b]Measured by N_2 adsorption-desorption at –196 °C.
[c]Total acid sites determined in the solid catalyst by NH_3 adsorption-desorption from 30 to 200 °C
[d]Total pore volume is 0.31 cm^3g^{-1}, average pore diameter is 30.9 Å for Zr-TMS.
[e]Numbers denote wt% (input) of sulphonic acid loading over Zr-TMS-BS.
[f]Total pore volume is 0.18 cm^3g^{-1}, average pore diameter is 18.2 Å for Zr-TMS-BSA-10.
[g]Total pore volume is 0.09 cm^3g^{-1}, average pore diameter is 4 Å for SO_4^{2-}/ZrO_2.
[h]A denotes amorphous
[i]Ammonia desorbed from 30 to 500 °C in six steps.

3.3.2. Template extraction optimization by XRD

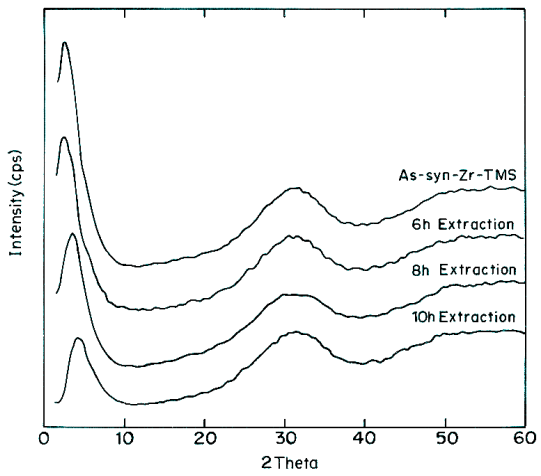

Figure 3.1. Powder X-ray diffraction pattern of Zr-TMS with respect to template extraction time As-syn-Zr-TMS, 6 h, 8 h, and 10 h.

Figure 3.1 shows the powder XRD pattern of as-synthesized Zr-TMS and different time of extraction (such as 6 h, 8 h and 10 h) to remove the template from the synthesized Zr-TMS for establishing the time of extraction without destroying the mesoporous structure. All spectra show a sharp peak at low 2θ (2°- 4°) range, which is characteristic of ordered porous structure of Zr-TMS [39-43], and two broad peaks at 30° (broad) and 50° (small), which are attributed to the amorphous nature of $Zr(OH)_4$ which can also be detected in the siliceous MCM-41 material [44]. Further, when it is calcined above 600 °C it may give sharp and intense peaks characteristic of tetragonal, monoclinic and cubic phases of ZrO_2, which are not shown here. The intensity of mesophase decreases with the increase in time of extraction. The decrease in intensity of Zr-TMS with the increase in time of extraction is attributed to the partial structure damage of Zr-TMS. The surface area of these samples, 6 h, 8 h and 10 h (Figure 3.1) was found to be 341, 370 and 364 $m^2 g^{-1}$, respectively. The surface area measurement revealed that after 6 h of extraction, the sample was

partially extracted. Though the 8 h and 10 h samples did not show much difference in surface area but the XRD intensity of 10 h sample decreased (Figure 3.1) indicating that there is structure damage to some extent and hence it is clear that 8 h extraction is the optimum time for removal of template from the synthesized material.

3.3.3. Influence of time of $ClSO_3H$ loading by XRD

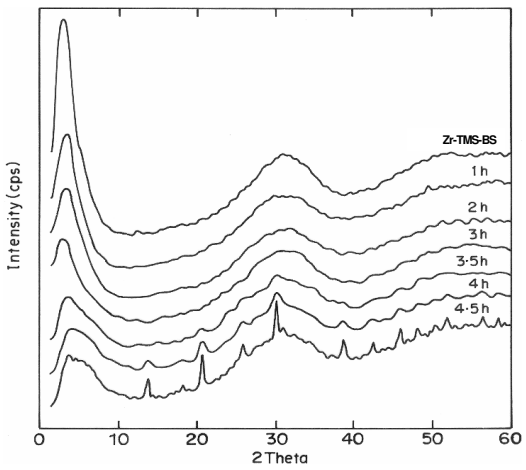

Figure 3.2. Powder XRD pattern of standardization of $ClSO_3H$ functionalization over Zr-TMS-BS material with respect to time.

The influence of time of chlorosulphonic acid functionalization on the mesoporous nature of Zr-TMS-BSA catalyst is shown in Figure 3.2 (Zr-TMS-BS, 1 h, 2 h, 3 h, 3.5 h, 4 h and 4.5 h). 10 wt% chlorosulphonic acid was used over Zr-TMS-BS to optimize the time without the structure collapse. The intensity of the mesophase in all the samples at low 2θ range (characteristic for mesoporous material) decreases with the increase in functionalization time, which showed that there was slow decay of mesoporous nature. Further, XRD pattern shows that after 3 h of reflux time extra peaks were noticed, which may be the prominent phases of zirconia, such as tetragonal, monoclinic and cubic. The intensity of these peaks increased with the increase in reflux time (Figure 3.2, 4 h and 4.5 h), which revealed that there was fast crystallization and consequently severe structure damage of the

material. The surface area of Zr-TMS-BS, 1 h, 2 h, 3 h, 3.5 h, 4 h and 4.5 h samples were found to be 308, 287, 229, 215, 201, 181 and 172 $m^2 g^{-1}$, respectively. The decrease in surface area may be attributed to the loading of $–SO_3H$ group over Zr-TMS-BS and a decrease in meso-phase of Zr-TMS-BS may be due to the formation of HCl as by product during functionalization, which destroys the mesoporous structure to some extent. It is clear from these data that time of functionalization cannot be extended beyond 3 h at our experimental condition to get optimum concentration of sulphonic acid over Zr-TMS-BS.

3.3.4. Influence of concentration of sulphonic acid by XRD

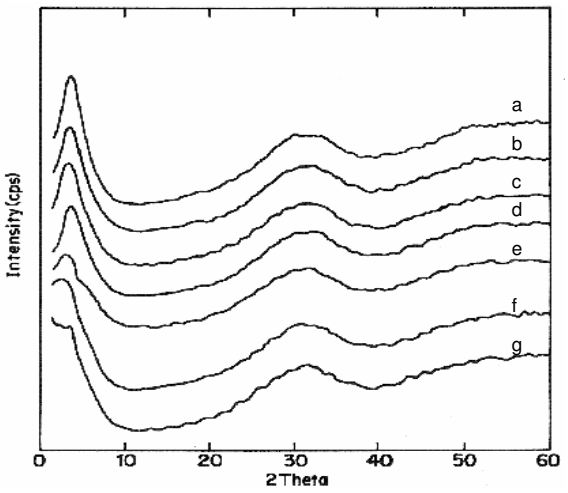

Figure 3.3. Powder XRD patterns of Zr-TMS, Zr-TMS-BS and different loadings of sulphonic acid over Zr-TMS-BS material. a. Zr-TMS, b. Zr-TMS-BS, c. Zr-TMS-BSA-5, d. Zr-TMS-BSA-10, e. Zr-TMS-BSA-15, f. Zr-TMS-BSA-20, and g. Zr-TMS-BSA-25 catalysts.

Figure 3.3 illustrates Zr-TMS, Zr-TMS-BS and the influence of $ClSO_3H$ concentration over Zr-TMS-BS (Zr-TMS-BSA-5, -10, -15, -20 and –25). The functionalization of Zr-TMS-BS by $ClSO_3H$ was done by varying the concentration of $ClSO_3H$ and keeping the functionalization time at 3 h. Various loading of sulphonic acid over Zr-TMS-BS such as 5, 10, 15, 20 and 25 wt % (input) was done and found

to be 4.7, 9.1, 10.3, 11.6 and 12 wt % (output) of SO_3H over Zr-TMS-BS, respectively (see Table 3.1, elemental analysis). The crystallinity of the sulphonic acid containing Zr-TMS-B materials decreased as the chlorosulphonic acid loading increased. Moreover, once the concentration of chlorosulphonic acid was increased >15 wt% (see Figure 3.3) the mesophase started to vanish and it was observed that at higher loading (25 wt %, Zr-TMS-BSA-25) the structure was completely destroyed. The surface areas of Zr-TMS, Zr-TMS-BS, Zr-TMS-BSA-5, Zr-TMS-BSA-10, Zr-TMS-BSA-15, Zr-TMS-BSA-20, and Zr-TMS-BSA-25 were found to be 370, 308, 229, 198, 179, 158 and 98 $m^2 g^{-1}$, respectively (Table 3.1). A decrease in surface area of Zr-TMS-BSA may be attributed to the sulphonic acid loading and due to the formation of HCl as by product during functionalization. The above results demonstrate that the Zr-TMS-BS can accommodate a maximum of 9.1 wt% of sulphonic acid at our experimental condition without destroying the mesostructure.

3.3.5. Nitrogen adsorption-desorption study

Incorporation or anchoring of any medium (acid or base) or metal in the framework positions and/or into the walls of the supporting medium leads to a progressive decrease in surface area [45, 46]. The BET surface areas of the Zr-TMS, Zr-TMS-BS, Zr-TMS-BSA, and SO_4^{2-}/ZrO_2 are given in Table 3.1. The surface area for the Zr-TMS was 370 $m^2 g^{-1}$, which is comparable to that measured previously for a Zr-TMS synthesized using a surfactant with C_{16} carbon chain [45]. The surface area gradually decreased with increasing sulphonic acid loading.

Figure 3.4 A, B and C show the nitrogen adsorption-desorption isotherm of Zr-TMS, Zr-TMS-BS and Zr-TMS-BSA-10 (10 represents the input concentration of sulphonic acid over Zr-TMS-BS), respectively. All the three isotherms are of type IV characteristic of mesoporous materials. Position of inflection of Zr-TMS-BSA-10 shows that there is structure damage in the materials. However, pore size distribution analysis indicates that mesoporosity was not lost.

Figure 3.5 A, B and C shows the BJH pore size distribution curves of Zr-TMS, Zr-TMS-BS and Zr-TMS-BSA-10. The surface area, total pore volume and average pore diameter of the Zr-TMS, Zr-TMS-BS and Zr-TMS-BSA-10 were found to be 370 m^2g^{-1}, 0.31cm^3 g^{-1}, 30.9 Å; 308 cm^2g^{-1}, 0.28 cm^3g^{-1}, 26.4 Å and 198 m^2g^{-1}, 0.18cm^3g^{-1} 18.2 Å, respectively (Table 3.1). The surface area of amorphous zirconia functionalized with BSA is found to be 49 m^2g^{-1}. These results demonstrate that the surface area, pore volume and pore diameter of the functionalized materials decrease [45,46] due to the anchoring of benzyl group over Zr-TMS and further functionalization of Zr-TMS-BS with $ClSO_3H$. The surface area, pore volume and average pore diameter of SO_4^{2-}/ZrO_2 are found to be 101 m^2g^{-1}, 0.09 cm^3g^{-1} and 9Å (Table 3.1), respectively, which shows that this material is not suitable for this particular reaction (benzoylation of diphenyl ether) because of the bulky nature of the product 4-PBP.

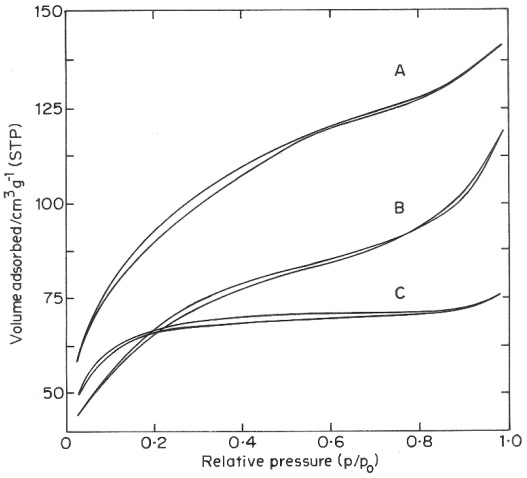

Figure 3.4. N_2 adsorption-desorption isotherms of (A) Zr-TMS, (B) Zr-TMS-BS and (C) Zr-TMS-BSA-10 samples.

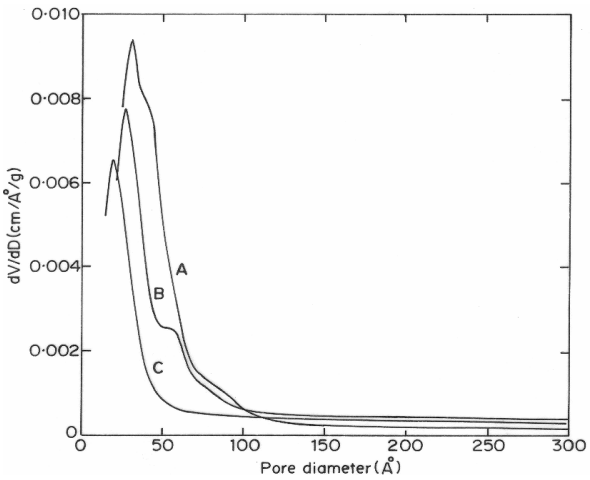

Figure 3.5. *BJH* pore size distributions of (A) Zr-TMS, (B) Zr-TMS-BS and (C) Zr-TMS-BSA-10 samples.

3.3.6. FT-Infrared spectroscopy study

The infrared spectra of as-synthesized-Zr-TMS, Zr-TMS and Zr-TMS-BS are shown in Figure 3.6. In all the spectra a weak unresolved band between 900-750 cm^{-1} is attributed to Zr-O stretching vibrations [39]. A broad band between 3400 to 3650 cm^{-1} corresponds to the O-H stretching vibration in $Zr(OH)_4$ and a sharp band between 1650-1600 cm^{-1} is due to the bending vibrations of surface O-H groups and water molecules occluded in the pores [39]. In addition to the above bands, the as-synthesized-Zr-TMS shows the additional weak bands at around 3200-2800 cm^{-1} and 1500-1300 cm^{-1} which are due to the C-H stretching and bending vibrations [47] of methylene group of template material. These bands are absent in the template extracted Zr-TMS, which shows that the template removal by ethanol and HCl mixture is complete and successful. After loading of benzyl alcohol over Zr-TMS (Zr-TMS-BS or -Zr-O-CH_2-Φ), the weak bands at around 3200-2800 cm^{-1} and 1500-1300 cm^{-1} are due to the C-H stretching and bending vibrations of methylene group as discussed earlier and a medium band at 1423 cm^{-1} indicates the C=C stretching in-plane vibration of benzene framework [47]. A band at 707cm^{-1} represents the C-H

bending vibration of methylene group of benzene [47]. A small and weak band at around 1000-1200 cm^{-1} is the characteristic band of C-O group in the catalyst.

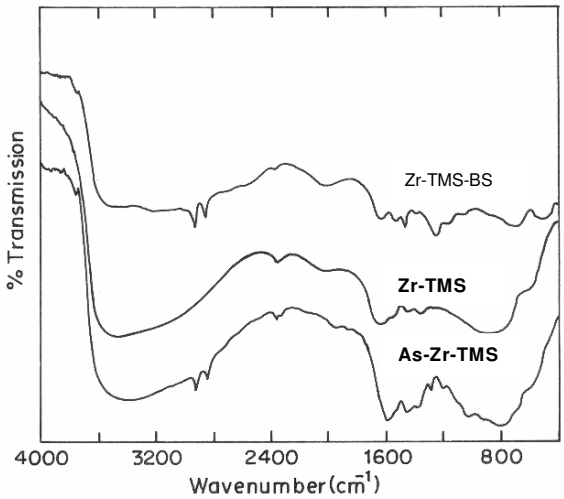

Figure 3.6. Fourier transform infrared spectrum of As-syn-Zr-TMS, Zr-TMS and Zr-TMS-BS material.

The FT-IR spectra of two loadings (5 and 10 wt % $ClSO_3H$) of sulphonic acid functionalized Zr-TMS-BS (Zr-TMS-BSA-5 and Zr-TMS-BSA-10) are shown in Figure 3.7. A small and intense band at 1298 cm^{-1} and the medium band at 1185 cm^{-1}, are due to S=O stretching mode of incorporated sulphonic acid [48]. The C-S link also gives a medium band between 600-700 cm^{-1} and the intensity is increased with the increase in acid loading. Further, it is noticed that the intensity of the stretching and bending modes of –C-H group remained unchanged in Zr-TMS-BS, Zr-TMS-BSA-5 and Zr-TMS-BSA-10 with the increase in sulphonic acid loading, which shows that the attachment of $–SO_3H$ is on the benzene ring. These observations confirm the successful anchoring of benzyl group over Zr-TMS to Zr-TMS-BS and its functionalization with $ClSO_3H$ to Zr-TMS-BSA.

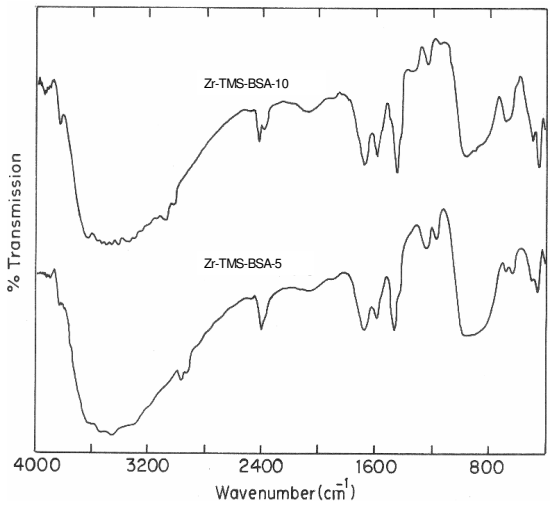

Figure 3.7. Fourier transform-infrared spectra of Zr-TMS-BSA-5 and Zr-TMS-BSA-10 catalysts.

3.3.7. Ammonia adsorption-desorption study

Temperature programmed desorption (TPD) of ammonia was performed for measuring the total acidity (acid sites) of the synthesized materials [38 and references therein]. The results of the step wise desorption of ammonia of Zr-TMS, Zr-TMS-BSA, and SO_4^{2-}/ZrO_2 are presented in Table 3.1. The values of acidity for Zr-TMS and functionalized Zr-TMS were obtained by desorbing ammonia in four stages from 30 to 200 °C (between 30 – 70 °C, 70 –110 °C, 110 –150 °C and 150 – 200 °C). Since the functionalized material is covalently bonded to the solid support, it could not be treated above 200 °C, which is evidenced by thermal analysis (shown below). Above this temperature benzyl sulphonic acid is lost from the solid support. Whereas, the ammonia was desorbed from SO_4^{2-}/ZrO_2 in six stages between 30 and 500 °C.

The results reveal that the total acidity and the acid site distribution are dependent on the type of catalyst and are strongly influenced by the amount of sulphonic acid loading over Zr-TMS-B. The total acidity of Zr-TMS, Zr-TMS-BSA-5, Zr-TMS-BSA-10, Zr-TMS-BSA-15, Zr-TMS-BSA-20 and Zr-TMS-BSA-25 are found to be 0.50, 0.72, 1.19, 1.22, 1.31 and 1.34 mmol g^{-1}, respectively (Table 3.1). These values are in agreement with the output of the elemental analysis result shown in

Table 3.1, where the total acidity of the material is increased with respect to the loading of sulphonic acid over Zr-TMS-B. Further, the total acidity of SO_4^{2-}/ZrO_2 was measured in six stages and found to be 1.45 mmol g^{-1}. These results demonstrate that the functionalization of benzyl group loaded Zr-TMS with sulphonic acid enhances the acidity of the material and consequently the conversion of diphenyl ether to 4-phenoxybenzophenone and condensation of 2-methylfuran to 2,2-bis(5-methylfuryl)propane.

3.3.8. Scanning electron microscopic study

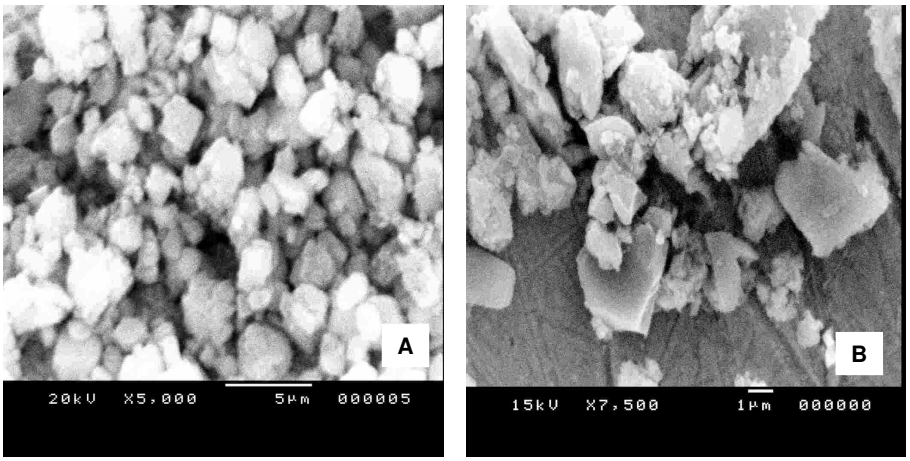

Figure 3.8. Scanning electron micrograph of (A) Zr-TMS, and (B) Zr-TMS-BSA-10 samples.

The particle size and morphology of Zr-TMS, and Zr-TMS-BSA-10 were studied by scanning electron microscopy technique. Support materials and the hydrolysis products associated with the support materials can control the morphology of mesoporous materials. The SEM micrograph of Zr-TMS (Figure 3.8A) shows clear ordered material with relatively uniform particle size (0.37µm). It is also observed that distorted hexagonal structure in the materials. Distorted, hard hexagonal and square like structure of Zr-TMS can be synthesized using the cationic surfactant CTMABr under basic condition. Thee explanations are in well agreement with the

earlier report for SBA-15 material [49]. It is noteworthy that previous authors have reported mesoporous zirconia to be very disordered [50], which is the case with our material also. It appears that functionalization alters the morphology and particle size of the material to a greater extent (Figure 3.8B). This decrease in ordering and crystallinity was also observed and clearly explained by XRD technique.

3.3.9. Transmission electron microscopic study

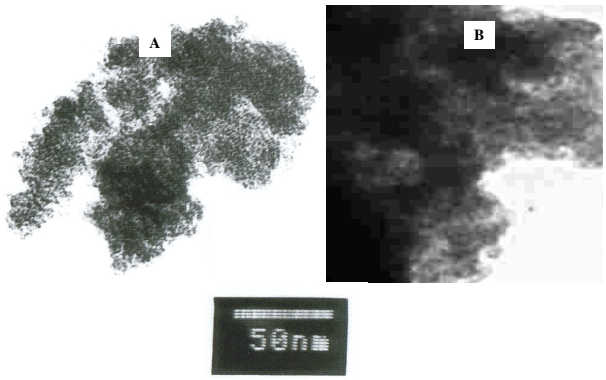

Figure 3.9. Transmission electron micrographs of (A) Zr-TMS, and (B) Zr-TMS-BSA-10 samples.

The samples were prepared for TEM analysis by dispersing the powder products as slurry in iso-propanol and subsequently deposited and dried on a honey carbon film on a copper grid. Transmission electron micrographs of Zr-TMS (Figure 3.9A), and Zr-TMS-BSA-10 (Figure 3.9B) reveal that these materials have a either disordered hexagonal and square planar structures. On the whole, the pores seemed to be packed together with no visible long-range order, consistent with the absence of low-angle XRD peaks. Its square like (or sponge like) pore morphology is characteristic of zirconia aerogels [14, 51]. Both Zr-TMS, and Zr-TMS-BSA-10 mesostructure contained a mixture of highly distorted hexagonal and square like regions and only the visibility of square like regions goes dark after functionalization (Figure. 3.9B).

3.3.10. Liquid phase benzoylation of diphenyl ether

Table 3.2. Liquid phase benzoylation of diphenyl ether with benzoyl chloride using Zr-TMS, Zr-TMS-BSA, A-Zr-BSA-10 and sulfated zirconia catalysts[a]

Catalysts	Conversion of DPE (wt %)	TOF[b] ($S^{-1}mol^{-1}S$)	Product selectivity to 4-PBP (wt %)[c]
Zr-TMS	11.7	--	100
Zr-TMS-BSA-5	33.7	21.5	100
Zr-TMS-BSA-10	57.5	29.4	100
Zr-TMS-BSA-15	60.1	27.5	97
Zr-TMS-BSA-20	57.0	22.8	81
Zr-TMS-BSA-25	52.4	20.2	75
A-Zr-BSA-10	53.0	26.1	72
SO_4^{2-}/ZrO_2	4.6	2.3	100

[a]Reaction conditions: diphenyl ether (mol) = 0.01; Benzoyl chloride (mol) = 0.01; Nitrobenzene (ml) = 20; Catalyst (g) = 0.5; Reaction time (h) = 0.5; Reaction temperature (°C) = 160.
[b]TOF is calculated as the number of moles of DPE converted per mol of sulfur per second.
[c]4-PBP= 4-phenoxybenzophenone.

Under similar reaction conditions, the Zr-TMS-BSA catalysts were more active than Zr-TMS, A-Zr-BSA-10 and SO_4^{2-}/ZrO_2. The less activity of Zr-TMS (11.7 wt %) and SO_4^{2-}/ZrO_2 (4.6 wt %) are due to the limited number of acid sites and non-availability of mesoporous nature, respectively. The geometry size of diphenyl ether was found to be 8.99 Å (horizontal), which clearly shows that the diffusion of product either from the pores or the interlayer distance of SO_4^{2-}/ZrO_2 is not easy. As evidenced from Figure 3.3, (more than 10 wt % sulphonic acid loading over Zr-TMS-BS leads to severe structure collapse) only two functionalized catalysts, Zr-TMS-BSA-5 and –10 were performed well in the reaction and the results are presented in Table 3.2. The Zr-TMS-BSA-5 and –10 gave the DPE conversion of 33.7 and 57.5 wt %, respectively, with 100 wt% selectivity to 4-PBP. The increase in DPE conversion is attributed to the increase in sulphonic acid loading over Zr-TMS-BS. Further, remaining three catalysts showed less conversion and very poor selectivity because of severe structure collapse. The activity and selectivity of Zr-TMS-BSA-10 (57.5 wt %) were found to be higher than that of A-Zr-BSA-10 (53 wt %), which shows that

high surface area and narrow pore size are essential of this reaction. Turn over frequency (TOF, $S^{-1}mol^{-1}S$) for all the catalysts are calculated as the number of moles of DPE converted per mol of sulfur per second. TOF for Zr-TMS-BSA-5, Zr-TMS-BSA-10, Zr-TMS-BSA-15, Zr-TMS-BSA-20, Zr-TMS-BSA-25, A-Zr-BSA-10 and SO_4^{2-}/ZrO_2 are found to be 21.5, 29.4, 27.5, 22.8, 20.2, 26.1 and 2.3 × $S^{-1}mol^{-1}S$, respectively. All these results demonstrate that the substrate needs acidic catalyst with well-defined mesoporous structure for enhanced activity.

3.3.11. Liquid phase condensation of 2-methylfuran

Table 3.3. Liquid phase condensation of 2-methylfuran with acetone using Zr-TMS, Zr-TMS-BSA, A-Zr-BSA-10 and sulfated zirconia catalysts[a]

Catalysts	Conversion of DPE (wt %)	TOF[b] ($h^{-1}mol^{-1}S$)	Product selectivity to BMP (wt %)[c]
Zr-TMS	6.2	--	100
Zr-TMS-BSA-5	13.2	13.5	100
Zr-TMS-BSA-10	40.5	34.2	100
Zr-TMS-BSA-15	44.7	34.1	98
Zr-TMS-BSA-20	46.0	28.2	92
Zr-TMS-BSA-25	40.5	26.2	81
A-Zr-BSA-10	37.2	30.5	76
SO_4^{2-}/ZrO_2	18.0	14.8	100

[a]Reaction conditions: 2-methylfuran (mol) = 0.02; acetone (mol) = 0.01 (excess used); Catalyst (g) = 0.1; Reaction time (h) = 3; Reaction temperature (℃) = 70.
[b]TOF is calculated as the number of moles of 2-MF converted per mol of sulfur per hour.
[c]BMP-2,2-bis(5-methylfuryl)propane

Condensation of 2-MF with acetone was by various researchers [25, 26] also performed and found the superiority of the catalysts. Under similar reaction conditions, the Zr-TMS-BSA catalysts were more active than Zr-TMS and SO_4^{2-}/ZrO_2. The poor activity of Zr-TMS (6.2 wt %) and SO_4^{2-}/ZrO_2 (18 wt %) are due to the limited number of acid sites and non-availability of mesoporous nature, respectively. Once again, as evidenced from Figure 3.3, (more than 10 wt% sulphonic acid loading over Zr-TMS-BS leads to severe structure collapse) only two functionalized catalysts, Zr-TMS-BSA-5 and –10 were show good conversion of 2-MF with 100 wt % selectivity and the results are presented in Table 3.3. The Zr-TMS-BSA-5 and –10

gave the 2-MF conversion of 13.2 and 40.5 wt %, respectively, with 100 wt % selectivity to BMP. The increase in 2-MF conversion is attributed to the increase in sulphonic acid loading over Zr-TMS-BS. Further, remaining three catalysts showed considerable conversion but very poor selectivity because of severe structure collapse. The activity and selectivity of Zr-TMS-BSA-10 (40.5 wt %) were found to be higher than that of A-Zr-BSA-10 (37.2 wt %), which shows that high surface area and narrow pore size are essential of this reaction. Turn over frequency (TOF, $h^{-1}mol^{-1}S$) for all the catalysts are calculated as the number of moles of 2-MF converted per mol of sulfur per hour. TOF for Zr-TMS-BSA-5, Zr-TMS-BSA-10, Zr-TMS-BSA-15, Zr-TMS-BSA-20, Zr-TMS-BSA-25 and SO_4^{2-}/ZrO_2 are found to be 13.5, 34.2, 34.1, 28.2, 26.2, 30.5 and 14.8 × $h^{-1}mol^{-1}S$, respectively. All these results demonstrate that the substrate needs acidic catalyst with well-defined mesoporous structure for enhanced activity.

3.3.12. Catalyst recycle study

Table 3.4. Catalyst recycle study by Zr-TMS-BSA-10 in condensation of 2-methylfuran with acetone reaction[a]

Cycle	Elemental analysis[b] (wt %)		Conversion of 2-MF (wt %)	TOF[c] (h^{-1} $mol^{-1}S$)[c]	Selectivity to BMP[d] (wt %)
	C	S			
Fresh	1.6	2.5	40.5	34.2	100
First recycle	1.6	2.4	40.0	35.5	100
Second recycle	1.2	2.1	34.0	34.7	98

[a]Reaction conditions: 2-methylfuran (mol) = 0.02; acetone (mol) = 0.01 (excess used); catalyst (g) = 0.1; Reaction time (h) = 3; Reaction temperature (°C) = 70.
[b]Measured by elemental analyzer
[c]TOF is calculated as the number of moles of 2-MF converted per mol of sulfur per hour.
[d]BMP-2,2-bis(5-methylfuryl)propane

Recycle of the synthesized catalysts was studied in the condensation reaction using Zr-TMS-BSA-10 in order to check the stability and recycled catalysts' activity (Table 3.4). Three reaction cycles (fresh and two recycles) were carried out under

similar reaction conditions, using the same catalyst. Elemental analysis (Table 3.4) and XRD analysis (not shown) showed that both sulphur content and catalyst crystallinity decreased after each cycle. The conversion of 2-MF decreased to some extent on recycling (from 40.5 to 34 wt %), whereas, the selectivity to BMP did change very little. The loss of sulfur and the decrease in the crystallinity of the catalyst were the likely causes of the decrease in catalytic activity.

3.3.13. Liquid phase condensation of anisole (Catalysts optimization study)

3.3.13.1. Catalytic activity of various catalysts

The results of the catalytic activities in the condensation of anisole with *p*-HCHO using conventional catalyst *p*-TSA, commercial ZrO_2/SO_4^{2-}, synthesized Zr-TMS and various amounts of benzylsulfonic acid anchored over Zr-TMS (Zr-TMS-BSA) catalysts are depicted in Table 3.5. The main product of the reaction is 4,4'-DMDPM. A considerable amount of 2,4'-DMDPM and a small amount of 2,2'-DMDPM are also observed over Zr-TMS and Zr-TMS-BSA catalysts. But with sulfated zirconia and *p*-TSA, considerable amount of other products are also observed which were not identified and may be polymerized products which are formed due to their strong acidic nature. The formation of DMDPM results from the aromatic substitution of anisole. The activities of various catalysts are compared under identical reaction conditions using data after 6 h run.

The conversion of anisole, rate of anisole conversion, product distribution and ratio of 4,4'-DMDPM to 2,2'-DMDPM depend on the type of catalysts used. As can be seen from the Table 3.5, Zr-TMS-BSA-15 catalyst is found to be more active than any other catalysts. Zr-TMS is less active due to its lower acidic nature. The conversion of anisole, rate of anisole conversion, selectivity for 4,4'-DMDPM and 4,4'-DMDPM/2,2'-DMDPM ratio over Zr-TMS-BSA-5, Zr-TMS-BSA-10, Zr-TMS-BSA-15 and Zr-TMS after 6 h of reaction time are found to be 12.6, 28.2, 43.9, 2.0 wt %; 6.7, 12.0, 16.7 $h^{-1}mol^{-1}S$; 75.1, 78.6, 78.2, 82.0 wt % and 20.3, 28.1, 29.2, 27.3,

respectively. P-TSA and sulfated zirconia produce 35.4, 61.1 wt% (conversion of anisole), 429.4, 25.1 $h^{-1}mol^{-1}S$ (TOF), 69.7, 68.7 wt % (selectivity for 4,4'-DMDPM), and 9.3, 10.1 (4,4'-DMDPM/2,2'-DMDPM ratio), respectively. Amongst the Zr-TMS-BSA-5, -10, -15, Zr-TMS-BSA-15 revealed the highest anisole conversion and rate of anisole conversion, which may be attributed to its higher acidity as seen from NH_3 desorption experiment (Table 3.1). The catalysts used in this study, show the following decreasing order of activity after 6 h of reaction time: ZrO_2/SO_4^{2-} > Zr-TMS-BSA-15 > *p*-TSA > Zr-TMS-BSA-10 > Zr-TMS-BSA-5 > Zr-TMS. Whereas the selectivity to 4,4'-DMDPM is in the order of Zr-TMS > Zr-TMS-BSA-10 > Zr-TMS-BSA-15 > Zr-TMS-BSA-5 > *p*-TSA > ZrO_2/SO_4^{2-}. The results indicate that mainly para- substitutions take place over Zr-TMS-BSA catalyst. The molecular size of 4,4'-DMDPM, 2,4'-DMDPM and 2,2'-DMDPM were found to be 12.40979, 10.65782 and 9.22677 Å (horizontal), respectively, which clearly show that the diffusion of products from pores of various Zr-TMS catalysts is highly possible and hindered from the pores or the interlayer distance of sulfated zirconia catalyst, which further shows that in sulfated zirconia, catalysis takes place on the surface.

Table 3.5. Catalytic activity of various catalysts in condensation of anisole reaction[a]

Catalysts	Conversion of anisole (wt %)	TOF[b] ($h^{-1}mol^{-1}S$)	Product distribution (wt %)[c]				4,4'-/ 2,2'-DADPM ratio[d]
			4,4'-DMDPM	2,4'-DMDPM	2,2'-DMDPM	Others	
Zr-TMS	2.00	--	82.0	15.0	3.0	0	21.16
Zr-TMS-BSA-5	12.62	6.73	75.0	21.24	3.76	0	19.94
Zr-TMS-BSA-10	28.20	12.03	78.53	18.60	2.85	0	27.55
Zr-TMS-BSA-15	43.96	16.74	78.18	19.14	2.68	0	29.17
p-TSA[e]	35.40	429.4	69.7	14.7	7.5	8.1	9.29
SO_4^{2-}/ZrO_2	61.10	25.06	68.7	23.5	3.1	4.7	22.16

[a]Reaction conditions: Catalyst (g) = 0.1; Anisole (mmol) = 20; *p*-HCHO (mmol) =10; Reaction temperature (°C) = 100; Reaction time (h) = 6.
[b]TOF = moles of anisole transformed per hour per mol of sulfur.
[c]4,4'-DMDPM = 4,4'-dimethoxydiphenylmethane; 2,4'-DMDPM = 2,4'-dimethoxydiphenylmethane; 2,2'-DMDPM = 2,2'-dimethoxydiphenylmethane.
[d]Ratio of 4,4'-dimethoxydiphenylmethane / 2,2'-dimethoxydiphenylmethane.
[e]Amount of catalyst used (g) = 0.01.

3.3.13.2. Influence of reaction time using Zr-TMS-BSA-10

The influence of reaction time on the conversion of anisole, rate of anisole conversion, product distribution and 4,4'-DMDPM/2,2'-DMDPM ratio using Zr-TMS-BSA-10 as catalyst at 100°C is presented in Figure 3.10. The conversion of anisole increased almost linearly up to 12 h of reaction time and then a marginal increase in the conversion of anisole is observed at 24 h of reaction time. The anisole along with p-HCHO leads mainly to 4,4'-DMDPM with 79.8 wt % selectivity within 0.5 h reaction time and ended with 79.0 wt % after 24 h. The anisole conversion, rate of anisole conversion, selectivity to 4,4'-DMDPM and 4,4'-/2,2'-DMDPM ratio after 24 h or reaction time were found to be 51.4 wt %, 5.5 $h^{-1}mol^{-1}S$, 79.0 wt % and 29.6, respectively. The results show that the reaction time influence the conversion of anisole, but did not affect significantly the 4,4'-DMDPM selectivity and 4,4'-DMDPM/2,2'-DMDPM isomer ratio.

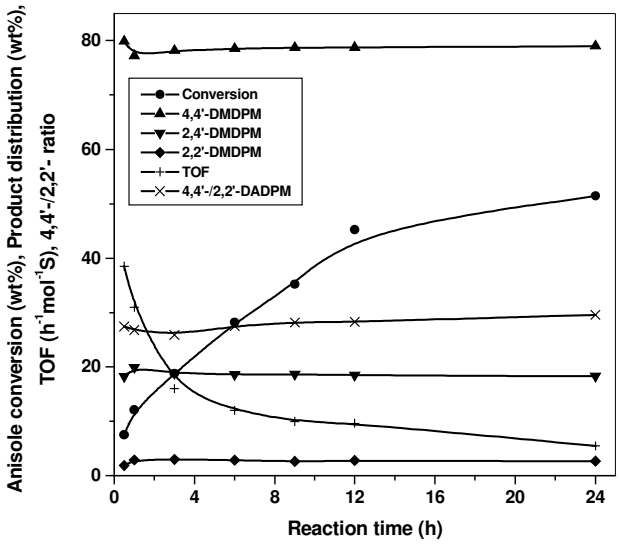

Figure 3.10. Conversion of anisole (wt %) vs. reaction time over Zr-TMS-BSA-10 catalysts; Reaction conditions: Catalyst (g) = 0.1; Anisole (mmol) = 20; p-HCHO (mmol) = 10; Reaction temperature (°C) = 100; Reaction time (h) = 6.

3.3.13.3. Influence of catalyst / anisole (wt. /wt.) ratio

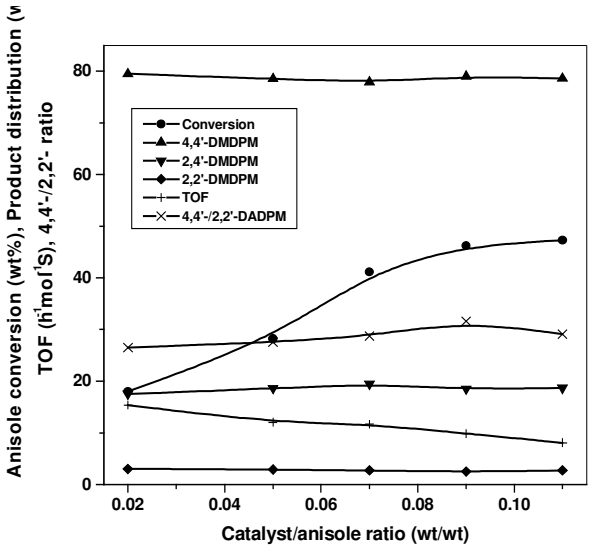

Figure 3.11. Effect of catalyst / anisole (wt./wt.) ratio on the conversion of anisole (wt%), product distribution (wt %), TOF ($h^{-1}mol^{-1}S$) and 4,4'-DMDPM/2,2'-DMDPM isomer ratio. Reaction conditions: Catalyst (g) = 0.05, 0.1, 0.15, 0.2 and 0.25; Anisole (mmol) = 20; p-HCHO (mmol) = 10; Reaction temperature (°C) = 100; Reaction time (h) = 6.

To study the effects of catalyst concentration on the conversion of anisole, rate of anisole conversion, product distribution and 4,4'-/2,2'- isomer ratio, the catalyst concentration (catalyst / anisole ratio (wt./wt.)) was increased from 0.02 to 0.11 and the results are depicted in Figure 3.11. The different ratios of catalyst / anisole were obtained by varying the amount of catalyst and keeping the concentration of anisole constant. The conversion of anisole increased from 18.0 to 47.3 wt % as the catalyst concentration increases from 0.02 to 0.11. Not much difference in the product distribution is seen against the change in catalyst concentration. The rate of anisole conversion (TOF) decreases continuously due to the increase in catalyst concentration due to the corresponding increase in the concentration of sulfur in the total amount of catalyst used. It may be seen that the catalyst / anisole (wt./wt.) ratio had a strong effect on the conversion of anisole. A

rapid increase in the conversion of anisole is observed from 0.02 to 0.07 of the reaction and very slow activity is observed from 0.07 to 0.11 of the catalyst / anisole (wt. / wt.) ratios. By using 0.11 ratio of catalyst/anisole, the conversion of anisole, rate of anisole conversion, 4,4'-DMDPM selectivity and 4,4'-/2,2'-DMDPM ratio are found to be 47.3 wt %, 8.1 $h^{-1}mol^{-1}S$, 78.6 wt %, and 29.1, respectively.

3.3.13.4. Influence of reaction temperature

The effect of reaction temperature was studied on the rate of condensation of anisole with *p*-formaldehyde over Zr-TMS-BSA-10 catalyst in the temperature range 90 to 120 ℃ using an anisole / *p*-HCHO molar ratio as 2 and the reaction time as 6 h (Figure 3.12). When the temperature is increased from 90 to 120 ℃, both the conversion of anisole and TOF increased from 17.8 to 37.4 wt % and 7.6 to 16.0 $h^{-1}mol^{-1}S$, respectively. However, the selectivity for 4,4'-DMDPM remains nearly unchanged with the increase in reaction temperature, as shown in Figure 3.12.

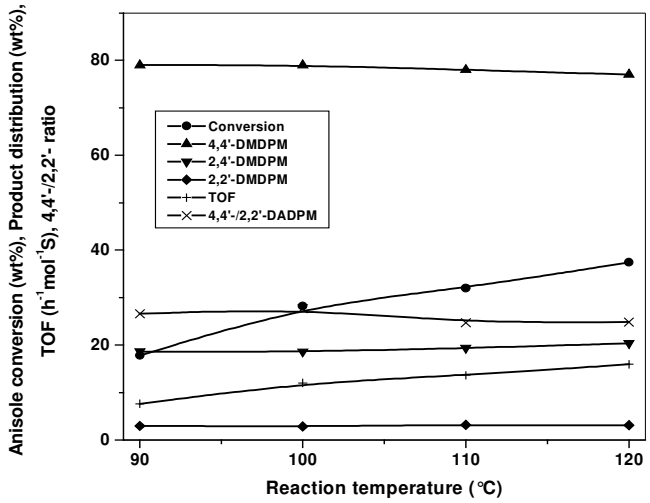

Figure 3.12. Effect of different reaction temperatures on the conversion of anisole (wt%), product distribution (wt%), TOF ($h^{-1}mol^{-1}S$) and 4,4'-DMDPM/2,2'-DMDPM isomer ratio. Reaction conditions: Catalyst (g) = 0.1; Anisole (mmol) = 20; p-HCHO (mmol) = 10; Reaction temperature (℃) = 90, 100, 110 and 120; Reaction time (h) = 6.

One of the reasons for the increased rates at higher temperature may be ascribed to an enhancement of the rate of diffusion of anisole inside the channel of the catalyst; however, reaction rates are usually more temperature dependant than rate of diffusion. The conversion of anisole increases sharply at the initial stages (12 h) of the reaction and finally (24 h) reaches a relatively steady state value over all temperatures as shown in Figure 3.12. The apparent activation energy of anisole conversion over Zr-TMS-BSA-10 catalyst is estimated to be 34.03 kJ/mol as it is depicted in Figure 3.13 in the temperature range of 90-120 °C.

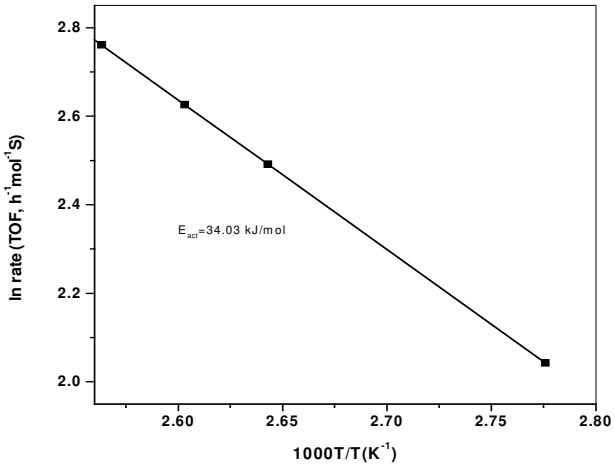

Figure 3.13. Arrehenius plot for the condensation of anisole with *p*-HCHO over Zr-TMS-BSA-10; Reaction conditions: Catalyst (g) = 0.1; Anisole (mmol) = 20; p-HCHO (mmol) = 10; Reaction temperature (°C) = 90, 100, 110 and 120; Reaction time (h) = 6.

3.3.13.5. Influence of molar ratios of the reactants

The results of the influence of anisole / *p*-HCHO molar ratios on the anisole conversion, TOF, product distribution and 4,4'-DMDPM/2,2'-DMDPM ratio is shown in Figure 3.14. The ratios were changed by keeping the amount of anisole as constant. The data show at 100 °C that, when anisole / *p*-HCHO ratio is increased from 1 to 3, the conversion of anisole and rate of anisole conversion decrease linearly from 58.3 to 16.6 wt % and 12.4 to 10.6 $h^{-1}mol^{-1}S$, respectively. Since the amount of anisole with respect to *p*-HCHO at the molar ratio of 1:1 (anisole / *p*-

HCHO=1) is less the conversion of anisole is found to be high. In addition, the selectivity to 4,4'-DMDBP is found to be decreased when the molar ratio is increased. Based on the observation, we found that 1:1 molar ratio of anisole: *p*-HCHO is optimum for high conversion of anisole, selectivity to 4,4'-DMDPM and 4,4'-DMDPM/2,2'-DMDPM ratio.

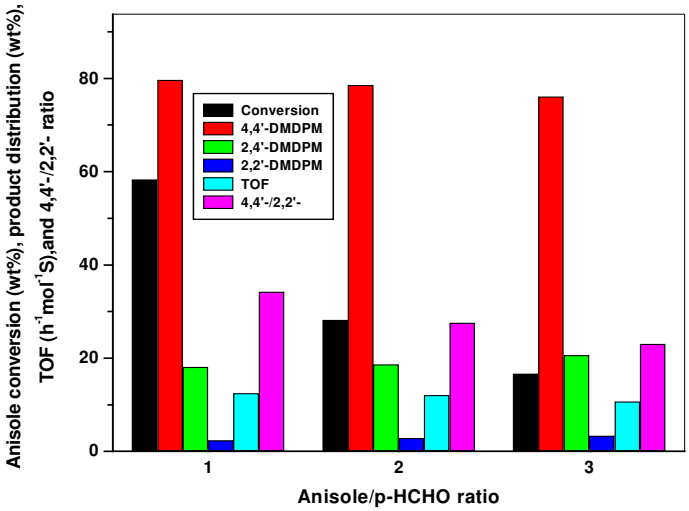

Figure 3.14. Effect of anisole / *p*-HCHO molar ratio on the conversion of anisole (wt %), product distribution (wt %), TOF ($h^{-1}mol^{-1}S$) and 4,4'-DMDPM/2,2'-DMDPM isomer ratio. Reaction conditions: Catalyst (g) = 0.1; Anisole (mmol) = 10, 20, 30; p-HCHO (mmol) = 10; Reaction temperature (°C) = 100; Reaction time (h) = 6.

3.3.13.6. Comparison of p-HCHO with aq-HCHO as condensation agent

The liquid phase condensation of anisole with formaldehyde was performed using *aqueous*-formaldehyde and *para*-formaldehyde. The 6 h reaction data over these two condensation agents is shown in Figure 3.15. As shown in Figure *aq*-HCHO showed very poor performance than p-HCHO. The presence of large quantity of water in the *aq*-HCHO may be deactivating the catalyst and the active species of the catalyst might be leached out from the surface of the support. Though *p*-HCHO is a polymer, it decomposes at about 120°C and gives monomer, which took part in the catalytic reaction. At 6 h reaction time, the conversion of anisole (wt %), TOF ($h^{-1}mol^{-1}S$), selectivity to 4,4'-DMDPM (wt %) and 4,4'-/2,2'-DMDPM ratio using aq-

HCHO and p-HCHO found to be 3.1, 1.3, 76.5, 22.4 and 28.2, 12.0, 78.5, 27.6, respectively. This experiment clearly shows that *p*-HCHO is a suitable and far better condensation agent than *aq*-HCHO for this particular reaction.

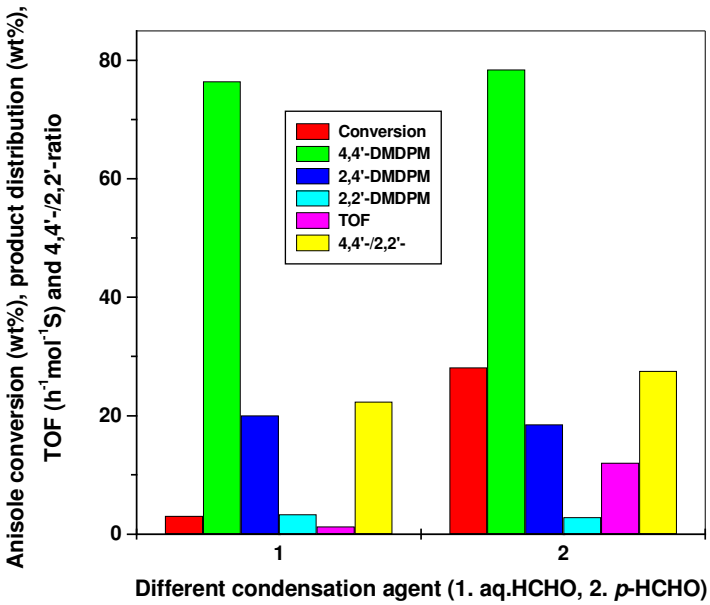

Figure 3.15. Effect of different condensation agents on the conversion of anisole (wt%), product distribution (wt%), TOF ($h^{-1}mol^{-1}S$) and 4,4'-DMDPM/2,2'-DMDPM isomer ratio. Reaction conditions: Catalyst (g) = 0.1; Anisole (mmol) = 20; p-HCHO/aq-HCHO (mmol) = 10; Reaction temperature (°C) = 100; Reaction time (h) = 6.

3.3.13.7. Catalyst recycle study

In order to check the stability and catalytic activity, the catalyst was recycled (fresh + two cycles) by using Zr-TMS-BSA-10 in the condensation of anisole. The results are presented in Table 3.6. After workup of the reaction mixture, the catalyst was separated by filtration, washed with acetone and activated for 10 h at 100 °C in the presence of air before use in the next experiment. Thus, the recovered catalyst after each reaction was characterized for its chemical composition by elemental analysis and crystallinity by X-ray diffraction (Figure 3.16). Elemental analysis showed a downward trend in the content of anchored benzylsulfonic acid of Zr-TMS-BSA-10 catalyst after second cycle. A slight decline was observed in the anisole

conversion from 28.2 to 25 wt %, and 25 to 15.3 wt %, when the catalyst was reused for first and second time, respectively. Whereas selectivity to 4,4'-DMDPM found to be unchanged to a greater extent. The leaching of the benzylsulfonic acid from the Zr-TMS catalysts by water (formed during the reaction) may be attributed for the decrease in catalytic activity after second cycle.

Table 3.6. Catalyst recycles study in condensation of anisole reaction[a]

Cycle	Element analysis (wt %)[b]		Conversion of anisole (wt %)	TOF[c] ($h^{-1}mol^{-1}$ S)	Selectivity to 4,4'-DMDPM (wt %)[d]	Catalyst crystallinity (%)
	C	S				
Fresh	1.6	2.5	28.20	12.03	78.53	100
1st Recycle	1.3	2.4	25.00	11.11	76.86	99.5
2nd Recycle	0.9	1.6	15.31	10.21	76.37	89.8

[a]Reaction conditions: Catalyst (g) = 0.1; anisole (mmol) = 20; *p*-HCHO (mmol) = 10; Reaction time (h) = 6; Reaction temperature (°C) = 100.
[b]Elemental analysis by EA1108 elemental analyzer (Carlo Erba).
[c]TOF is given as moles of anisole transformed per hour per mol of Sulfur.
[d]4,4'-DMDPM = 4,4'-dimethoxydiphenylmethane; 2,4'-DMDPM = 2,4'-dimethoxydiphenlymethane; 2,2'-DMDPM = 2,2'-dimethoxydiphenylmethane.

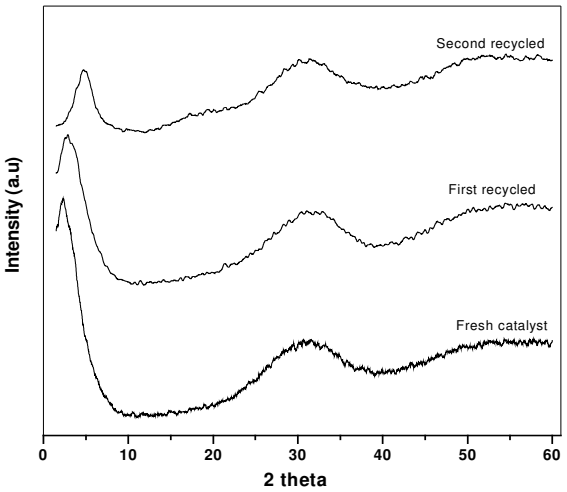

Figure 3.16. Powder XRD pattern of fresh, first and second recycled catalyst.

3.4. CONCLUSIONS

In summary, Zr-TMS has been synthesized with high surface area and functionalized with benzyl sulphonic acid using post synthetic route by applying the

etherification and subsequent sulphonation reactions to get covalently bonded Zr-TMS-BSA (-Zr-O-CH_2-Φ-SO_3H) catalysts. Various amounts of sulphonic acid were loaded over Zr-TMS-BS and the maximum amount of sulphonic acid loading was optimized to 9.1 wt % (input 10 wt %) without destroying the mesoporous structure of the material. The powder XRD confirms the mesoporous nature of the materials. The N_2 adsorption-desorption studies ascribed the high surface area and considerable pore size distribution, which is in general agreement with previous values reported for mesoporous ZrO_2. The FT-IR study revealed the successful anchoring of benzyl group and the subsequent functionalization of $–SO_3H$ group. The NH_3 TPD measurements showed that the catalysts are acidic in nature with proper acid strength. The synthesized catalysts were used in the benzoylation of diphenyl ether with benzoyl chloride and found to be more active and selective due to their mesoporosity and to an increase in the number of acid sites. Zr-TMS, A-Zr-BSA-10 and SO_4^{2-}/ZrO_2 were found to be poorly active because of the lower acidic and non-mesoporous nature, respectively. The higher activity of the synthesized materials may be attributed to its higher acidity and mesoporous characteristics.

In another summary, condensation of anisole to 4,4'-DMDPM reactions were performed on Zr-TMS-BSA-5, Zr-TMS-BSA-10, Zr-TMS-BSA-15, Zr-TMS, sulfated zirconia and *p*-TSA catalysts. Zr-TMS-BSA-15 catalyst catalyzes the condensation of anisole efficiently with *para*-formaldehyde and is superior to other Zr-TMS-BSA catalysts due to its higher acidity. *P*-TSA, the conventional homogeneous catalyst and sulfated zirconiaa showed higher active than Zr-TMS and Zr-TMS-BSA catalysts. Whereas Zr-TMS-BSA catalysts found to be higher selective than any other catalysts studied. Total acidity obtained at 30 ℃ of Zr-TMS and Zr-TMS-BSA with different wt% loading of benzylsulfonic acid show direct co-relationship between acidity and catalytic activity in the condensation of anisole. The influence of the duration of the run, catalyst concentration, reaction temperature and anisole / *p*-HCHO molar ratio

on the catalyst performance was examined in order to optimize the conversion of anisole and selectivity to 4,4'-DMDPM. The conversion of anisole using Zr-TMS-BSA-10 increased significantly with an increase in reaction time, catalyst concentration, and reaction temperature and decreased for anisole to *p*-HCHO molar ratio. Zr-TMS-BSA-10 was recycled two times and a decrease in anisole conversion was observed after two cycles, which is related to a minor leaching of benzylsulfonic acid from the catalyst.

3.5. REFERENCES

1. C.T. Kresge, M.E. Leonowicz, W.J. Roth, J.C. Vartuli, J.S. Beck, *Nature,* 359, **1992**, 710.
2. F. Marlow, D. Demuth, G.D. Stucky, F, Schuth, *J. Phys. Chem.,* 99, **1995**, 1306.
3. D.M. Antonelli, J.Y. Ying, *Angew. Chem., Int. Ed. Engl.,* 34, **1995**, 2014.
4. H. Yoshitake, T. Sugihara, T. Tatsumi, *Chem. Mater.,* 14, **2002**, 1023.
5. J.A. Knowles, M.J. Hudson, *J. Chem. Soc., Chem. Commun.,* **1995**, 2083
6. U. Ciesla, M. Froba, G.D. Stucky, K.K. Unger, F. Schuth, *Chem. Mater.,* 11, **1999,** 227.
7. N. Ulagappan, V.N. Raju, C.N.R. Rao, *Chem. Commun.,* **1996**, 2243.
8. B. Lee, D.L. Lu, J.N. Kondo, K. Domen, *J. Am. Chem. Soc.,* 124, **2002**, 11256.
9. D.M. Antonelli, J.Y. Ying, *Chem. Mater.,* 8, **1996**, 874.
10. S.A. Bagshaw, T.J. Pinnavaia, *Angew. Chem. Int. Ed. Engl.,* 35, **1996**, 1102.
11. P. Liu, J. Liu. A. Sayari, *Chem. Commun.,* **1997**, 577.
12. K.G. Servin, T.M. AbdeFattah, T.J. Pinnavaia, *Chem. Commun.,* **1998**, 1471.
13. Z. Tian, W. Tong, J. Wang, N. Duan, V.V. Krishnan, S.L. Suib, *Science,* 276, **1997**, 926.

14. M.S. Wong, J.Y. Ying, *Chem. Mater.,* 10, **1998**, 2067.

15. Y. Inoue, H. Yamazaki, *Bull. Chem. Soc. Jpn.*, 60, **1987**, 891.

16. A. Clearfield, *Inorg. Chem.,* 3, **1964**, 146.

17. G.D. Yadav, J.J. Nair, *Micropor. Mesopor. Mater.,* 33, **1999**, 1.

18. Z.R. Tian, W. Tong, J.Y. Ying, N.G. Duan, V.V. Krishnan, S. L. Suib, *Science*, 276, **1997**, 926.

19. R.A. Boyse, E.I. Ko, *Catal. Lett.,* 38, **1996**, 225.

20. T. Jin, T. Yamaguchi, K. Tanabe, *J. Phys. Chem.*, 90, **1986**, 4794.

21. B.H. Davis, R.A. Keogh, R. Srinivasan, *Catal. Today,* 20, **1994**, 219.

22. X. Song, A. Sayari, *Catal. Rev.-Sci. Eng.,* 38, **1996**, 329.

23. Y.Y. Huang, T. J. McCarthy, W. M.H. Sachtler. *Appl. Catal. A: Gen.*, 148 **1996**, 135.

24. F. Mohino, I. Díaz, J. P. Pariente, E. Sastre, *Stud. Surf. Sci. Catal.*, 142, **2002**, 1275.

25. I. Díaz, F. Mohino, J. P. Pariente, E. Sastre, *Appl. Catal. A: Gen.*, 205, **2001**, 19.

26. I. Díaz, F. Mohino, J. P. Pariente, E. Sastre, P.A. Wright, W. Zhou, *Stud. Surf. Sci. Catal.,* 135, **2001**, 1248.

27. I. Díaz, C. M. Alvarez, F. Mohino, J. P. Pariente, E. Sastre, *J. Catal.*, 193, **2000**, 295.

28. W.M. Van Rhijin, D.E.De Vos, B.F. Sels, W.D. Bossaert, P.A. Jacobs, *J. Chem. Soc., Chem. Commun.,* **1998**, 317.

29. I. Diaz, C. Marquez-Alvarez, F. Mohino, J. Perez-Pariente, E. Sastre, *J. Catal.*, 193, **2000**, 295.

30. W.D. Bossaert, D.E.De Vos, W.M. Van Rhijin J. Bullen, P.J. Grobet, P. A. Jacobs, *J. Catal.,* 182, **1999**, 156.

31. K. Wilson, A. F. Lee, D. J. Macquarrie, J. H. Clark, *Appl. Catal A: Gen.*, 228, **2002**, 127.

32. D. Margolese, J. A. Melero, S.C. Christiansen, B.F. Chmelka, G.D. Stucky, *Chem. Mater.,* 12, **2000**, 2448.

33. S. Inagaki, S. Guan, T. Ohsuna, O. Terasaki, *Nature,* 416, **2002**, 304.

34. Y. Goto, S. Inagaki. *Chem. Commun.,* **2002**, 2410.

35. N. Bion, P. Ferreira, A. Valente, I.S. Goncalves, J. Rocha. *J. Mater. Chem.,* 13, **2003**, 1910.

36. K. Okamoto, M.P. Kapoor, S. Inagaki, *Chem. Commun.,* **2005**, 1423.

37. J. R. Sohn, S. G. Ryu, Y. I. Pae, S. J. Chol, *Bull. Korean Chem. Soc.*, 11 **1990**, 403.

38. M. Chamumi, D. Brunel, F. Fajula, P. Geneste, P. Moreau, J. Solof, *Zeolites,* 14, **1994**, 283.

39. M.J. Hudson, J.A. Knowles, *J. Mater. Chem.,* 6, **1996**, 89.

40. G. Pacheco, E. Zhao, E.D. Valdes, A. Garcia, J.J. Fripiat, *Micropor. Mesopor. Mater.,* 32, **1999**, 175.

41. J.L. Blin, R. Flamant, B.L. Su, *Int. J. Inorg. Mater.,* 3, **2001**, 959.

42. G. Larsen, E. Lotero, M. Nabity, L.M. Petkovic, D.S. Shobe, *J. Catal.,* 164, **1996**, 246.

43. E. Zhao, S.E. Hardcastle, G. Pacheco, A. Garcia, A.L. Blumenfeld, J.J. Fripiat, *Micropor. Mesopor. Mater.,* 31, **1999**, 9.

44. U. Ciesla, S. Schacht, G.D. Stucky, K.K. Unger, F. Schuth, *Angew. Chem. Int. Ed. Engl.,* 35, **1996**, 541.

45. A.N. Parvulescu, B.C. Gagea, M. Alifanti, V. Parvulescu, V.I. Parvulescu, S. Nae, A. Razus, G. Poncelet, P. Grange, *J. Catal.,* 202, **2001**, 319.

46. N.C. Marziano, L.D. Ronchin, C. Tortato, A. Zingales, A.A. Sheikh-Osman, *J. Mol. Catal. A: Chem.,* 174, **2001**, 265.

47. M. Suzuki, S. Ito, T. Kuwahara, *Bull. Chem. Soc. Jpn.,* 56, **1983**, 957.

48. L.J. Bellamy, *Infrared spectra of complex molecules*, Chapman and Hall, **1975**.

49. D. Zhao, J. Sun, Q. Li, G.D. Stucky, *Chem. Mater,* **2000,** 12, 275.

50. V.I. Parvulescu, H. Bonnemann, V. Parvulescu, B. Endruschar, A.Ch.W. Rufinska, B. Tesche, G. Poncelet, *Appl. Catal. A: Gen.* **2001,** 214, 273.

51. D.A. Ward, E.I. Ko, *Chem. Mater,* **1993,** 5, 956.

CHAPTER-4

TRIFLIC ACID FUNCTIONALIZED Zr-TMS CATALYSTS (Zr-TMS-TFA)

4.1. INTRODUCTION

Synthesis of highly acidic inorganic materials by heterogenization of homogeneous systems is currently the subject of a great deal of research effort in green chemistry that aims to facilitate the recovery of the catalyst and to minimize the pollution. Many acidic catalysts have been developed using silica, alumina, metal oxides and microporous zeolites as supports [1-5]. However, there are still many problems because of limited acidity and diffusion. Soon after the discovery of the MCM-41 materials, it was demonstrated that it is also possible to synthesize non-silica-based mesostructured materials. niobium-, hafnium-, or cerium-based materials are now frequently cited [6-8]. However, as noted in a recent review by Sayari and Liu [9], although a large number of elements are able to form such materials, only few of these exhibits ordered porous structures.

Transition metal oxides are widely used as industrial catalysts and as catalyst supports. Unfortunately they usually have poorly defined pore structures. The synthesis of mesoporous silica partially substituted by titanium and zirconium has been attempted to circumvent the difficulty of preparing stable mesoporous titania and zirconia. Zirconium oxide is of particular interest because it contains both acidic and basic surface sites. These are critical for some reactions that need bifunctional (amphoteric) catalysts. The search for zirconium oxide as supports for various catalysts has received keen interest in the past decade. In the recent years SO_4^{2-}/ZrO_2 has attracted attention as it catalyzes various industrially important reactions such as: isomerization; condensation; Friedel-Crafts acylation reactions; etc. [10]. However, its non-uniform pore size, low porosity, and small surface area limit its potential application for catalyzing reactions of bulky molecules. Despite these limitations zirconia has a high melting point, low thermal conductivity, high corrosion resistance, and amphoteric behavior, all of which can be useful properties for a

support material. The possibility of obtaining such material with a mesoporous texture has made this oxide even more interesting [11].

The recent discoveries of ordered, high surface area, porous zirconia in the presence of cationic surfactants by Knowles and Hudson [12,13], mesoporous zirconia from anionic and neutral surfactants by Pacheco et al. [14], nano-structured mesoporous zirconia by Blin et al. [15], mesoporous sulfated zirconium dioxide by Huang et al. [16], surfactant-assisted synthesis of mesoporous zirconia by Larsen et al. [17], and aluminum-doped mesoporous zirconia by Zhao et al. [18] are attracting increased interest in the use of zirconia as a catalyst support. Great effort has been made to prepare mesoporous zirconium hydroxide with high surface area via a surfactant templating route.

"Triflic acid (triflluromethanesulfonic acid, CF_3SO_3H) is known to be a 'strong' acid". It is widely used in many organic reactions such as: Koch carbonylations [19]; Friedel-Crafts reactions [20]; polymerizations [20]; etc. [21, 22]. However, the recovery of the triflic acid from the reaction mixture results in the formation of large amounts of waste, which is environmentally unacceptable. The desire to perform acid-catalyzed reactions over solids has resulted in new research in this area and supported triflic acid is now becoming available to replace homogeneous acid solutions [23-25].

Trifluoromethanesulfonic acid and its conjugate base have extremely high thermal stability and resistance to both reductive and oxidative cleavage. They do not provide a source of fluoride ions even in the presence of strong nucleophiles. In addition, the use of triflate or triflic acid as homogeneous acid catalysts has received attention because of the electron-withdrawing effect exerted by the triflluromethanesulfonic group. Recently, a silica-supported polytrifluoromethanesulfosiloxane solid superacid [26], a silica-embedded triflate [27], and metal-triflate [28] were reported to be heterogeneous catalysts for reactions of

bulkier molecules. Hence, we thought that the immobilization of triflic acid over Zr-TMS would develop a novel class of heterogeneous solid acid catalysts with enhanced acidity. Moreover, the use of a heterogeneous CF_3SO_3H system would offer ease of catalyst recovery and reuse, and minimize the production of waste currently formed during triflic acid recovery.

In this chapter, I describe the first preparation of triflic acid functionalized Zr-TMS (Zr-TMS-TFA, Zr-TMS-O-SO_2-CF_3, mesoporous ≡Zr-O-SO_2-CF_3) materials using Zr-TMS as solid support and triflic acid as an acidic component (added by post synthesis). Sol-gel method was employed for the synthesis of Zr-TMS. The environment of the triflic acid on the walls of Zr-TMS was determined by different techniques. Since the catalysts are highly acidic, acetalization of ethylacetoacetate (EAA) to ethyl 3, 3-ethylenedioxybutyrate (fructone) and benzoylation of biphenyl (BP) to 4-phenylbenzophenone (4-PBP), benzoylation of toluene to 4,4'-dimethylbenzophenone (4,4'-DMBP) were carried out to check the catalytic activity of the synthesized catalysts. Acetalization of EAA and benzoylation of BP reactions were also carried out by using functionalized amorphous zirconia (A-Zr-TFA) catalysts, Zr-TMS, SO_4^{2-}/ZrO_2, and triflic acid for comparison. Fructone, an apple scent has been used as fragrances, in detergents, in pharmaceutical industries, as food and beverage additives, and also in cosmetics [29]. The 4-PBP is an important intermediate in the pharmaceutical industry to synthesize an anti-fungal agent (bifonazole) and as a photo-initiator [30, 31]. Complete study of benzoylation of toluene reaction is reported to demonstrate the synthesized catalysts are highly efficient for any acid catalyzed reactions. 4,4'-dimethylbenzophenone (4,4'-DMBP, Di-*p*-toluoyl ketone) is used mainly as a photosensitizer and applied to the UV-curable coatings and UV-curable inks. Disubstituted diphenyl ketones are also used as intermediates for pharmaceutical and agricultural chemicals [32]. It gives high whiteness background and high d. images showing good resistance to plasticizers

[33]. Also, 4,4'-DMBP is extensively used as UV light stabilizers in plastics, cosmetics (as fixative in perfumes) and films [34]. 4,4'-DMBP is usually synthesized by the Friedel-Crafts reaction of toluene with phosgene as an acylation agent using $AlCl_3$ as catalyst, resulting in lower yield of 4,4'-DMBP [35-37]. Recently, 4,4'- DMBP is prepared by reacting *p*-toluic acid, toluene and various metal (Praseodymium, Dysprosium, Indium, Bismuth, Cerium, Thorium, Scandium and Yttrium) triflate catalysts; the yield of 4,4'-DMBP obtained was in the range of 4-30% [38].

4.2. EXPERIMENTAL

4.2.1. Materials

The syntheses of Zr-TMS-TFA catalysts were carried out using zirconium (IV) butoxide (80 wt % solution in 1-butanol, Aldrich, USA), a 25 wt % aqueous solution of tetramethyl ammonium hydroxide (TMAOH, Loba Chemie, India), a 25 wt % aqueous solution of N-cetyl-N, N, N trimethyl ammonium bromide (CTMABr, Loba Chemie, India), and trifluoromethanesulphonic acid (CF_3SO_3H, Lancaster, UK).

4.2.2. Synthesis of Zr-TMS material

The synthesis of Zr-TMS was carried out using the following gel composition and procedure:

0.07 $Zr(OC_4H_9)_4$:1.4 BuOH:0.02 CTMABr:0.014 TMAOH:1.7 H_2O

A mixture of zirconium (IV) butoxide (80 wt % solution in 1-butanol) and 1-butanol was stirred for 10 min. Then the required amount of water was added drop wise into this mixture under stirring to hydrolyze the zirconium (IV) butoxide to $Zr(OH)_4$. The precipitated $Zr(OH)_4$ mixture was added to an aqueous solution of CTMABr (25 wt % aq. solution) and TMAOH (25 wt % aq. solution) under continuous stirring. After further stirring for 2 h, the resulting synthesis gel (pH =10.5 -11.0) was transferred to a round bottom flask, sealed and refluxed at 90°C for 48 h under stirring. The solid product was recovered by filtration, washed with deionised water and acetone, and dried at 100 °C for 2 h. The surfactant was removed from the

synthesized material by extraction with a mixture containing 100 g of ethanol and 2.5 g of HCl (36 wt %) per gram of the solid material [20, 39] under reflux for 48 h. The Zr-TMS was washed with water and acetone and dried at 100 °C for 6h.

4.2.3. Synthesis of Zr-TMS-TFA catalysts

The resulting solid mesoporous material, Zr-TMS, was functionalized with triflic acid by post synthesis procedure using the molar composition

0.07 Zr-TMS: 0.7 dry toluene: 0.03 CF_3SO_3H

Triflic acid (0.03 mol) was added drop wise into the mixture of toluene and Zr-TMS at 90 °C under nitrogen atmosphere and further refluxed for 2 h. Then the mixture was cooled, filtered, washed with acetone and dried at 100 °C for 6 h. Soxhlet extraction of the material (to remove the unreacted triflic acid) was carried out at 75 °C for 24 h using a mixture of dichloromethane (100 g) and diethyl ether (100 g) per gram of catalyst. The sample was then dried at 200 °C for 10 h. The synthesis of the catalyst is shown in Scheme 4.1. The syntheses of different loadings of triflic acid (5 to 25 wt %) on Zr-TMS were carried out by varying the molar ratios of zirconium (IV) butoxide, CTMABr, TMAOH, water, and CF_3SO_3H. Henceforth, triflic acid functionalized mesoporous zirconia catalysts will be designated as Zr-TMS-TFA.

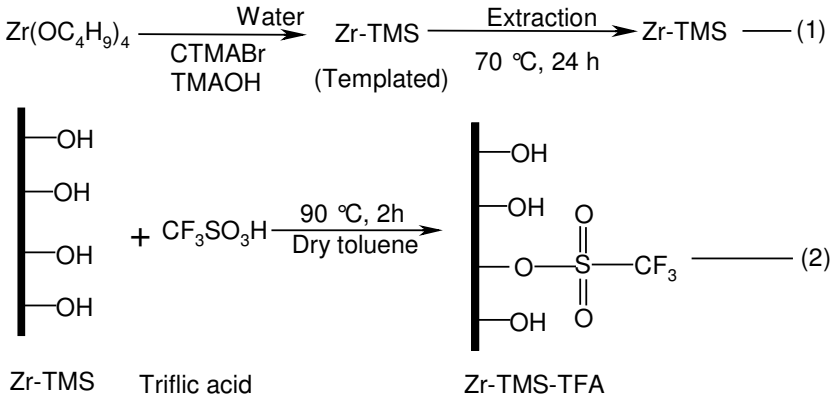

Scheme 4.1. Synthesis of triflic acid functionalized mesoporous zirconia (Zr-TMS-TFA) catalysts; (1) Synthesis and template removal of Zr-TMS material, (2) Functionalization of triflic acid over Zr-TMS material by post synthesis route.

4.2.4. Synthesis of A-Zr-TFA catalysts

Synthesis of triflic acid functionalized amorphous ≡Zr-O-SO_2-CF_3 (A-Zr-TFA) catalysts was carried out via the following procedure. A mixture of zirconium (IV) butoxide (0.07 mol) and 1-butanol (1.4 mol) was placed in a three-necked 250 ml round bottom flask equipped with a magnetic stirrer and a septum. The flask was held at 90 °C and stirred for 10 min. Then 0.28 mol of water was added drop-wise into this mixture under stirring to hydrolyze the zirconium (IV) butoxide to $Zr(OH)_4$. Further, after 30 min of stirring, triflic acid (0.03 mol) was slowly added by syringe into the above mixture and stirring was continued for 2 h. The mixture was cooled, filtered, washed with deionised water and acetone and then dried at 100 °C for 6 h. Soxhlet extraction was carried out for 24 h. Then the sample was dried at 200 °C for 10 h. The syntheses of different loadings of triflic acid over amorphous $Zr(OH)_4$ (5 to 25 wt %) were carried out by varying the molar ratios of zirconium (IV) butoxide, water, and CF_3SO_3H. The synthesized materials were white in colour. Henceforth, functionalized amorphous catalysts will be designated as A-Zr-TFA.

The SO_4^{2-}/ZrO_2 was obtained from MEL Chemicals, Manchester. UK and activated at 500°C for 10 h in static air prior to the catalytic run.

4.2.5. Catalyst Characterization

The synthesized materials were mainly characterized by powder X-ray diffraction (XRD) for phase purity and crystallinity, N_2 adsorption-desorption techniques for specific surface area, total pore volume and average pore diameter, Fourier transform infrared (FTIR) spectroscopy for functional group confirmation, elemental analysis for C and S to measure the triflic acid loading in the material, solid state ^{13}C CP/MAS (cross polarisation/magic angle spinning) and ^{13}C DD/MAS (dipolar decoupled/magic angle spinning) NMR for the confirmation of functional group (-CF_3) in the catalyst, FT-Raman analysis for the binding mode of the triflate, temperature programmed desorption (TPD) of NH_3 measurement for total acidity,

scanning electron microscopy (SEM) for the particle size and morphology, transmission electron microscopy (TEM) to view the crystalline structure and thermogravimetric-differential thermal analysis (TG-DTA and DTG) to study the decomposition and thermal stability of the catalysts.

The powder X-ray diffraction patterns of synthesized Zr-TMS, Zr-TMS-TFA and A-Zr-TFA catalysts were recorded on a Rigaku Miniflex instrument using Cu K_α radiation (30 kV, 15 mA), λ=1.5404 Å between 1.5 to 60° (2θ) with a scan rate of 4°/min. The BET surface area, total pore volume, and average pore diameter were measured by N_2 adsorption-desorption method by NOVA 1200 (Quantachrome) at –196°C. For this particular measurement, the samples were activated at 180°C for 3 h under vacuum and then the adsorption-desorption was conducted by passing nitrogen onto the sample, which was kept under liquid nitrogen. The FT-IR spectra were obtained in a range of 400 to 4000 cm^{-1} on a Shimadzu FTIR 8201 PC using a Diffuse Reflectance scanning disc technique. Elemental analysis for C and S were done by EA1108 Elemental Analyzer (Carlo Erba Instruments).

^{13}C CP/MAS and ^{13}C DD/MAS solid-state NMR studies were carried out on a Bruker DRX-500 NMR spectrometer. The resonance frequency was 125.757 MHz. The finely powdered sample Zr-TMS-TFA-30 was placed in 4.0 mm zirconia rotors and spun at 810 kHz. The CP/MAS spectrum was recorded under Hartmann-Hahn match condition using a contact time of 1 m/sec. A relaxation delay of 10 and 4 sec were used for DD/MAS and CP/MAS spectra, respectively. The chemical shift was referred to an external adamantane CH_2 peak reference taken as 28.7 ppm with respect to TMS. The raw data obtained for DD/MAS (2000 scans) and CP/MAS (3000 scans) were processed with an exponential function of line broadening of 20 Hz and 60 Hz, respectively, prior to Fourier transformation for sensitivity enhancement.

Powder samples (*ca.* 10 mg) were compressed into a small stainless steel holder. Raman spectra of these samples were measured at room temperature, exposed to atmosphere, using a Bruker RFS/100S FT-Raman spectrometer. A Nd-YAG laser (1064 cm^{-1}; 50 mW) was used as an excitation source. Scattered radiation was collected at 180 ℃ and detected using an InGaAs detector. Spectra were recorded in the Stokes region between 2000 and 25 cm^{-1} at 4 cm^{-1} resolutions. 100 scans were coadded. For comparison, the Raman spectrum of liquid triflic acid (Aldrich, synthesis grade; in a standard 4 mm NMR tube) was collected under similar conditions. Only 50 scans needed to be coadded.

Temperature programmed desorption (TPD) were carried out to determine the total acidity and strength of acid sites on the catalysts using ammonia as an adsorbate [40]. In a typical run, 1.0 g of activated sample was placed in a silica tubular reactor and heated at 200 ℃ under nitrogen flow of 50-ml min^{-1} for 6 h. The reactor was then cooled at 30 ℃ and adsorption conducted at that temperature by exposing the sample to ammonia (10 ml min^{-1}) for 30 min. Physically adsorbed ammonia was removed by purging the sample with a nitrogen stream flowing at 50 ml min^{-1} for 15 h at 30℃. The acid strength distribution was obtained by raising the catalyst temperature (10 K min^{-1}) from 30 to 300 ℃ in a number of steps with the flow of nitrogen (50 ml min^{-1}). The NH_3 evolved was trapped in the HCl solution and titrated with a standard NaOH solution.

The SEM micrographs of Zr-TMS and Zr-TMS-TFA-30 materials were taken by JEOL-JSM-5200 scanning microscopy. TEM was performed on a JEOL JEM-1200EX instrument with 100 kV of acceleration voltage to probe the mesoporosity of the materials. The TG-DTA and DTG analysis of the Zr-TMS and Zr-TMS-TFA-30 catalysts were carried out with Mettler Toledo 851^e equipment using an alumina pan under a nitrogen (80ml min^{-1}) atmosphere from ambient to 1000℃ with the increasing rate of 20 ℃ min^{-1}.

4.2.6. Liquid phase acetalization of ethylacetoacetate

The catalytic activity of all Zr-TMS-TFA was examined in the acetalization of ethylacetoacetate (EAA) with ethylene glycol (EG) using toluene as a solvent (Scheme 4.2). The reactions were carried out in a batch reactor equipped with two-necked 50 ml round bottom flask with septum, an oil bath and condenser. AR grade chemicals were used without further purification. In a typical run, EAA and EG were added in a required molar ratio to the activated catalyst (0.1 g) in the required molar ratio. The reaction mixtures were magnetically stirred and heated to the required temperature at atmospheric pressure. The products were analyzed in a gas-chromatograph (HP 6890) equipped with a flame ionization detector (FID) and a capillary column (5 μm thick cross-linked methyl silicone gum, 0.2 x 50 m). The products were also identified by GC-MS (Shimadzu 2000 A) analysis and confirmed by ^{1}H and ^{13}C NMR spectra (Bruker AC-200).

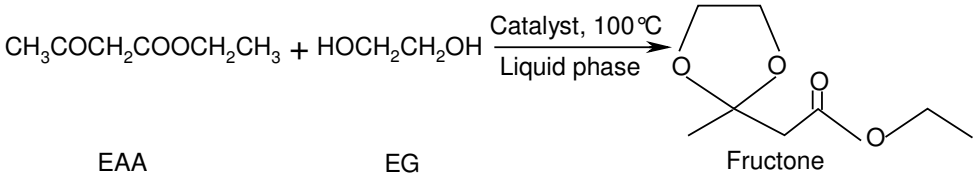

Scheme 4.2. Liquid phase acetalization of ethylacetoacetate with ethylene glycol to fructone.

Conversion of EAA is defined as the weight percentage of EAA consumed. The turnover frequency (TOF) for EAA conversion (in mol^{-1} S h^{-1}) was calculated as the moles of EAA converted per hour over per mol of sulfur. The selectivity to a product is expressed as the amount of a particular product divided by the amount of total products and multiplied by 100.

4.2.7. Liquid phase benzoylation of biphenyl

In another reaction, the catalytic activity of all Zr-TMS-TFA was examined in the benzoylation of biphenyl (BP) with benzoyl chloride (BOC) using nitrobenzene as

a solvent (Scheme 4.3). The reactions were carried out in a batch reactor equipped with two-necked 50 ml round bottom flask with septum, an oil bath and condenser. AR grade chemicals were used without further purification. In a typical run, BP and BOC were added to the activated catalyst (0.5 g) in the required molar ratio. The reaction mixtures were magnetically stirred and heated to the required temperature at atmospheric pressure. The products were analyzed in a gas-chromatograph (HP 6890) equipped with a flame ionization detector (FID) and a capillary column (5 μm thick cross-linked methyl silicone gum, 0.2 x 50 m). The products were also identified by GC-MS (Shimadzu 2000 A) analysis and confirmed by ^{1}H and ^{13}C NMR spectra (Bruker AC-200).

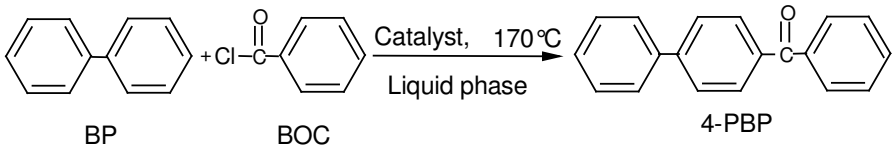

Scheme 4.3. Liquid phase benzoylation of biphenyl with benzoyl chloride to 4-phenylbenzophenone (4-PBP).

Conversion of BP is defined as the weight percentage of BP consumed. The turnover frequency (TOF) for BP conversion (in $10^{-1}mol^{-1}$ S h^{-1}) was calculated as the moles of BP converted per hour over per mol of sulfur. The selectivity to a product is expressed as the amount of a particular product divided by the amount of total products and multiplied by 100.

4.2.8. Catalysts recycle study

Recycling of the catalyst was done during the acetalization reaction by using Zr-TMS-TFA-30. After work-up of the reaction, the catalyst was separated by filtration, washed with acetone, and dried at 200 °C for 10 h in the presence of air. The recovered catalyst after each cycle was characterized for its crystallinity by XRD and its chemical composition by elemental analysis.

4.2.9. Liquid phase benzoylation of toluene (Catalysts optimization study)

High purity dry toluene, A.R. grade *p*-T-Cl and nitrobenzene were used without further purification. The catalyst was activated at 200 °C for at least 2 h before use in the experiments, so as to maintain the dry conditions. The liquid phase catalytic benzoylation was performed in a 50 ml round bottom flask fitted with a condenser, N_2 gas supply tube and a septum. The temperature of the reaction vessel was maintained using an oil bath. In a typical run, a mixture of toluene (0.01 mol), *p*-T-Cl (0.01 mol), nitrobenzene (10 ml) and activated catalyst (0.5 gm), was magnetically stirred and heated to attain the reaction temperature (130 °C) in the presence of N_2 gas. The product samples were withdrawn at regular intervals of time and analyzed periodically on a gas-chromatograph (HP 6890) equipped with a flame ionization detector and a capillary column (5 μm thick cross-linked methyl silicone gum, 0.2mm x 50 m long). The product samples were also identified by injecting authentic samples and GCMS (Shimadzu 2000 A) analysis.

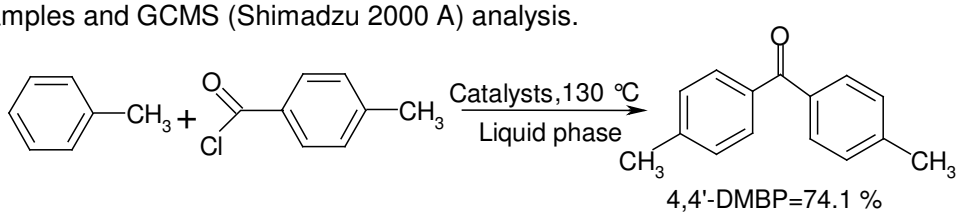

Scheme 4.4. Liquid phase benzoylation of toluene with para-toluoyl chloride to 4,4'-dimethylbenzophenone.

Conversion of *p*-T-Cl is defined as the weight percentage of *p*-T-Cl consumed. The turnover rate for p-T-Cl conversion (TOF, $10^{-1}h^{-1}mol^{-1}S$) was calculated as the moles of *p*-T-Cl converted per hour over per mol of sulfur. The selectivity to a product is expressed as the amount of a particular product divided by the amount of total products and multiplied by 100.

4.3. RESULTS AND DISCUSSION

4.3.1. Catalysts synthesis strategy

Organic functionalization of the internal surfaces of any mesoporous materials can be achieved, either by covalently grafting of various organic species onto the surface or by incorporating of functionalities directly during the synthesis. Zr-TMS material has been synthesized by the procedure given in experimental part and obtained dry material before functionalization. For functionalization of TFA over Zr-TMS, two different methods were adopted and based on our preliminary instrumental techniques; the procedure given in experimental part was found suitable for the preparation of proposed Zr-TMS-TFA catalysts. By first method, In situ preparation of Zr-TMS-TFA was tried and ended with bulk material having very poor mesoporous structure. By second method, TFA was added into the Zr-TMS material, which was taken in dry toluene by post synthetic route and obtained the material with highest loading without collapsing the mesoporous structure.

Six samples of TFA functionalized Zr-TMS (denoted as Zr-TMS-TFA-5, -10, -15, -20, -25 and -30) and six samples of OSA functionalized over non-porous zirconia (denoted as AZr-TFA-,-5, -10, -15, -20, -25, and -30 wt %) were prepared and their compositions are listed in Table 4.1 and the generalized synthesis scheme of Zr-TMS-OSA is given in Scheme 4.1. Zr-TMS material (Formula 1 of Scheme 4.1.) was treated with TFA to get Zr-TMS-TFA material having the Formula 2 of Scheme 4.1. Six different loading of TFA, such as 5, 10, 15, 20, 25, and 30 wt % over Zr-TMS was done and designated as Zr-TMS-TFA-5, Zr-TMS-TFA-10, Zr-TMS-TFA-15, Zr-TMS-TFA-20, Zr-TMS-TFA-25, and Zr-TMS-OSA-30, respectively, where as the effective loading is tabulated in Table 4.1., based on the sulfur concentration by elemental analysis of sulfur. In the same manner, functionalizations of TFA over non-porous zirconia were designated as A-Zr-TFA-5, A-Zr-TFA-10, A-Zr-TFA-15, A-Zr-TFA-20, A-Zr-TFA-25, and A-Zr-TFA-30.

Table 4.1. Physico-chemical properties of Zr-TMS, A-Zr-TFA, Zr-TMS-TFA and sulfated zirconia catalysts.

Catalyst	Elemental analysis (wt %)		Loading of CF_3SO_3H (wt %)		BET Surface area[a] ($m^2 g^{-1}$)	Crystal size[b] (μm)	NH_3 desorbed (mmol g^{-1}) between temperature (° C)[c]					NH_3 Chemisorbed[d] at 30° C (mmol g^{-1})
	C	S	Input	Output			30-70 (%)	70-110 (° C)	110-150 (%)	150-200 (%)	200-300 (%)	
Amor- $Zr(OH)_4$	--	--	--	--	80	0.35	12	27	33	20	8	0.49
A-Zr-TFA[e]-5[f]	0.7	1.00	5.0	4.7	72	0.40	11	33	37	12	6	0.81
A-Zr-TFA-10	1.5	2.04	10.0	9.6	68	0.35	10	33	38	15	3	1.05
A-Zr-TFA -15	1.5	2.6	15.0	12.2	63	0.38	17	29	35	15	3	1.27
A-Zr-TFA -20	1.7	3.19	20.0	15.2	59	0.37	14	30	37	15	3	1.36
A-Zr-TFA -25	2.0	5.16	25.0	24.2	56	0.40	13	29	38	17	3	1.53
A-Zr-TFA -30	2.7	5.91	30.0	27.7	52	0.39	13	29	37	17	4	1.67
SO_4^{2-}/ZrO_2[g]	---	3.08	10.0	7.8	101	0.45	--	--	--	--	--	1.45
Zr-TMS[h]	----	---	---	---	371	0.33	14	26	32	20	8	0.50
Zr-TMS-TFA-5[f]	0.98	1.01	5.0	4.7	355	0.37	16	26	34	17	8	0.77
Zr-TMS-TFA-10	0.97	1.52	10.0	7.1	344	0.34	17	28	33	16	6	0.87
Zr-TMS-TFA-15	1.52	2.78	15.0	13.0	320	0.38	17	29	33	15	6	1.05
Zr-TMS-TFA-20	1.62	3.54	20.0	16.6	309	0.40	13	27	37	17	6	1.31
Zr-TMS-TFA-25	1.82	3.85	25.0	18.0	292	0.36	12	27	41	16	4	1.47
Zr-TMS-TFA-30[i]	2.00	4.86	30.0	22.8	284	0.40	12	28	41	16	3	1.55

[a]Measured by N_2 adsorption-desorption at –196 °C.
[b]Measured by JEOL SEM (JSM-5200).
[c] Percent of acid strength distribution calculated based on NH_3 desorbed from 30 to 300 °C.
[d]Total acid sites determined in the solid catalyst by NH_3 adsorption-desorption
[e]A-denotes Amorphous.
[f]Numbers denote wt% (input) of triflic acid loading over Zr-TMS.
[g]NH_3 desorbed from 30 to 600 °C
[h]Total pore volume ($cm^3 g^{-1}$) = 0.31 and average pore diameter (Å) = 44.3 measured by N_2 adsorption isotherm.
[i]Total pore volume ($cm^3 g^{-1}$) = 0.25 and average pore diameter (Å) = 34.0 measured by N_2 adsorption isotherm.

4.3.2. Powder X-ray diffraction study

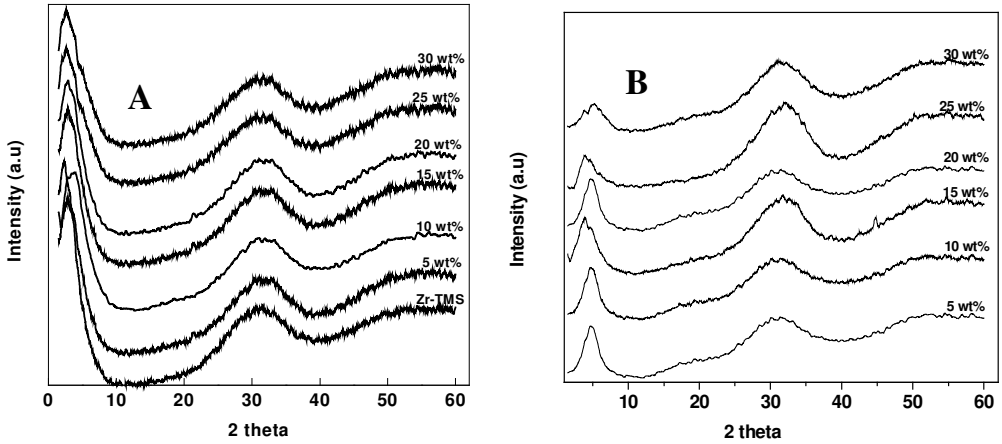

Figure 4.1. Powder X ray diffraction patterns of (A) Zr-TMS and Zr-TMS-TFA (5-30wt %) and (B) A-Zr-TFA (5-30 wt %).

The powder X-ray diffraction (XRD) patterns of all the synthesized catalysts are shown in Figures 4.1 A and B. The template-extracted Zr-TMS (Figure 4.1A, Zr-TMS) and Zr-TMS-TFA (Figures 4.1A, 5-30 wt %) catalysts exhibited a single, broad reflection at low 2θ (2.5° – 4.0°). This reflection corresponds to the XRD pattern of ordered mesoporous ZrO_2 [11, 13-18] and Si-Zr mesoporous materials [41]. However, in these studies no higher order reflections were observed. The presence of these in our spectra may indicate that the pore walls are rather amorphous or that there is a lack of correspondence between the structures of adjacent pores. Other reflections were observed at about 31° (broad) and at about 50° (small) in all the samples. They are attributed to the tetragonal, monoclinic and cubic phases of ZrO_2. They are readily formed after calcination of the sample at higher temperature [15]. The broad reflection at 2θ = 31° may also be partially due to presence of amorphous materials as was reported in siliceous MCM-41 [42]. The crystallinity of the triflic acid containing Zr-TMS materials decreased as the triflic acid loading increased. Moreover, low intensity and the absence of higher order reflections show that the order and mesostructure were entirely different from that measured for the

mesoporous silica [11]. A-Zr-TFA catalysts (Figures 4.1B, 5-30 wt %) were indeed purely amorphous showing low intensity reflections at about 5, 31 and 50° (2 θ).

4.3.3. Nitrogen adsorption-desorption study

The incorporation or anchoring of any medium (acid or base) or metal in the framework positions and/or into the walls of the supporting medium leads to a progressive decrease in surface area [27, 41, 43]. The BET surface areas of the Zr-TMS, Zr-TMS-TFA, A-Zr-TFA, and SO_4^{2-}/ZrO_2 are given in Table 4.1. The surface area for the Zr-TMS was 371 $m^2 g^{-1}$, which is comparable to that measured previously for a Zr-TMS synthesized using a surfactant with C_{16} carbon chain [11, 13]. Surface area gradually decreased with increasing triflic acid loading. The surface area decreased to 284 m^2 g^{-1} for the maximum loading of triflic acid (30 wt %) over Zr-TMS. In the same way, the surface area of amorphous $Zr(OH)_4$ was 80 m^2 g^{-1} and decreased to 52 m^2 g^{-1} for A-Zr-TFA-30. The surface area of SO_4^{2-}/ZrO_2 was found to be 101 $m^2 g^{-1}$.

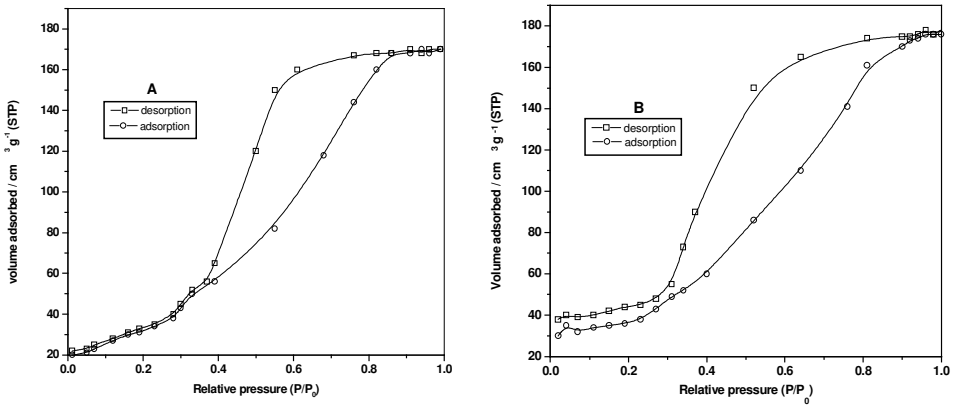

Figure 4.2. N_2 adsorption-desorption isotherms of (A) Zr-TMS and (B) Zr-TMS-TFA-30.

Zr-TMS and Zr-TMS-TFA-30 were analyzed by detailed N_2 sorption studies. The BET surface area, average pore diameter and total pore volume of Zr-TMS and Zr-TMS-TFA-30 were 371m^2 g^{-1}, 44.3 Å, 0.31 cm^3 g^{-1}, and 284 m^2 g^{-1}, 34.0 Å, 0.25 cm^3 g^{-1}, respectively (Table 4.1.). The decrease in surface area, pore diameter and

pore volume of Zr-TMS-TFA-30 may be attributed to the functionalization of Zr-TMS by triflic acid. The isotherms and pore size distributions of Zr-TMS confirm the presence of mesopores. These results are comparable with those previously reported for a mesoporous ZrO_2 [13].

Figures 4.2A and B show the nitrogen adsorption isotherm of Zr-TMS and Zr-TMS-TFA-30, respectively. Both the isotherms are indicative of type IV behavior characteristic of mesoporous materials [11, 13]. The hysteresis in the desorption branch clearly shows the existence of mesopores. The desorption isotherm of Zr-TMS is similar to the calcined ZrO_2 aerogels previously reported [13]. Before the functionalization (Figure 4.2A) the position of the inflection in the P/P_0 = 0.4 to 0.83 region depends on the diameter of the mesopores (broad pore size distribution) and its sharpness indicates the uniformity of the pore size distributions. After the functionalization (Figure 4.2B), the position of the inflection is changed in the P/P_0 = 0.35 to 0.90 region. This is indicative of a slight structural collapse in the material. However, pore size distribution analysis still indicates that mesoporosity was not lost.

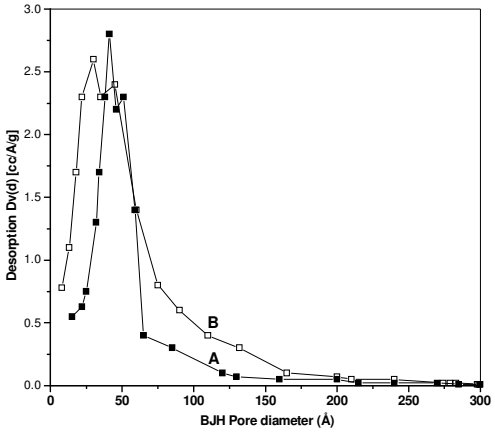

Figure 4.3. Barrett-Joyner-Halenda (BJH) pore size distributions of (A) Zr-TMS (B) Zr-TMS-TFA-30.

Figures 4.3 A and B show the BJH pore size distributions of Zr-TMS and Zr-TMS-TFA-30, respectively. Zr-TMS possesses a fairly narrow distribution of

mesopores centred at circa 40 to 50 Å with some as large as 100 Å. After functionalization the distribution is clearly broadened. The material also contains smaller pores of 10 to 20 Å and the amount of larger pores (between 75 and 150 Å) is greatly increased. It is apparent that a pore formation mechanism may be in effect that differs from that of M41S materials. Pore size uniformity does not necessarily imply bi- or three-dimensional X-ray detectable ordering [11, 13].

4.3.4. Elemental analysis study

The carbon and sulfur contents of the samples are shown in Table 4.1. To a first approximation, the sulfur content was assigned to the loading of triflic acid over Zr-TMS and it was observed that acid loading over Zr-TMS indeed increased with the increase in the amount of CF_3SO_3H introduced. After removal of surfactant no nitrogen was detected in the elemental analysis as expected. These results were confirmed by infrared and NMR spectroscopies (see below).

4.3.5. FT-Infrared spectroscopy study

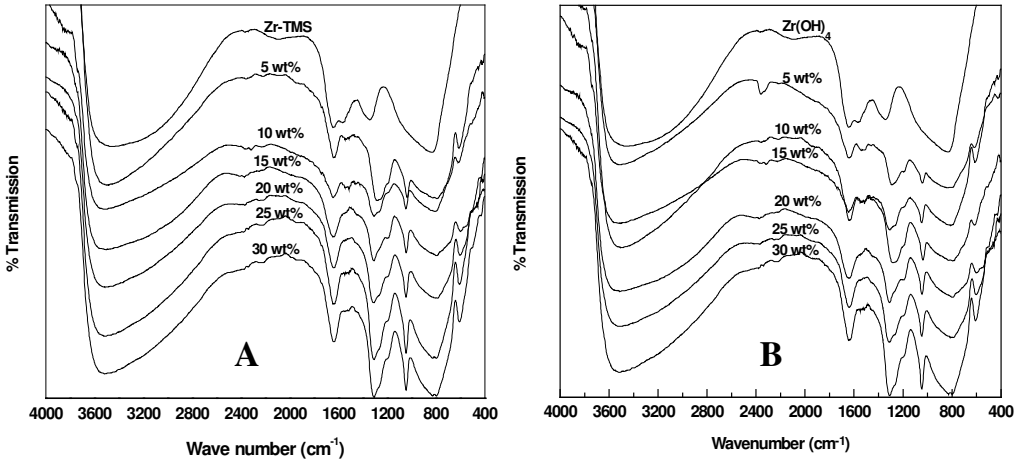

Figure 4.4. Fourier transform-infrared spectrum of (A) Zr-TMS and Zr-TMS-TFA (5-30 wt %) and (B) A-Zr-TFA (5-30 wt %).

The infrared spectra of Zr-TMS, Zr-TMS-TFA and A-Zr-TFA catalysts are shown in Figures 4.4A and B, respectively. The strong and broad band between

3600-3200 cm^{-1} corresponds to the stretching mode of hydroxyl groups present on the surface (as $Zr(OH)_4$). The weak unresolved band between 850-700 cm^{-1} is attributed to Zr-O stretching modes. The sharp band in the region 1650-1600 cm^{-1} is due to the bending mode of associated water molecules. The Zr-TMS-TFA (Figures 4.4.A, 5-30 wt %) and A-Zr-TFA (Figures 4.4B, 5-30 wt %) spectra show additional bands (at 1296, 1184, 1043 and 601 cm^{-1}) that are absent in Zr-TMS (Figure 4.4A, Zr-TMS). The broad and intense band at 1296 cm^{-1} and medium band at 1184 cm^{-1} are due to S=O stretching mode of the incorporated triflic acid [44, 45]. The C-S link in Zr-TMS-TFA also gives a medium band at 601 cm^{-1}. This band is assigned to the SO_2 deformation mode and a sharp band at 1043 cm^{-1} is assigned to C-F band [44, 45]. Moreover, the spectra of Zr-TMS-TFA and A-Zr-TFA are similar to the reported silver triflate spectrum [46]. Further, from the Figure 4.4A-Zr-TMS, it can be seen that the stretching (3200-2800 cm^{-1}) and bending (1500-1300 cm^{-1}) modes of the methyl groups of CTMABr completely disappear after 48 h of extraction [13, 15]. Thus, all these results indicate that the final material was free from surfactant and that triflic acid was functionalized onto the walls of Zr-TMS.

4.3.6. Solid-State ^{13}C-CP/MAS and ^{13}C-DD/MAS NMR studies

In order to confirm that the $–CF_3$ group exists in the material, the solid state ^{13}C-CP/MAS and DD/MAS NMR spectra were recorded at 125.757 MHz at a rotational speed of 8 kHz for Zr-TMS-TFA-30. The DD/MAS NMR spectrum (Figure 4.5) was found to be more sensitive than the CP/MAS NMR spectra indicating the absence of a proton environment in the proximity of the carbon under observation. The quartet nature of the ^{13}C spectrum, arising due to the ^{13}C –^{19}F scalar coupling ($J_{C\text{-}F} \approx 310$Hz), unambiguously shows the presence of CF_3 groups. Moreover, the chemical shift observed at ≈119 ppm is very close to that reported for Na-O-SO_2-CF_3 (≈120 ppm) [47]. These features indicate that the $–CF_3$ group is intact in the sample.

Further, no peak corresponding to the surfactant was observed, which would normally appear in the range 10-100 ppm in the ^{13}C CP/MAS NMR spectrum.

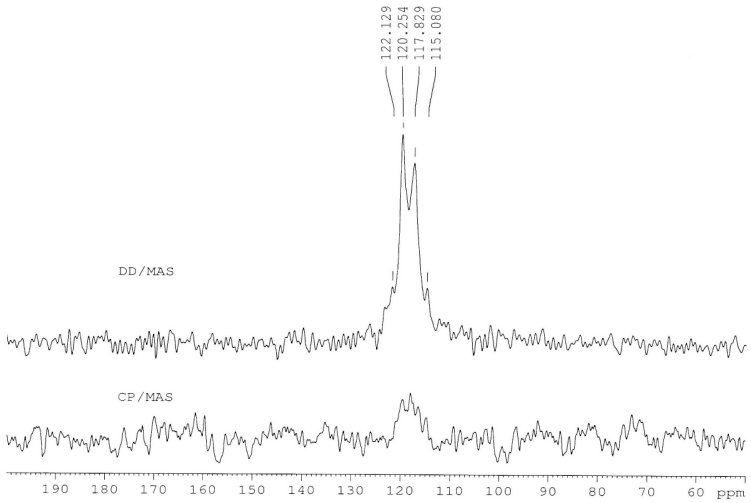

Figure 4.5. Solid-state ^{13}C CP/MAS and ^{13}C DD/MAS NMR spectra of Zr-TMS-TFA-30.

4.3.7. FT-Raman spectroscopic study

Figure 4.6 shows the Raman spectra of Zr-TMS and amorphous $Zr(OH)_4$. The spectra of the two zirconia materials are identical, with bands at 120 cm^{-1}(w), 84 cm^{-1}(m), and 39 cm^{-1}(w). Apparently these low frequency modes are not sensitive to the presence or absence of mesopores. Figure 4.7A shows the Raman spectra of Zr-TMS-TFA with triflic acid loadings between 5 and 30 wt %. The spectrum of the Zr-TMS support was subtracted from each. Also shown is the spectrum of liquid triflic acid. Clearly, the spectra of all the Zr-TMS-TFA samples are very similar to each other and to that of liquid trifluoromethanesulphonic acid. No bands appear in the spectra of the Zr-TMS-TFA samples that do not appear in the spectrum of the acid itself. Only small peak shifts exist for some bands on the supported samples relative to the liquid acid. These will be discussed in detail later. Comparing Figure 4.7A-5-30 wt % one observes that the intensity of each band increases with increased loading of triflate. Figure 4.7A-20 wt % is somewhat anomalous and may indicate that the

sample actually contains more than 20 wt % triflate. Elemental analysis in fact revealed that the sulfur content was lower than 20 wt % (16.6 wt %). According to Table 4.1 the actual change in S content between spectra 7A-20-30 wt % was smaller than theoretically calculated (13–22.8 wt % rather than 15–30 wt %). Figure 4.7B shows the spectra for the A-Zr-TFA samples. Again the spectrum of the support was subtracted. These spectra are again very similar to that of the liquid acid.

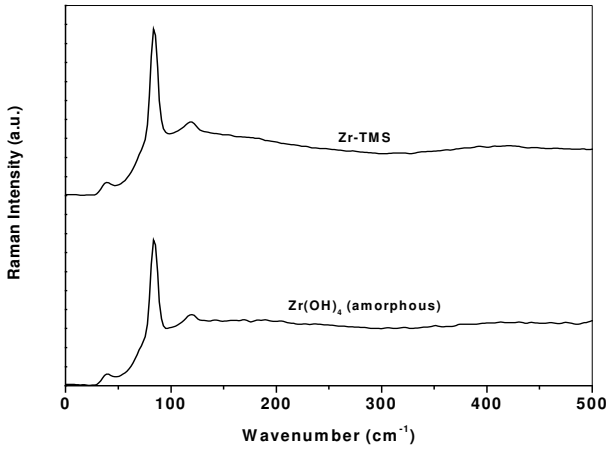

Figure 4.6. FT-Raman spectra of amorphous $Zr(OH)_4$ and Zr-TMS, 4 cm^{-1}, 100 scans, 50 mW.

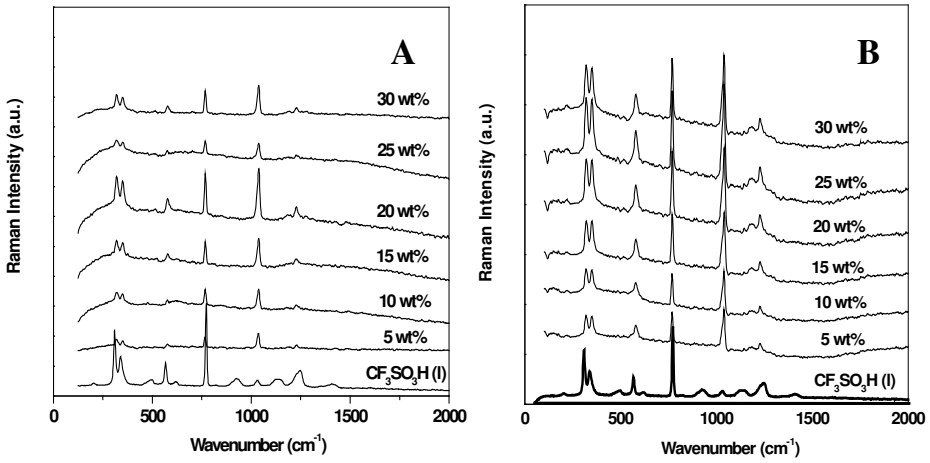

Figure 4.7. FT-Raman spectra of adsorbed triflate at different acid loadings (A) A-Zr-TFA, (B) Zr-TMS-TFA. The spectra of the solid material were subtracted in each case (4 cm^{-1}, 100 scans, 50 mW). The spectrum of liquid triflic acid is also shown in each case of comparison.

The peak data from Figure 4.7A and B are compiled in Table 4.2. Also listed are previously published data regarding the Raman spectrum of liquid trifluoromethanesulphonic acid and the band assignments previously made for this molecule [48, 49]. As shown in Table 4.2, excellent agreement exists between the measured and the previously reported Raman spectra of liquid triflic acid. The assignments are from the work of Katsuhara et al. [48] who were the first to measure and assign the complete spectrum between 1500–0 cm^{-1}. They assumed that the CF_3SO_3H molecule belonged to the point group C_s with, however, local C_{3v} symmetry (the CF_3 group). They also assumed that this group was free to rotate around the C-S bond. The most relevant bands for this study are the SOH deformation mode at 1122 cm^{-1} and the symmetric and asymmetric stretching modes of SO_2 (at 1248 and 1410 cm^{-1} respectively). The symmetric stretching band of the triflate anion ($CF_3SO_3^-$) is also included in Table 4.2 (1034 cm^{-1} [49], 1038 cm^{-1} [50]). This peak was not observed in very pure acid since there is very little dissociation. We observed a small band at 1030 cm^{-1}. Since no attempt was made to purify the acid or to keep it totally dry, trace water obviously led to some dissociation in our case. Finally, the OH stretching frequency, previously reported at 2997 cm^{-1} [49], was observed at 2999 cm^{-1} in this study. Previous work on bulk samples of metal sulphonate salts [50] showed that the sulphonate oxygen atoms were in equivalent, symmetric positions. Normal coordinate analyses of IR and Raman spectra indicated that the $CX_3SO_3^-$ anions (x = H, D, F, Cl) had C_{3v} symmetry in which the three oxygen atoms coordinate in an equivalent manner to a metal ion with three-fold rotational symmetry about the C-S bond. Essentially the sulphonate group acts as a tripod.

The C_{3v} point group has 18 normal vibrational modes that can be classified by the symmetry types: T_{vib} = 5 A′ + A″ + 6E. All modes, excepting the A″ mode, are both IR and Raman active.

Table 4.2. Compilation of Raman bands measured (cm^{-1}) for Zr-TMS-TFA, A-Zr-TFA and for liquid CF_3SO_3H. The band assignments were made previously [49, 50] and apply to the liquid acid molecule only.

Zr-TMS-TFA	A-Zr-TFA	CF_3SO_3H (liquid)		Assignment[48,a]
This Study			Literature[48,a]	
-	-	2999	2997[49]	υ (OH) A′ [49]
1412	1396	1410	~ 1400	υ_{as} (SO_2) A″
1256	1266	1248	1244	υ_s (SO_2) A′
1229	1228	~ 1228	~ 1232	υ_d (CF_3) E
-	1185	1151	~ 1152	υ_s (CF_3) A_1
-	-	1130	1122	δ (SOH) A′
1038	1040	1030	1034[49],1038[50]	υ_s (S-O_3^-)[49,50]
929	924	929	930	υ (SO(H)) A′
768	769	773	775	δ_s (CF_3)A′[48], υ (CS) A′[49]
~ 620	619	619	622	δ (SO_2 bend) A′
576	578	568	570	δ_d (CF_3) E
513	518	499	499	δ (SO(H) wag) A′
~ 480	492	478 (sh)	478 (sh)	δ (SO_2 rock) A″
350	351	339	340	δ (SCF_3 wag) A′
319	321	309	312	υ (CS) A′ [48], CF_3 wag A″[49]
~ 223	213	202	201	ρ (CF_3) E

[a] Assignments were made assuming that the CF_3SO_3H molecule belongs to the point group C_s however has local C_{3v} symmetry (CF_3 group).

Table 4.3. Vibrational modes of S-O_3^- group (assuming C_{3v} symmetry) for $CF_3SO_3^-$ and their measured IR and Raman frequencies (cm^{-1}).

Mode	IR[50]	Raman[50]	Raman[this study]	
			Zr-TMS-TFA	A-Zr-TFA
υ_s (S-O_3^-) A′	1019-1049 (s-vs)	1038 (s-vs) p	1038	1041
υ_a (S-O_3^-) E	1152-1194 (s-vs)	1188 (vw) dp	-	1185
δ_s (S-O_3^-) A′	630- 676 (s-vs, br)	635 (s) p	~620	619
δ_a (S-O_3^-) E	515- 531 (w-s)	520 (vw) dp	513	518
ρ_a (S-O_3^-) E	350- 356 (w-s)	353- 359 (m) dp	350	351

Hall and Hansma [50] studied the adsorption and orientation of sulphonic acids on alumina using inelastic tunneling spectroscopy and found that sulphonate groups also bind through three equivalent oxygen atoms in a tridentate form on this surface. The four possible binding modes of $CF_3SO_3^-$ (a) monodentate (b) bidentate

(c) tridentate and (d) tridentate (distorted) can be distinguished by their spectra in the following manner. The lowered symmetry of monodentate sulphonates (bound via only one oxygen) leads to splitting of the three degenerate $S\text{-}O_3^-$ stretching modes and produces a spectrum containing three distinct modes spanning about 500 cm^{-1}, centred around 1100 cm^{-1}. Bidentate ligands (bound via two oxygen atoms) also produce three different S-O stretching modes centred around 1150 to 1250 cm^{-1} and separated by at least 300 cm^{-1}. The totally symmetric tridentate sulphonate group (C_{3v}) has only two different S-O stretching modes, the symmetric stretch υ_s and the doubly degenerate asymmetric stretch υ_a. Slight distortion from C_{3v} symmetry results in loss of degeneracy of these two modes resulting in two asymmetric S-O bands slightly split ($\leq$ 32 cm^{-1}) about their degenerate position. The vibrations involving the $S\text{-}O_3^-$ group for the $CF_3SO_3^-$ anion and their measured frequencies (using IR and Raman) are shown in Table 4.3. In a recent previous publication [51] some of us reported the transmission infrared spectrum of Zr-TMS-TFA. The spectrum contained four bands not present in the IR spectrum of the Zr-TMS support. These bands appeared at 1296 cm^{-1} (vs), 1184 cm^{-1} (m), 1043 cm^{-1} (vs), and 601 cm^{-1} (m, br). The first two bands were previously assigned to υ_a and υ_s of the $CF_3S\text{-}O_3^-$ group bound to the surface. However, a more careful examination of the spectrum shows an unresolved shoulder at 1200 cm^{-1}. As shown in Table 4.3, this band should be assigned to υ_a ($CF_3S\text{-}O_3^-$) E. This very weak mode was observed at 1038 cm^{-1} on the A-Zr-TFA samples (see Table 4.2). The band at 1296 cm^{-1} should be assigned to υ_a ($C\text{-}F_3$) E. According to [50], this band has been observed in the IR between 1259 and 1280 cm^{-1} (vs, br) and at 1285 cm^{-1} (vw, dp) in some Raman spectra. Very weak bands were detected at 1256 and 1266 cm^{-1} in the spectra of the Zr-TMS-TFA and A-Zr-TFA materials, respectively. In addition, the band previously reported at 601 cm^{-1} in the IR spectrum is more probably two unresolved bands. Table 4.3 shows that the

symmetric deformation mode of triflate anion, δ_s (S-O_3^-) A′ appears at slightly higher frequencies (630- 676 cm^{-1} (s-vs, br)) in the IR, and at 635 cm^{-1} (s, p) in the Raman. Bands were observed at ~620 cm^{-1} on both the amorphous and the mesoporous samples. The second component of the band is probably due to the asymmetric deformation mode of the CF_3 group [δ_d (C-F_3) E]. As reported in [50], this mode appears between 577 and 591 cm^{-1} (vw-s) in the IR, and at 580 cm^{-1} in the Raman (vw, dp). Bands were observed at 576 cm^{-1} in this study.

4.3.8. Ammonia adsorption-desorption study

Experimental data obtained using the *Hammett* acidity function have shown that triflic acid and perfluorinated acid resins are superacids with H_o values between –12 and –14 [52, 53]. However discrepancies and uncertainties in the practical applications of *Hammett* acidity made us to look for other methods to determine the acid strength of our functionalized materials. Marziano et al. [43] and Corma et al. [54] used potentiometric titration with standardized NaOH and ammonia TPD measurement to obtain the total acidity and the distribution of their acid strengths of triflate and SO_4^{2-}/ZrO_2 materials, respectively. Hence, ammonia TPD technique was used to measure the acidity of the synthesized catalysts.

In addition to the total number of acid sites, a quantitative distribution of acid strengths of the sites on the functionalized materials was obtained by measuring the amounts in five arbitrarily-defined temperature regions during the ammonia TPD experiment (between 30 -70 °C, 70 -110 °C, 110 -150 °C, 150 -200 °C and 200 -300 °C). Since the functionalized materials are covalently bonded to the solid support, it could not be treated above 300 °C (above this temperature triflic acid is lost from the solid support [20, 26, 27, 43]). Table 4.1 shows the total number of acid sites (determined via NH_3 chemisorbed at 30 °C) of Zr-TMS, Zr-TMS-TFA and A-Zr-TFA. The quantitative distributions of the acid sites (in the 5 regions) are also shown.

The total number of acid sites on the catalysts was found to increase proportionally with increased loading of triflic acid supported on Zr-TMS. The same trend of increasing the total number of acid sites with increasing triflic acid loading was observed in the A-Zr-TFA catalysts (see Table 4.1). A larger number of acid sites were observed for the amorphous catalyst (A-Zr-TFA-30) than for the mesoporous catalyst (Zr-TMS-TFA-30). This is consistent with the results of elemental analysis (see Table 4.1).

The total number of acid sites on the Zr-TMS was found to be 0.50 mmol g^{-1}; the Brönsted acid sites are formed by the hydroxyl groups that exist in the Zr-TMS material. The total amount of NH_3 chemisorbed at 30 °C was 0.77 mmol g^{-1} for Zr-TMS-TFA-5 and 1.55 mmol g^{-1} for Zr-TMS-TFA-30. The total number of acid sites on SO_4^{2-}/ZrO_2 (measured between 30 to 600 °C) was found to be 1.45 mmol g^{-1}. Silica-supported triflic acid showed superacid character (*i.e.* the acidity was greater than that of 100 % H_2SO_4 [26]. Triflic acid alone is also known to be a superacid [20].

Further, the acid strength distribution (in %) of Zr-TMS, Zr-TMS-TFA, amorphous $Zr(OH)_4$, and A-Zr-TFA are given in Table 4.1. The results of ammonia TPD measurements reveal that the total acidity (mmol g^{-1} at 30 °C) increases with the increase in loading of triflic acid over amorphous $Zr(OH)_4$ and Zr-TMS. However, the acid strength distribution (measured in five steps) remains nearly unchanged except between 110-150 °C. It is observed that the percentage of the acid sites (between 110-150 °C) increases from 33 to about 38 %, and 32 to 41 % when the triflic acid loading was increased from 0 to 30 wt % over amorphous Zr(OH) and Zr-TMS, respectively.

4.3.9. Scanning electron microscopic study

The particle size and morphology of Zr-TMS and Zr-TMS-TFA-30 were studied by SEM. SEM micrographs of Zr-TMS (Figure 4.8 A) and Zr-TMS-TFA-30 (Figure 4.8 B) are typical of ordered ZrO_2 [55] and MCM-41 [56] type materials

exhibiting the winding-worm type. It is noteworthy that previous authors have reported mesoporous zirconia to be very disordered [11]. Zr-TMS consisted of ordered particles (winding-worm type) of approximately 0.33 µm in size. The particle size of Zr-TMS-TFA-30 was slightly larger (approximately 0.4 µm). The particles appeared to be of a distorted winding-worm type. It appears that functionalization alters the particle size to some extent. The increase in the particle size with the increase of CF_3SO_3H loading is attributed to anchoring of triflic acid on Zr-TMS. This decrease in ordering and crystallinity was also observed by XRD.

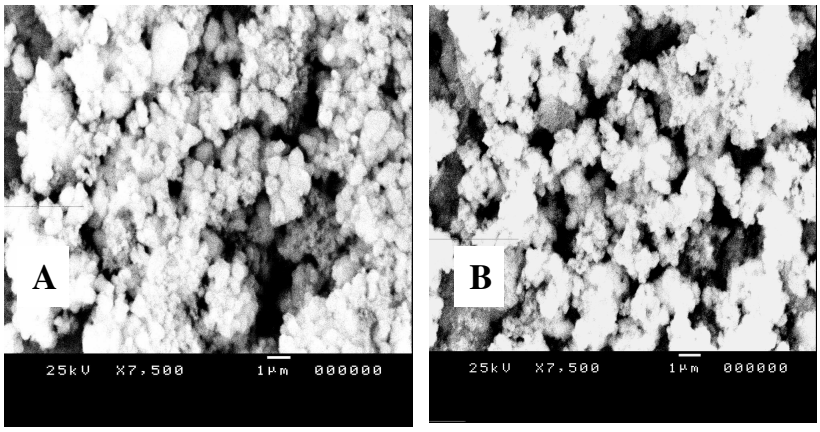

Figure 4.8. Scanning electron micrographs of (A) Zr-TMS, (B) Zr-TMS-TFA-30.

4.3.10. Transmission electron microscopic study

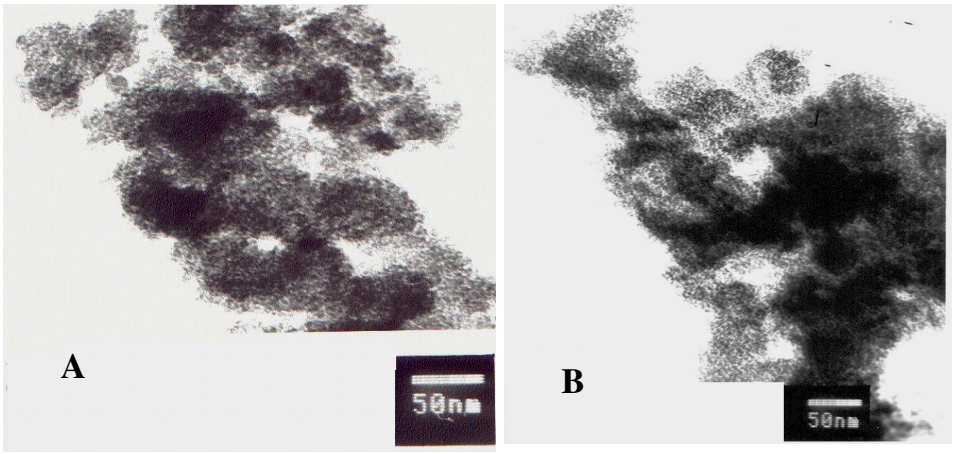

Figure 4.9. Transmission electron micrographs of (A) Zr-TMS, (B) Zr-TMS-TFA-30.

The samples were prepared for TEM analysis by sonification in iso-propanol followed by deposition on carbon-coated copper grids. Transmission electron micrographs of Zr-TMS (Figure 4.9 A) and Zr-TMS-TFA-30 (Figure 4.9 B) reveal that these materials have a highly porous nature and contain either disordered hexagonal phases or pseudo-hexagonal arrays. These results are in good agreement with the earlier studies of Zr-TMS [57, 58].

4.3.11. Thermal analysis (TG, DTA & DTG) study

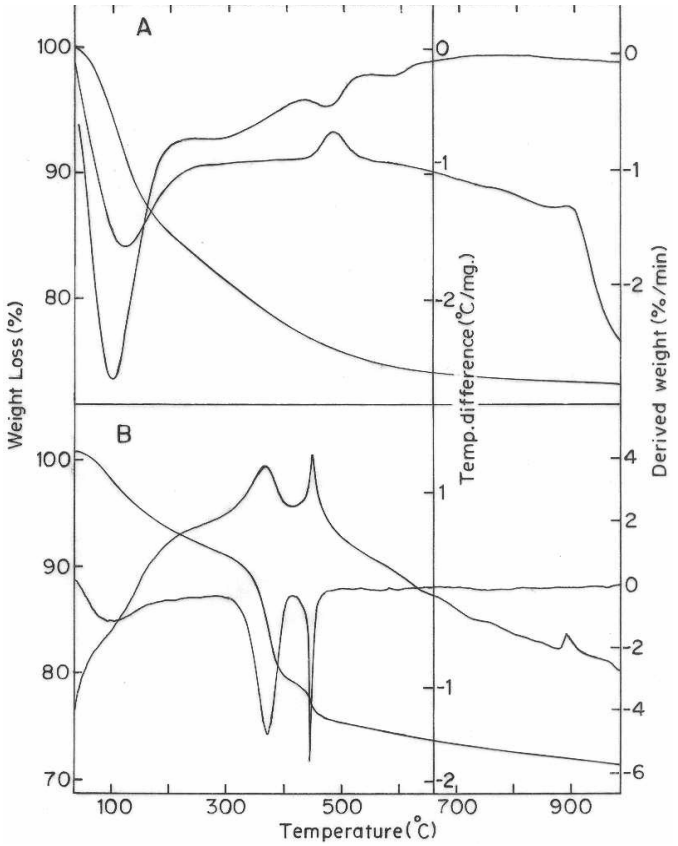

Figure 4.10. Thermo Gravimetric Differential thermal analysis (TG, DTA & DTG) profiles of (A) Zr-TMS (B) Zr-TMS-TFA-30.

Thermal analysis of all synthesized catalysts showed similar results. Figures 4.10 A and B show typical TG, DTA and DTG profiles measured for Zr-TMS and Zr-TMS-TFA-30 samples, respectively. The TG curve of Zr-TMS shows three stages of

weight loss. The weight loss (endothermic) between 70 and 200 °C corresponds to the loss of loosely bound water (Desorption of adsorbed water) [57] and residual butanol (the latter was used as solvent in the synthesis mixture). Further, the weight loss between 200 to 400 °C corresponds to the decomposition of $Zr(OH)_4$ into ZrO_2 [11, 13]. A slight decrease at about 450 °C in the TG curve and a corresponding sharp exothermic peak at the same temperature in the DTA curve are indicative of an additional phase coexisting with zirconia. This may be a quasi-amorphous tetragonal phase produced in the decomposition process of $Zr(OH)_4$ [59]. No further weight losses were observed above 650 °C. At this point the residue is anhydrous ZrO_2.

The TG curve of Zr-TMS-TFA-30 (Figure 4.10 B) shows four stages of weight loss as described above. The decrease between 70 and 200 °C corresponds to the loss of loosely bound water and residual butanol. The large weight losses between 320 and 400 °C [28] and between 400 and 440 °C correspond to the loss of the trifluoromethane sulfonate ($O\text{-}SO_2\text{-}CF_3$) group from the zirconia surface and to the complete phase change of $Zr(OH)_4$ to ZrO_2, respectively. Hence these functionalized materials cannot be treated above 300 °C.

Differential thermal gravimetric (DTG) analysis of the catalysts agreed well with the results obtained by TG-DTA. Figure 4.10A shows the DTG profile of the Zr-TMS catalyst. Two endothermic peaks were observed at about 110 and 450 °C), for Zr-TMS whereas three endothermic peaks were observed (at about 100, 370 and 440 °C) for Zr-TMS-TFA-30 (Figure 4.10 B). The endothermic peak at 360 °C corresponds to the loss of trifluoromethane sulfonate. The sharp endothermic peak at 440 °C is attributed to the additional phase and the phase change of zirconia. In addition, a sharp exothermic peak exhibits at about 900 °C in DTA curve corresponds to the crystallization of material and the phase change from tetragonal to monoclinic and it is also observed in Zr-TMS (Figure 4.10 A).

4.3.12. Liquid phase acetalization of ethylacetoacetate

Table 4.4. Liquid phase acetalization of ethylacetoacetate with ethylene glycol using Zr-TMS, Zr- TMS-TFA, A-Zr-TFA, CF_3SO_3H, and sulfated zirconia catalysts[a]

Catalyst	Conversion of EAA (wt %)	TOF[b] (h^{-1} mol^{-1} S)	Product distribution (wt %)[c]	
			EDBA	Fructone
Amor- $Zr(OH)_4$	18.0	--	3	97
A-Zr-TFA[e]-5[f]	83.0	265.6	36	64
A-Zr-TFA-10	83.0	130.2	18	82
A-Zr-TFA -15	89.0	105.5	27	73
A-Zr-TFA -20	94.0	94.1	21	79
A-Zr-TFA -25	89.0	55.2	22	78
A-Zr-TFA -30	92.0	49.8	35	65
CF_3SO_3H[d]	95.0	54.0	26	74
SO_4^{2-}/ZrO_2	93.0	96.6	10	90
Zr-TMS	21.0	--	0	100
Zr-TMS-TFA-5	82.0	259.0	0	100
Zr-TMS-TFA-10	87.0	183.0	0	100
Zr-TMS-TFA-15	88.0	101.3	0	100
Zr-TMS-TFA-20	88.0	79.5	0	100
Zr-TMS-TFA-25	91.0	75.6	0	100
Zr-TMS-TFA-30	93.0	61.2	0	100

[a]Reaction conditions: Catalyst (g) = 0.1; Ethylacetoacetate (mmol) = 10; Ethylene glycol (mmol) = 10; Reaction time (h) = 1; Reaction temperature (°C) = 100; Toluene (g) = 25.
[b]TOF is given as moles of EAA transformed per hour per mole of Sulfur.
[c]EDBA: 3,3-ethylenedioxy butanoic acid; Fructone: ethyl 3,3-ethylenedioxybutyrate.
[d]Catalyst (g) = 0.125; Reaction time (h) = 1.

The catalytic activity of the synthesized materials was examined in the acetalization of ethylacetoacetate with ethylene glycol to fructone in batch reactors at 100 °C for 1 h. The results of acetalization of ethylacetoacetate to fructone are given in Table 4.4. Under similar reaction conditions, the Zr-TMS-TFA catalysts were more active than Zr-TMS and comparable to SO_4^{2-}/ZrO_2 and A-Zr-TFA. The Zr-TMS and amorphous $Zr(OH)_4$ showed 21 and 18 wt % conversion of EAA, respectively, due to the limited number of acid sites. However, in terms of selectivity amorphous $Zr(OH)_4$ gave 97 wt % to fructone whereas Zr-TMS was 100 wt % selectivity to fructone. This higher selectivity is attributed to the presence of well-defined pores. Since the acidity of the functionalized mesoporous and the amorphous catalysts are similar with

respect to the triflic acid loading (Table 4.1), both series of catalysts showed more or less similar conversion of EAA. The EAA conversion was 82 wt % for Zr-TMS-TFA-5 and 93 wt % for Zr-TMS-TFA-30. Further, the EAA conversion over A-Zr-TFA-5 and A-Zr-TFA-30 was 83 and 92 wt %, respectively. All the Zr-TMS-TFA catalysts showed the conversion of EAA between 82 and 93 wt % with 100 wt % selectivity to fructone (Table 4.4). The selectivity of the A-Zr-TFA catalysts to fructone was much poorer (between 64 and 82 wt %) than over the Zr-TMS-TFA catalysts. SO_4^{2-}/ZrO_2 showed 93 wt % conversions of EAA and 90 wt % selectivity to fructone. The lower selectivity of SO_4^{2-}/ZrO_2 may be correlated due to its non-uniform pore size, low porosity and smaller surface area. Pure CF_3SO_3H showed higher conversion (95 wt %) than all the catalysts, with a selectivity of 74 wt %. The homogeneous medium of strong acid and the water formed during this reaction can cause the hydrolysis of the ester, producing the corresponding EDBA (3,3-ethylenedioxy butanoic acid). The formation of this product not only reduces the yield of fructone, but also it can alter the organoleptic characteristics of the final product. The turnover frequency (TOF) was calculated as number of moles of EAA converted per moles of sulfur per hour. Since the conversions were almost the same in all the cases with respect to the loading of triflic acid, TOF was found to be approximately similar for both types of catalysts (Table 4.4). The TOF (in mol^{-1} S h^{-1}) for Zr-TMS-TFA-5, Zr-TMS-TFA-30, and A-Zr-TFA-5 and A-Zr-TFA-30 were 259, and 61.2, and 265.6 and 49.8, respectively. The TOF of triflic acid and SO_4^{2-}/ZrO_2 were 54.0 and 96.9, respectively.

4.3.13. Liquid phase benzoylation of biphenyl

The catalytic activity of the synthesized materials was examined in the benzoylation of biphenyl with benzoyl chloride to 4-PBP in batch reactors at 170 °C for 6 h, The results for the benzoylation reaction of BP to 4-PBP are given in Table 4.5. As in the acetalization reaction, due to the limited acidity, both Zr-TMS and amorphous $Zr(OH)_4$ showed comparable conversion of BP, 3.2 and 3.1 wt %,

respectively. Further, the biphenyl conversion dramatically increased after the functionalization of triflic acid over Zr-TMS. All the Zr-TMS-TFA catalysts showed higher conversion of BP with 100 wt % selectivity to 4-PBP. The conversion of BP over the Zr-TMS-TFA catalysts was between 22 and 41 wt % when the triflic acid loading was increased from 5 to 30 nominal wt %. In the same manner, the conversion of BP over the A-Zr-TFA catalysts was between 5 and 20 wt % for nominal loadings of triflic acid increasing from 5 to 30 wt %. In terms of selectivity, the Zr-TMS-TFA catalysts showed 100 wt % to 4-PBP whereas the A-Zr-TFA catalysts produced a small amount of 2-PBP due to its non-porous structure. Triflic acid and SO_4^{2-}/ZrO_2 showed 63.7 and 7.2 wt % conversions of BP, respectively.

Table 4.5. Liquid phase benzoylation of biphenyl with benzoyl chloride using Zr-TMS, Zr-TMS-TFA, A-Zr-TFA, CF_3SO_3H and sulfated zirconia catalysts[a]

Catalyst	Conversion of Biphenyl (wt %)	TOF[b] (10^{-1} $h^{-1}mol^{-1}$ S)	Product distribution (wt %)[c]	
			2-PBP	4-PBP
Amor- $Zr(OH)_4$	3.1	--	0	100
A-Zr-TFA[e]-5[f]	5.0	5.34	3	97
A-Zr-TFA-10	10.2	5.55	2	98
A-Zr-TFA -15	15.5	6.36	2	98
A-Zr-TFA -20	16.0	5.34	4	96
A-Zr-TFA -25	19.1	4.2	3	97
A-Zr-TFA -30	20.5	3.7	2	98
CF_3SO_3H[d]	63.7	54.3	7	93
SO_4^{2-}/ZrO_2	7.2	0.98	0	100
Zr-TMS	3.2	--	0	100
Zr-TMS-TFA-5	22.0	23.2	0	100
Zr-TMS-TFA-10	27.0	21.9	0	100
Zr-TMS-TFA-15	31.5	12.1	0	100
Zr-TMS-TFA-20	35.0	10.5	0	100
Zr-TMS-TFA-25	37.0	10.2	0	100
Zr-TMS-TFA-30	41.0	9.0	0	100

[a]Reaction conditions: Catalyst (g) = 0.5; Biphenyl (mmol) = 10; Benzoyl chloride (mmol) = 10; Reaction time (h) = 6; Reaction temperature (° C) = 170; Nitrobenzene (ml) = 20.
[b]TOF is given as moles of BP transformed per hour per mole of Sulfur.
[c]2-PBP= 2-phenylbenzophenone; 4-PBP= 4-phenylbenzophenone
[d]Catalyst (g) = 0.125; Reaction time (h) = 3.

The selectivity to 4-PBP over CF_3SO_3H was only 93 wt % due to its nonshape-selective nature. These results demonstrate that the BP benzoylation reaction essentially needs a porous catalyst with uniform pore size and higher acidity. The TOF was calculated as the number of moles of BP converted per mole of sulfur per hour. TOF (in $10^{-1}mol^{-1}$ S h^{-1}) of BP conversion over Zr-TMS-TFA-5, Zr-TMS-TFA-30, A-Zr-TFA-5, and A-Zr-TFA-30 were 23.2, 9.0, and 5.34, and 3.7, respectively. The TOF (in $10^{-1}mol^{-1}$ S h^{-1}) of CF_3SO_3H and SO_4^{2-}/ZrO_2 were 54.3 and 0.98, respectively.

4.3.14. Catalyst recycles study

Recycle of the synthesized catalysts was studied in the acetalization reaction using Zr-TMS-TFA-30 in order to check the stability and activity of recycled catalysts (Table 4.6). Three reaction cycles (fresh and two recycles) were carried out under similar reaction conditions, using the same catalyst. Elemental analysis (Table 4.6) and XRD analysis (Figure 4.11) showed that both sulphur content and catalyst crystallinity decreased after each cycle. The conversion of EAA decreased to some extent on recycling (from 93 to 86 wt %), whereas the selectivity to fructone did not change. The loss of sulfur and the decrease in the crystallinity of the catalyst were the likely causes of the decrease in catalytic activity.

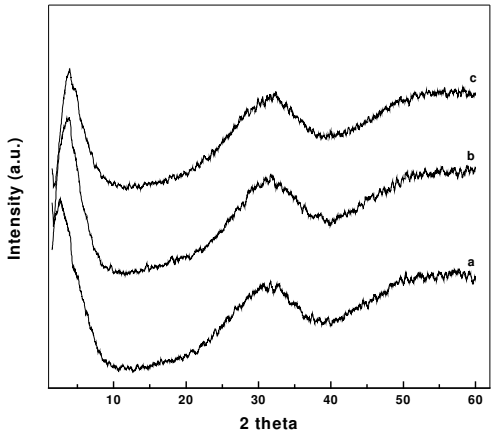

Figure 4.11. Powder X ray diffraction patterns of fresh and recycled catalysts (a) fresh Zr-TMS-TFA-30; (b) after one recycle; (c) after two recycles.

Table 4.6. Recycling study of Zr-TMS-TFA-30 catalyst in acetalization of ethylacetoacetate with ethylene glycol reaction[a]

Cycle	Elemental analysis[b] (wt %)		Conversion of EAA (Wt %)	TOF[c] ($h^{-1}mol^{-1}$ S)	Selectivity to fructone (wt %)
	C	S			
Fresh	2.0	4.86	93.0	61.2	100
1st Recycle	1.96	4.79	86.0	61.8	100
2nd Recycle	1.92	4.71	86.0	68.7	100

[a]Reaction conditions: Catalyst (g) = 0.1; Ethylacetoacetate (mmol) = 10; Ethylene glycol (mmol) = 10; Reaction time (h) = 1; Toluene (g) = 25; Reaction temperature (°C) = 100.
[b]Elemental analysis by EA1108 elemental analyzer (Carlo Erba).
[c]TOF is given as moles of EAA transformed per hour per mole of Sulfur.

4.3.15. Liquid phase benzoylation of toluene (Catalysts optimization study)

4.3.15.1. Catalytic activity of various catalysts

The results of the catalytic activities in the benzoylation of toluene with *p*-T-Cl using conventional catalyst CF_3SO_3H, Zr-TMS and various amounts of CF_3SO_3H anchored over Zr-TMS (Zr-TMS-TFA) are depicted in Table 4.7. The main product of the reaction is 4,4'-DMBP. A small amount of 2,4'-DMBP is also observed. The formation of 4,4'-DMBP and 2,4'-DMBP results from the aromatic substitution of toluene. The activities of various catalysts are compared under identical reaction conditions using data after 8 h run.

The conversion of *p*-T-Cl, rate of *p*-T-Cl conversion, product distribution and 4,4'-DMBP to 2,4'-DMBP ratio depend on the type of catalysts used. As can be seen from the Table 4.7, Zr-TMS-TFA-30 catalyst is found to be more active than any other catalysts. Zr-TMS is less active due to its lower acidic nature. The conversion of *p*-T-Cl (wt %), rate of *p*-T-Cl conversion ($10^{-1}h^{-1}mol^{-1}S$) and selectivity (wt %) for 4,4'-DMBP over Zr-TMS-TFA-5, Zr-TMS-TFA-15, Zr-TMS-TFA-30 and Zr-TMS after 8 h of reaction time are found to be 46.0, 50.7, 54.0, 22.4 (wt %), 13.2, 14.5, 15.5, 6.4 ($10^{-1}h^{-1}mol^{-1}S$) and 75.9, 73.5, 74.2, 78 (wt %), respectively. CF_3SO_3H produces 20.1

wt % 2,4'-DMBP and 76.4 wt % 4,4'-DMBP at 87.5 wt % conversion level of *p*-T-Cl after 0.25 h reaction time. Amongst the Zr-TMS-TFA with various loadings of triflic acid studied, Zr-TMS-TFA-30 revealed the highest *p*-T-Cl conversion and rate of *p*-T-Cl conversion, which may be attributed to its stronger acid sites as seen from NH_3 desorption experiment, which is given in Table 4.1.

The total number of acid sites on the catalysts was found to increase proportionally with increased loading of triflic acid over Zr-TMS. The total number of acid sites on the Zr-TMS was found to be 0.50 mmol g^{-1}**.** The total amount of NH_3 chemisorbed at 30 °C was 0.77 mmol g^{-1} for Zr-TMS-TFA-5, 1.05 mmol g^{-1} for Zr-TMS-TFA-15 and 1.55 mmol g^{-1} for Zr-TMS-TFA-30. The catalysts used in this study, show the following decreasing order of activity after 8 h of reaction time: CF_3SO_3H > Zr-TMS-TFA-30 > Zr-TMS-TFA-15 > Zr-TMS-TFA-5 > Zr-TMS. The results indicate that mainly *ortho*- and *para*- substitutions take place over Zr-TMS-TFA catalyst, which is expected for an electrophilic aromatic substitution pathway [60].

Table 4.7. Liquid phase benzoylation of toluene with p-toluoyl chloride using Zr-TMS-TFA and CF_3SO_3H catalysts [a]

Catalysts	Reaction time (h)	PTC Conversion (wt %)[b]	TOF[c] (10^{-1} $h^{-1}mol^{-1}$ S)	Product distribution[d] (wt %)		
				2,4'-DMBP	4,4'-DMBP	Others
Zr-TMS	8 24	22.4 42.2	-- --	22 15.5	78 78.6	0 5.9
Zr-TMS–TFA-5	8 24	46.0 72.0	13.2 6.8	22.1 23.0	75.9 73.3	2.0 3.7
Zr-TMS–TFA-15	8 24	50.7 82.1	14.5 7.8	22.5 21.4	73.5 74.1	4.0 4.5
Zr-TMS–TFA-30	8 24	54.0 85.0	15.5 8.1	22.5 22.8	74.2 73.9	3.3 3.3
CF_3SO_3H	0.25 3	87.5 100	420.1 40.0	20.1 21.2	76.4 75.2	3.5 3.6

[a]Reaction conditions: Catalyst (g) = 0.5; Toluene (mol) = 0.01; *p*-Toluoyl chloride (mol) = 0.01; Reaction temperature (°C) = 130; Nitrobenzene (ml) = 10

[b]*P*-T- Cl = *para*-toluoyl chloride.

[c]TOF = moles of *p*-T-Cl transformed per second per mol of sulfur.

[d]2,4'-DMBP = 2,4'-dimethylbenzophenone; 4,4'-DMBP = 4,4'-dimethylbenzophenone.

4.3.15.2. Duration of the run

The conversion of *p*-T-Cl as a function of reaction time for the benzoylation of toluene over various Zr-TMS-TFA (5, 15, and 30 wt % TFA) and other catalysts such as Zr-TMS and TFA are given in Figure 4.12. Increasing reaction time increased the conversion of *p*-T-Cl over all catalysts. Zr-TMS-TFA-30 showed considerably superior performance throughout the reaction and its activity is found to be higher compared with those of other catalysts. The reason could be the higher strength and number of acid sites. Zr-TMS is found to be much less active. CF_3SO_3H is the most active catalyst and within 0.25 h, 87.5 wt% conversion of *p*-T-Cl is obtained (Figure 4.12). The catalytic activity of various catalysts used in this study after 24 h of reaction time can be arranged in the following order: CF_3SO_3H > Zr-TMS-TFA-30 > Zr-TMS-TFA-15 > Zr-TMS-TFA-5 > Zr-TMS.

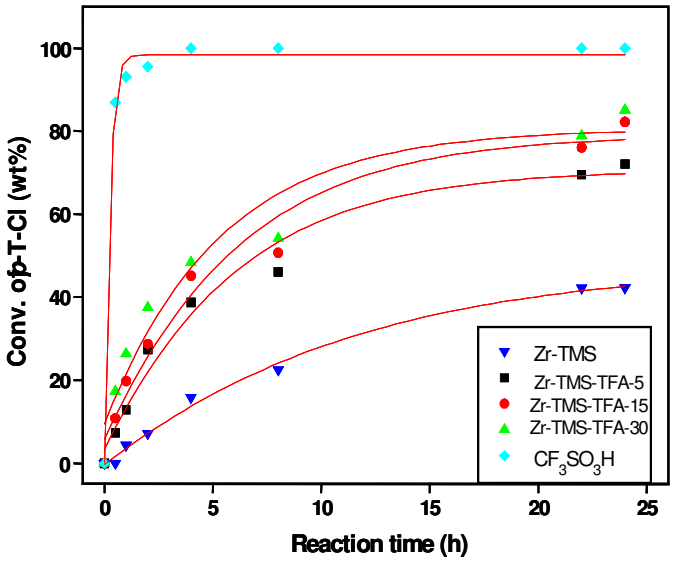

Figure 4.12. Conversion of *p*-T-Cl (wt %) vs. reaction time over various catalysts; Reaction conditions: Catalyst (g) = 0.5; Toluene (mol) = 0.01; p-T-Cl (mol) = 0.01; Reaction temperature (°C) =130; Reaction time (h) =0.25, 0.5, 2, 4, 8, 22 and 24.

4.3.15.3. Influence of reaction time using Zr-TMS-TFA-15.

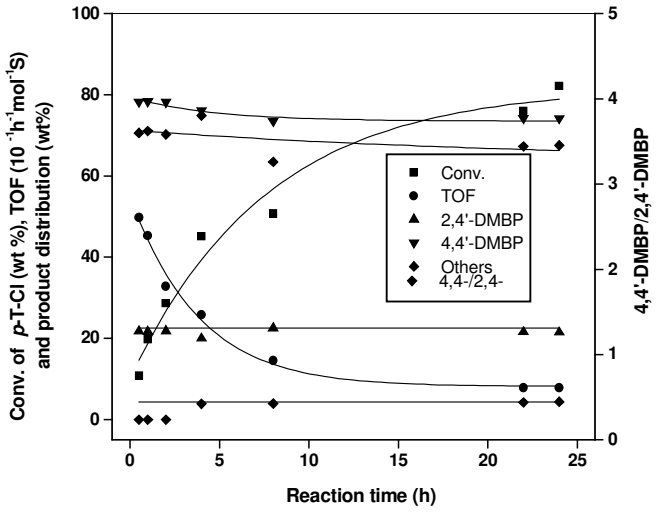

Figure 4.13. Effect of reaction time on the conversion of *p*-T-Cl (wt %), TOF ($10^{-1}h^{-1}mol^{-1}S$), product distribution (wt %) and 4,4'-DMBP/2,4'-DMBP isomer ratio using Zr-TMS-TFA-15. Reaction conditions: Catalyst (g) = 0.5; Toluene (mol) = 0.01; p-T-Cl (mol) = 0.01; Reaction temperature (°C) =130; Reaction time (h) =0.25, 0.5, 2, 4, 8, 22 and 24.

The influence of reaction time on the conversion of *p*-T-Cl, product distribution and 4,4'-DMBP/2,4'-DMBP using Zr-TMS-TFA-15 as catalyst at 130 °C is presented in Figure 4.13. The conversion of *p*-T-Cl increased almost linearly up to 22 h of reaction time and then a marginal increase in the conversion of *p*-T-Cl is observed. *P*-T-Cl along with toluene leads mainly to 4,4'-DMBP with 78 wt % selectivity within 0.5 h reaction time and decreases to 74.1 wt % after 24 h. The results show that the reaction time influenced the conversion of *p*-T-Cl, but did not affect significantly the 4,4'-DMBP/2,4'-DMBP isomer ratio to a great extent.

4.3.15.4. Influence of catalyst / p-T-Cl (wt./wt.) ratio

To study the effects of catalyst concentration on the conversion of *p*-T-Cl, rate of *p*-T-Cl conversion, product distribution and 4,4'-/2,4'- isomer ratio, the catalyst concentration (catalyst / *p*-T-Cl ratio (wt./wt.)) was increased from 0.06 to 0.45 and

the results are depicted in Figure 4.14. The different ratios of catalyst / *p*-T-Cl were obtained by varying the amount of catalyst and keeping the concentration of *p*-T-Cl constant. The conversion of *p*-T-Cl increased from 12.6 to 59.1 wt % as the catalyst concentration increases from 0.06 to 0.45. No change in the product distribution is seen against the change in catalyst concentration. The rate of *p*-T-Cl conversion (TOF) decreases continuously due to the increase in catalyst concentration and a corresponding increase in the concentration of sulfur in the total amount of catalyst used in the benzoylation of toluene.

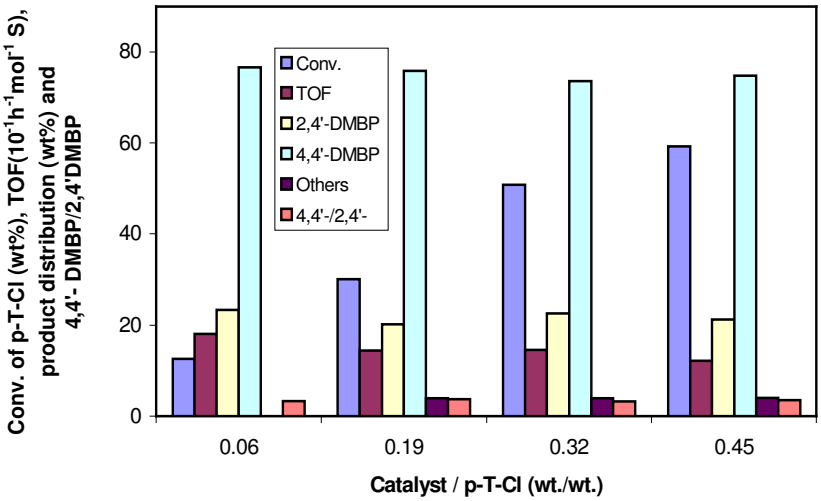

Figure 4.14. Effect of catalyst / *p*-T-Cl (wt./wt.) ratio on the conversion of *p*-T-Cl (wt%), TOF ($10^{-1}h^{-1}mol^{-1}S$), product distribution (wt %) and 4,4'-DMBP/2,4'-DMBP isomer ratio. Reaction conditions: Catalyst (g) = 0.25, 0.5; 0.75 and 1.0; Toluene (mol) = 0.01; p-T-Cl (mol) = 0.01; Reaction temperature (°C) =130; Reaction time (h) = 24.

4.3.15.5. Influence of reaction temperature

The effect of reaction temperature was studied on the rate of benzoylation of toluene with *p*-toluoyl chloride as benzoylating agent over Zr-TMS-TFA-15 catalyst in the temperature range 110 to 140 °C using a toluene / *p*-T-Cl molar ratio as 1. When the temperature is increased from 110 to 140 °C, both the conversion of *p*-T-Cl and TOF increased from 28.3 to 69.5 wt % and 8.1 to 19.9 ($10^{-1}h^{-1}mol^{-1}S$), respectively.

However, the selectivity for 4,4'-DMBP remains nearly unchanged with the increase in reaction temperature, as shown in Figure 4.15. One of the reasons for the increased rates at higher temperature may be ascribed to an enhancement of the rate of diffusion of *p*-T-Cl inside the channel of the catalyst; however, reaction rates are usually more temperature dependant than rate of diffusion [61]. Increasing the reaction temperature increases the catalytic activity and the conversion of *p*-T-Cl increases sharply at the initial stages (8 h) of the reaction and finally (22 h) reaches a relatively steady state value over all temperatures. The apparent activation energy of *p*-T-Cl conversion over Zr-TMS-TFMSA-15 catalyst is estimated to be 38.11kJ/mol as it is depicted in Figure 4.16 in the temperature range of 110 to 140 °C.

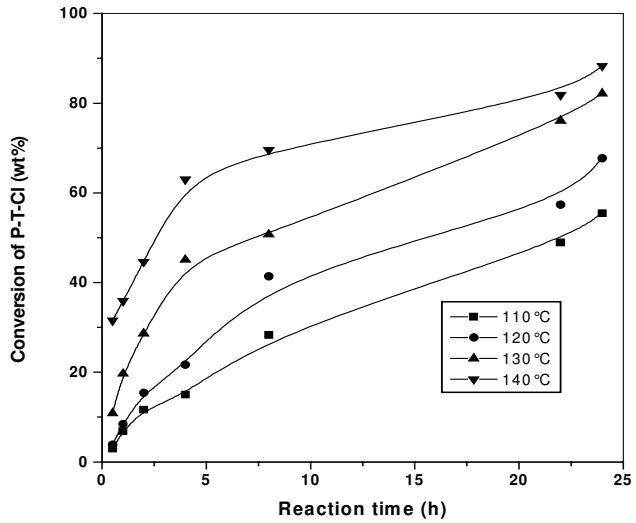

Figure 4.15. Effect of reaction temperature (°C) on the conversion of *p*-T-Cl (wt %) over Zr-TMS-TFA-15 catalyst with reaction time (h). Reaction conditions: Catalyst (g) = 0.5; Toluene (mol) = 0.01; p-T-Cl (mol) = 0.01; Reaction temperature (°C) =110, 120, 130 and 140; Reaction time (h) =0.25, 0.5, 2, 4, 8, 22 and 24.

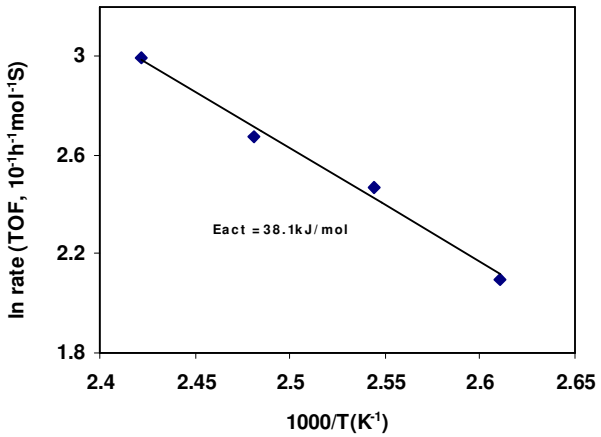

Figure 4.16. Arrehenius plot for the benzoylation of toluene by *p*-T-Cl over Zr-TMS-TFA-15

4.3.15.6 Influence of molar ratios of the reactants

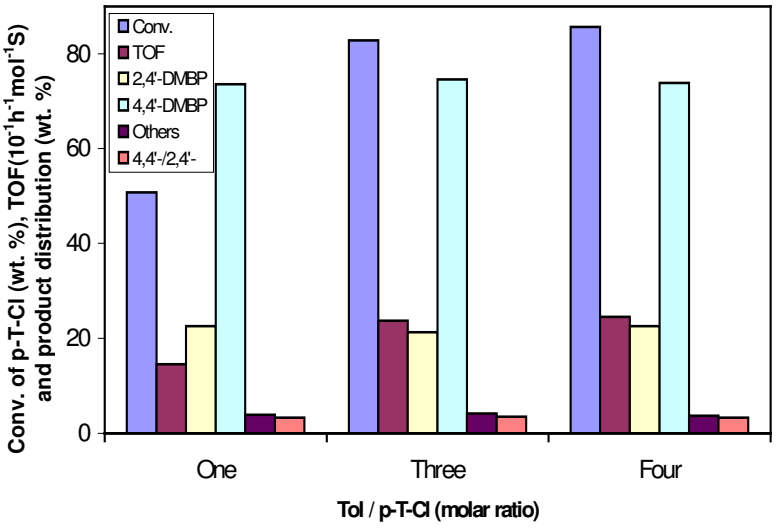

Figure 4.17. Effect of Toluene / *p*-T-Cl molar ratio on the conversion of *p*-T-Cl (wt %), TOF ($10^{-1}h^{-1}mol^{-1}S$), product distribution (wt %) and 4,4'-DMBP/2,4'-DMBP isomer ratio. Reaction conditions: Catalyst (g) = 0.5; Toluene (mol) = 0.01; p-T-Cl (mol) = 0.01, 0.03 and 0.04; Reaction temperature (°C) =130; Reaction time (h) = 24.

The results of the influence of Toluene / *p*-T-Cl molar ratios on the *p*-toluoyl chloride conversion, TOF, product distribution and 4,4'-DMBP/2,4'-DMBP ratio is shown in Figure 4.17. The ratios were changed by keeping the amount of *p*-T-Cl as constant. The data at 130 °C show that, when Toluene / *p*-T-Cl ratio is increased

from 1 to 4, the conversion of *p*-T-Cl and rate of *p*-T-Cl conversion increase linearly from 50.7 wt % and 14.5 ($10^{-1}h^{-1}mol^{-1}S$) to 85.6 wt % and 24.5 ($10^{-1}h^{-1}mol^{-1}S$), respectively. In addition, the selectivity to 4,4'-DMBP is found to be unaffected over the wide range of Toluene / *p*-T-Cl ratio. The conversion of *p*-T-Cl vs. reaction time increases with all molar ratios of Toluene / *p*-T-Cl. A higher increase in the *p*-T-Cl conversion with reaction time is observed when Toluene / *p*-T-Cl molar ratio of four is used in the benzoylation of toluene.

4.3.15.7. Catalyst recycle study

Table 4.8. Recycling of Zr-TMS-TFA-15 in benzoylation of biphenyl with benzoyl chloride reaction[a]

Cycle	Loading of TFA (wt %)	Conv. of *p*-T-Cl[b] (wt %)	Product distribution[c] (wt %)			TOF[b] ($10^{-1}h^{-1}$ $mol^{-1}S$)	crystallinity (%)[e]
			2,4'-DMBP	4,4'-DMBP	Others		
Fresh	15.0	50.7	22.5	73.5	4.0	14.5	100
1st cycle	14.1	49.2	21.6	74.5	3.9	14.9	98
2nd cycle	13.8	45.1	21.5	75.0	3.5	13.6	98

[a-d]see footnotes to Table 4.7.
[e]By X-ray diffraction.

In order to check the stability and catalytic activity, the catalyst was recycled (fresh + two cycles) by using Zr-TMS-TFA-15 in the benzoylation of toluene. The results are presented in Table 4.8. After workup of the reaction mixture, the catalyst was separated by filtration, washed with acetone and activated for 16 h at 200 °C in the presence of air before use in the next experiment. Thus, the recovered catalyst after each reaction was characterized for its chemical composition by elemental analysis and crystallinity by X-ray diffraction (XRD). Elemental analysis showed a downward trend in the content of anchored CF_3SO_3H of Zr-TMS-TFA-15 catalyst after two cycles. A slight decline was observed in the *p*-T-Cl conversion from 50.7 to 45.1 wt %, when the catalyst was reused for first time. The leaching of the CF_3SO_3H from the Zr-TMS catalysts by HCl (formed during the reaction) may be attributed for the decrease in catalytic activity after one cycle.

4.4. CONCLUSIONS

In conclusion, Zr-TMS catalysts have been synthesized based on the sol-gel method by using CTMABr and TMAOH. The template was extracted from the synthesized materials with by using ethanol and HCl. The extracted Zr-TMS was successfully functionalized with triflic acid by post synthesis treatment to obtain covalently-bonded Zr-TMS-TFA catalysts. Various loadings of triflic acid over Zr-TMS were prepared by varying the molar ratios of $Zr(OC_4H_9)_4$, CTMABr, TMAOH, H_2O and CF_3SO_3H. Triflic acid functionalized amorphous (A-Zr-TFA) catalysts were also synthesized and characterized for comparison. The catalysts were characterized by various physico-chemical techniques such as XRD, N_2 adsorption-desorption, FTIR, FT-Raman, elemental analysis, ^{13}C DD/MAS NMR, TPD of NH_3, SEM, TEM, and thermal analysis. BET surface area and pore size distribution results were in general agreement with previous values reported for mesoporous ZrO_2. The NH_3 TPD measurements showed that the catalysts were highly acid. ^{13}C DD/MAS NMR revealed that the $–CF_3$ group remained intact in the material. FT-Raman analysis demonstrated that the triflic acid was bonded in an identical fashion on both amorphous $Zr(OH)_4$ and Zr-TMS at all loadings. Triflate ligands bound via 3 equivalent oxygen atoms to zirconium atoms forming tripod structures. TEM studies teach that the material contained disordered channels, unlike MCM-41 mesoporous molecular sieves. Acetalization of EAA to fructone and benzoylation of BP to 4-PBP reactions were performed on Zr-TMS-TFA, A-Zr-TFA, triflic acid and SO_4^{2-}/ZrO_2. Zr-TMS-TFA catalysts were found to be the most active and selective in both reactions due to their mesoporosity and to an increase in the number of acid sites with the “right” acid strength. The stability and recycle effect of the catalysts were checked in the acetalization reaction by using Zr-TMS-TFA-30. No major loss of activity was observed after two recycles, but a decrease of the sulfur content and catalyst crystallinity was observed.

In another summary, benzoylation of toluene to 4,4'-DMBP reactions were performed on Zr-TMS-TFA-5, Zr-TMS-TFA-15, Zr-TMS-TFA-30, Zr-TMS and TFA catalysts. Zr-TMS-TFA-30 catalyst catalyzes the benzoylation of toluene efficiently with *para*-toluoyl chloride and is superior to other Zr-TMS-TFA catalysts due to its higher acidity. The conventional homogeneous catalyst, CF_3SO_3H, shows higher activity. Total acidity obtained at 30℃ of Zr-TMS and Zr-TMS-TFA with different wt% loading of triflic acid show direct co-relationship between acidity and catalytic activity in the benzoylation of toluene. The influence of the duration of the run, catalyst concentration, reaction temperature and toluene / *p*-T-Cl molar ratio on the catalyst performance is examined in order to optimize the conversion of *p*-T-Cl and selectivity to 4,4'-DMBP. The conversion of *p*-T-Cl using Zr-TMS-TFA-15 increased significantly with an increase in reaction time, catalyst concentration, reaction temperature and toluene to *p*-T-Cl molar ratio. Zr-TMS-TFA-15 was recycled one time and a decrease in *p*-T-Cl conversion is observed after one cycle, which is related to a minor leaching of CF_3SO_3H from the catalyst. The formation of acylated products of toluene is explained by an electrophilic attack of acyl cation ($R\text{-}CO^+$; where R = $CH_3\text{-}C_6H_5$-) on the toluene ring, whose formation is facilitated by acid sites on Zr-TMS-TFA catalysts.

4.5. REFERENCES

1. Y.D. Xia, W.M. Hua, Y. Tang, Z. Goa, *Chem. Commun.,* **1999**, 1899.
2. T. Jin, T. Yamaguchi, K. Tanabe, *J. Phys. Chem.,* 90, **1986**, 4797.
3. M. Hino, K. Arata, *J. Chem. Soc., Chem. Commun.,* **1979**, 1148.
4. A. Corma, *Chem. Rev.,* 95, **1995**, 559.
5. Z. Liu, W. Ji, L. Dong, Y. Chen, *Mater. Chem. Phys.,* 56, **1998**,134.
6. D.M. Antonelli, J.Y. Ying, *Angew. Chem. Int. Ed. Engl.,* 35, **1996**, 426.
7. D.M. Antonelli, J.Y. Ying, *Chem. Mater.,* 8, **1996**, 874.
8. D. Terrible, A. Trovarelli, J. Llorca, C. de Leitenburg, G. Dolcettin, *J. Catal.,*

178, **1998**, 299.

9. A. Sayari, P. Liu, *Micropor. Mater.,* 12, **1997**, 149.
10. G.D. Yadav, J.J. Nair, *Micropor. Mesopor. Mater.,* 33, **1999**, 1.
11. V.I. Parvulescu, H. Bonnemann, V. Parvulescu, B. Endruschat, A. Rufinska, B. Tesche, G. Poncelet, *Appl. Catal. A: Gen.,* 214, **2001**, 273.
12. J.A. Knowles, M.J. Hudson, *J. Chem. Soc., Chem. Commun.,***1995**, 2083.
13. M.J. Hudson, J.A. Knowles, *J. Mater. Chem.*, 6, **1996**, 89.
14. G. Pacheco, E. Zhao, E.D. Valdes, A. Garcia, J.J. Fripiat, *Micropor. Mesopor. Mater.,* 32**, 1999**, 175.
15. J.L. Blin, R. Flamant, B.L. Su, *Int. J. Inorg. Mater.,* 3, **2001**, 959.
16. Y.Y. Huang, T.J. Mccarth, W.M.H. Sachtler, *Appl. Catal. A: Gen.,* 148, **1996**, 135.
17. G. Larsen, E. Lotero, M. Nabity, L.M. Petkovic D.S. Shobe *J. Catal.,* 164, **1996**,246.
18. E. Zhao, S.E. Hardcastle, G. Pacheco, A. Garcia, A.L. Blumenfeld, J.J. Fripiat, *Micropor. Mesopor. Mater.,* 31, **1999**, 9.
19. D.S. Sood, S.C. Sherman, A.V. Iretskii, J.C. Kenvin, D.A. Schiraldi, M.G. White, *J. Catal.,* 199, **2001**,149.
20. R.D. Howells, J.D.Mc. Cown, *Chem. Rev.,* 77, **1977**, 69.
21. A. Senning, *Chem. Rev.*, 65, **1965**, 385.
22. D.G. Russel, J.B. Senior, *Can. J. Chem.,* 52, **1974**, 2975.
23. J.W. Brockington, R.H. Bennett, *US Patent.* US3970721, **1976**.
24. J.F. Joly, C. Marcilly, E. Benazzi, *US Patent,* US5336833, **1994**.
25. S.I. Hommeltoft, *Eur. Pat.*, EP0987237A, **2000**.
26. D.Q. Zhou, J.H. Yang, G.M. Dong, M.Y. Huang, Y.Y. Jiang, *J. Mol.Catal. A: Chem.,* 159, **2000**, 85.

27. A.N. Parvulescu, B.C. Gagea, M. Alifanti, V. Parvulescu, V.I. Parvulescu, S. Nae, A. Razus, G. Poncelet, P. Grange, *J. Catal.,* 202, **2001**, 319.

28. K. Wilson, A. Renson, J.H. Clark, *Catal. Lett.,* 61, **1999**, 51.

29. K. Bauer, D. Garbe, H. Surburg, *Common Fragrances and Flavors Materials,* 2nd Ed., VCH, New York, **1990**.

30. A. Walczak, J. Rzasa, S. Labus, *Pol. Pat.,* PL170632, **1997**.

31. J.I. Kroschwitz, M. Howe-Grant, Ed. Kirk-Othmer, *Encyclopedia of Chemical Technology,* 4th Edn., Wiley, New York, **1995**, 454.

32. U. Beck, *Ullmann's Encyclopedia of Industrial Chemistry,* Eds. W. Gerhartz, Y.Y. Stephen, F.T. Campbell, R. Pfeffekorn, J.F. Rounsaville, VCH, Weinheim, vol. A15, **1986**, p. 91.

33. M. Nakatsuka, Y. Tanabe, K. Yoshikawa, *Jpn. Patent,* JP 08290668, **1996**.

34. M. Windholz (Ed.), Merck Index, *An Encyclopedia of chemical drugs and Biochemicals,* 10th ed., published by Merck and Co. Inc., Rahway, NJ, **1983**, p. 7199.

35. H. Limpricht, *Annalen,* 91, **1900**, 312.

36. A.L. Klebanski, K.K. Tchevychatova, *Zh. Obshch. Khim.,* 5, **1935**, 535.

37. R.E. Wilson, E.W. Fuller, *J. Ind. Eng. Chem.,* 14, **1922**, 406.

38. M. Walker, *US Patent,* US6362375, **2002**.

39. S. Hitz, R. Prins, *J. Catal.*, 168, **1997**, 194.

40. M. Chamumi, D. Brunel, F. Fajula, P. Geneste, P. Moreau, J. Solof, *Zeolites,* 14, **1994**, 283.

41. A.O. Bianchi, M. Champanati, P.M. Torres, E.R. Castellon, A.J. Lopez, A. Vaccari, *Appl. Catal. A: Gen.,* 220, **2001**, 105.

42. U. Ciesla, S. Schacht, G.D. Stucky, K.K. Unger, F. Schuth, *Angew. Chem. Int. Ed. Engl.,* 35, **1996**, 541.

43. N.C. Marziano, L.D Ronchin, C. Tortato, A. Zingales, A.A. Sheikh-Osman, *J. Mol. Catal. A: Chem.,* 174, **2001**, 265.

44. G. Herzberg, *Infrared and Raman Spectra of Polyatomic Molecules* (Van Nostrand, **1945**, p. 285.

45. L.J. Bellamy, *The Infrared Spectra of Complex Molecules,* Ed. John Wiley & Sons. Inc., **1960**, p. 328.

46. C.J. Pouchert, *The Aldrich Library of IR Spectra*. Ed. III, **1981**, p. 533.

47. C.J. Pouchert, J. Behnke, *The Aldrich Library of ^{13}C and ^{1}H FT NMR Spectra*, Ed..I, Vol.1, p.1431.

48. Y. Katsuhara, R.M. Hammaker, D.D. DesMarteau, *Inorg. Chem.,* 19, **1980**, 607.

49. H.G.M. Edwards, *Spectrochim. Acta.,* 45A, **1989**, 715.

50. T. Hall, P.K. Hansma, *Surf. Sci.* 71, **1978**, 1 and references therein.

51. M. Chidambaram, C. Venkatesan, P.R. Rajamohanan, A.P. Singh, *Appl. Catal. A: Gen.,* 244, **2003**, 27.

52. C.H. Rochester, *Acidity Functions,* Academic Press, London, **1970**.

53. G.A. Olah, G.K. Surya Prakash, J. Sommer, *Science,* 206, **1973**, 13.

54. A. Corma, M.I. Fornes, J.M. Juan-Rajadell, L. Neito, *Appl. Catal. A: Gen.,* 116, **1994**, 151.

55. X. Ju, P. Huang, N. Xu, J. Shi, *J. Memb. Sc.,* 166, **2000**, 41.

56. S.C. Laha, P. Mukherjee, S.R. Sainkar, R. Kumar, *J. Catal.,* 207, **2002**, 213.

57. M.S. Wong, J.Y. Ying, *Chem. Mater.,* 10, **1998**, 2067.

58. D.M. Antonelli, *Adv. Mater.,* 11, **1999**, 487.

59. J.A. Wang, M.A. Valenzuela, J. Salmones, A. Vazquez, A.G. Ruiz, X. Bokhimi, *Catal. Today,* 68, **2001**, 21.

60. G.A. Olah, R. Malhotra, S.C. Narang, J.A. Olah, *Synthesis,* **1978**, 672.

61. J.S. Reddy, S. Sivasanker, P. Ratnasamy, *Zeolites,* 12, **1992**, 135.

CHAPTER-5

ORGANOSILANOLSULFONIC ACID FUNCTIONALIZED Zr-TMS CATALYSTS (Zr-TMS-OSA)

5.1. INTRODUCTION

There has been considerable interest in the development of heterogeneous solid acid catalysts to avoid the use of traditional homogeneous acid catalytic systems (H_2SO_4, HF, $AlCl_3$, BF_3, etc.) which present serious drawbacks including difficult in handling, corrosiveness, production of toxic waste, and difficulties in separation.

Discovery of silica-based mesoporous materials raised an enormous interest in catalysis because of possibility to extent the concept of shape selectivity to large molecules [1]. Soon after the discovery of M41S materials, oxides of titanium [2, 3], zirconium [4-6], niobium [7], tantalum [8], aluminum [9], hafnium [10], tin [11], and manganese [12] have been synthesized using ionic or neutral surfactants as structure directing agents. Most of them were comprised of mainly amorphous framework walls, which would limit their thermal and hydrothermal stability and greatly compromise their usefulness in catalytic applications.

Hudson and Knowels were first synthesized zirconium-based mesoporous materials [4] as zirconia based mixed oxides are of great importance due to their multiple applications, including catalysis and solid-oxide fuel cells [13, 14]. Porous zirconia was reported to be one of the best candidates as a catalyst support due to its chemical stability and further catalytic efficiency which can easily be tuned either by doping the metal oxide with metals and/or other metal oxides or by functionalizing with organic species through active OH groups [15, 16].

In the recent years SO_4^{2-}/ZrO_2 has been attracted much attention among the researchers and it has been studied in various industrially important reactions such as: isomerization; condensation; Friedel-Crafts acylation reactions; etc [17]. However, non-uniform pore size, low porosity, and small surface area limit the potential application of SO_4^{2-}/ZrO_2 for catalyzing reactions where shape selectivity is expected. In this context, as an alternative, the covalent attachment of alkylsulfonic

acid groups to the surface of mesoporous molecular sieves based on silica has been proposed by several authors and successfully implemented in several acid catalyzed reactions, including esterification and condensations [18, 19].

Though the alkyl/aryl sulfonic acid groups can be successfully attached to the surface of M41S and SBA-n (n=1-15) molecular sieve materials by secondary synthesis as well as via direct synthesis methods, it would be obvious to look for better system than silica based support because of smooth surface of silica would possibly allow leaching and lack of chemical stability [20, 21]. Singh et al. reported trifluromethanesulfonic acid and benzylsulfonic acid functionalized Zr-TMS as efficient acid catalysts for the acylation, acetalization and condensation reactions of bulky molecules [22, 23]. Monoglycerides are widely used as emulsifier in food, pharmaceutical and cosmetic industries [24, 25]. Condensation of aniline to 4,4'-diaminodiphenylmethane is an industrially important intermediate and till now there is no efficient procedure based on environmentally benign route, and hence we adopted a heterogeneous route using *p*-formaldehyde instead of aqueous formaldehyde (formalin) to avoid the catalyst deactivation within short period by the water. Its major uses are as a chemical intermediate in the synthesis of certain isocyanates and polyurethane polymers, as a corrosion inhibitor, in the preparation of azo dyes, as a rubber preservative, and in the curing of epoxy resins and neoprene [26]. In continuation of our effort to increase hydrophobicity and stability of catalytic active species here we report the synthesis of organosilanolsulfonic acid functionalized Zr-TMS catalysts (Zr-TMS≡Si-R_3S-R_4SO_3H). The attachment and chemical nature of the OSA on the walls of Zr-TMS were characterized by various physico-chemical techniques. The catalytic activity of the synthesized catalysts has been tested in liquid phase esterification of glycerol and liquid phase condensation of aniline reactions.

5.2. EXPERIMENTAL

5.2.1. Materials

Zirconium (IV) butoxide (80 wt % solution in 1-butanol, Aldrich, USA), tetramethyl ammonium hydroxide (25 % aq. solution, TMAOH, Loba Chemie, India), N-cetyl-N,N,N trimethyl ammonium bromide (CTMABr, Loba Chemie, India), acetyl acetone (acac, Merck, India), 3-mercaptopropyltrimethoxysilane (3-MPTS, Alrdich, USA), 1,4-butanesultone (1,4-BS, Lancaster, UK), sodium hydroxide (NaOH, Merck, India), methanol (Merck, India) and HCl (Merck, India). All chemicals were used as received without further purification for the synthesis of materials. Lauric acid, aniline, glycerol, p-formaldehyde were used as received for catalytic reactions.

5.2.2. Synthesis of Zr-TMS material

The synthesis of Zr-TMS was carried out using the following gel composition and procedure:

0.1 $Zr(OC_4H_9)_4$:0.05 acac:0.5 CH_3OH:0.025 CTMABr:0.02 TMAOH:8.5 H_2O

In a typical synthesis of Zr-TMS, zirconium (IV) butoxide, methanol and acetyl acetone were mixed well by stirring at room temperature. Then the mixture was slowly added to an aqueous solution of CTMABr and TMAOH, which are well dissolved in required amount of water. After further stirring for 4 h, at about pH =10.5-11, the resulting synthesis gel was refluxed at 90°C for about 50 h. The solid product was recovered, washed with deionised water, acetone, and dried at 100°C for 10 h. The surfactant was removed from the synthesized material by solvent extraction with a mixture containing 100 g of ethanol and 2.5 g of HCl (36 wt %) per gram of the solid material under reflux condition in 48 h. The solid product was recovered by filtration, washed with deionised water, acetone, and dried at 100°C for 6 h.

5.2.3. Synthesis of Zr-TMS-OSA-n catalysts

Well-dried Zr-TMS was taken in a two-necked round bottom flask connected with water condenser through one neck, which was equipped with nitrogen

atmosphere. Dry toluene was added through another neck fitted with septum and stirred for 10 min at 100°C. Then 3-MPTS was introduced into the mixture by syringe and continued the stirring for another 2 h under nitrogen atmosphere (solution A).

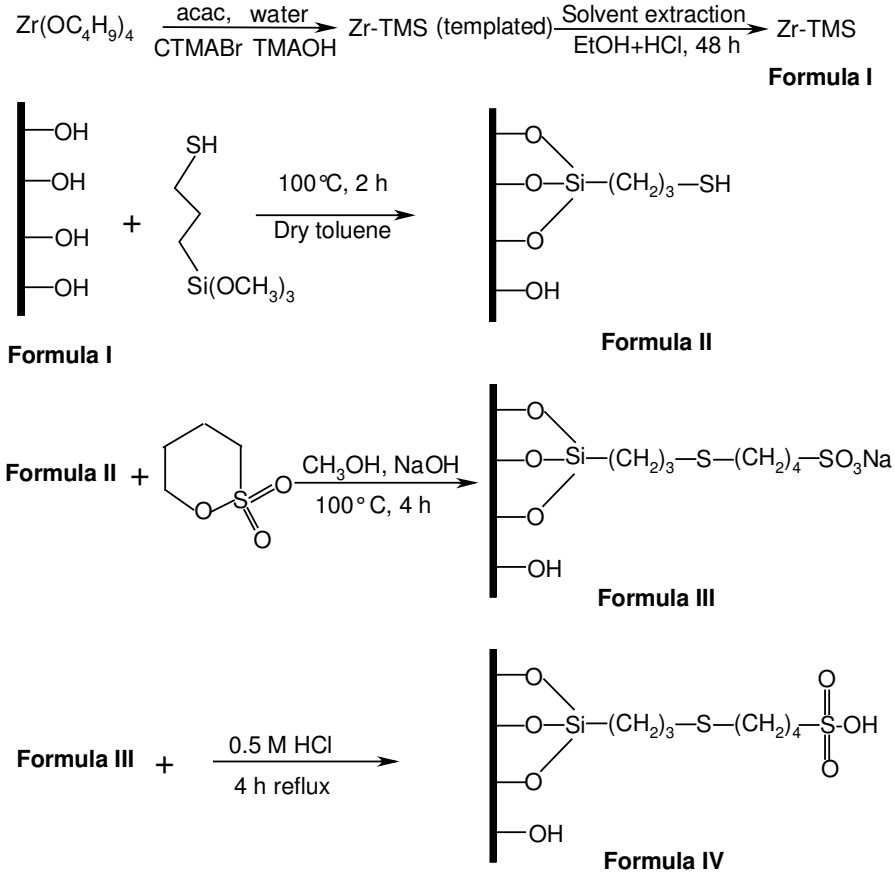

Scheme 5.1. Generalized synthesis scheme of Zr-TMS-OSA catalysts: (I) Zr-TMS; (II) Zr-TMS-SH; (III) Sodium salt of Zr-TMS-OSA; and (IV) Zr-TMS-OSA.

Sodium hydroxide was dissolved in methanol, and stirred at room temperature in an another single necked round bottom flask equipped with septum and to this 1,4-butane sultone was added drop wise and continued the stirring for another 30 min (solution B). Solution B was added in to the solution A and the reflux was continued for another 4 h. Then the mixture was cooled to room temperature, filtered, washed with water, acetone and then dried at 100°C for 10 h. Soxhlet extraction was carried out using a mixture of dichloromethane and diethyl ether (1:1)

mixture to remove the unreacted organic moieties. The sample was then dried at 100 ℃ for 10 h. Organosilanolsulfonic acid functionalized mesoporous Zr-TMS catalyst is designated as Zr-TMS-OSA-n where n denotes the amount of loading.

5.2.4. Synthesis of A-Zr-OSA-20 catalyst

A mixture of zirconium (IV) butoxide (0.08 moles) and 1-butanol (1.6 moles) was taken in a two-necked 250 ml round bottom flask equipped with a magnetic stirrer and a septum. The flask was kept at 100℃ and stirred for 10 min. Then 0.32 mol of water was added drop-wise into this mixture under stirring to hydrolyze the zirconium (IV) butoxide to $Zr(OH)_4$. Further, after 30 min of stirring, 3-MPTS (0.02 mol), and mixture of CH_3OH, NaOH (0.02 mol) and 1,4-BS (0.02 mol) was slowly added by syringe and stirring was continued for 2 h. The mixture was cooled, filtered, washed with deionised water, acetone and then dried at 100℃ for 6 h. Soxhlet extraction was carried out for 24 h. Then the sample was dried at 100 ℃ for 10 h and is designated as A-Zr-OSA-20.

5.2.5. Synthesis of Zr-TMS-SO_3H-20 catalyst

Well-dried Zr-TMS was taken in a two-necked round bottom flask connected with water condenser through one neck, which was equipped with nitrogen atmosphere. Dry toluene was added through another neck fitted with septum and stirred for 10 min at 100 ℃. Then 3-MPTS (20 wt %) was introduced into the mixture by syringe and continued the stirring for another 2 h under nitrogen atmosphere. Then the mixture was cooled to room temperature, filtered, washed with acetone and then dried at 100 ℃ for 10 h. The obtained Zr-TMS-SH-20 was oxidized with three fold excess of H_2O_2 at room temperature under nitrogen atmosphere for 10 h, filtered and washed with water, acetone and then dried at 100 ℃ for 10 h (Zr-TMS≡Si-R_3SO_3H-20). The obtained catalyst is designated as Zr-TMS-SO_3H-20.

5.2.6. Characterization of catalysts

The powder X-ray diffraction of synthesized Zr-TMS, and Zr-TMS-OSA were recorded on a monochromatic Rigaku Miniflex with Ni-filtered Cu K_α radiation, λ=1.5404 Å, 30kV, 15mA between 1.5 to 60° (2θ) with a scan rate of 4° min^{-1}. The BET surface area, total pore volume and average pore diameter were measured by N_2 adsorption-desorption method on a NOVA 1200 (Quantachrome) at –196 °C. Prior to analysis the sample was evacuated at 180 °C for 3 h. The FT-IR spectra were obtained in a range of 400 to 4000 cm^{-1} on a Shimadzu FTIR 8201 PC using a diffuse reflectance scanning mode. Elemental analysis for C and S were done by EA1108 Elemental Analyzer (Carlo Erba Instruments). Atomic absorption spectroscopy (AAS) was used to determine extend of sodium (Na^+) exchange during treatment with HCl using instrument Varian Spectra AA220.

Solid-state ^{13}C CP/MAS and ^{29}Si/MAS NMR studies of Zr-TMS-SH-20 and Zr-TMS-OSA-20 were carried out on a Bruker DSX-300 NMR spectrometer at room temperature. The resonance frequencies of ^{29}Si and ^{13}C were 59.6 and 75.5 MHz, respectively. Finely powdered samples were placed on 5.0 mm dual zirconia rotors and spun at 2.5-3.5 kHz. The chemical shifts were determined using tetramethyl silane (δ=82.4 ppm from TMS) and adamantane (δ =28.7 ppm from TMS) as the reference compounds for ^{29}Si and ^{13}C, respectively. For FT-Raman spectroscopy, powder samples (*ca.* 10 mg) were compressed into a small stainless steel holder. Raman spectra of these samples were measured at room temperature, exposed to atmosphere, using a Bruker RFS/100S FT-Raman spectrometer. NdYAG laser (1.064 μm; 400 mW) was used as an excitation source. Scattered radiation was collected at 180° and detected using an NdYAG detector. Spectra were recorded in the Stokes region between -1000 and 4000 cm^{-1} at 4 cm^{-1} with unpolarised beam resolution. 1024 Scans were coadded.

X-ray photoelectron spectra (XPS) of Zr-TMS-SH-20 and Zr-TMS-OSA-20 were obtained using a VG Microtech Multilab-ESCA3000 spectrometer equipped with a twin anode of Al and Mg. All the measurements were made on as received powder samples using Mg K_α X-ray at room temperature. Base pressure in the analysis chamber was 4 x 10^{-10} Torr. Multichannel detection system with nine channels is employed to collect the data. The overall energy resolution of the instrument is better than 0.7 eV, determined from the full width at half maximum of $4f_{7/2}$ core level of gold surface. The errors in all BE (binding energy) values were with in ±0.3 eV. Temperature programmed desorption (TPD) measurements were carried out to measure the total acidity and strength of acid sites on the catalysts using ammonia as an adsorbate by the procedure given in earlier literatures [27, 22].

The SEM micrographs of Zr-TMS, Zr-TMS-SH-20 and Zr-TMS-OSA-20 materials were taken by JEOL-JSM5200 scanning microscopy. TEM was performed on a JEOL JEM-1200EX instrument with 120 kV of acceleration voltage to probe the size and shape of the materials. The TG-DTA and DTG analysis of the Zr-TMS, Zr-TMS-SH-20 and Zr-TMS-OSA-20 catalysts were carried out by Mettler Toledo 851^e instrument using an alumina pan under air (80ml min^{-1}) atmosphere from ambient to 1000 °C with the increasing rate of 10°C min^{-1}.

5.2.7. Liquid phase esterification of glycerol

The catalytic activity of all Zr-TMS-OSA was examined in the esterification of glycerol with lauric acid at 100 °C (Scheme 5.2). The reactions were carried out in a batch reactor equipped with two-necked 50 ml round-bottomed flask with septum, an oil bath and condenser with nitrogen atmosphere. AR grade chemicals were used without further purification. In a typical run, glycerol and lauric acid were added to the activated catalyst (0.1 g) in the required molar ratio (1:1). The reaction mixture was magnetically stirred and heated to the required temperature at atmospheric pressure. The products were analyzed by a gas-chromatograph (Agilent 6890N) equipped with

a flame ionization detector (FID) and a capillary column (5 μm thick cross-linked methyl silicone gum, 0.2 x 50 m). The products were also identified by GC-MS (Shimadzu 2000 A) analysis and confirmed by ^{1}H and ^{13}C NMR spectra (Bruker AC-200).

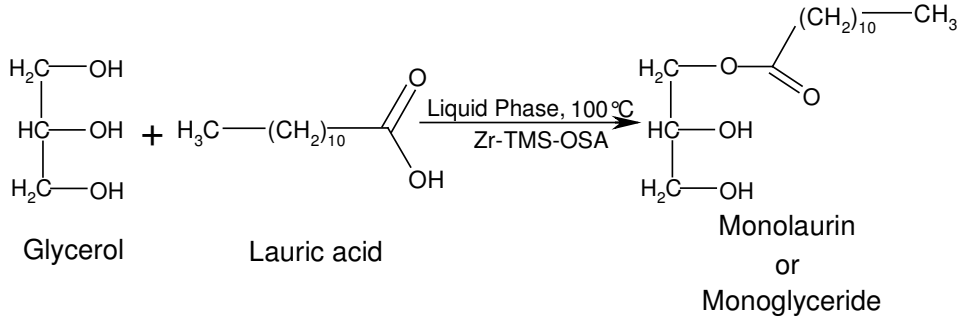

Scheme 5.2. Liquid phase esterification of glycerol with lauric acid to Monolaurin or Monoglyceride.

5.2.8. Liquid phase condensation of aniline

Another activity of the catalysts was checked in condensation of aniline with *p*-formaldehyde at 150 °C (Scheme 5.3). The reactions were carried out in a batch reactor equipped with two-necked 50 ml round-bottomed flask with septum, an oil bath and condenser with nitrogen atmosphere. AR grade chemicals were used without further purification. In a typical run, aniline and p-formaldehyde were added in a required molar ratio (2:1) to the activated catalyst (0.1 g). The reaction mixture was magnetically stirred and heated to the required temperature at atmospheric pressure. The products were analyzed by a gas-chromatograph equipped with a flame ionization detector (FID) and a capillary column (5 μm thick cross-linked methyl silicone gum, 0.2 x 50 m). The products were also identified by GC-MS (Shimadzu 2000 A) analysis and confirmed by ^{1}H and ^{13}C NMR spectra (Bruker AC-200).

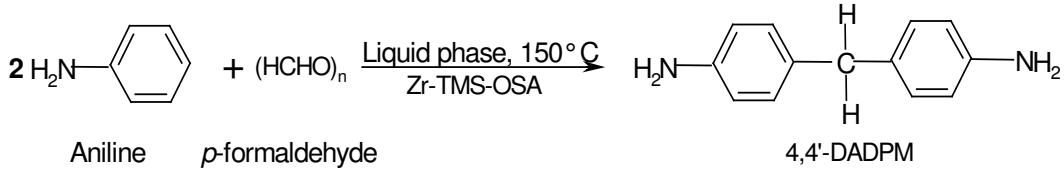

Scheme 5.3. Liquid phase condensation of aniline with *p*-formaldehyde to 4,4'-diaminodiphenylmethane (4,4'-DADPM).

5.2.9. Catalyst recycles study

Recycling of the catalyst was done during the esterification reaction by using Zr-TMS-OSA-20. After workup of the reaction, the catalyst was separated by filtration, washed with acetone and dried at 100 ℃ for 10 h in the presence of air. Thus, the recovered catalyst after each cycle was characterized for its crystallinity by XRD and its chemical composition by elemental analysis.

5.3. RESULTS AND DISCUSSION

5.3.1. Synthesis of catalysts

In order to immobilize the catalytically active species on a heterogeneous solid surface, an organic linker group is used. Organic functionalization of mesoporous materials can be achieved, either by covalently grafting of various organic species onto the surface or by incorporating of functionalities directly during the synthesis. The organosilane having ligands such as thiol, chloro or amine is directly grafted to the silica surfaces by an in situ silylation procedure [20, 21, 28, 29].

Organo functionalized Zr-TMS material has been synthesized by the post-synthesis functionalization procedure as the insitu preparation of Zr-TMS-OSA ended with bulk material with poor surface area. In an attempt to reduce the synthesis steps, OSA was synthesized separately and reacted with Zr-TMS, and found that loading was minimum which can be accounted by two reasons: the bulky nature of the OSA and the competition among two reactive groups, $RSi(OMe)_3$ and SO_3H to react with the surface active OH groups. Hence, stepwise functionalization (bottom up) procedure was adopted and higher loading of OSA up to 20 wt % without loss of meso structure was obtained.

Four different concentrations of 3-MPTS loaded Zr-TMS were prepared by refluxing Zr-TMS with 3-MPTS in anhydrous toluene. Zr-TMS-SH-n was treated with mixture of methanol, NaOH, and 1,4-BS to get sodium salt of OSA functionalized Zr-TMS (Zr-TMS-OSA-n-Na). The final acid form was obtained by treating Zr-TMS-

OSA-n-Na with 0.5 M HCl solution. Their compositions are listed in Table 5.1 and the generalized synthesis procedure is given in scheme 5.1.

Table 5.1. Physico-chemical properties of Zr-TMS, Zr-TMS-OSA, A-Zr-OSA and Zr-TMS-SO_3H catalysts

Catalyst	Elemental analysis (Output) (wt %)		Loading of organosilane/ sulfonic group (wt %)[a]		BET Surface area ($m^2 g^{-1}$)[b]	Sodium exchange (%)[c]	Crystal size (μm)[d]	NH_3 desorbed (mmol g^{-1}) at (°C)[e]				NH_3 chemisorbed[f] at 30°C (mmol g^{-1})
								70-110	110-150	150-200	200-300	
	C	S	Input	Output								
Zr-TMS[g]	----	---	---	---	365	---	0.35	0.13	0.16	0.10	0.04	0.43
Zr-TMS-OSA-5[h]	2.7	1.0	5	4.5	312	99.5	0.37	0.14	0.21	0.12	0.05	0.52
Zr-TMS OSA-10	3.6	2.1	10	9.5	275	99.4	0.38	0.19	0.26	0.15	0.07	0.67
Zr-TMS-OSA-20[i]	5.2	3.9	20	17.7	218	99.6	0.41	0.22	0.33	0.19	0.09	0.83
Zr-TMS-OSA-30	5.3	4.3	30	19.5	109	99.5	0.40	0.26	0.37	0.22	0.08	0.93
A-Zr-OSA-20[j]	6.8	4.1	20	18.6	45	99.7	0.41	0.26	0.34	0.19	0.08	0.87
Zr-TMS-SO_3H-20	4.8	3.5	20	17.2	267	--	0.39	0.20	0.29	0.16	0.08	0.73
Zr-TMS-SH-20	5.0	3.6	20	17.3	260	---	0.37	--	--	--	--	--

[a]Elemental analysis by EA1108 elemental analyzer (Carlo Erba).
[b]Measured by N_2 adsorption-desorption at –196°C.
[c]Measured by Atomic Absorption Spectroscopy (Spectra AA220, Varian).
[d]Measured by JEOL SEM (JSM-5200).
[e]Percent of acid strength distribution calculated based on NH_3 desorbed from 30 to 300°C.
[f]Total acid sites determined in the solid catalyst by NH_3 adsorption-desorption
[g]Total pore volume ($cm^3 g^{-1}$) = 0.36 and average pore diameter (Å) = 40.0 measured by N_2 adsorption isotherm.
[h]Numbers denote wt % (input) of OSA loading over Zr-TMS.
[i]Total pore volume ($cm^3 g^{-1}$) = 0.25 and average pore diameter (Å) = 27.0 measured by N_2 adsorption isotherm.
[j]A-denotes Amorphous $Zr(OH)_4$.

Table 5.2. Degree of sodium exchange of Zr-TMS-OSA-20-Na by HCl of different strength and its catalytic activity

Strength of HCl (mole)	Elemental analysis (output) (wt %)[a]		Loading of OSA(wt %)[b]		Surface area (m^2/g)	(%) sodium exchange[c]	Crystallinity (%)	Convn. of LA (wt %)[d]	TOF[e] ($10^{-1}h^{-1}$ mol^{-1} S)	MG/ML selectivity (wt %)[f]
	C	S	Input	Output						
0.1	5.5	3.9	20	17.7	220	99.2	100	83.4	22	95
0.5	5.8	3.9	20	17.7	218	99.6	100	85.2	23	97
0.7	5.7	3.9	20	17.7	181	99.0	91	85.6	21	90
1.0	5.2	3.8	20	17.2	155	99.8	83	85.0	20	82

[a]Measured by EA1108 elemental analyzer (Carlo Erba).
[b]Calculated based on elemental (Sulfur) analysis value.
[c]Atomic absorption spectroscopy (Spectra AA220, Varian), acetylene used for analysis
[d]Reaction conditions: lauric acid (mmol)=10; glycerol (mmol)=10; catalyst (g)=0.1; reaction time (h)=10; reaction temperature (°C)=100.
[e]TOF is given as moles of lauric acid converted per hour per more of sulfur (amount of Sulfur in $–SO_3H$ group).
[f]MG/ML= monoglycerides/monolaurin.

The influence of different concentration of HCl over the degree of Na-exchange of Zr-TMS-OSA-20-Na has been investigated by treating with different concentration of HCl solutions (Table 5.2). The results reveal that though the degree of Na exchange were almost >99% in all the four cases, the surface area was found to be 220, 218, 181, and 155 $m^2 g^{-1}$ for the sample treated with 0.1, 0.5, 0.7 and 1 M HCl solution, respectively. At higher concentration of HCl, i.e., above 0.5 M the surface area of the sample was found to be decreased drastically which may be attributed to the degradation of meso structure. The above observation was further confirmed by measuring crystallinity of all the four HCl treated samples (Table 5.2). Further, the efficiency of sodium exchange was tested in esterification of glycerol with lauric acid and found similar conversion level of lauric acid (~85 wt %) over samples treated with different strengths of HCl (0.1, 0.5, 0.7 and 1.0 M) and the selectivity to monoglyceride was found to be 95, 97, 90 and 82 wt %, respectively, which demonstrate that the severe structure collapse by using more than 0.5 M HCl solution. Hence, 0.5 M HCl solution was found to be the optimum concentration to obtain high sodium exchange (>99%) without damaging the mesostructure.

5.3.2. Powder X-ray diffraction study

The powder X-ray diffraction (XRD) patterns of the synthesized catalysts are shown in Figure 5.1. The template extracted Zr-TMS (Figure 5.1a), different amount of OSA loaded Zr-TMS (Figure 1b-e), and Zr-TMS-SH-20 (Figure 5.1f) catalysts exhibited a single, broad reflection at low 2θ (2.5° – 4.0°). This reflection corresponds to the XRD pattern of ordered mesoporous ZrO_2 [18, 30, 31] and Si/Zr mesoporous materials [32]. However, the absence of higher order reflections suggest that the pore walls are rather amorphous or there is a lack of correspondence between adjacent pores. A broad peak at about 31° (broad) and a small hump at about 50° are possibly due to the nano crystalline zirconia phases. The broad halo reflection at 2θ = 31° can be distinguished from the peak centered at 2θ = 30° normally observed

for amorphous material and siliceous MCM-41 material [5]. As expected a gradual loss of long-range ordering is observed with increasing the loading of OSA in the Zr-TMS samples. Moreover, low intensity and the absence of higher order reflections show that the order and mesostructure were entirely different from mesoporous silica [18].

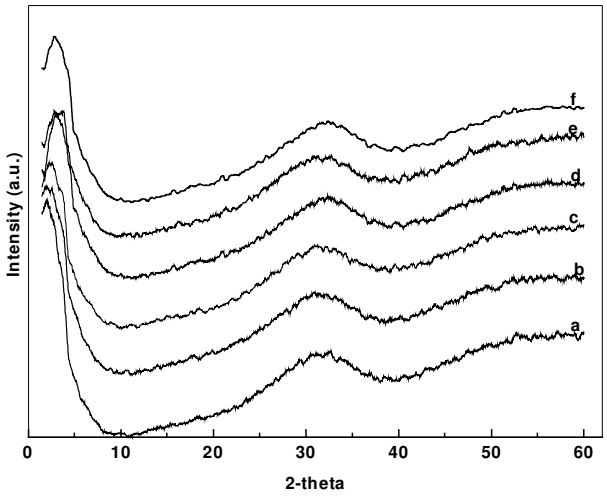

Figure 5.1. X-ray diffraction patterns of Zr-TMS and four different loading of organosilanolsulfonic acid over Zr-TMS: (a) Zr-TMS; (b) Zr-TMS-OSA-5; (c) Zr-TMS-OSA-10; (d) Zr-TMS-OSA-20; (e) Zr-TMS-OSA-30; and (f) Zr-TMS-SH-20 samples.

5.3.3. Nitrogen adsorption-desorption study

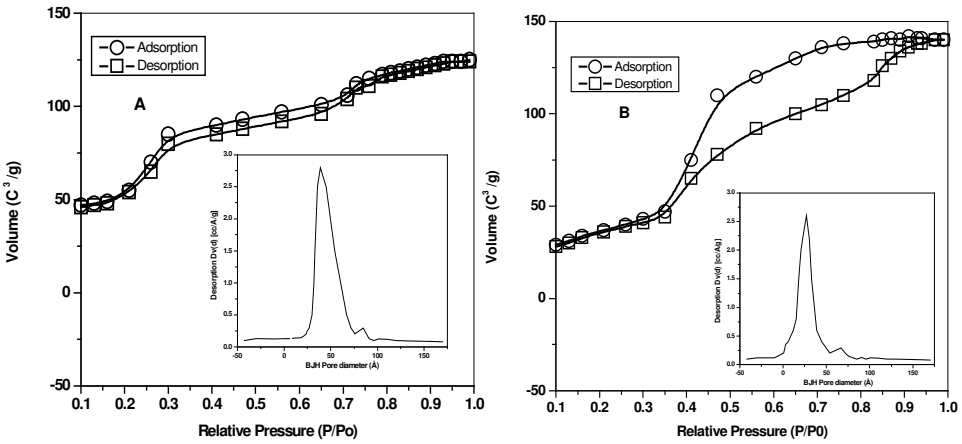

Figure 5.2. N_2 adsorption-desorption isotherm of (A) Zr-TMS (Inset-*BJH* Pore size distribution); and (B) Zr-TMS-OSA-20 (Inset-*BJH* Pore size distribution).

Two important factors that can influence the selectivity of heterogeneously catalyzed organic transformations are the pore size and the nature of active sites at interior pore surface of the catalyst. These properties can have larger effects on the internal mass transfer of reactant, product, and intermediate species within the internal pore spaces. The pore sizes of Zr-TMS materials can be adjusted by controlling the template materials and the synthesis conditions [21]. The BET surface areas of the Zr-TMS, Zr-TMS-OSA-20, A-Zr-OSA-20 and Zr-TMS-SO_3H-20 are given in Table 5.1. The observed surface area for the Zr-TMS was found to be decreased after stepwise functionalization with 3-MPTS and 1,4-BS [30]. The surface area of Zr-TMS-SH-20, Zr-TMS-SO_3H-20 and A-Zr-OSA-20 were found to be 260, 267 and 45 m^2g^{-1}, respectively. Zr-TMS and Zr-TMS-OSA-20 were analyzed by detailed N_2 sorption studies. The specific surface area, average pore diameter and total pore volume of Zr-TMS and Zr-TMS-OSA-20 were 365 m^2 g^{-1}, 40.0 Å, 0.36 cm^3 g^{-1} and 218 m^2 g^{-1}, 27.0 Å, 0.25 cm^3 g^{-1}, respectively (Table 5.1). The decrease in surface area, pore diameter and pore volume of Zr-TMS-OSA-20 may be attributed to the functionalization of Zr-TMS by OSA.

Figures 5.2A and 2B show the nitrogen adsorption isotherms and pore size distributions (inset) of Zr-TMS and Zr-TMS-OSA-20, respectively. Both the isotherms are indicative of type IV behavior demonstrated for mesoporous materials. The position of inflection (Figure 5.2A) in the P/P_0 = 0.25 to 0.75 region depends on the diameter of the mesopores (sharp and narrow pore size distribution) and its sharpness indicates the uniformity of the pore size distributions. After functionalization (Figure 5.2B), the position of inflection is changed in the P/P_0 = 0.35 to 0.93 region. This is indicative of a slight structural collapse in the material. This is also consistent with degradation of the structure leading to materials with larger pore sizes due to collapse of walls between neighboring pores. The insets of figures 5.2A and 5.2B show the BJH pore size distributions of Zr-TMS and Zr-TMS-OSA-20,

respectively. The Zr-TMS possesses a sharp and narrow distribution of mesopores centred at circa 40 Á. After functionalization (Figure 5.2B inset) the distribution is clearly broadened with the pore size distribution of 27 Á.

5.3.4. Elemental analysis study

The carbon and sulfur contents of the samples are shown in Table 5.1. To a first approximation the sulfur content was assigned to the loading of OSA over Zr-TMS and it was observed that acid loading of Zr-TMS indeed increased with the increase in the amount of OSA introduced. After the removal of surfactant, nitrogen was not detected in the elemental analysis as expected. These results were further confirmed by infrared and ^{13}C CP/MAS NMR spectroscopy. For the maximum loading of OSA (20 wt %) over Zr-TMS, output of OSA was found to be only 17.7 wt % without major structure collapse. For A-Zr-OSA-20 material, 18.6 wt % output was observed for the same input loading and increase in loading can be attributed to the insitu functionalization.

5.3.5. FT-Infrared spectroscopic study

The infrared spectra of Zr-TMS, Zr-TMS-SH-20, Zr-TMS-OSA-5, Zr-TMS-OSA-10, Zr-TMS-OSA-20, Zr-TMS-OSA-30 and A-Zr-OSA-20 catalysts are shown in Figure 5.3. The strong and broad band between 3500-3200 cm^{-1} corresponds to the stretching mode of hydroxyl groups present on the surface. The weak unresolved band between 850-750 cm^{-1} is attributed to Zr-O stretching modes. The band observed at about 1450 cm^{-1} corresponds to zirconia. The Zr-TMS-OSA-n (Figure 5.3c-f) and A-Zr-OSA-20 (Figure 5.3g) show additional bands at 2900 cm^{-1}, 1412 cm^{-1}, 1550 cm^{-1} , 1250 cm^{-1} , 1190 cm^{-1}, 1100 cm^{-1} and 740 cm^{-1}, which are absent in Zr-TMS confirm the organic functionalization over surfactant free Zr-TMS. The band at 1190 cm^{-1} and a medium band at 740 cm^{-1} are due to S=O stretching mode and C-S-C bond, respectively. The C-S-C band is merged with Zr-O stretching mode. The short bands at 1412, 1550 cm^{-1} and medium band at 2900 cm^{-1} correspond to the C-

H bending and C-H stretching vibrations of alkyl sulfonic acid groups, respectively. The band at 1250 cm^{-1} is assigned to Si-CH_2 stretching [33]. The stretching mode of Si-O band is observed at 1100 cm^{-1}. Further, a short band at 2553 cm^{-1} in Zr-TMS-SH-20 (Figure 5.3b) is assigned to S-H stretching vibration of thiol group, which disappears after the functionalization of Zr-TMS-SH-20 with 1,4-BS (Figure 5.3c-f). Thus, all these results indicate that the organosilanol sulfonic acid group was incorporated into the walls of surfactant free Zr-TMS.

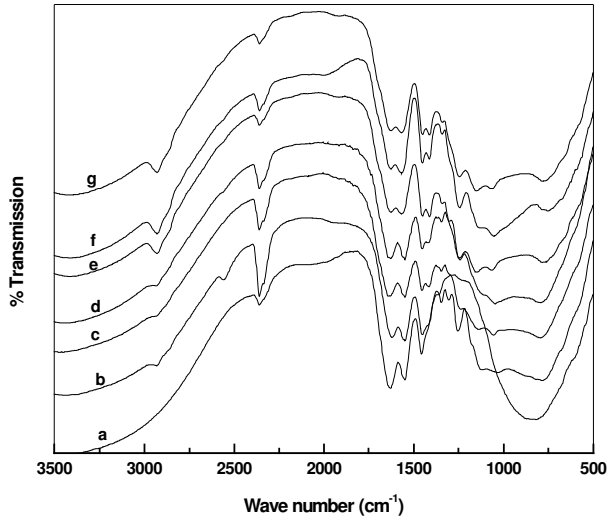

Figure 5.3. Fourier transform-infrared spectra of (a) Zr-TMS; (b) Zr-TMS-SH-20; (c) Zr-TMS-OSA-5; (d) Zr-TMS-OSA-10; (e) Zr-TMS-OSA-20; (f) Zr-TMS-OSA-30; and (g) A-Zr-OSA-20 samples.

5.3.6. Solid-state ^{13}C-CP/MAS NMR study

The Chemical nature of organic moieties anchored on the Zr-TMS surface is further demonstrated by NMR techniques. The solid state ^{13}C-CP/MAS spectra of Zr-TMS-SH-20 (Figure 5.4A) and Zr-TMS-OSA-20 (Figure 5.4B) show characteristic resonance peaks that can be assigned to carbons of different environment present in the sample after functionalization of 3-MPTS and 1,4-BS. Zr-TMS-SH-20, show two peaks at 12.86 and 28.42 ppm due to carbon atom adjacent to the silicon (C_3) and central (C_2) + adjacent to SH group (C_1), which confirm the presence of mercaptopropyl groups attached to the walls of Zr-TMS [21]. Further, absence of

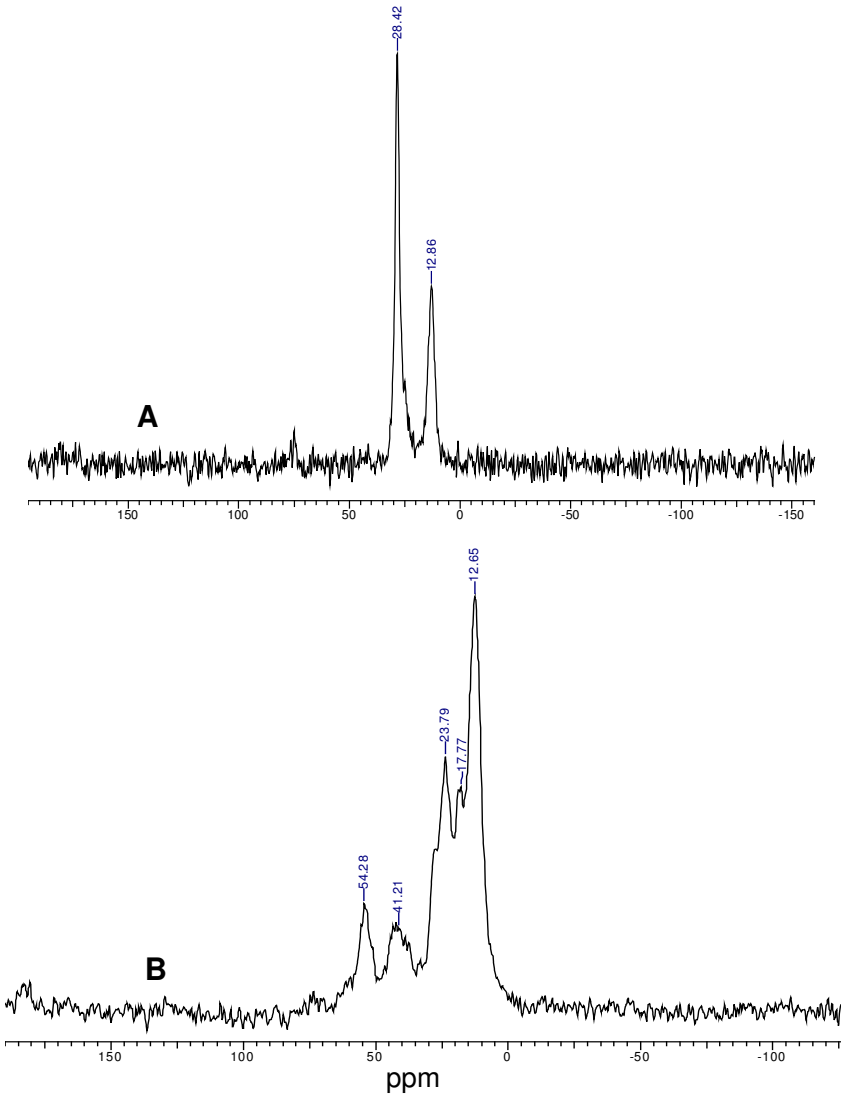

Figure 5.4. Solid-state ^{13}C CP/MAS NMR spectra of (A) Zr-TMS-SH-20; and (B) Zr-TMS-OSA-20 samples.

band in the range of 50 to 52 ppm, characteristic for methoxy carbon confirms that silica is anchored on the walls of Zr-TMS in the tripod form, which is also confirmed by FT-Raman spectroscopy (see below). After functionalization of Zr-TMS-SH-20 with 1,4-BS and further treatment with HCl, Zr-TMS-OSA-20, number of intense and broad bands have been obtained which are characteristic of organosilanolsulfonic acid group anchored on Zr-TMS (Figure 5.4B). The spectrum shows two distinct

peaks at 12.65 and 23.79 ppm for C_3, C_2+ C_1 carbons, respectively, and peaks at 17.77 and 41.21 ppm are assigned to carbon $C_{2'}$ (second carbon from SO_3H group) and $C_{1'}$ (adjacent to sulfonic acid group), respectively [34]. Remaining two carbons ($C_{3'}$ and $C_{4'}$) from sulfonic acid group will behave similarly as C_1 and C_2 carbons as they are located on either sides of sulfur. The peak at 54.28 ppm is due to methoxy carbon which may be formed during treatment with 1,4-butane sultone in methanol solvent.

5.3.7. Solid-state ^{29}Si/MAS NMR study

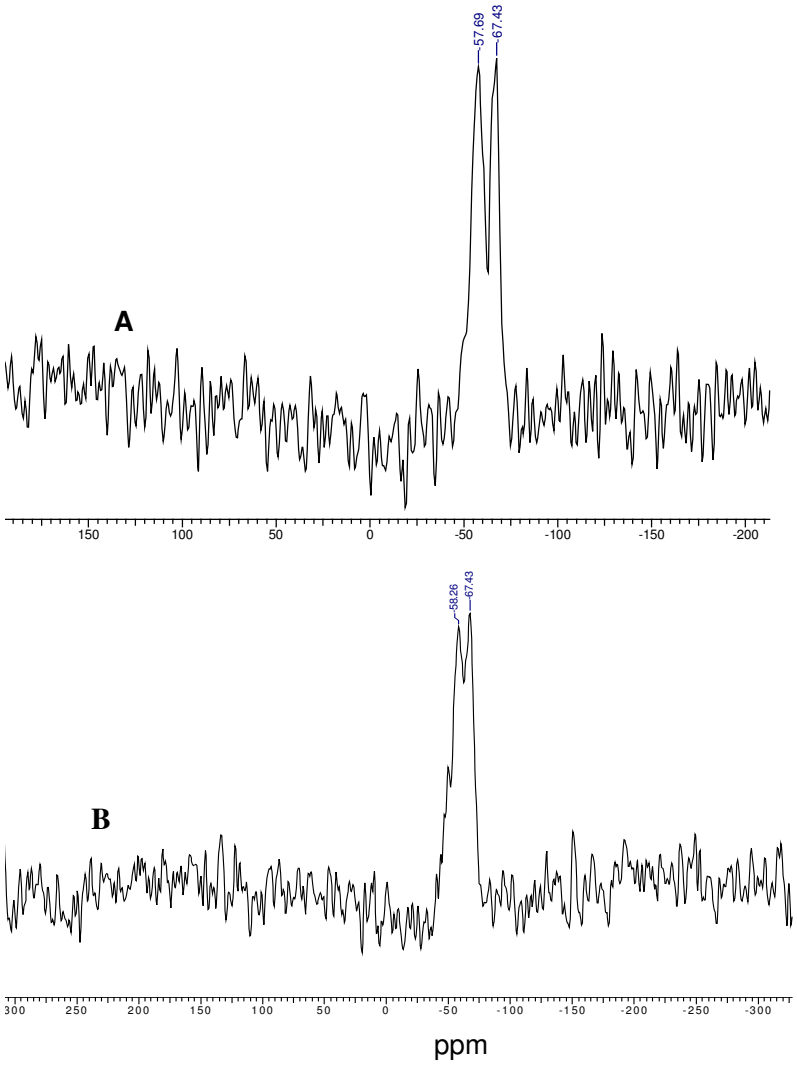

Figure 5.5. Solid-state ^{29}Si MAS NMR spectra of (A) Zr-TMS-SH-20; and (B) Zr-TMS-OSA-20 samples.

Solid-state ^{29}Si/MAS NMR was recorded for Zr-TMS-SH-20 (Figure 5.5A) and Zr-TMS-OSA-20 (Figure 5.5B) and the results were compared with tetramethyl silane. In both the spectra, distinct resonances have been observed for organosilane groups. Signals at –67.43 ppm (T^3) and at –57.69 ppm (T^2) in Zr-TMS-SH-20, show the presence of terminal organic group in the materials [35]. After functionalization of Zr-TMS-SH-20 with 1,4-BS, the T^2 group has shifted from -57.69 to -58.26 ppm, which confirms the reaction of 1,4-BS with –SH group of organosilane molecule of Zr-TMS-SH-20. These results further confirm the successful incorporation of the organo functional groups in the framework of Zr-TMS material.

5.3.8. FT-Raman spectroscopic study

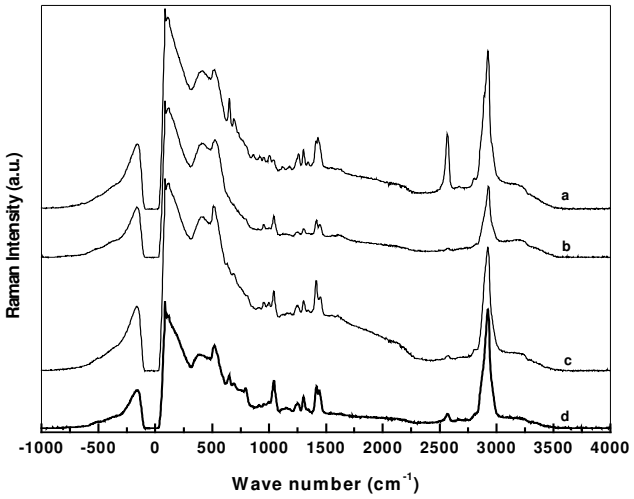

Figure 5.6. FT-Raman spectra of (a) Zr-TMS-SH-20; (b) Zr-TMS-OSA-5; (c) Zr-TMS-OSA-20; and (d) A-Zr-OSA-20 samples.

Nature of functional groups in organo functionalized Zr-TMS were further explored by FT-Raman spectroscopy. Figure 5.6 shows the FT-Raman spectra of Zr-TMS-OSA-5, and Zr-TMS-OSA-20, Zr-TMS-SH-20, and A-Zr-OSA-20. Medium bands at about 123 cm^{-1}(m) and 91 cm^{-1}(m) are characteristic of zirconium material, which are identical in all samples [22]. Apparently these low frequency modes are not sensitive to the presence or absence of mesopores. Prior to addition of 1,4-BS in

the synthesis mixture, Figure 5.6a, Zr-TMS-SH-20 exhibited a strong peak at 2565 cm^{-1} characteristic of the thiol group of mercaptopropyl silica [36].

After addition of 1,4-BS to the Zr-TMS-SH-20, and subsequent treatment with HCl, decrease of intensity due to thiol group was observed in Zr-TMS-OSA-5, Zr-TMS-OSA-20, and A-Zr-OSA-20 (Figure 5.6 b, c, d, respectively) catalysts. The appearance of two new bands in OSA functionalized Zr-TMS catalysts at 954 and 1043 cm^{-1} are attributed to the symmetric and asymmetric vibrational modes of SO_3^-, respectively. It should be noted that Si-O and Si-OH modes obscure S=O stretching vibrations using conventional techniques, however, the present Raman measurements enable us to identify the creation of surface sulfonic acid groups [37]. Further, the retention of modes at 1246 cm^{-1} in Zr-TMS-OSA-20 or 1254 cm^{-1} in A-Zr-OSA-20 and 1304 cm^{-1} in Zr-TMS-OSA-20 or 1312 cm^{-1} in A-Zr-OSA-20, are assigned to CH_2-S and CH_2-Si wagging modes, respectively, confirming the integrity of alkyl linker between the sulfonic acid and silicon centers. The CH_2-S deformation band was observed at 1417 cm^{-1} in Zr-TMS-OSA-20 or 1415 cm^{-1} in A-Zr-OSA-20, however, it was not observed in Zr-TMS-SH-20 (Figure 5.6a). Further, the C-S stretching mode was also observed at 644 or 653 cm^{-1}. FT-Raman spectra show the vibrational mode at around 514 cm^{-1} in Zr-TMS-OSA-20 or 522 cm^{-1} in A-Zr-OSA-20, which shall be assigned to SO_3 asymmetric stretching vibration based on Raman study by Ristova et al. [38]. The disulfide species vibration is also observed in this region. Since disulfide formation was not observed by any other experimental techniques, 514 or 522 cm^{-1} vibration mode can be strongly assigned to SO_3 asymmetric stretching vibration. The band at 1450 cm^{-1} in functionalized Zr-TMS-OSA-20 or 1445 cm^{-1} in Zr-TMS-SH-20 is assigned to C-CH_2-C vibrational mode. The band observed at about 410 cm^{-1} can be assigned to C-C bond stretching vibration. Another observation of strong band at 2924 cm^{-1} is attributed to the asymmetric stretching vibration of CH_2 group. The peak intensity of Zr-TMS-OSA-20

is found to be higher than the intensity of Zr-TMS-OSA-5 (Figure 5.6), which shows the anchoring of OSA over Zr-TMS increased with the increase of OSA concentration. Further, we observed no vibrational mode at about 3500 cm^{-1}, suggesting that under our reaction conditions no Si-OH species were formed. Based on the above observation and NMR studies for the absence of residual methoxy groups confirm that the catalyst synthesis scheme given in scheme 5.1 is acceptable for the final form of catalysts. Small peak shifts exist for some bands on the supported samples relative to the literature assignment. But it should be noted that the literature assignments are not based on the organic specific species (long chain aliphatic group) supported over any bulk materials.

Table 5.3. Compilation of Raman bands measured (cm^{-1}) for Zr-TMS-OSA-20, A-Zr-OSA-20 and Zr-TMS-SH-20 and assignments for the observed vibrations.

Zr-TMS-OSA-20	A-Zr-OSA-20	Zr-TMS-SH-20	Literature [36-39]	Assignment [36-39]
Experimentally measured (in cm^{-1})			(in cm^{-1})	
91	91	81	-	-
123	123	115	-	-
409	406	400	399	υ_s(C-C)
514	522	514	510	$\delta_{as}(SO_3)$
-	644	653	~650	δ_{as}(C-S)
954	955	-	960	$\upsilon_s(S\text{-}O_3^-)$
1043	1043	-	~1050	$\upsilon_{as}(S\text{-}O_3^-)$
1246	1254	1254	1250	$_{wag}(CH_2\text{-}S)$
1304	1312	1304	~1320	$_{wag}(CH_2\text{-}Si)$
1417	1415	-	~1430	$\delta_s(CH_2\text{-}S)$
1450	1450	1445	~1450	$\upsilon_s(C\text{-}CH_2\text{-}C)$
2565	2565	2565	~2570	δ_s(S-H)
2924	2924	2924	2930	$\upsilon_{as}(CH_2)$

The peak data from Figure 5.6, previously reported assignments of Raman spectrum for propylsulfonic acid and some standard peak values of organic species, which are present in the synthesized catalysts [36-38], are compiled in Table 5.3. As shown in Table 5.3, well agreement exists between the measured and the previously

reported Raman spectra for comparable samples. The assignments are from the work of Wilson et al. [37], Ristova et al. [38] and Jones et al. [39]. Finally, the OH stretching frequency, previously reported at 2997 cm^{-1} was observed at 2999 cm^{-1} in this study [40]. All the experimentally observed peak values are matched with previously reported Raman values and found correct with minor shifts, which may be due to the interference of support material.

5.3.9. X-ray photoelectron spectroscopic study

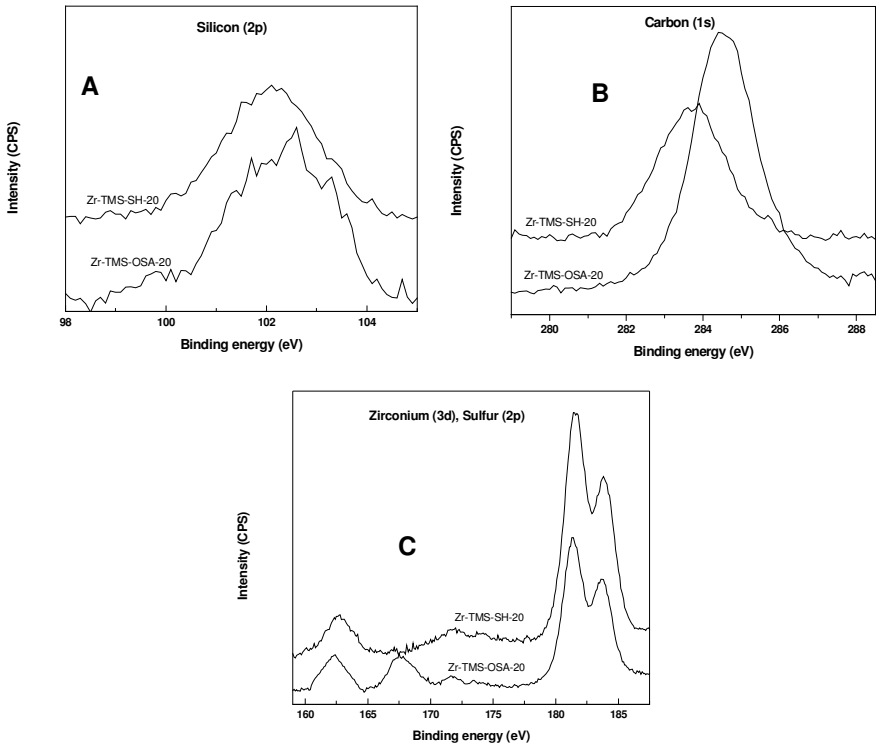

Figure 5.7. X-ray photoelectron spectra of Zr-TMS-SH-20 and Zr-TMS-OSA-20 (A) Silicon; (B) Carbon; and (C) Zirconium and sulfur samples.

To confirm the presence of long linear chain of OSA over Zr-TMS, X-ray photoelectron spectroscopy technique has also been used. The photoelectron spectra were recorded for Zr-TMS-SH-20 and Zr-TMS-OSA-20 samples and the peaks of silicon 2p, carbon 1s, and zirconium 3d, sulfur 2p [41] are shown in Figure

5.7A, B and C, respectively. The accuracy of the measured binding energy (BE) was ±0.3 eV. Figure 5.7A shows the 2p silicon spectra of Zr-TMS-SH-20 and Zr-TMS-OSA-20 samples attached to zirconia with the peak maximum centered at around 102 eV, which further confirms the absence of methoxy group attached to silicon atom [41]. The observed intensities of both the samples were approximately same, but the resolution of spectrum of Zr-TMS-OSA-20 was lower because of bulkiness of the sample. Figure 5.7B explains the carbon 1s XPS spectra of Zr-TMS-SH-20 and Zr-TMS-OSA-20, where one can easily understand that after functionalization of Zr-TMS-SH-20 with 1,4-BS, carbon concentration has increased enormously with binding energy centered at around 284 eV [41, 42]. Further, Figure 5.7C demonstrates the different types of sulfur and zirconium species, which are present in Zr-TMS-SH-20 and Zr-TMS-OSA-20 samples. Both the samples exhibit same environment of zirconium binding energy at about 181.5 eV for $3d_{5/2}$ and 183 eV for $3d_{3/2}$ species confirming the formation of stable zirconium [41]. A small hump observed at about 172 eV is the satellite peak of zirconium, which normally appears along with major peaks. Zr-TMS-SH-20 shows a line broadening at about 162.5 eV characteristic for sulfide sulfur of thiol group of 3-MPTS. After functionalization of Zr-TMS-SH-20 with 1,4-BS and treatment with HCl (Figure 5.7C, Zr-TMS-OSA-20) another line broadening observed with the binding energy of 167.5 eV corresponding for sulfate sulfur of the sample along with sulfide sulfur at about 162.5 eV [41, 42]. The photoelectron spectra pertaining to oxygen 1s has also been recorded and found that there was increase in intensity in Zr-TMS-OSA-20 sample (the spectra not shown). All the above results clearly show that the OSA chain is linearly attached to the zirconia on the surface of Zr-TMS to take active participation in catalysis. Thus this experiment strongly confirms the proposed catalyst's structure (Formula IV of Scheme 5.1).

5.3.10. Ammonia adsorption-desorption study

Marziano et al. [43] and Corma et al. [44] used potentiometric titration with standardized NaOH and ammonia TPD measurement, respectively, to obtain the total acidity and the distribution of their acid strengths of triflate and SO_4^{2-}/ZrO_2 materials, respectively. Here ammonia TPD technique was used to measure the acidity of the synthesized catalysts. In addition to the total number of acid sites, a quantitative distribution of acid strengths of the sites of the functionalized materials was obtained by measuring the desorbing amounts of ammonia in four arbitrarily defined temperature regions during the ammonia TPD experiment (between 70 and 300°C). The organic groups are covalently bonded to the solid support, and as determined from thermal analysis, the maximum temperature (320°C) up to which the organosilanol sulfonic acid can survive was kept as maximum temperature in TPD experiment. Table 5.1 shows the total number of acid sites of Zr-TMS, Zr-TMS-OSA-5, Zr-TMS-OSA-10, Zr-TMS-OSA-20, and Zr-TMS-OSA-30. The quantitative distributions of the acid sites and the total number of acid sites on the catalysts were found to increase with increased loading of OSA over Zr-TMS. A larger number of acid sites were observed on the A-Zr-OSA-20 (0.93 mmol g^{-1}) than on the Zr-TMS≡Si-R_3S-R_4SO_3H-20 (0.67 mmol g^{-1}), which is consistent with the results of elemental analysis (Table 5.1).

5.3.11. Scanning electron microscopic study

The particle size and morphology of Zr-TMS, Zr-TMS-SH-20 and Zr-TMS-OSA-20 were studied by scanning electron microscopy (SEM). The SEM micrograph of Zr-TMS (Figure 5.8A) shows average particle size between 1-2 μm. Distorted hexagonal structure is also found in the materials. After functionalization with 3-MPTS (Figure 5.8B), fine particles disappeared and winding-worm type of particles were observed with bulky materials. Anchoring of 1,4-BS over Zr-TMS-SH-groups (Zr-TMS-OSA-20, Figure 5.8C) leads to further increase in particle size [39]. The

particles appeared to be of a distorted winding-worm type with bulk and clear particles, which are typical of ordered ZrO_2 [18, 45] and MCM-41 [46] type materials. It appears that functionalization alters the morphology and particle size of the material to a greater extent. This decrease in ordering and crystallinity was also observed after functionalization of Zr-TMS with OSA.

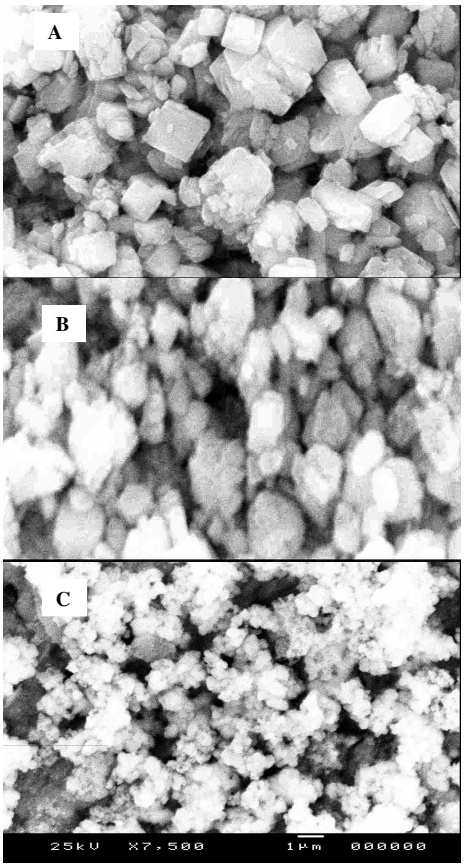

Figure 5.8. Scanning electron micrographs of (A) Zr-TMS; (B) Zr-TMS-SH-20; and (C) Zr-TMS-OSA-20 samples.

5.3.12. Transmission electron microscopic study

Transmission electron micrographs of Zr-TMS (Figure 5.9A), Zr-TMS-SH-20 (Figure 5.9B), and Zr-TMS-OSA-20 (Figure 5.9C) reveal that these materials have mesopores in disordered nature. On the whole, the pores seemed to be packed together with no visible long-range order, consistent with the absence of higher order peaks in low-angle XRD spectra. Its sponge like pore morphology is characteristic of

zirconia aerogels [47, 48]. These results are in good agreement with the earlier studies of Zr-TMS [47].

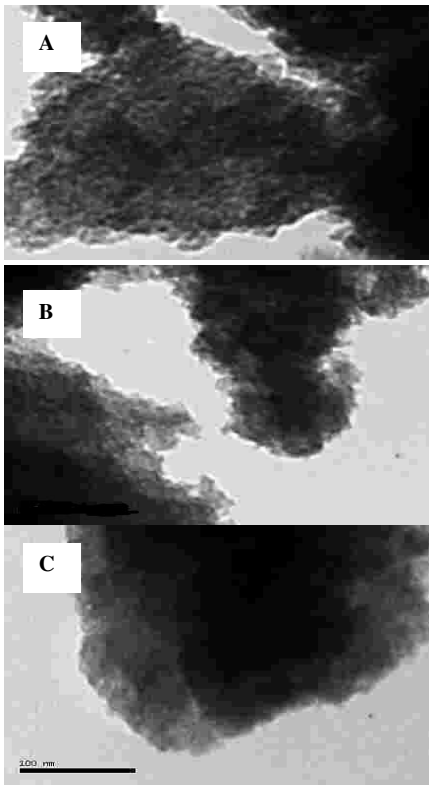

Figure 5.9. Transmission electron micrographs of (A) Zr-TMS; (B) Zr-TMS-SH-20; and (C) Zr-TMS-OSA-20 samples.

5.3.13. Thermal (TGA, DTA & DTG) study

Thermal stability of these catalysts was studied by thermo gravimetric analysis in air atmosphere from ambient temperature to 1000 °C with temperature ramp of 10 °C min^{-1}. Figures 5.10A, B, C and D show typical thermal analysis profiles measured for Zr-TMS, Zr-TMS-SH-20, Zr-TMS-SO_3H-20, and Zr-TMS-OSA-20 samples, respectively. The TGA curve of Zr-TMS (Figure 5.10A) shows three stages of weight loss. The weight loss between 70 and 150 °C corresponds to the loss of loosely bound water, adsorbed moisture and residual butanol, which is clearly evidenced by the large endothermic peak of DTA and then by differential thermal gravimetric peak. Further, the weight loss between 200 to 400 °C corresponds to the annealing of $Zr(OH)_4$ into ZrO_2 [30]. A slight decrease at about 480 °C in the TGA

curve and a corresponding sharp exothermic peak at the same temperature in the DTA curve are indicative of an additional phase coexisting with zirconia. This may be a quasi-amorphous tetragonal phase produced in the annealing process of $Zr(OH)_4$. No further weight losses were observed above 650 °C. At this point the residue is anhydrous ZrO_2.

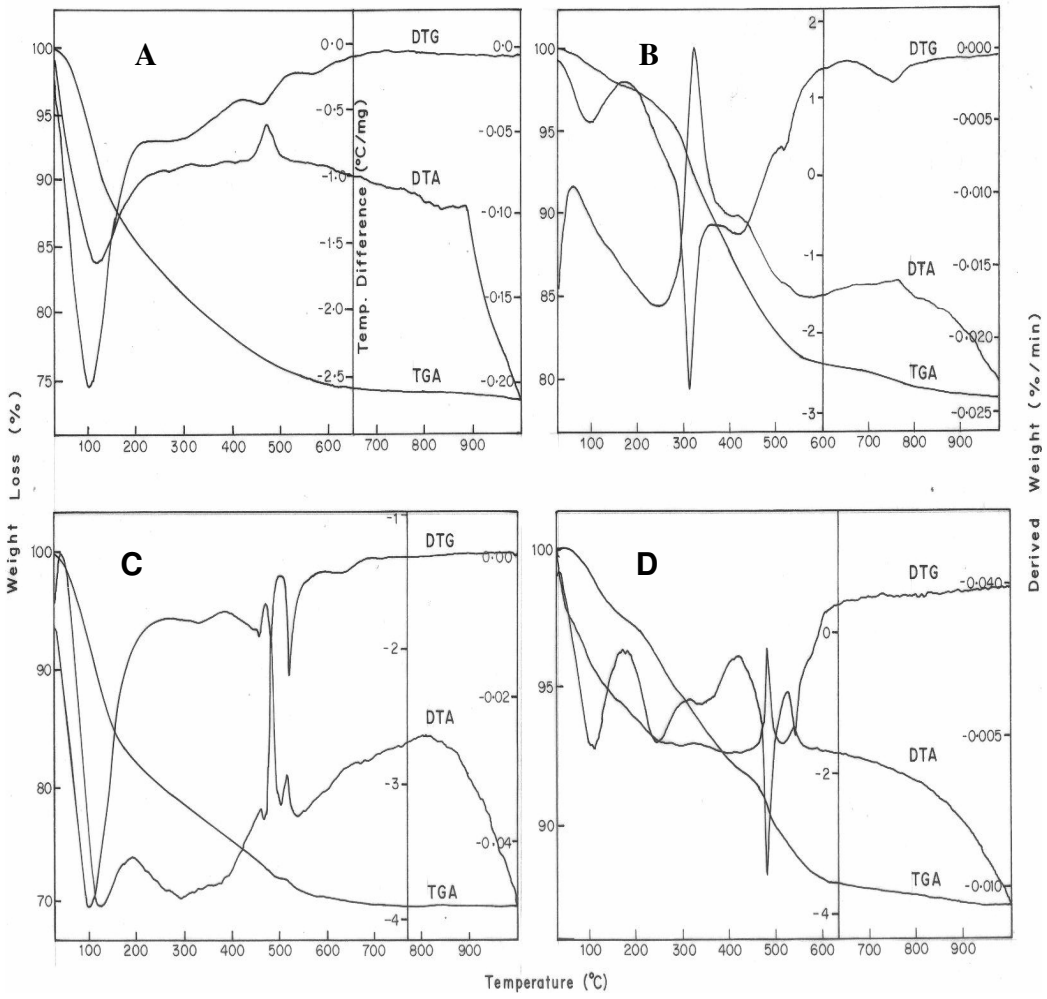

Figure 5.10. TG-DTA and DTG of (A) Zr-TMS; (B) Zr-TMS-SH-20; (C) Zr-TMS-SO_3H-20 and (D) Zr-TMS-OSA-20 samples.

The TGA curves of Zr-TMS-SH-20 (Figure 5.10B), shows four stages of weight losses, which can be clearly explained by its DTA and DTG curves. The weight loss at 100 °C is because of the loss of adsorbed water and moisture. The

large exothermic peak of DTA and its derived weight loss observed at 300°C is characteristic peak for the decomposition of mercaptopropyl group [21, 37]. A small decrease at about 440 °C in the TGA curve and a corresponding exothermic peak at the same temperature in the DTA curve are indicative of an additional phase coexisting with zirconia. The weight loss found above 600 °C shows that the material is anhydrous zirconia.

The thermo gravimetric analysis, differential thermal analysis and differential thermo gravimetric curves of Zr-TMS-SO_3H-20 and Zr-TMS-OSA-20 (Figure 5.10C and D, respectively), show five stages of weight losses. The loss at 100 °C in both the catalysts corresponds to the loss of loosely bound water and adsorbed moisture. The weight loss at about 200 °C in Zr-TMS-SO_3H-20 and at about 250 °C in Zr-TMS-OSA-20 are characteristic losses of unreacted organic moieties, which is clearly observed by an exothermic peak of DTA analysis in Zr-TMS-SO_3H-20 and in Zr-TMS-OSA-20 by DTG curve. The bulky nature (high concentration, long chain) of organosilanolsulfonic acid in Zr-TMS-OSA-20 might be the reason for not observing sharp peak of DTA, since the concentration of unreacted molecule might be very less. The large weight loss at 470 °C in both the catalysts and corresponding sharp exothermic peak of DTA curve (Figure 5.10C and D) corresponds to the loss of sulphonic acid group from the support material [21, 37, 52], which is further evidenced by the differential thermogravimetric (DTG) peak. A small weight loss observed at 520 °C in both the cases may be attributed to the existence of an additional phase of zirconia. The weight loss observed about 700 °C shows that the material is completely anhydrous ZrO_2. This technique reveals that sulfonic acid group is stable at least up to 450 °C. All these results show that the material is pure and the long chain organosilanolsulfonic acid is formed and principally located on the mesoporous surfaces, where they are accessible for adsorption and catalytic reaction processes. Moreover, the amount of weight loss observed from Zr-TMS-SO_3H-20

and Zr-TMS-OSA-20 was nearly same, which is the clear indication of formation of long organosilanolsulfonic acid group present. These results show that the material is stable up to 450 ℃ and can be used conveniently in reactions at moderate temperatures.

5.3.14. Liquid phase esterification of glycerol

The organosilanolsulfonic acid functionalized materials were studied in the esterification of lauric acid with glycerol to monoglyceride and the results are given in Table 5.4. Under similar reaction conditions, Zr-TMS-OSA catalysts were found to be more active than that of Zr-TMS which shows that the Brönsted acid sites of sulfonic acids are responsible for the same. Apart from the pore size and strength of active acid sites, relative affinity of the catalyst for highly hydrophilic glycerol and the rather hydrophobic lauric acid also influence the catalytic activity. The Zr-TMS showed 10 wt % conversion of lauric acid due to the limited number of acid sites, however, the selectivity, to monolaurin was 100 wt %. The lauric acid conversion was found to be 31, 60, 82, 85 and 52 wt %, respectively over Zr-TMS-OSA-5, Zr-TMS-OSA-10, Zr-TMS-OSA-20, A-Zr-OSA-20 and Zr-TMS-SO_3H-20. Even though the acid sites concentrations of Zr-TMS-OSA-20 (0.67 mmol g^{-1}) and the A-Zr-OSA-20 (0.93 mmol g^{-1}) catalysts are different (Table 5.1), both catalysts showed nearly similar conversion of lauric acid (Table 5.4) which shows that the acid sites in Zr-TMS-OSA-20 are well exposed to the reactants through the mesopores where as in A-Zr-OSA-20 the acid sites may be buried inside the framework. The selectivity to monolaurin over Zr-TMS-OSA-20 was higher (90 wt %) than the A-Zr-OSA-20 (70 wt %) and the lower selectivity of A-Zr-OSA-20 (70 wt %) may be ascribed to surface reaction and possibly di and tri-glycerides were also formed over the later (Table 5.4). The activity of Zr-TMS-OSA-20 was found to be 82 wt % with 90 wt % selectivity to monolaurin, which shows that the hydrophobic nature of Zr-TMS-OSA-20 facilitates the selective formation of monolaurin. The TOF (10^{-1} h^{-1} mol^{-1} S) for Zr-TMS-OSA-5, Zr-TMS-OSA-

10, Zr-TMS-OSA-20, A-Zr-OSA-20 and Zr-TMS-SO_3H-20 were found to be 41, 38, 29, 28 and 26, respectively. Bossaert et al. [20] have reported in their studies that 53 % yield of monoglyceride was obtained using propylsulfonic acid functionalized MCM-41 whereas Diaz et al. [19] have got 63 % yield of monoglyceride using combined alkyl sulfonic acid functionalized MCM-41 using 1:1 molar ratio of reactants. Based on these reports it is clearly seen that organosilanolsulfonic acid functionalized Zr-TMS catalysts are more effective catalyst for the esterification of lauric acid even at moderate reaction condition with high selectivity to monolaurin (>90 wt %).

Table 5.4. Liquid phase esterification of glycerol with lauric acid over Zr-TMS, Zr-TMS-OSA, A-Zr-OSA and Zr-TMS-SO_3H catalysts[a]

Catalysts	Conversion of LA (wt %)	TOF[b] ($10^{-1}h^{-1}$ mol^{-1} S)	Product distribution (wt %)[c]	
			MG/ML	Others
Zr-TMS	10	--	100	0
Zr-TMS-OSA-5[d]	31	41	90	10
Zr-TMS-OSA-10[d]	60	38	86	14
Zr-TMS-OSA-20[d]	82	29	90	10
A-Zr-OSA-20[d]	85	28	70	30
Zr-TMS-SO_3H-20[d]	52	26	88	12

[a]Reaction conditions: Catalyst (g) = 0.1; Glycerol (mmol) = 10; Lauric acid (mmol) = 10; Reaction time (h) = 24; Reaction temperature (°C) = 100.
[b]TOF is given as moles of lauric acid transformed per hour per mole of sulfur
[c]MG/ML: monoglyceride/monolaurin.
[d]Numbers denote wt % of OSA loading over Zr-TMS.

5.3.15. Liquid phase condensation of aniline

Since the condensation of aniline with formaldehyde is one of important processes, there are plentiful reports using homogeneous and heterogeneous acid catalysts to improve the yield of 4,4'-diaminodiphenylmethane (4,4'-DADPM) [49-51]. Corma et al. reported 81.5 % diamines with 42.5 % selectivity for 4,4'-DADPM using

dealuminated zeolite catalysts [53]. Here in this study, p-formaldehyde was used instead of aqueous formaldehyde and found that higher conversion of aniline to 4,4'-DADPM (Table 5.5). The p-formaldehyde cleaved at the reaction condition and reacted with aniline was enhanced by the presence of Brönsted acid sites. As observed in the esterification reaction, Zr-TMS showed lower aniline conversion (20 wt %) and the conversion significantly increased after the functionalization of OSA over Zr-TMS.

Table 5.5. Liquid phase condensation of aniline with *p*-formaldehyde over Zr-TMS, Zr-TMS-OSA, A-Zr-OSA and Zr-TMS-SO_3H catalysts[a]

Catalysts	Conversion of aniline (wt %)	TOF[b] ($10^{-1}h^{-1}$ mol^{-1} S)	Product distribution (wt %)[c]	
			4,4'-DADPM	Others
Zr-TMS	20	--	90	10
Zr-TMS-OSA-5[d]	55	73	86	14
Zr-TMS-OSA-10[d]	84	54	85	15
Zr-TMS-OSA-20[d]	91	32	86	14
A-Zr-OSA-20[d]	86	28	64	36
Zr-TMS-SO_3H-20[d]	56	28	82	18

[a]Reaction conditions: catalyst (g) = 0.1; aniline (mmol) = 20; *p*-formaldehyde (mmol) =10; reaction time (h) = 24; reaction temperature (°C) = 150.
[b]TOF is given as moles of aniline transformed per hour per mole of sulfur.
[c]4,4'-DADPM: 4,4'-diaminodiphenylmethane
[d]Weight % of OSA loading over Zr-TMS

The conversion of aniline over Zr-TMS-OSA catalysts was found to increase from 55 to 91 wt % when the loading of OSA was increased from 5 to 20 wt %. When the loading of OSA was increased further from 20 to 30 wt %, the conversion of aniline and selectivity to 4,4'-DADPM decreased (not shown). The lower activity and selectivity may be ascribed to decrease in long range order and formation of amorphous like material where the active sites are buried inside the framework and the reaction is expected to take place at the surface. The conversion of aniline and

selectivity to 4,4'-DADPM over Zr-TMS-OSA-20 and A-Zr-OSA-20 were found to be 91, 86 wt % and 86, 64 wt %, respectively. Under similar reaction conditions, the conversion of aniline and selectivity to 4,4'-DADPM over Zr-TMS-SO_3H-20 was found to be 56 and 82 wt %, respectively, which is lower than Zr-TMS-OSA-20. The increase in carbon chain length enables the hydrophobic nature of the catalyst which significantly increases the tolerance limit of the catalyst towards water which forms as co-product during the reaction and also enhances the selectivity to monolaurin.

5.3.16. Catalyst recycles study

Table 5.6. Recycling of Zr-TMS-OSA-20 in esterification reaction[a]

Cycle	Elemental analysis[b] (wt %)		Convrsion of LA (wt %)	TOF[c] ($10^{-1}h^{-1}$ mol^{-1} S)[c]	Selectivity to MG/ML[d] (wt %)	Crystallinity (%)
	C	S				
Fresh	5.2	3.8	82	29	90	100
1st recycle	5.0	3.7	78	28	90	98
2nd recycle	4.7	3.3	70	29	86	94

[a]Reaction conditions: catalyst (g) = 0.1; glycerol (mmol) = 10; lauric acid (mmol) = 10; reaction time (h) = 24; reaction temperature (°C) = 100
[b]Measured by elemental analysis (EA1108,Carlo Erba).
[c]TOF is given as moles of Lauric acid transformed per hour per mole of Sulfur
[d]MG/ML: monoglyceride/monolaurin.

The stability of the catalysts was studied with Zr-TMS-OSA-20 catalyst (Table 5.6) by recycling in glycerol esterification reaction. After the reaction the catalyst was filtered washed with solvent and dried before using. Three cycles (fresh and two recycles) were carried out under similar reaction conditions, using the same catalyst. Elemental (Table 5.6) analyses showed that sulfur content of catalyst decreased marginally after each cycle which also reflected in the conversion of lauric acid on recycling (from 82 to 70 wt %), whereas, the selectivity to monolaurin remains nearly the same. The marginal decrease in sulfur content can be attributed to loss of organosilane which were less covalently attached to the zirconia wall work. From this

study it was confirmed that almost >90% of organosilanol sulfonic acid groups were firmly attached to the zirconia walls which can survive at reaction temperature even with the presence of water which formed as a co-product during the reaction.

5.4. CONCLUSIONS

A simple and efficient procedure has been developed for the syntheses of organosilanol sulfonic acid functionalized Zr-TMS by post synthesis modification of Zr-TMS. Different characterization techniques have been applied for characterizing the synthesized catalysts and found that the organosilanolsulfonic acid groups were firmly attached to the porous walls of mesoporous zirconia. The mesostructure of zirconia was retained during the post-synthetic functionalization of Zr-TMS with OSA up to 20 wt % loading and after that structural disintegration was observed and the material behaves like the one obtained by in-situ synthesis, A-Zr-OSA-20. The Zr-TMS-OSA-20 was found to be an active and selective catalyst for the esterification of lauric acid with glycerol and condensation of aniline with p-formaldehyde. The recycling studies support the stability of the catalyst at the reaction temperature even in the presence of water.

5.5. REFERENCES

[1] C.T. Kresge, M.E. Leonowicz, W.J. Roth, J.C. Vartuli, J.S. Beck, *Nature,* 359, **1992**, 710.

[2] D.M. Antonelli, J.Y. Ying, *Angew. Chem., Int. Ed. Engl.,* 34, **1995**, 2014.

[3] H. Yoshitake, T. Sugihara, T. Tatsumi, *Chem. Mater.,* 14, **2002**, 1023.

[4] J.A. Knowles, M.J. Hudson, *J. Chem. Soc., Chem. Commun.,* **1995**, 2083.

[5] U. Ciesla, S. Schacht, G.D. Stucky, K.K. Unger, F. Schuth, *Angew. Chem. Int. Ed. Engl.,* 35, **1996**, 541.

[6] U. Ciesla, M. Froba, G.D. Stucky, K.K. Unger, F. Schuth, *Chem. Mater.*, 11, **1999**, 227.

[7] B. Lee, D.L.Lu, J.N. Kondo, K. Domen, *J. Am. Chem. Soc.*, 124, **2002**, 11256.

[8] D.M. Antonelli, J.Y. Ying, *Chem. Mater.*, 8, **1996**, 874.

[9] S.A. Bagshaw, T.J. Pinnavaia, *Angew. Chem. Int. Ed. Engl.*, 35, **1996**, 1102.

[10] P. Liu, J. Liu. A. Sayari, *Chem. Commun.*, **1997**, 577.

[11] K.G. Servin, T.M. AbdeFattah, T.J. Pinnavaia, *Chem. Commun.*, **1998**, 1471.

[12] Z. Tian, W. Tong, J. Wang, N. Duan, V.V. Krishnan, S.L. Suib, *Science*, 276, **1997**, 926.

[13] T. Takahashi, N.Q. Minh, *Science and Technology of Ceramic Fuel Cells,* Elsevier, New York, **1995**.

[14] S.Y. Lai, W. Pan, C.F. Ng, *Appl. Catal. B:* 24, **2000**, 207.

[15] J.B. Miller, E.I. Ko, *Catal. Today*, 35, **1997**, 269.

[16] C.N. Satterfield, *Mass Transfer in Heterogeneous Catalysis,* MIT Press, Cambridge, MA, **1970**.

[17] G.D. Yadav, J.J. Nair, *Micropor. Mesopor. Mater.*, 33, **1999**, 1.

[18] I. Diaz, C. Marquez-Alvarez, F. Mohino, J. Perez-Pariente, E. Sastre, *J. Catal.*, 193, **2000**, 295.

[19] W.D. Bossaert, D.E. De Vos, W.M. Van Rhijin J. Bullen, P.J. Grobet, P.A. Jacobs, *J. Catal.,* 182, **1999**, 156.

[20] V.I. Parvulescu, H. Bonnemann, V. Parvulescu, B. Endruschar, A.Ch.W. Rufinska, B. Tesche, G. Poncelet, *Appl. Catal. A: Gen.*, 214, **2001**, 273.

[21] D. Margolese, J.A. Melero, S.C. Christiansen, B.F. Chmelka, G.D. Stucky, *Chem. Mater.*, 12, **2000**, 2448.

[22] M. Chidambaram, D. Curulla-Ferre, A.P. Singh, B.G. Anderson, *J. Catal.*, 220, **2003**, 442.

[23] S. Parambadath, M. Chidambaram, A.P. Singh, *Catal. Today*, 97, **2004**, 233.

[24] E. Jungermann, *Cosmet. Sci. Technol.*, 11, **1991**, 97.

[25] H. Baumann, M. Buhler, H. Fochem, F. Hirsinger, H. Zoebelein, J. Falbe, *Angew. Chem.,* 100, **1988**, 41.

[26] J.I. Kroschwitz, *Kirk-Othmer Encyclopedia of Chemical Technology*, Vol.2, p.461, **1944**.

[27] M. Chamumi, D. Brunel, F. Fajula, P. Geneste, P. Moreau, J. Solof, *Zeolites,* 14, **1994**, 283.

[28] C. Venkatesan, M. Chidambaram, A.P. Singh, *Appl. Catal. A: Gen.*, 292, **2005**, 344.

[29] Anirban Ghosh, Rajiv Kumar, *J. Catal.*, 228, **2004**, 386.

[30] M.J. Hudson, J.A. Knowles, *J. Mater. Chem.*, 6, **1996**, 89.

[31] G. Larsen, E. Lotero, M. Nabity, L.M. Petkovic, D.S. Shobe, *J. Catal.*, 164, **1996**, 246.

[32] A.O. Bianchi, M. Champanati, P.M. Torres, E.R. Castellon, A.J. Lopez, A. Vaccari, *Appl. Catal. A: Gen.*, 220, **2001**, 105.

[33] L.J. Bellamy, *Infrared spectra of complex molecules*, Chapman and Hall, **1975**.

[34] C.J. Pouchert, J. Behnke, *The Aldrich Lib. Of ^{13}C and ^{1}H NMR Spectra,* Edn.1, Vol.1, p. 1445, **1993**.

[35] X. Feng, G.E. Fryxell, L.Q. Wang, A.Y. Kim, J. Liu, K.M. Kemner, *Science,* 276, **1997**, 923.

[36] N.B. Colthup, L.H. Daly, S.E. Wiberly, *Introduction to Infrared and Raman Spectroscopy,* Academic Press, New York, **1964**.

[37] K. Wilson, A.F. Lee, J.M. Macquarrie, J.H. Clark, *Appl. Catal. A: Gen.*, 228 **2002**, 127.

[38] M. Ristova, L. Pejov, M. Zugic, B. Soptrajanov, *J. Mol. Str.*, 482-483, **1999**, 647.

[39] C.W. Jones, M. Tsapatsis, T. Okubo, M.E. Davis, *Micropor. Mesopor. Mater.,* 42, **2001,** 21.

[40] H.G.M. Edwards, *Spectrochim. Acta.,* 45A, **1989**, 715.

[41] C.D. Wagner, W.M. Riggs, L.E. Davis, J.F. Mounder, G.E. Muilenberg, *Hand*

Book of X-ray photoelectron spectroscopy, Perkin-Elmer corpn, Minnesota, **1979**.

[42] E. Godocikova, P. Balaz, Z. Bastl, L. Brabec, *Appl. Sur. Sci.*, 200, **2002**, 36.

[43] N.C. Marziano, L.D. Ronchin, C. Tortato, A. Zingales, A.A. Sheikh-Osman, *J. Mol. Catal. A: Chem.,* 174, **2001**, 265.

[44] A. Corma, M.I. Fornes, J.M. Juan-Rajadell, L. Neito, *Appl. Catal. A: Gen.,* 116, **1994**, 151.

[45] X. Ju, P. Huang, N. Xu, J. Shi, *J. Memb. Sc.*, 166, **2000**, 41.

[46] S.C. Laha, P. Mukherjee, S.R. Sainkar, R. Kumar, *J. Catal.*, 207, **2002**, 213.

[47] M.S. Wong, J.Y. Ying, *Chem. Mater.,* 10, **1998**, 2067.

[48] Y-Y. Lyu, S.H. Yi, J.K. Shon, L.S. Pu, S-Y. Lee, J.E.Yie, K. Char, G.D. Stucky, J.M. Kim, *J. Am. Chem. Soc.*, 126, **2004**, 2310.

[49] J.L. Nafziger, L.A. Rader, I.J. Jr. Seward, *US 4554378 A,* **1985**.

[50] S. Klein, D. Grotjohann, C. Mendoza-Frohn, D. Koch, H.H. Mueller, H.G. Pirkl, R. Uchdorf, G. Wegener, *WO 2001058847 A1,* **2001**.

[51] V. Peesapati, P.L. Pauson, R.A. Pethrick, *J. Chem. Res., Synop.*, 6, **1987**, 194.

[52] I. Diaz, C. Marquez-Alvarez, F. Mohino, J. Perez-Pariente, E. Sastre, *J. Catal.*, 193, **2000**, 295.

[53] A. Corma, P. Botella, C. Mitchel, *Chem. Commun.*, **2004**, 2008.

CHAPTER-6

SUMMARY AND CONCLUSIONS

The background of the present work lies in the fact to fabricate new mesoporous zirconia (Zr-TMS, zirconia based transition metal oxide mesoporous molecular sieves) catalyst for the acid catalysis. Different amounts of acidic functionalities such as benzylsulfonic acid, trifluromethanesulfonic acid and organosilanolsulfonic acid have been introduced in the high surface area Zr-TMS material. With this view, the present work is composed of six chapters. Apart from the main thesis work (synthesis of three types of catalysts, their characterization and catalytic application), the introduction & literature survey and synthesis methodologies and characterization techniques have also been discussed in first and second chapters, respectively.

Chapter 3 describes the synthesis, characterization and catalytic application of Zr-TMS-BSA catalysts. Zr-TMS has been synthesized with high surface area and functionalized with benzyl sulphonic acid using post synthetic route by applying the etherification and subsequent sulfonation reactions to get covalently bonded Zr-TMS-BSA (-Zr-O-CH_2-Φ-SO_3H) catalysts. Different amounts of sulphonic acid (5, 10, 15, 20 and 25 wt %) were loaded over Zr-TMS-BS and the maximum amount of sulphonic acid loading was optimized to 9.1 wt % (input 10 wt %) without destroying the mesoporous structure of the material and compared with A-Zr-BSA-10. The powder XRD patterns and the N_2 adsorption-desorption confirm the mesoporous nature of the material with high surface area and considerable pore size distributions in agreement with conventional mesoporous ZrO_2. The FT-IR study revealed the successful anchoring of benzyl group and the subsequent functionalization of –SO_3H group. The NH_3 TPD measurements showed that the catalysts are acidic in nature with proper acid strength. The synthesized catalysts were used in the benzoylation of diphenyl ether with benzoyl chloride to 4-phenoxybenzophenone, liquid phase condensation of 2-methylfuran with acetone to 2,2-bis(5-methylfuryl)propane and found to be more active and selective due to their increase in the number of acid

sites and mesoporosity, respectively. Zr-TMS, A-Zr-BSA-10 and SO_4^{2-}/ZrO_2 were found to be poorly active because of the lower acidic and non- mesoporous nature, respectively. The catalysts optimization study for different reaction parameters was done on the liquid phase condensation of anisole with p-HCHO to 4,4'-dimethoxydipneylmethane at 100°C. Zr-TMS-BSA-10 was recycled two times and a decrease in anisole conversion is observed after second cycle, which is related to a minor leaching of benzylsulfonic acid from the catalyst. The higher activity of the synthesized materials may be attributed to its higher acidity and mesoporous characteristics.

Chapter 4 describes synthesis, characterization and catalytic application of Zr-TMS-TFA catalysts. Zr-TMS has been synthesized based on the sol-gel method. The extracted Zr-TMS was successfully functionalized with triflic acid by post synthesis treatment to obtain covalently-bonded Zr-TMS-TFA (≡ Zr-O-SO_2-CF_3) catalysts with high surface area. Different amounts of triflic acid (5, 10, 15, 20, 25 and 30 wt %) were loaded over Zr-TMS and the maximum amount of triflic acid loading was optimized to 22.8 wt % (input 30 wt %) without destroying the mesoporous structure of the material and compared with A-Zr-TFA catalysts. The catalysts were characterized by various physico-chemical techniques such as XRD, N_2 adsorption-desorption, FTIR, FT-Raman, elemental analysis, ^{13}C DD/MAS NMR, TPD of NH_3, SEM, TEM, and thermal analysis. The low angle powder XRD patters show the existence of mesoporous nature. The BET surface area and pore size distribution results were in general agreement with previous values reported for mesoporous ZrO_2. The NH_3 TPD measurements showed that the catalysts were highly acid. ^{13}C DD/MAS NMR revealed that the $–CF_3$ group remained intact in the material. FT-Raman analysis demonstrated that the triflic acid was bonded in an identical fashion on both amorphous $Zr(OH)_4$ and Zr-TMS at all loadings. Triflate ligands bound via 3 equivalent oxygen atoms to zirconium atoms forming tripod structures. TEM studies

teach that the material contained disordered channels, unlike MCM-41 mesoporous molecular sieves. Acetalization of ethylacetoacetate to fructone and benzoylation of biphenyl to 4-phenylbenzophenone reactions were performed on Zr-TMS-TFA, A-Zr-TFA, triflic acid and SO_4^{2-}/ZrO_2. Zr-TMS-TFMSA catalysts were found to be the most active and selective in both reactions due to their mesoporosity and to an increase in the number of acid sites with the "right" acid strength. The stability and recycle effect of the catalysts were checked in the acetalization reaction by using Zr-TMS-TFMSA-30. No major loss of activity was observed after two recycles, but a decrease of the sulfur content and catalyst crystallinity was observed. Further, the catalysts optimization study with different reaction parameters was done in the benzoylation of toluene with p-toluoyl chloride to 4,4'-dimethylbenzophenone. Zr-TMS-TFA-15 was recycled one time and a decrease in *p*-T-Cl conversion is observed after one cycle, which is related to a minor leaching of CF_3SO_3H from the catalyst. The formation of acylated products of toluene is explained by an electrophilic attack of acyl cation ($R\text{-}CO^+$; where R = $CH_3\text{-}C_6H_5\text{-}$) on the toluene ring, whose formation is facilitated by acid sites on Zr-TMS-TFA catalysts.

Chapter 5 describes the synthesis, characterization and catalytic application of Zr-TMS-OSA catalysts. A simple and efficient procedure has been developed for the syntheses of Zr-TMS and functionalization of OSA by bottom-up approach over Zr-TMS to achieve Zr-TMS-OSA catalysts. Four different loadings of OSA (5, 10, 20 and 30 wt %) over Zr-TMS were prepared by varying the molar ratios. OSA functionalized non-porous catalyst (A-Zr-OSA-20) was also synthesized for comparison study. After successful syntheses, the catalysts were characterized by various physico-chemical techniques. The low angle powder XRD patterns and the high BET surface area and uniform pore size distribution explains that the material is in mesoporous range with well-defined pore size. AAS experimental results reveal that more than 99 % of sodium (Na^+) was replaced by H^+ to form organosilanolsulfonic acid Zr-TMS

catalysts. The NH_3 TPD measurements proved that the catalysts were comparatively highly acidic in nature. Solid-state ^{13}C CP/MAS NMR demonstrated that the OSA group remained intact in the material and there is no disulphide formation under the present synthesis condition. FT-Raman analysis illustrate that organosilanolsulfonic acid was bonded in an identical fashion on Zr-TMS at all loadings measured and found correct. The XPS measurements show peak broadening and shift in the binding energies of zirconium 3d, Silicon 2p, carbon 1s, sulfur 2p (both sulfide and sulfate sulfur) and lines in the case of Zr-TMS-OSA catalysts. Further, it explains that the OSA is anchored on the surface of zirconia linearly and sulfonic acid group is easily accessible for catalysis. Thermal analytical results demonstrate that the material is highly pure and it cannot be treated above 300°C. After having demonstrated the syntheses of stable, mesoporous, OSA functionalized Zr-TMS catalysts; their catalytic performance was assessed for the liquid phase esterification of glycerol with lauric acid to monolaurin and liquid phase condensation of aniline with p-formaldehyde to 4,4'-diaminodiphenylmethane, which are industrially equally important reactions. Zr-TMS-OSA catalysts were found to be the most active and selective in both the reactions due to their acidity and mesoporosity. The stability and recycle effect of the catalysts were checked in the liquid phase esterification reaction using Zr-TMS-OSA-20. No major loss of reactivity was observed after two recycles however a decrease in sulfur content and catalyst crystallinity were observed.

PUBLICATIONS / SYMPOSIA / CONFERENCES

LIST OF RESEARCH PUBLICATIONS

1. Selective benzoylation of Biphenyl to 4-Phenylbenzophenone over Zeolite H-beta.

   M. Chidambaram, C. Venkatesan, A.V. Ramaswamy, P. Moreau, A. Finiels and A.P, Singh.

   Applied Catalysis A: General. 224 ***(2002)*** *129.*

2. Synthesis of acid functionalized mesoporous ≡Zr-O-SO_2-CF_3 catalysts; heterogenization of CF_3SO_3H over mesoporous $Zr(OH)_4$.

   M. Chidambaram, C. Venkatesan, P.R. Rajamohanan and A.P. Singh.

   Applied Catalysis A: General. 244 ***(2003)*** *27.*

3. Preparation of isobutyl cumenes by liquid phase isopropylation of isobutyl benzene with 2-propanol using zeolite H-beta.

   C. Venkatesan, **M. Chidambaram,** K.R. Kamble and A.P. Singh,.

   Catalysis Letters 85 ***(2003)*** *171.*

4. Synthesis and Characterization of Triflic Acid Functionalized Mesoporous Zr-TMS Catalysts; Heterogenization of CF_3SO_3H over Zr-TMS and its Catalytic Activity.

   M. Chidambaram, D. Curulla-Ferre, A.P. Singh and B.G. Anderson.

   Journal of Catalysis 220 ***(2003)*** *442.*

5. Preparation of benzylsulphonic acid functionalized mesoporous Zr-TMS and its application in acylation reaction.

   Surendran Parambadath, **M. Chidambaram** and A.P. Singh.

   Catalysis Today 97 ***(2004)*** *233.*

6. Benzoylation of toluene with p-toluoyl chloride over triflic acid functionalized Zr-TMS catalysts.

   Shainaz M. Landge, **M. Chidambaram** and A. P. Singh.

   Journal of Molecular Catalysis A: Chemical. 213 ***(2004)*** *257.*

7. 3-Aminopropyltriethoxysilyl functionalized Na-Al-MCM-41 solid base catalyst for selective preparation of 2-phenylpropionitrile from phenylacetonitrile.

   C. Venkatesan, **M. Chidambaram** and A.P. Singh

   Appl. Catal. A: Gen. 292 ***(2005)*** *344.*

8. Condensation of anisole with p-formaldehyde over benzylsulphonic acid functionalized mesoporous Zr-TMS catalyst.

   M. Chidambaram, S. Selvakumar, T. Tamil Selvi and A. P. Singh

Journal of Molecular Catalysis A: Chemical, (in press 2005).

9. Organosilanolsulfonic acid functionalized mesoporous Zr-TMS catalysts; Synthesis, characterization and catalytic applications in esterification and condensation reactions.
   M. Chidambaram, C. Venkatesan and A.P. Singh.
   Journal of Catalysis (Under review).
10. Preparation of coumarin derivatives using triflic acid functionalized mesoporous Zr-TMS catalysts.
    S. Selvakumar, **M. Chidambaram** and A.P. Singh
    Journal of Organic Chemistry (To be communicated).
11. Studies on the X-ray diffraction analysis of $Li_xCo_{1/6}Mn_{11/6}O_4$ cathode material synthesized through solution route.
    K. Ragavendran, **M. Chidambaram**, D. Vasudevan, Bosco Emmanuel and A. Veluchamy.
    Journal of Material Chemistry Physics (To be Communicated).

PATENTS

1. An improved process for the production of Phenyl ketones.
   M. Chidambaram, C. Venkatesan, A.P. Singh and A.V. Ramaswamy
   U.S. Patent No. 6,593,499, ***2003.***
2. An improved process for the production of 4,4'-Dimethylbenzophenones.
   S.M. Landge, A.P. Singh and **M. Chidambaram**
   U.S. Patent. PCT No.PCT/IN03/00459, 2003.
3. A process for the production of 4,4'-diaminodiphenylmethane by sulfonic acid functionalized Zr-TMS catalyst.
   M. Chidambaram and A.P. Singh.
   Indian Patent filed
4. An improved process for the production of Phenyl ketones.
   M. Chidambaram, C. Venkatesan, A.P. Singh and A.V. Ramaswamy
   Indian Patent, Appl. No. 1107/DEL/2001.
5. An improved process for the production of 4,4'-dimethylbenzophenones.
   S.M. Landge, A.P. Singh and **M. Chidambaram**
   Indian Patent, Appl. No. NF-462/2003.

CONTRIBUTIONS TO NATIONAL/INTERNATIONAL SYMPOSIA/CONFERENCES

1. *Sulfated zirconia for condensation reaction*. C. Venkatesan, **M. Chidambaram** and A.P. Singh.
   Participated in 15th National catalysis symposium and 2nd Indo-Pacific catalysis symposium held at National Chemical Laboratory, Pune India on January 2001***(Poster presentation).***
2. *Selective Monomethylation of phenylacetonitrile to 2-Phenylpropionitrile using solid base catalysts.* C. Venkatesan, M. Muthukumar, **M. Chidambaram** and A.P. Singh
   4th National Symposium in Chemistry held at National Chemical Laboratory, Pune. India on February 2002. ***(Poster Presentation).***
3. *Selective acetylation of 2-methoxynaphthalene over solid acid catalysts.*
   C. Venkatesan, P. Muthukumar, Sachin N. Shah, **M. Chidambaram** and A.P. Singh.
   "Catalysis: Concepts to practice" held on June 2002 at N.C.L. Pune, India conference in honor of Dr. Paul Ratnasamy on his 60th birth anniversary. ***(Poster Presentation).***
4. *Heterogenization of CF_3SO_3H over Zr-TMS and its catalytic activity*
   M. Chidambaram, C. Venkatesan and A.P. Singh
   "Catalysis Research in India-Some highlights" held on May 2003 at N.C.L, Pune, India. A symposium in honor of Dr. A.V. Ramaswamy on his 60th birth anniversary. ***(Poster Presentation).***
5. *Triflic acid functionalized Zr-TMS catalysts and its catalytic activity.*
   M. Chidambaram and A.P. Singh
   National workshop on advances in catalysis held on January 2003 conducted by catalysis society of India at Loyola college, Chennai, India. (***Poster presentation***).
6. *Benzoylation of toluene with p-toluoyl chloride over triflic acid functionalized mesoporous Zr-TMS catalyst.*
   M. Chidambaram, S. Parambadath, S. Selva kumar and A.P. Singh.
   17th National symposium on catalysis held on January 2005 at CSMCRI, Bhavnagar, India. ***(Oral presentation).***